

General Disclaimer

One or more of the Following Statements may affect this Document

- This document has been reproduced from the best copy furnished by the organizational source. It is being released in the interest of making available as much information as possible.
- This document may contain data, which exceeds the sheet parameters. It was furnished in this condition by the organizational source and is the best copy available.
- This document may contain tone-on-tone or color graphs, charts and/or pictures, which have been reproduced in black and white.
- This document is paginated as submitted by the original source.
- Portions of this document are not fully legible due to the historical nature of some of the material. However, it is the best reproduction available from the original submission.

NASA CR-156682

ADVANCED VERY HIGH RESOLUTION RADIOMETER
FINAL ENGINEERING REPORT

PREPARED BY

ITT AEROSPACE/OPTICAL DIVISION
FORT WAYNE, INDIANA

46803

(NASA-CR-156682) ADVANCED VERY HIGH
RESOLUTION RADIOMETER Final Engineering
Report (ITT Aerospace/Optical Div.) 305 p
HC A14/MF A01 CSCI 14B

N78-16345

Unclas
G3/35 03616

CONTRACT #NAS5-21900

PREPARED FOR

NATIONAL AERONAUTICS AND SPACE ADMINISTRATION
GODDARD SPACE FLIGHT CENTER
GREENBELT, MARYLAND
20771



TABLE OF CONTENTS

		<u>PAGE</u>
1.0	INTRODUCTION-----	1-1
1.1	General Instrument Description-----	1-1
1.1.1	The Scanner Module-----	1-2
1.1.2	Electronics Module-----	1-7
1.1.3	Radiant Cooler-----	1-8
1.1.4	Optical Subsystem-----	1-9
1.1.5	Baseplate Unit-----	1-10
2.0	SYSTEM SENSITIVITY-----	2-1
2.1	Solar Channels 1 and 2-----	2-1
2.1.1	Detector-----	2-1
2.1.2	Detector Responsivity-----	2-1
2.1.3	Solar Channels System Sensitivity-----	2-4
2.2	Channel 3 Detector and Sensitivity-----	2-11
2.2.1	Mercury-Cadmium-Telluride Detector-----	2-11
2.2.2	Channel 3 Sensitivity-----	2-15
2.3	Channel 4-----	2-20
2.3.1	Detector-----	2-20
2.3.2	Channel 4 Sensitivity-----	2-20
3.0	OPTICAL DESIGN-----	3-1
3.1	General Description-----	3-1
3.2	Scan Mirror-----	3-4
3.3	Telescope Design-----	3-4
3.4	Channels 1 and 2 Lens Design-----	3-9
3.5	Channel 3 and 4 Lens Design-----	3-13
3.6	AVHRR Tolerance Analysis-----	3-18
3.6.1	Summary of Mechanical Tolerances-----	3-18
3.6.2	Surface Quality for Filters, Beamsplitters-----	3-22
3.6.3	Mechanical Adjustment Data (Inches)-----	3-22
3.7	Dichroics, Beamsplitters and Cooler Windows-----	3-22
3.8	Spectral Definition-----	3-25
3.8.1	Spectral Definition of Solar Channels-----	3-25
3.8.2	Spectral Definition of Thermal Channels-----	3-40
3.9	Channel Registration-----	3-44
3.10	Polarization Sensitivity-----	3-45
3.11	Scattered Sunlight-----	3-48
3.11.1	Honeycomb Temperature Gradient-----	3-49
3.11.2	Sunlight Reflections from In-Flight Target-----	3-49
3.11.3	Signal Contamination-----	3-52
3.11.4	Sun Scatter Test Results-----	3-54
4.0	MECHANICAL DESCRIPTION-----	4-1
4.1	Overall Instrument Configuration-----	4-1
4.1.1	Structure-----	4-1
4.1.2	Materials in Structure-----	4-4
4.2	Scanner Subassembly-----	4-4
4.2.1	Scan Motor-----	4-4
4.2.2	Bearings-----	4-10

TABLE OF CONTENTS (CONTINUED)

		<u>PAGE</u>
4.2.3	Bearing Fits-----	4-10
4.2.4	Lubrication-----	4-13
4.2.5	Jitter-----	4-13
4.2.6	Life Test-----	4-14
4.2.7	Angular Momentum-----	4-14
4.2.8	Venting of the Scanner Housing-----	4-15
4.3	Radiant Cooler Subassembly-----	4-15
4.3.1	Support Body-----	4-15
4.3.2	Detector Location-----	4-19
4.3.3	Deployable Earth Shield-----	4-19
4.3.4	Materials and Finishes in Cooler-----	4-21
4.4	Optics Subassembly-----	4-21
4.4.1	Optics Outline-----	4-21
4.4.2	Materials and Finishes Used in Optics-----	4-21
4.5	Electronics Package-----	4-21
4.5.1	Electronics Package Layout-----	4-21
4.5.2	Accessibility-----	4-21
4.5.3	Thermal Considerations-----	4-25
4.5.4	Radiation Considerations-----	4-25
4.5.5	Materials and Finishes in Electronics-----	4-25
4.6	Weight Breakdown-----	4-25
4.7	Materials-----	4-25
5.0	ELECTRICAL SYSTEM-----	5-1
5.1	Electronic Packaging-----	5-1
5.2	Electrical Design Considerations-----	5-4
5.3	Video Scan Timing-----	5-4
5.4	Power Subsystem-----	5-6
5.4.1	General-----	5-6
5.4.2	Turn on Transient-----	5-6
5.4.3	Electronics Switching Regulator-----	5-6
5.4.4	Power Converter-----	5-9
5.4.5	+5V Regulators-----	5-9
5.4.6	±15V Regulators-----	5-9
5.4.7	Motor Power Supply Switching Regulator-----	5-10
5.5	Commands and Digital TM-----	5-11
5.6	Analog TM and Patch Control-----	5-17
5.6.1	Analog Telemetry-----	5-17
5.6.2	Patch Temperature Control-----	5-25
5.7	Motor Logics-----	5-29
5.8	Scan Count and Decode-----	5-30
5.9	Output Data Control-----	5-34
5.10	Ramp Calibration Generator-----	5-42
5.11	Auxiliary Scan Timing-----	5-46
5.12	Ch 3 Data Amplifier-----	5-50
5.13	Channel 4 Amplifier-----	5-55
5.14	Daylight Amplifiers-----	5-55
5.15	Multiplexer Board-----	5-59
5.16	Black Body Mux-----	5-60
5.17	Motor Power Supply-----	5-60
5.18	Power Profile-----	5-64
5.19	Interface Connectors-----	5-64
5.20	Electronics Drawings-----	5-64

TABLE OF CONTENTS
(CONTINUED)

		<u>PAGE</u>
6.0	RADIANT COOLER-----	6-1
6.1	Field of View-----	6-3
6.2	Shield-----	6-5
6.2.1	Cover Temperature-----	6-5
6.2.2	Shielding and View Factors-----	6-7
6.3	Radiator-----	6-10
6.4	Patch-----	6-14
6.5	Solar Exposure-----	6-16
6.6	Anti-Contamination Provisions-----	6-19
6.7	Optical Port Loading-----	6-20
6.7.1	Optical Loading on the Radiator-----	6-21
6.7.2	Optical Loading on the Patch-----	6-21
6.7.3	Absorptivity of the Instrument Patch Opening (Theoretical Model)-----	6-27
7.0	CALIBRATION-----	7-1
7.1	Thermal Channels Calibration-----	7-1
7.1.1	Calibration Accuracy-----	7-1
7.1.2	Chamber Calibration Targets-----	7-7
7.1.3	In-Flight Calibration Target-----	7-19
8.0	THERMAL DESIGN-----	8-1
9.0	TEST AND CALIBRATION DATA-----	9-1
10.0	LIST OF DESIGN INFORMATION REPORTS-----	10-1

1.0 INTRODUCTION

The Advanced Very High Resolution Radiometer (AVHRR) was developed under Contract NAS5-21900 over the period from January 1973 to December 1976. The program covered the design, construction, and test of a Breadboard Model, Engineering Model, Protoflight Model, Mechanical/Structural Model, and a Life Test Model. Special bench test and calibration equipment was also developed for use on the program.

Initially, the instrument was to operate from a 906 n.m. orbit and be thermally isolated from the spacecraft. The Breadboard Model and the Mechanical/Structural Model were designed and built to these requirements. During the Engineering Model assembly phase, the spacecraft altitude was changed to 450 n.m., IFOVs and spectral characteristics were modified, and spacecraft interfaces were changed. In addition, the final spacecraft design provided a temperature-controlled Instrument Mounting Platform (IMP) to carry the AVHRR and other instruments. The design of the AVHRR was modified to these new requirements and the modifications were incorporated in the Engineering Model. The Protoflight Model and the Flight Models (being built on Contract NAS5-22497) conform to this design.

1.1 General Instrument Description

The AVHRR is a four channel scanning radiometer providing two channels in the visible-near IR region and two IR channels. The instrument utilizes an 8 inch diameter optical system. Cross-track scanning is accomplished by a continuously rotating mirror direct-

driven by a hysteresis synchronous motor. The two IR detectors are cooled to 105K by a two-stage passive radiant cooler. The data from the four channels is simultaneously sampled at a 40 KHz rate and converted to 10-bit binary from within the instrument.

A summary of the AVHRR characteristics is given in Table 1-1. Figure 1-1 is a photograph of the Engineering Model instrument and Figure 1-2 shows the configuration of the Protoflight Model.

The AVHRR is comprised of five modules which are assembled together into a single unit instrument. These modules are:

- Scanner Module
- Electronics Module
- Radiant Cooler Module
- Optical Subsystem
- Baseplate Unit

These modules are shown in the exploded view of Figure 1-3.

1.1.1 The Scanner Module

This module includes the scan motor, the mirror and the scan motor housing. The scan motor design is based on the motor developed for the SCMR, an 80 pole hysteresis synchronous motor. The motor has two power modes of operation. High power ($\approx 4-5$ watts) will be utilized for driving the scan mirror in air and low power (≈ 3.8 W) will be used for nominal in-orbit operation. The scanner housing is an integral part of the motor and is made of beryllium. The scan mirror is also made of beryllium and is ≈ 11.6 inches across the major axis and 8.25 inches across the minor axis. The scan motor

Table 1-1 Summary of Characteristics

	<u>Ch 1</u>	<u>Ch 2</u>	<u>Ch 3</u>	<u>Ch 4</u>
Spectral Range (μM)	.55 -.9	.725 - 1.0	10.5 - 11.5	3.55 - 3.93
Detector	Silicon	Silicon	HgCdTe	InSb
Resolution (N.M.)	.59	.59	.59	.59
IFOV (MR)	1.3 sq.	1.3 sq.	1.3 sq.	1.3 sq.
S/N @ .5% Albedo	>3:1	>3:1	-	-
NETD @ 300K	-	-	.12K	.12K
MTF (1 IFOV/Single Bar)	.30	.30	.30	.30
Optics	- 8 inch diameter afocal cassegrainian telescope			
Scanner	- 360 rpm hysteresis synchronous motor with beryllium scan mirror.			
Cooler	- Two-stage radiant cooler, IR detectors controlled at 105K			
Data Output	- 10 bit binary, simultaneous sampling at 40 KHz rate.			
Commands	- 28			
Telemetry	- 14 Digital, 20 Analog			

REPRODUCIBILITY OF THE
ORIGINAL PAGE IS POOR

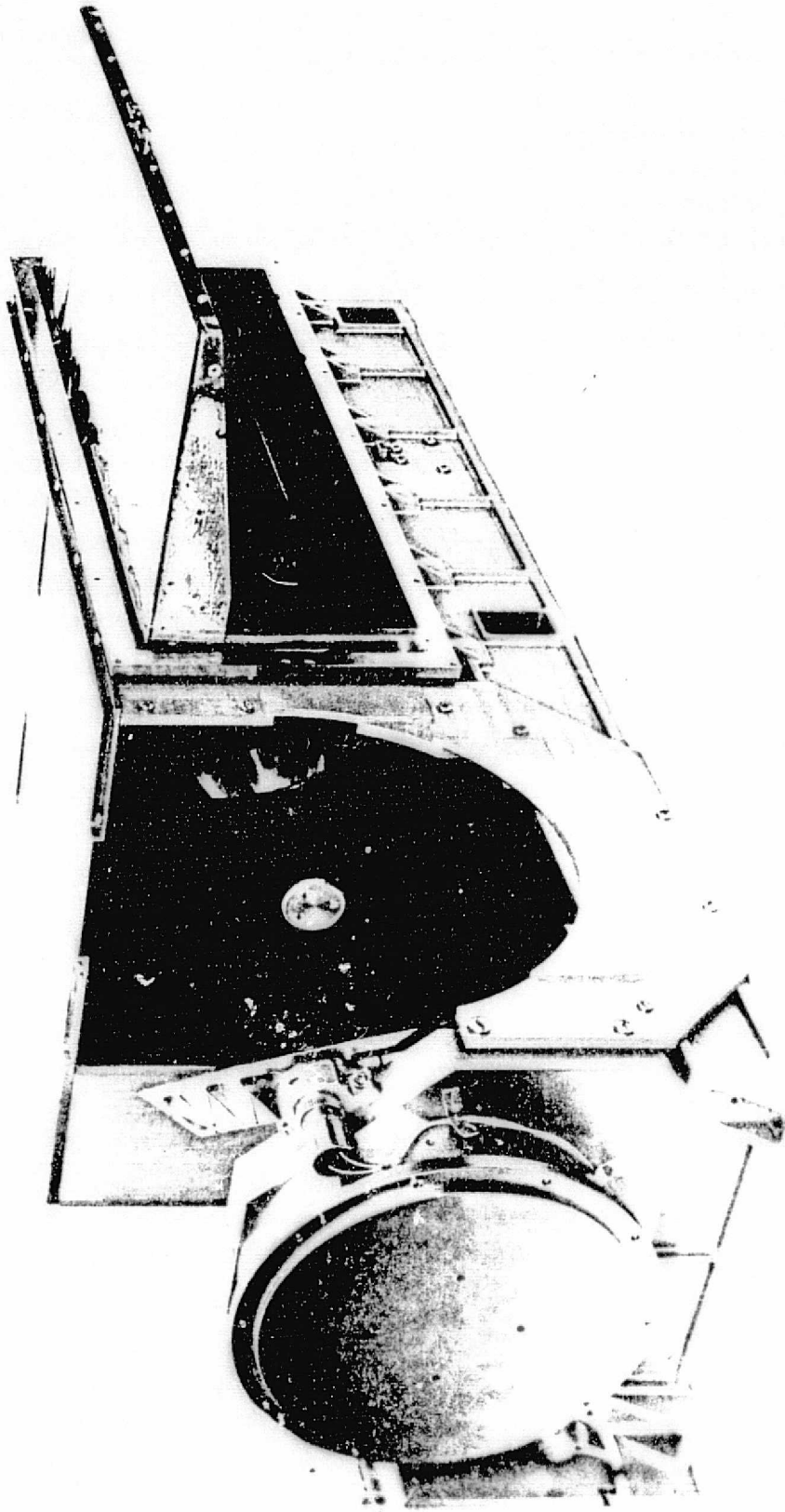
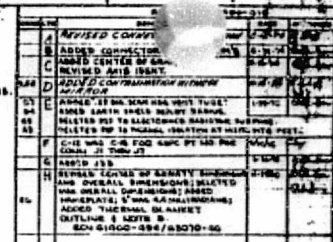


FIG. 1-1



REPRODUCIBILITY OF THE
ORIGINAL PAGE IS POOR

FIG 1-2

[illegible]

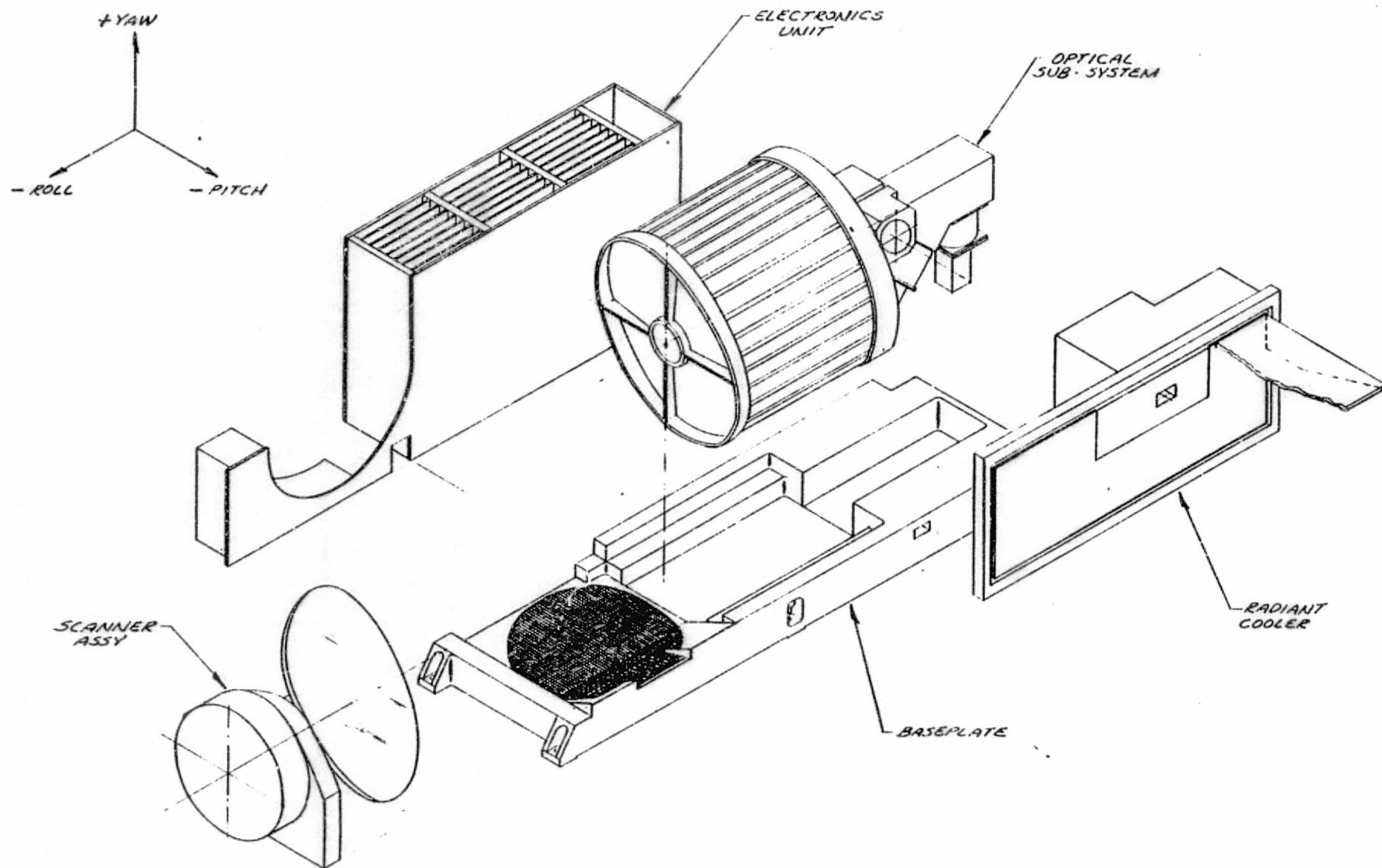


Figure 1-3 AVHRR Modules

rotates the mirror at the 360 RPM to produce a contiguous scan of the earth scene. The line-to-line jitter is less than 17 microseconds.

1.1.2 Electronics Module

The electronics module is in two sections both of which bolt on to the instruments inboard side panel. The curved box (Reference Figure 1-3) is the motor power supply. Twenty-five electronic modules are used to make up the electrical system of the AVHRR. Nineteen of these are located in the electronics box. The solar channel preamplifiers for the solar channels and IR channel 3 are located in the area of the secondary optics. The IR channel 4 preamplifier is located on the rear of the radiant cooler housing.

Except for Channels 1, 2 and 4 preamplifiers, all of the modules are accessible without the removal of the instrument from the spacecraft.

The following is a list of the electronics modules:

1. Power Converter and Switching Regulator
2. Logics Regulators
3. $\pm 15V$ Regulators
4. Command Relay #1
5. Command Relay #2
6. Command Relay #3
7. Patch Temperature Control and T/M
8. T/M Board #2
9. Motor Logics
10. Scan Count and Decode
11. Interface Logics #1

12. Interface Logics #2
13. Ramp Calibration Generator
14. Auxiliary Scan Logics
15. IR Post Amplifier
16. Daylight Post Amplifier
17. Multiplexer
18. Black Body MUX logics
19. A to D Converter
20. IR Preamplifier
21. Channel 4 Preamplifier
22. Daylight Preamplifier (Ch. 2)
23. Daylight Preamplifier (Ch. 1)
24. Motor Power Supply
25. Switching Regulator

1.1.3 Radiant Cooler

The radiant cooler module is made up to four basic assemblies. These are (1) the cooler housing, (2) the first stage radiator, (3) the patch or second stage radiator, and (4) the cooler cover. The first stage radiator is configured in such a manner as to shade most of its 55.2 inch² area from the earth by the cooler cover when the cover is deployed. A "single shot" solenoid actuated, spring driven deployment system is used to deploy the cover. Mounted on the patch are the two infrared detectors. The patch has a 22.4 in² radiating area. The cooler housing surrounds the cooler on all sides except

for the radiation area. The housing is vacuum sealed so that when the bench cooler is clamped to the front of the housing a vacuum can be pulled on the entire cooler and the system permitted to cool as it would in space; i.e. radiation to a cold target located in the bench cooler (except that the cold target is at liquid nitrogen temperature).

Multilayer insulation thermally separates the first stage radiator from the housing and the first stage optical window is thermally isolated and heated several degrees warmer than the 171K radiator temperature. The patch is thermally isolated from the first stage by low emissivity surfaces (gold to gold) and runs at 95K with no control power. During nominal operation the patch temperature will be controlled at 105K.

1.1.4 Optical Subsystem

The optical subsystem was designed by Ferson Optics, a division of Bausch and Lomb, to ITT Specification. (Ferson fabricated the BBM ETM and PTM optics; however, the Flight Model Optics are being fabricated by Perkin-Elmer, Costa Mesa, California.) The subsystem consists of an afocal 8.0 inch aperture telescope (two coaxial confocal paraboloidal mirrors) followed by secondary optics which split the radiant input into four discrete spectral bands and focus them onto their respective field stops. The spectral bands are:

Channel 1: 0.55 to 0.90 microns

Channel 2: 0.72 to 1.05 microns

Channel 3: 10.5 to 11.5 microns

Channel 4: 3.55 to 3.92 microns

The instantaneous field of view is 1.3 milliradians in all channels and is defined by an aperture plate in Channels 1 and 2 and by the detector active areas in Channels 3 and 4. In addition the optical subsystem has been designed to meet the total system MTF requirements with the detectors registered off axis by as much as 1.5 milliradians in Channels 1 & 2 and 1 milliradian in Channels 3 & 4.

Polarization effects have been minimized (<7% in Channels 1 and 2) by orienting the polarization sensitive elements in a predetermined way, thus having elements compensate for other elements.

1.1.5 Baseplate Unit

The baseplate unit is the common structure in which all other modules are secured. Dowel pins are used to establish and maintain alignment of the scanner and optics modules. Alignment of the cooler to the optics is established by shims.

2.0 SYSTEM SENSITIVITY

2.1 Solar Channels 1 and 2

2.1.1 Detector

Both solar channels use the same detectors with the same operating characteristics as before the modifications. The detectors used are Harshaw Chemical Co. silicon detectors. The detector is an oxide passivate, planar diffused, silicon PIN photodiode with a guard ring and operated at -15 volts bias. The device has an active area of 0.100 inch square and is packaged in a TO-5 can using a metallic hermetic seal. Some of the most pertinent characteristics of the device are given in Table 2-1.

The detector will be used as a current source for an op-amp preamplifier. In the current-to-voltage transducer operating mode, the combination gives excellent sensitivity and frequency response using a 4M ohm feedback resistor as the effective detector load.

The detectors are used as energy collection devices behind the 0.0238 inch square apertures which are the defining field stops for Channels 1 and 2. Optical analysis showed that using a 0.100 inch square detector active area at an effective optical distance of 0.146 inch behind the field stop, resulted in a well over 99% of the rays, which passed through the field stop, being collected by the detectors of both channels.

2.1.2 Detector Responsivity vs. Temperature

The question was raised early in the AVHRR program as to the effect of temperature upon the responsivity of the silicon detectors. Harshaw ran spectral response versus temperature data for two of the delivered units. The measured data is of historical

Table 2-1 Solar Channel Detector Characteristics

Type	Passivated, Planar Diffused Silicon Pin Photodiode
Manufacturer	Harshaw Chemical Co.
Active Area Size	0.100 Inch Square
Bias	-15 Volts
Spectral Peak	975 \pm 25 nmeters
Responsivity - Peak	0.62 Amp/Watt
Responsivity - Ch 1 Avg.	0.37 Amp/Watt
Responsivity - Ch 2 Avg.	0.54 Amp/Watt
Leakage Current at -15 V	17 Namp Maximum
Capacitance at -15 V	15 pf Maximum

Table 2-2 Measured Temperature Vs. Responsivity For Detector Q-3

Wavelength Microns	Responsivity at Temperature		
	-10°C	+24°C	+50°C
0.50	NC	1.00	NC
0.60	NC	1.00	1.017
0.70	NC	1.00	NC
0.80	1.006	1.00	0.998
0.90	1.008	1.00	1.005
0.95	0.987	1.00	0.997
1.00	0.932	1.00	1.021
1.10	0.541	1.00	1.425

Responsivity (Amp/watt) at +24°C is baseline for each wavelength measured.

interest only since the latest predictions indicate a maximum detector operating temperature of about 24°C . The data is shown in Table 2-2. The data shows that as Harshaw predicted, no sensible change occurs at wavelengths shorter than about 1.0 micron. This means, of course, no change would occur in Channel 1.

The AVHRR temperature is more controlled by the TIROS-N TCE and the maximum operating temperature is within a few degrees of the nominal detector test temperature of $+24^{\circ}\text{C}$. The maximum overall temperature change under various operating conditions is about 10°C . The detector responsivity changes are insignificant over so small an excursion and so the AVHRR output will not sensibly change due to detector temperature variations.

2.1.3 Solar Channels System Sensitivity

For channels 1 & 2, the signal to noise ratio, S/N, is given by

$$S/N = \frac{\Phi_{\Delta\lambda}}{\alpha \text{ NEP}}$$

where $\Phi_{\Delta\lambda}$ = solar spectral flux incident on the detector

α = degradation factor due to electronic noise pickup, 1/f noise, etc.

NEP = effective detector Noise Equivalent Power

$\Phi_{\Delta\lambda}$ is given by

$$\Phi_{\Delta\lambda} = \frac{1}{\pi} I_{\Delta\lambda} \tau \rho_s A_o \theta^2 = \frac{1}{4} I_{\Delta\lambda} \tau \rho_s D_o^2 \theta^2$$

where $I_{\Delta\lambda}$ = solar spectral irradiance in the spectral band incident on the Earth's atmosphere

τ = transmission of optical system

ρ_s = scene spectral albedo

D_o = diameter of the collection aperture

θ = instantaneous field of view

The NEP is given by

$$\text{NEP} = \frac{\sqrt{i_s^2 + i_d^2 + i_l^2}}{R}$$

where i_s = shot noise current due to signal flux on the detector

i_d = photodiode leakage current noise.

i_l = load resistor Johnson noise current

R = detector responsivity in ampere/watt

Using Thekaekara's Tables we find that the total solar irradiance incident on the atmosphere in channels 1 and 2 (weighted by the relative response in each band) is:

$$I_{\Delta\lambda}^1 = 4.24 \times 10^{-2} \text{ W/cm}^2$$

$$I_{\Delta\lambda}^2 = 3.00 \times 10^{-2} \text{ W/cm}^2$$

This is the solar power in the 0.50 to 0.91 micron region (channel 1) and the 0.71 to 1.10 micron region of channel 2.

2.1.3.1 System Transmission

The elements affecting the system transmission can be divided into two broad categories, those that are spectrally variant and those that are not. The elements that are variant are the scan, telescope, and folding mirrors, and the gold dichroic beamsplitter. These elements are analysed in the section defining the spectral response. Also analyzed are the bandpass filters and detectors; however, for S/N purposes, it is assumed that the bandpass filters are invariant across the band and that the detector has an average responsivity in the spectral band of interest.

Table 2-3 gives the spectral efficiencies of the mirrors and gold dichroic used in these calculations. These are measured PTM values and represent expected flight model values. Combining the three mirror reflections and gold dichroic transmission for Channel 1 gives an average transmittance of 0.60 for this channel. Doing likewise for channel 2 (with one more mirror reflectance) gives 0.43. These are the transmissions through the spectrally variant elements only.

The elements which can be considered spectrally invariant are the inconel beamsplitter separating channel 1 and 2, the relay lenses in each channel, and each bandpass filter (the filter has a relatively flat response across each band). In addition the obscuration caused by the secondary mirror and its support must be considered. The values used in calculating the transmissions are also shown in Table 2-3. There are three relay lenses in each

Table 2-3 Optical Efficiency of AVHRR Elements
(PTM Measured)

SPECTRALLY INVARIANT ELEMENTS

Reflectivity of Inconel beamsplitter	=	.225
Transmittance of Inconel beamsplitter	=	.375
Transmittance of Chan. 1 filters	=	0.85
Transmittance of Chan. 2 Filter	=	0.90
Telescope Obscuration	=	0.94
Lens Transmittance	=	0.95

SPECTRALLY VARIANT ELEMENTS

<u>SPECTRAL POINT MICRON</u>	<u>SCAN MIRROR REFLECTIVITY</u>	<u>TELESCOPE MIRROR REFLECTIVITY</u>	<u>CH 2 FOLDING MIRROR REFLECTIVITY</u>	<u>GOLD DICHROIC TRANSMISSION</u>
0.50	.92	.88	-	.73
0.55	.93	.92	-	.772
0.60	.925	.93	-	.80
0.65	.92	.93	-	.81
0.70	.90	.93	.84	.81
0.75	.90	.93	.81	.79
0.80	.88	.92	.79	.765
0.85	.875	.915	.79	.73
0.90	.88	.93	.80	.69
0.95	.89	.935	.815	.642
1.00	.89	.93	.825	.59
1.05	.89	.93	.835	.56
1.10	.885	.925	.845	.54

channel so that the combined transmission for the invariant elements is 0.154 for channel 1 and 0.272 for channel 2. Combining these with the values for the variant elements gives:

$$\tau_1 = 0.092$$

$$\tau_2 = 0.117$$

for the expected total system transmission for each channel.

Allowing a degradation factor for dirt, dust, etc. on each element, will result in, perhaps, a more realistic overall system transmission. It is reasonable that lens surfaces sealed from ambient will not markedly degrade. For sensitivity calculations assume that each channel will suffer a 50% degradation overall thus

$$\tau_1 = .046$$

$$\tau_2 = .058$$

2.1.3.2 Detector NEP

The Harshaw detector has a peak responsivity (ampere/watt) of at least 0.62. The average responsivity across the channel 1 spectral band is 0.37 ampere/watt while that in channel 2 is 0.54 ampere/watt.

Several factors contribute to the noise. The shot noise due to the detector dark current, the shot noise due to the detector scene generated current, and the Johnson noise in the preamplifier feedback resistor are the major noise sources. $1/f$ noise is negligible across the 14.5 KHz bandpass of the electronic filter. Contribution of preamplifier transistor noise is also very small compared to the above sources and so can be ignored.

Both channels use a 4 megohm feedback resistance in the preamplifier so that the Johnson noise at a 300K temperature over a 14.5 KHz bandwidth is 7.75×10^{-12} ampere. The detector dark current is 17 nanoamperes maximum in each channel giving a dark current noise of:

$$(i_d^1) = (i_d^2) = (2 \varepsilon I_d \Delta f)^{1/2} = 8.88 \times 10^{-12} \text{ ampere}$$

The signal shot noise under minimum signal condition is based on the current flowing in the detector under that illumination. The minimum signal flux is calculated later to be 1.68×10^{-9} watt in channel 1 and 1.43×10^{-9} watt in channel 2. The minimum DC current out of the detectors then is 6.22×10^{-10} amp and 7.72×10^{-10} amp for channels 1 and 2. The shot noise then is

$$i_s^1 = 1.70 \times 10^{-12} \text{ amp rms}$$

$$i_s^2 = 1.89 \times 10^{-12} \text{ amp rms}$$

The total noise current in channel 1 is:

$$i_{T1} = ((7.75)^2 + (8.88)^2 + (1.70)^2)^{1/2} \times 10^{-12}$$

$$i_{T1} = 1.19 \times 10^{-11} \text{ amp}$$

similarly for channel 2

$$i_{T2} = 1.19 \times 10^{-11} \text{ amp}$$

The noise is essentially the same in both channels due to the predominance of i_ℓ and i_d .

A degradation factor α is included in the calculation. This accounts for stray noises as well as degradations in operation of the system. For this analysis a degradation factor of 1.6 based on the measured BBM and ETM values was used.

The detector NEP then is

$$NEP_1 = \frac{1.19 \times 10^{-11}}{0.37} = 3.22 \times 10^{-11} \text{ watt}$$

$$NEP_2 = \frac{1.19 \times 10^{-11}}{0.54} = 2.20 \times 10^{-11} \text{ watt}$$

2.1.3.3 Signal to Noise Ratio Calculation

Using the equation previously given and assuming a minimum scene as described in the AVHRR specification ($\rho_s = 0.5\%$), a collection aperture of 8.0 inches, and an IFOV of 1.31 milliradians, we have

$$\Phi_{\Delta\lambda}^1 = 1.73 \times 10^{-9} \text{ watt}$$

$$\Phi_{\Delta\lambda}^2 = 1.54 \times 10^{-9} \text{ watt}$$

and so

$$S/N = \frac{\Phi_{\Delta\lambda}}{\alpha NEP}$$

$$S/N_1 = \frac{1.73 \times 10^{-9}}{1.6 \times 3.22 \times 10^{-11}} = 33:1$$

$$S/N_2 = \frac{1.54 \times 10^{-9}}{1.6 \times 2.20 \times 10^{-11}} = 44:1$$

Table 2-4 Solar Channel Sensitivity

	CH 1	CH 2
System Transmission (Degraded)	0.046	0.058
Detector Responsivity	0.37 A/W	0.54 A/W
Detector NEP (25°C)	3.22×10^{-11} W	2.20×10^{-11} W
S/N Ratio at Minimum Albedo (25°C)	33:1	44:1
Specified Minimum Signal to Noise Ratio	3:1	3:1

2.1.3.4 Sensitivity vs Temperature

The foregoing calculation is based on a detector dark current of 17 nanoamps. This is true at 25°C. At higher temperatures, the detector dark current (and the load Johnson noise to some extent) increases, thus increasing the noise and increasing the detector NEP. Based on data from Harshaw and the results of the thermal math model which indicates very little variation in detector temperature, the signal to noise ratio for the solar channels will not perceptibly change in operation.

2.2 Channel 3 Detector and Sensitivity

2.2.1 Mercury-Cadmium-Telluride Detector

The mercury-cadmium-telluride detector is optimized for best sensitivity between 10.5 and 11.5 μm wavelengths when cooled to 105 Kelvin by the radiant cooler. The important characteristics of the detector are summarized in Table 2.2-1.

The Hg Cd Te element is mounted in a small metal enclosure shown in ITT-A/OD Figure 2.2-1. The aplanat lens is bonded directly to the metal enclosure and also serves as the window through which the optical beam passes. The alignment and spacing of the aplanat lens with respect to the sensing element is accurately maintained with this arrangement. The detector is tested by the manufacturer both before and after attachment of the lens to assure a qualified unit. The internal volume is filled with an inert gas and then sealed by the manufacturer. The detectors are inspected both before and after lens attachment by an ITT-A/OD Quality Control representative who also witnesses the important acceptance tests at the manufacturer's plant.

MERCURY-CADMIUM-TELLURIDE DETECTOR

<u>ITEM</u>	<u>CHANNEL 3</u>
Spectral Band	10.5-11.5 μm
Width of Sq. Sensitive Area	0.0068 \pm 0.0004"
Operating & Spec. Temperature	105 Kelvin
Field of View, Min.	100 $^{\circ}$
Minimum Resistance	10 Ohms
Max. Bias Power	1.2 M.W.
Avg. D* In Spectral Band At 105K, 2KHz, 100 $^{\circ}$ FOV, 1.2 M.W., 1 HZ	2.0 \times 10 ¹⁰ $\frac{\text{CMHZ}}{\text{Watt}}^{1/2}$
Avg. Spectral Responsivity, Min.	5,500 $\frac{\text{Volts}}{\text{Watt}}$
Max. Change in Responsivity Per Kelvin at 105 Kelvin	5%
Long Wavelength Response	<1% at 18 μm
Time Constant	<1 μs
Spatial Responsivity Uniformity	<2 to 1
I/f Knee Frequency	<1 KHz

Table 2.2-1 MCT Detector Characteristics

NOTE:

- 1 THE PLANE OF THE DETECTOR FACE IS TO COINCIDE WITH SURFACE -B- WITHIN .001. THE CENTER OF THE ACTIVE AREA OF THE DETECTOR SHALL BE LOCATED ON THE CENTER OF DIA -A- WITHIN .001 DIA. THE CENTER OF THE LENS SHALL BE CENTERED ON THE ACTIVE AREA OF THE DETECTOR WITHIN .001.
- 2 TOLERANCE FOR LOCATION OF .0637 DIA. HOLES: $\pm .0005$
TOLERANCE FOR LOCATION OF THREADED HOLES: $\pm .0050$
- 3 THE CENTER LINE OF THE .0637 DIA. HOLES SHALL COINCIDE WITH SURFACE -B- WITHIN .002 AND SHALL BE PARALLEL TO SURFACE -B- WITHIN .001.
- 4 THIS DIMENSION SHALL NOT EXCEED THE MEASURED LENS HEIGHT (.216 NOM.) PLUS THE MEASURED DIMENSION FROM SURFACE -B- TO THE INDICATED SURFACE (.180 NOM.).
- 5 THESE DIMENSIONS ARE TO BE MEASURED FROM THE CENTER LINE OF DIA. -A-.
- 6 APPLY PLUS (+) VOLTAGE MARKING AT PROPER PIN TO INDICATE OPTIMUM BIAS DIRECTION.
- 7 LENS TO BE SUPPLIED BY ITT A/OD.
- 8 ATTACH 3" MIN. LENGTH OF #32 AWG COPPER WIRE, POLYTHERMALEZE COATED, TO EACH ELECTRICAL LEAD PER NASA DOCUMENT NHB 5300.4 (3A); MIN. OF TWO TURNS OF WIRE AROUND PIN.
9. ONE SIDE OF SQUARE SENSITIVE AREA OF DETECTOR TO BE PARALLEL TO MOUNTING BASE WITHIN 10°.
10. BOND LENS TO HOUSING USING "TORR SEAL" EPOXY RESIN AND HARDENER. (VARIAN ASSOCIATES, VACUUM DIV.)

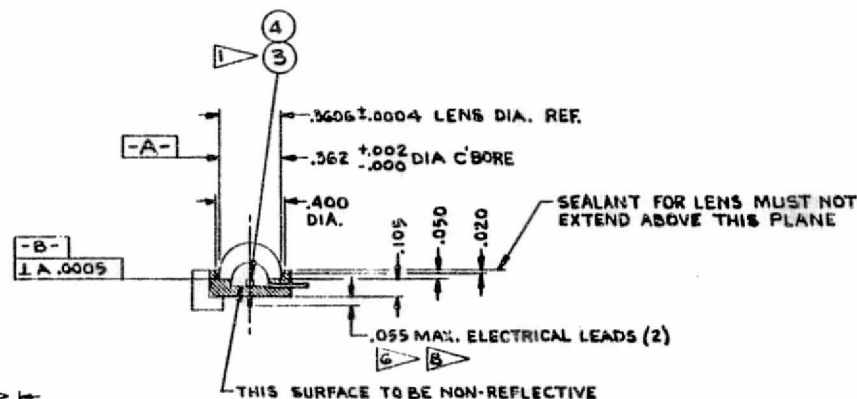


FIG 2.2-1

REF	Q	B	8008307-2	WITNESS PLATE - APLANAT
AR	5		VARIAN ASSOCIATES "TORR SEAL"	ADHESIVE
REF.	4	A	8008755	SPECIFICATION, IR. DETECTOR
1	3		WHITWELL, INC. RADIATION CENTER	DETECTOR
1	2	C	8009232-1	LENS
1	1		THIS DWG - 1	HOUSING

Q7	Q8	Q9	Q4	Q3	Q2	Q1	ITEM NO.	PART OR IDENTIFYING NO.	NOMENCLATURE OR DESCRIPTION
QUANTITY PER GROUP							LIST OF MATERIALS OR PARTS LIST		
UNLESS OTHERWISE SPECIFIED							CONTRACT NO.		
DIMENSIONS ARE IN INCHES AND INCLUDE CHEMICALLY APPLIED OR PLATED FINISHES							NAS 5-21900		
TOLERANCES							APPROVALS		
BASIC		DECIMALS		ANGLES		DRAWN 7-15-74			
DIMENSION		PLACE		PLACE		CHECKED 7-15-74			
UNDER 8		± .02		± .005		ENGR 7-15-74			
8-24 INCL.		± .03		± .010		7-15-74			
OVER 24		± .04		± .030		7-15-74			
DO NOT SCALE PRINT							ITTAOD 7/15/74		
COML. TOL. TO STOCK SIZES							OTHER 7/15/74		
SHOP PRACTICE, 30.101 APPLIES							SCALE 2/1		
MATERIAL							ITTA AEROSPACE/OPTICAL DIVISION		
AS NOTED							PORT WAYNE, INDIANA, U.S.A.		
FINISH							INTERNATIONAL TELEPHONE AND TELEGRAPH CORPORATION		
8008799 61400							HOUSING, INFRARED		
NEXT ASSEMBLY USED ON							DETECTOR, CHANNEL 3 -		
APPLICATION							ASSY OF AVHRR		
EXCEPT AS MAY BE OTHERWISE PROVIDED BY CONTRACT, THESE DRAWINGS AND SPECIFICATIONS ARE THE PROPERTY OF ITTA AEROSPACE/OPTICAL DIVISION AND SHALL NOT BE REPRODUCED, COPIED, OR USED AS THE BASIS FOR THE MANUFACTURE OR SALE OF APPARATUS WITHOUT PERMISSION.							C 31550 8008791		
FORM NO. 17-11-60 (11-60)							LINCOLN-BRADY CORP.		

REPRODUCIBILITY OF THE ORIGINAL PAGE IS POOR

The size of the sensitive area is determined by the effective focal length (EFL) of the optical system and the instantaneous field of view (IFOV), which is obtained from the specified resolution. They are related by the equation

$$w = \theta \times \text{E.F.L.}$$

where w = edge width of square sensitive area

θ = angular width of square IFOV

For Channel 3, EFL is 132.3 mm (= 5.209 inches) and θ = 1.31 milliradians which gives w equal to 0.0068 inch. A tolerance of ± 0.0004 inch has been established as being a reasonable amount consistent with detector fabrication capabilities and size of the IFOV. In the electrode-to-electrode direction, the length of the sensing element will be slightly greater (by 0.0005 inch) to compensate for electrode end effects where the detector normally has very little response.

A uniformity specification has been incorporated into the detector specification in order to minimize non-uniformity of response across the sensitive area. A total of nine equally spaced readings arranged in a 3 by 3 grid will be taken across the sensitive area and all readings must be equal to or greater than 50% of the largest reading. The diameter of the test spot is about 0.0015 inch and the readings are spaced by 0.002 inch; the measurements will be made on a standard "spot scan" test station by the manufacturer.

Acceptance tests are based on measurements made at the anticipated operating temperature of 105 Kelvin. Measurements are

made at 90, 95, 100, 110, 115 and 120 Kelvin in the event that the cooler must be operated at the backup temperature of 107 Kelvin or

a cooler malfunction occurs. Details of what measurements are made at the different temperatures are given in the procurement specification for the detector.

2.2.2 Channel 3 Sensitivity

System sensitivity in the infrared channels (numbers 3 and 4) is expressed in terms of the noise-equivalent-temperature difference, NEAT (NETD). The NETD is the difference in temperature between two targets (several times larger than the instantaneous field of view) which is required to produce a change in signal voltage equal to the rms noise of the radiometer. The equation used to calculate the NETD is given in Table 2.2-3, which also defines the various parameters used in the equation. The degradation factor, α , and the optical f-number have been made as small as feasible whereas factors in the denominator of the NETD equation have been maximized as much as possible. The detector detectivity is the highest available from any vendor for the spectral bands, operating temperature, field of view, etc. imposed by instrument requirements. The field of view, element dwell time (or electrical bandwidth) and change in scene radiance are all set by instrument performance specifications. We will discuss in this section only the degradation factor and the optical transmission since additional information on the other factors are given in the Optical Section (3.0) of this report.

The degradation factor, α , consists of two factors for the case under consideration, that due to $1/f$ noise from the infrared detector, and a second factor to account for some additional electronic noise. Diffraction effects are negligible

$$\text{NETD} = \frac{2 \sqrt{2} \alpha \text{fn}}{\pi D_o D_m^* \tau \theta \sqrt{t_d} \left(\frac{dN}{dT} \right)_T}$$

NETD = Noise Equivalent Temperature Difference

α = Degradation Factor Including 1/f Detector Noise

fn = Optical F-number

D_o = Diameter of Optical Entrance Aperture

D_m^* = Average detector detectivity in spectral band at the measuring frequency

τ = Transmission of optics including obscuration effects

θ = Angular width of square instantaneous field of view

t_d = Elemental dwell time (= $\frac{1}{2\Delta f}$ where Δf_o is the 3 db bandwidth of presampling filter)

$\left(\frac{dN}{dT} \right)_T$ = Change in scene radiance for small temperature change at temperature T

Table 2.2-3 Noise Equivalent Temperature Difference Equation (Channel 3)

DEGRADATION FACTOR (α)

$$\alpha_{\text{total}} = \alpha_{1/f} \cdot \alpha_2$$

$$\alpha_{1/f} = \left[1 + \frac{f_c}{f_u - f_l} \cdot \ln \left(\frac{f_u}{f_l} \right) \right]^{1/2}$$

f_c = frequency where 1/f detector noise power equals G-R white noise

f_u = upper cutoff frequency of the system

f_l = lower cutoff frequency of the system

$$f_c \leq 1 \text{ KHz}$$

$$f_l \approx 1 \text{ Hz}$$

$$f_u = 14.5 \text{ KHz}$$

<u>ITEM</u>	<u>CHANNEL 3</u>
$\alpha_{1/f}$	1.29
α_2 (See text)	1.4
α_{total}	1.8

Table 2.2-4 Degradation Factor

AVHRR OPTICAL TRANSMISSION

<u>Item Description</u>	<u>Reflectance or Transmittance</u>	
	<u>Channel 3</u>	<u>Channel 4</u>
Scan Mirror	0.95	0.95
Telescope Mirrors (2 @ 0.97 Ea)	0.94	0.90
Transp. Gold B.S. (D1)	0.88	0.82
Folding Mirror (M3)	0.96	0.95
Ge Focus Lens (L1)	0.819	0.846
Ch 3 (2 @ .905)		
Ch 4 (2 @ .920)		
Irtran II Windows Inner	0.92	0.95
	Outer 0.82	0.95
Infrared Dichroic (D2)	0.81 (T)	0.92 (R)
(OCLI Guaranteed Minimum)		
Ge Aplanat Lens (L2, L3)	0.94	0.94
Bandpass Filters (F4)		0.80
Telescope Obscuration	0.94	0.94
System Transmission	0.333	0.331
(Product of Above)		

Values Given Above Are Measured PTM Values.

Table 2.2-5 Optical Transmission For Channels 3 and 4

since we are considering scenes which are several times larger than an IFOV. The equation and parameters used to calculate the degradation factors are given in Table 2.2-4. The degradation factor for the electronic noise has been calculated by determining the noise voltage level from the infrared detector and from measurements on the BBM and ETM.

The apparent electronic pick up was somewhat higher on the ETM than expected. The apparent, α_2 , on the ETM was about 1.6 and the total degradation factor α_T was about 2.1. Several areas of potential pickup were redesigned on the PTM and a lower α_2 is expected. A value for α_2 of 1.4 and a total α of 1.8 seems reasonably conservative.

The optical transmission, τ , was determined from the measured transmittance or reflectance value for each optical component in the PTM optical system. The value for each component is listed in Table 2.2-5 for both Channels 3 and 4. Assuming some optical degradation as in the solar channels we assign a value of

$$\tau_3 = .20$$

$$\tau_4 = .20$$

for use in the sensitivity calculations.

Table 2.2-6 gives the parameters used and the calculated NEAT. As shown, the spec. value will be achieved.

2.3 Channel 4

2.3.1 Detector

The detector chosen for use in the channel 4 (3.55 to 3.93 microns) is a photovoltaic indium antimonide photodiode built by Cincinnati Electronics Corp. The detector has a 0.007 inch square active area and is used in a configuration identical to the silicon detectors of channels 1 and 2. That is, it is a current source to an amplifier used as a current to voltage amplifier with a 16.4 M ohm feedback resistance. The detector is mounted in a Kovar housing like the channel 3 detector with the aplanat forming a hermetic seal.

Photovoltaic InSb has better noise characteristics with a small amount of reverse bias; therefore, a bias on the order of -30 millivolts is used. The exact bias is determined by C.E.C. during acceptance testing of the photodiodes. The method used for bias generation and control is discussed in the section of the electronics describing the channel 4 preamplifier. Table 2.3-1 summarizes the channel 4 detector parameters.

2.3.2 Channel 4 Sensitivity

The sensitivity of the InSb photodiode is specified in terms of its quantum efficiency, η , and its noise output for a given thermal background irradiance. Since noise sources external to the detector-amplifier system are significant (i.e., background flux and signal shot noise), this concept is most applicable. The

use of D^* implies a situation where system and detector noise are the limiting factors.

The following analysis determines the sensitivity of the system in terms of the detector output current for both the noise sources and the NEAT. The initial section determines the system noise. Following that are sections which define the detector output for the NEAT, effects of an albedo signal in this spectral region, and postamp gain and digitizer effects on the system sensitivity.

2.3.2.1 System Noise

For Channel 4 there are four noise sources. These are:

1. Background flux noise
2. Preamp noise
3. Signal shot noise
4. Stray pickup

These are discussed separately below. The stray pickup is handled as a degradation to the total noise.

In the nominal 3.55 to 3.93 micron band, a 300K background scene causes a signal current out of the detector given by:

$$I_{bs} = K A q n Q_B \quad \text{Eq. 1}$$

K = optical filtering factor

n = quantum efficiency (average in band)

q = 1.6×10^{-19}

A = detector area - $2.98 \times 10^{-4} \text{ cm}^2$

Q_B = background photon flux

This assumes that the filter is cold and mounted on the detector. The optical filtering factor accounts for the fact that when the detector is mounted in the system on a cold patch, the incidence

Table 2.3-1 Channel 4 Detector Parameters

Spectral Band	3.55 to 3.93 Micron
Type of Detector Source	Indium Antimonide Cincinnati Electronics
Operating Temperature	105K
Operating Mode	Photovoltaic
Sensitive Area	0.007" Square
Quantum Efficiency in Spectral Band	0.75 Minimum
Background Noise Level	Maximum 10% over Theoretical Level
Bias Voltage	~ 30 mvolts
Preamplifier Gain	16×10^6

angle, θ , of the background is limited by the cooler windows and reduced by the transmissions of the inner window (τ_w), the band-pass filter (τ_F), and the aplanat (τ_a).

$$K = \tau_F \cdot \tau_w \cdot \tau_a \cdot \pi \sin^2 \theta \quad \text{Eq. 2}$$

For $\tau_w = \tau_F = \tau_a = .85$ and $\theta = 75^\circ$

$$K = 1.80 \text{ ster}$$

For a 300K scene, the photon flux, Q_B , in the nominal spectral band is 3.22×10^{14} photon cm^{-2} ster^{-1} sec^{-1} . Using $n = 0.75$, we have

$$I_{bs} = 2.07 \times 10^{-8} \text{ amp}$$

The noise in this background signal is given by:

$$i_b = \sqrt{2q I_{bs} \Delta f} \quad \text{Eq. 3}$$

The bandwidth, Δf , is 14.5 KHz and so

$$i_b = 9.80 \times 10^{-12} \text{ amp rms.}$$

The second noise source (the preamp) really consists of two sources. The input transistor contributes noise as does the feedback resistance which contributes Johnson noise. Noise data was measured by G.E. Sonnek on a preamp similar to that required for Channel 4. His measured data indicated that with a 16 Mohm feedback a total rms preamp noise of 4.42×10^{-12} amp is obtained in a 14.5 KHz bandwidth.

The third noise source, the signal shot noise, depends on signal level. Since the NEAT spec is at 300K, this is the scene level of interest. The maximum scene to be viewed is a 320K scene.

The detector output current due to the scene is given by:

$$I_s = N_s T R_\lambda \quad \text{Eq. 4}$$

where N_s = scene radiance

T = system thruput

R_λ = detector responsivity (amp/watt)

The system thruput T is given by:

$$T = A\Omega\tau \quad \text{Eq. 5}$$

where A = collecting area

Ω = solid angle of view

τ = system transmission

For AVHRR, A is 324 cm^2 , Ω is 1.72×10^{-6} ster, τ is about 0.33; therefore, T is $1.83 \times 10^{-4} \text{ cm}^2 \text{ ster}$. Using the minimum specified quantum efficiency of 0.75 gives a R_λ of 2.26 amp/watt. The radiance of a 300K scene in the nominal spectral band is $1.70 \times 10^{-5} \text{ w/cm}^2 \text{ ster}$. The detector output then, with no albedo contribution, using equation 4, is:

$$I_s = 7.03 \times 10^{-9} \text{ amp}$$

The rms noise, i_s , is

$$i_s = 5.71 \times 10^{-12} \text{ amp rms}$$

The last source, stray pickup is a source which is minimized by design, but never entirely eliminated. We will assume a 1.60 degradation in the TOTAL system noise performance since ETM and PTM noise degradation appeared to be less in this channel than in channel 3. This includes a 4% 1/f noise contribution. The total

noise current, i_n , under these conditions is:

$$i_n = 1.6 \left[(9.80)^2 = (4.42)^2 + (5.71)^2 \right]^{1/2} \times 10^{-12} \text{ amp Eq. 6}$$

$$i_n = 1.95 \times 10^{-11} \text{ amp rms.}$$

2.3.2.2 System Output for NEAT

The detector output caused by a 0.12K scene change at 300K is determined as follows. Using the Lowan & Blanch "Tables of Plancke Radiation and Photon Functions", we find that the photon flux of 301K scene in our band is 3.36×10^{14} photons cm^{-2} ster^{-1} sec^{-1} . For a 300K scene it is 3.22×10^{14} . The change in flux due to a 1.0K temperature change in the scene is then 1.37×10^{13} photon cm^{-2} ster^{-1} sec^{-1} K^{-1} . For a 0.12K NEAT, the Noise Equivalent Photon Flux is:

$$\text{NEF} = 1.64 \times 10^{12} \text{ photon cm}^{-2} \text{ ster}^{-1} \text{ sec}^{-1}$$

The noise equivalent flux on the detector is simply:

$$\text{NEF}_D = T \cdot \text{NEF}$$

$$\text{NEF}_D = 1.83 \times 10^8 \text{ photon sec}^{-1}$$

The detector output current change caused by the scene temperature change is:

$$I_{\text{NEF}} = n q (\text{NEF}_D)$$

$$I_{\text{NEF}} = 2.19 \times 10^{-11} \text{ amp}$$

By definition the NEAT of the system is the ΔT which causes a I_{NEF} equal to the total system rms noise i_n . This analysis then indicates that with the nominal spectral band, an NEAT of 0.12K is achievable with a S/N ratio of

$$(S/N)_4 = \frac{2.14 \times 10^{-11}}{1.95 \times 10^{-11}} = 1.12:1$$

The effective NEAT is expected to be .107K as shown in Table 2.3-2

Table 2.3-2 Channel 4 Sensitivity Parameters

Collection Optics	8.00" Diameter
System Transmission	0.20
IFOV	1.3 mrad
Bandwidth	14.5 KHz
Background Temp	300K
Degradation Factor	1.6
Quantum Efficiency	0.75
Specified NEAT	0.12K at 300K
Calculated NEAT	0.107K at 300K

2.3.2.3 Albedo Radiance

In this spectral channel, the sunlight reflected from the Earth Scene contributes to the total scene radiance. Using Thekaekara's table of solar irradiance we find that a 1.0 albedo scene at noon at the subsatellite point has a reflected radiance in the nominal spectral band of $1.06 \times 10^{-4} \text{ w/cm}^2 \text{ ster}$. According to NASA personnel, the maximum actual albedo of a scene in this band is about 0.10. Further, since the spacecraft is never over a noon nadir, this value of reflected radiance is reduced by $\sin 67^\circ$ (which is the maximum orbit normal to sun angle). These factors make the maximum reflected solar radiance $9.76 \times 10^{-6} \text{ w/cm}^2 \text{ ster}$. If we assume no atmospheric attenuation, this is the albedo contribution on the day side of the orbit.

The maximum scene temperature is specified as 320K. The spectral radiance of this scene is $3.76 \times 10^{-5} \text{ w/cm}^2 \text{ ster}$. The albedo radiance is then about 25% of the maximum thermal radiance, and the total scene radiance for a daylight 320K scene is $4.74 \times 10^{-5} \text{ w/cm}^2 \text{ ster}$, if the maximum albedo is 0.10 in this band.

2.3.2.4 Post Amp Gain and Digitizer Effects

The post amp gain is determined by the output voltage range and the maximum scene radiance level. As discussed previously, the maximum scene radiance for a 320K scene is $3.76 \times 10^{-5} \text{ w/cm}^2 \text{ ster}$. This causes a detector output of $2.04 \times 10^{-8} \text{ amp}$

(using equation 4). With a 16 Mohm feedback, the preamp output is a 0.326 volts. If 6.1 volts represents the output voltage swing for a full to zero radiance change, then the post-amp gain must be 18.1.

Since the A-D converter digitizes to 10 bits (1024 levels), each level corresponds to:

$$\frac{6.39375}{1823} = 6.25 \text{ m volts}$$

The detector current change caused by the NEAT is 2.19×10^{-11} amp. At the digitizer input this is:

$$2.19 \times 10^{-11} \times 16 \times 10^6 \times 18.7 = 6.5 \text{ m volts}$$

Thus each data bit will be about the same as the estimated noise level of this channel.

3.0 OPTICAL DESIGN

3.1 General Description

The optical configuration of the AVHRR is shown in Figure 3.1-1 (the rotating scan mirror is not illustrated for simplicity). The energy from the scene is collected by an 8.0 inch diameter clear aperture afocal telescope, the primary mirror being the entrance aperture. In the afocal design, the secondary mirror recollimates an incoming collimated beam with the angular spread of the exit beam being increased over that of the input beam by the ratio of diameters of the input to the exit beams.

Dichroic No. 1 transmits Channels 1 and 2 (solar channels) and reflects Channels 3 and 4 (infrared channels). The latter two channels are then partially focused by a germanium lens doublet (L1) which is axially adjustable for focusing. The beam passes through a window on the cooler housing and a window on the gold box (or low emissivity shield), the windows being used to provide a vacuum seal for bench testing the cooler and to prevent moisture from the multilayer getting onto a 105 Kelvin patch-detector assembly respectively. Channels 3 and 4 are separated by dichroic No. 2 which is mounted on the patch along with the detectors, bandpass filters and aplanat lenses (L2 and L3). Dichroic D2 is actually the Channel 3 bandpass filter designed for the 45° incident beam and is used also as the dichroic since it reflects the Channel 4 energy. The bandpass filters are multilayer interference type filters which provide the spectral response required by the AVHRR specification. Mounting of the two infrared detectors and dichroic No. 2 in a precision-machine mounting structure simplifies registration of these two channels to each other.

M1 MIRROR, TELESCOPE PRIMARY
 M2 MIRROR, TELESCOPE SECONDARY
 D1 DICHOIC, THIN GOLD ON GLASS
 M3, M4 FLAT FOLDING MIRRORS
 L1 INFRARED FOCUS LENS
 W1, W2 IRTRAN II WINDOWS
 D2/F4 INFRARED DICHOIC & CHANNEL 3 FILTER
 F1, F2, F3 BANDPASS FILTERS
 L2, L3 INFRARED APLANAT LENSES
 L4 FOCUS ACHROMAT LENS ASSY, CH.1
 L5 FOCUS ACHROMAT LENS ASSY, CH.2
 D3 BEAMSPLITTER, INCONEL

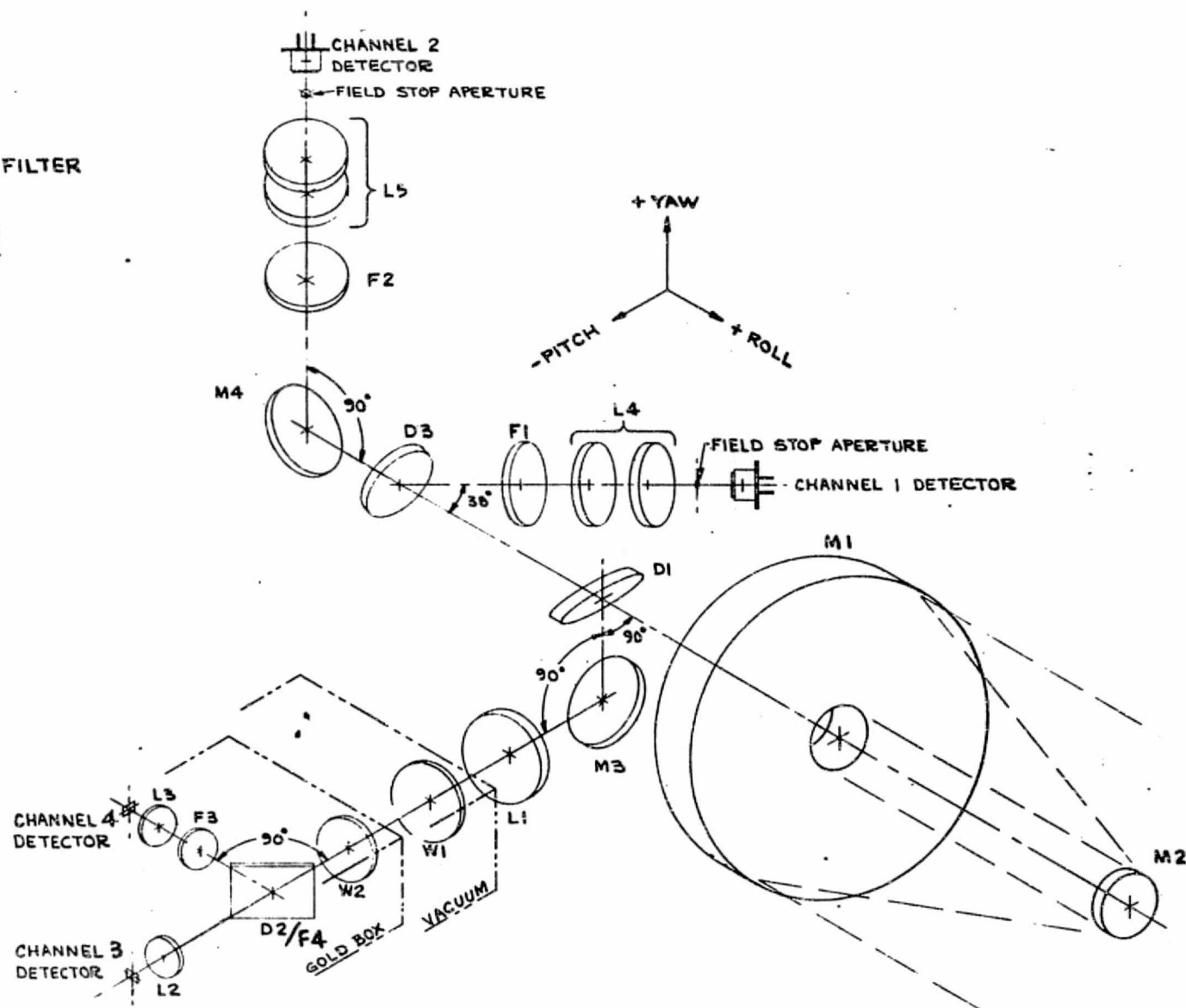


Figure 3.1-1 AVHRR OPTICAL LAYOUT

The beam which is transmitted by dichroic No. 1 is subsequently separated by beamsplitter D3 which reflects Channel 1 and transmits Channel 2. Mirror M4 and beamsplitter D3 are used to minimize polarization. Elements F1 and F2 are the spectral shaping filters for Channels 1 and 2 respectively; they both have flat faces on both sides and produce no focusing effect since they are in the collimated beam from the telescope. Lens assemblies L4 and L5 are re-focusing elements which form an image of the scene at the "field stop aperture" (i.e. an aperture plate located in the final focal plane of the system which contains an opening that determines the field of view for these two channels). The energy which passes through the aperture opening is then detected by silicon detectors are mounted in TO-5 housing with a flat glass window hermetically sealed to the housing).

The optical performance requirements are summarized in Table 3.1-1. In addition to the instantaneous field of view (IFOV) requirement, ITT imposed a larger, extended FOV on the optical subcontractor. That is, the optical system is designed so that the minimum MTF values given in Table 3.1-1 are obtained over a larger field of view than would be required by the IFOV. The reason for this is so that the detectors can be moved individually in their respective focal planes in order to register all channels simultaneously without losing MTF performance. In Channels 3 and 4, only the focus lens assembly L1 is designed for the EFOV since Channel 3 will be used as the reference channel (i.e. it will be located on the optical axis and the other detectors will be adjusted until aligned with it). Since the telescope operates over all four channels, it must cover the EFOV in all channels. The spatial frequencies listed in Table 3.1-1 correspond

to the subsatellite target sizes given in the AVHRR specification, i.e., 385 cycles/radian corresponds to a 0.59 nautical mile ground target, etc. A complete detailed description of the optical sub-assembly requirements is given to ITT-A/OD Spec. No. 8007907. A more detailed description of the optical system and components and the calculated performance is given in the following sections.

The initial design and fabrication of the development models of AVHRR (BEM, ETM, PTM) was performed by Ferson Optics Div. of Bausch and Lomb. The Flight Model optics are being obtained from Perkin Elmer, Costa Mesa, California.

3.2 Scan Mirror

The scan mirror configuration is shown in Figure 3.2-1 (ITT-A/OD Dwg. No. 8007928). It is made using a waffle or egg-crate construction to reduce weight while maintaining rigidity. The basic material is HP21 beryllium with a precision elastic limit of 4000 PSI minimum. After machining of the blank it is electroless nickel plated to provide a good polishing surface. After polishing to the specified flatness, the flat surface is aluminized and overcoated to give a high reflectance in all four spectral channels. The back surface is gold plated for thermal reasons. The scan mirror is mounted to the drive motor shaft and dynamically balanced as described in Section 4.0. The scan mirrors are being procured from Applied Optics Center, Burlington, Massachusetts.

3.3 Telescope Design

The telescope assembly is shown in Figure 3.3-1 (ITT Drawing #8009383). The telescope collects energy from an infinitely distant source (i.e., the earth) that subtends a solid angle of one IFOV which is located within the extended FOV. The diameter of the

OPTICAL PERFORMANCE REQUIREMENTS

	<u>CH 1</u>	<u>CH 2</u>	<u>CH 3</u>	<u>CH 4</u>
INSTANTANEOUS F.O.V. $\left(\begin{smallmatrix} \text{EDGE} \\ \text{OF SQ} \end{smallmatrix} \right)$	1.31 M.R.	1.31 M.R.	1.31 M.R.	1.31 M.R.
SPECTRAL BAND (μm)	0.55-0.90	0.725-1.1	10.5-11.5	3.55-3.93
EDGE WIDTH OF SQ. FIELD STOP	0.0238"	0.0238"	0.0068"	0.0068"
EXTENDED FOV (RADIUS)	1.1 M.R.	1.1 M.R.	2.2 M.R.*	2.2 M.R.*

TELESCOPE--AFOCAL CASSEGRAIN (TWO COAXIAL, CONFOCAL PARABOLOIDS)

TELESCOPE PRIMARY MIRROR--APERTURE STOP & ENTRANCE PUPIL

DIAMETER OF ENTRANCE PUPIL 8.00 \pm 0.01 INCHES

DIAMETER OF EXIT, AXIAL TELESCOPE BUNDLE 1.00 INCH

MAX. SECONDARY OBSCURATION (INC. BAFFLE) 2.00 INCHES

SPATIAL FREQUENCY (ALL CHANNELS)	<u>CYCLES</u> <u>RADIAN</u>		<u>MINIMUM SYSTEM M.T.F.</u>			
	<u>CH 1</u>	<u>CH 2</u>	<u>CH 3</u>	<u>CH 4</u>		
19	0.96	0.96	0.96	0.96		
257	0.91	0.93	0.90	0.91		
385	0.88**	0.90	0.86**	0.88**		

TELESCOPE MIRROR MATERIAL (OWENS-ILLINOIS) "CERVIT"

CHANNEL REGISTRATION SAME AS NASA/GSFC SPEC.

* APPLIES TO FOCUS LENS ONLY.

**DESIGN GOAL MTF IS 90%

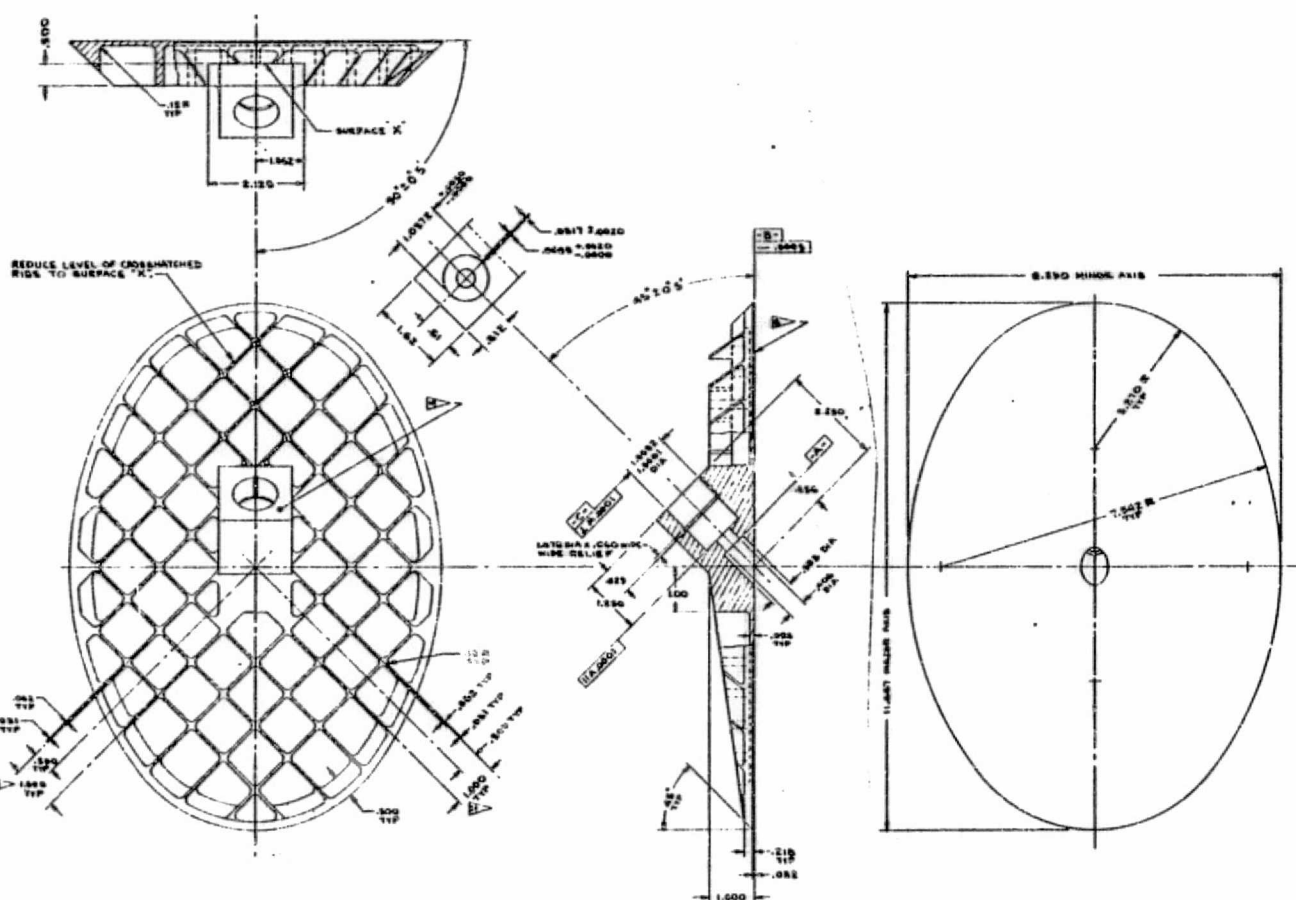
Table 3, 1-1 - Summary of Optics Requirements

- NOTE: THIS DRAWING IS TO BE USED IN CONJUNCTION WITH THE INSTRUCTIONS TO THE DRAWING.
1. REMOVE SURFACE TO BE FINISHED.
 2. HEAT TREAT TO REMOVE INTERNAL STRESS.
 3. FINISH MACHINE TO FINAL DIMENSIONS WITH ALLOWANCE FOR FINISHING AND PLATING.
 4. CLEAN WITH SUITABLE SOLVENT OR CLEANER AND POLISH WITH FINISHING AND DRIVING.
 5. ETCH SURFACE WITH SUITABLE REAGENT TO REMOVE SURFACE TOOL MARKS.
 6. ELECTROPLATING (HARD): PLATE ALL SURFACES BY THE HARDENED PROCESS (OR EQUIV). PLATING MUST BE OF SUFFICIENT THICKNESS SO THAT THERE IS NO EVIDENCE OF FINISHING TURN ON FINISHED REFLECTIVE SURFACE.
 7. INSPECT ALL DIMENSIONS.

- PER POLISHING:
1. OPTICAL POLISH SURFACE TO APLATINUM FINISH. POLISHES MAINTAIN OVER CLEAR APERTURE.
 2. POLISHING (TYPE 1) FINISH THROUGH OVER CLEAR APERTURE.
 3. CLEAR APERTURE IS ELLIPTICAL WITH 0.125 IN. MINOR AXIS AND 0.250 IN. MAJOR AXIS. SURFACE QUALITY 50-50 PPM. PPM. 0.1 IN. MIN. AFTER POLISHING, STAIN SURFACES WITH GOLD AND ELECTROPLATE REMAINING SURFACES WITH GOLD IN ACCORDANCE WITH MIL-B-42248B, TYPE 2, GRADE 2.
 4. AFTER POLISHING, SUBMERGE INTO SURFACE TO A HIGH REFLECTIVITY COATING OF ALUMINUM WITH A PROTECTIVE OVERLAYER. THIS REFLECTIVE COATING SHALL MEET ALL OF THE REQUIREMENTS OF ITT-AERO SPECIFICATION SUBSTITUTION COATING FOR ANVHR, EXCEPT THAT THE ACTUAL ANVHR BEAM SURFACE DOES NOT HAVE TO BE SUBJECTED TO THE HUMIDITY TEST AS SPECIFIED IN PARA. 5.5.

10. FINAL INSPECTION - ITT AERO MUST BE NOTIFIED 5 DAYS IN ADVANCE OF FINAL INSPECTION SO THAT ITT AERO QUALITY ASSURANCE PERSONNEL CAN BE PRESENT TO WITNESS FINAL INSPECTION.
11. DISCLOSE INTERNAL DEFECTS.
12. FINISHES MUST TO DISCLOSE ADEQUACY OF REFLECTIVE COATING FOR (TYPE 1) AND SAMPLE PLATE MUST BE INSPECTED VERTICALLY WITH MICROSCOPE.
13. POLISHING LABRATORY TEST ON REFLECTIVE METALIC FILM (NOTE 7) ON SAMPLE PLATE.
14. ACTUAL POLISHED SURFACES ON PLATING MUST BE SUBMITTED WITH PHOTOGRAPH. PHOTOGRAPH MUST BE SUBMITTED WITH PHOTOGRAPH OF FINISHES.
15. CERTIFICATION OF MATERIALS AND PRECISION ELASTIC LIMIT MUST BE SUBMITTED WITH FINISHES.
16. TOLERANCE BUILD-UP ON CIRCULAR SPACING TO BE NON-CUMULATIVE.
17. SURFACES FINISHED WITH FINISHES, TYPE 2, BARBER HALL (EQUIV. WITH FIN.) PER MANUFACTURER'S INSTRUCTIONS. ITT AERO HAS THE FINAL ACCEPTANCE OF THE FINISHES.

REVISIONS		DATE	BY
1	REPLACE REV C WITH E	1-10-70	W. J. HALL
2	REPLACE REV E WITH F	1-10-70	W. J. HALL
3	ADDENDUM 1000-100	1-10-70	W. J. HALL
4	ADDENDUM 1000-100	1-10-70	W. J. HALL



REPRODUCIBILITY OF THE ORIGINAL PAGE IS POOR

FIG 3.2-1

REVISIONS		DATE	BY
1	REPLACE REV C WITH E	1-10-70	W. J. HALL
2	REPLACE REV E WITH F	1-10-70	W. J. HALL
3	ADDENDUM 1000-100	1-10-70	W. J. HALL
4	ADDENDUM 1000-100	1-10-70	W. J. HALL

31550	61490	AS NOTED
31550	61450	AS NOTED

31550	61490	AS NOTED
31550	61450	AS NOTED

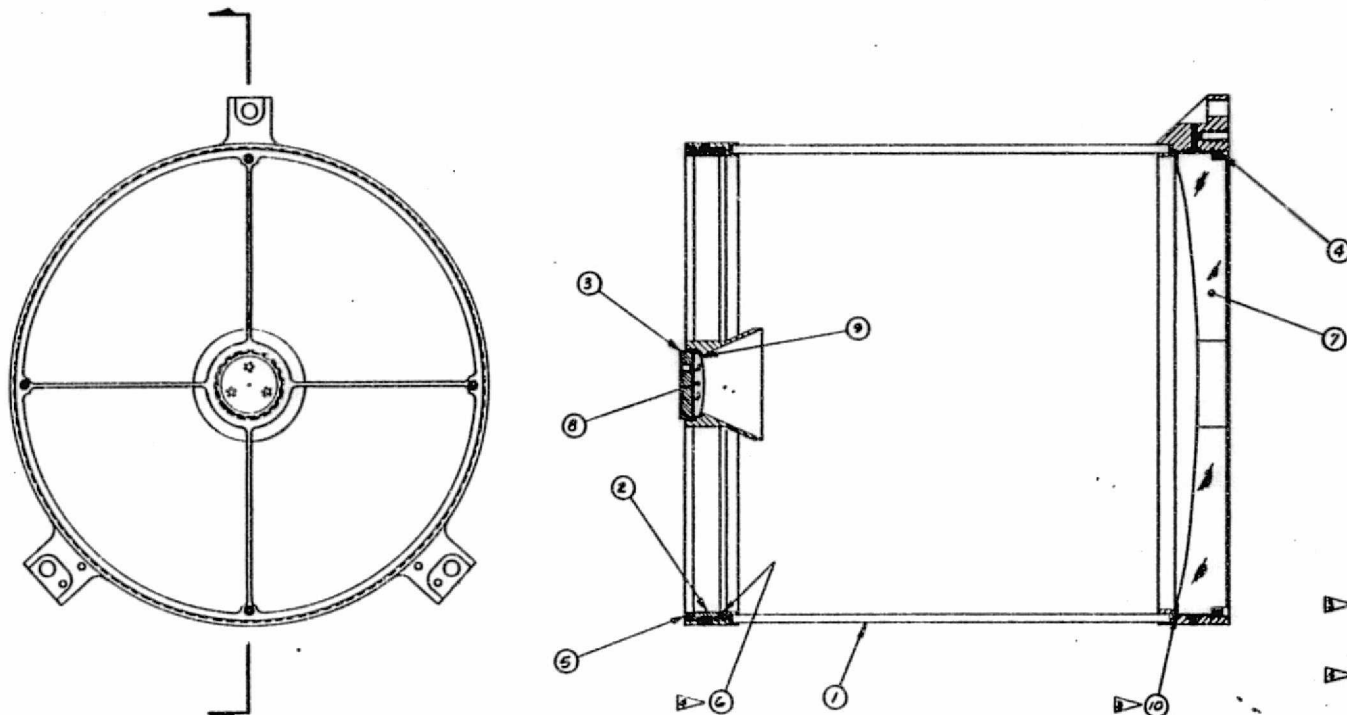
31550	61490	AS NOTED
31550	61450	AS NOTED

NOTES:

1. IDENTIFY PER MIL-STD-130, NO MARKING PERMITTED ON PART.
2. ALIGN AND TEST PER ALIGNMENT PROCEDURE 8007992.
3. QTY OF ITEM 10 TO BE DETERMINED DURING ALIGNMENT PER 8007992.
4. QTY A DASH 10. FOR ITEM G TO BE DETERMINED DURING ALIGNMENT PER 8007992.

		DEVERMOND		6100-755	
DATE	TYPE	DESCRIPTION	DATE	TYPE	DESCRIPTION
		YOUNG & BROS. CO., LINDSEY, WIS - 11 ARROW ITEMS IN TORN FR; REMISED NOTE #;	4-4-78		<i>[Signature]</i>
		ARROW NOTE #;	9-28-78		R. J. [Signature]
		SEN 6100-576.			

REPRODUCIBILITY OF THE
ORIGINAL PAGE IS POOR

[illegible]

entrance beam into the telescope is 8.00 inches and the diameter of the exit beam, which leaves through the center hole of the primary mirror, is 1.0 inch. This reduction in beam diameter caused a corresponding increase in angular extent, i.e. the IFOV of 1.31 mr (milliradian) by 1.31 mr into the telescope leaves with 10.5 mr by 10.5 mr beam spread. The largest field angle over which the telescope must operate is the extended FOV which has a 4.4 mr diameter in object space (without the extended FOV, the telescope would have to cover a field of 1.85 mr).

The telescope consists of two confocal, coaxial paraboloidal mirrors which are called the primary (large) and secondary mirrors. The primary mirror clear aperture is both the aperture stop and entrance pupil of the optical system. It has an 8.00 inch diameter clear aperture and a focal length of 10 inches giving it an optical speed of 1.25. The intervertex distance (the axial separation of the primary and secondary mirrors) is 8.75 inches. This gives a 1.0 inch diameter beam reflected by the secondary for a collimated, axial beam into the telescope. Because of the extended field of view, the clear aperture of the secondary mirror must be a minimum of 1.040 inches. In order to re-collimate the beam, the secondary mirror must have the same optical speed of the primary mirror, i.e. 1.25. The focal length of the secondary mirror is therefore 1.25 inches.

A conical baffle is located around the secondary mirror to prevent radiation within the EFOV from getting past the secondary mirror and into the aft optics (i.e. the optical components behind the telescope). The telescope barrel is made of invar metal which has a very low coefficient of thermal expansion and therefore maintains

mirror alignment over the temperature range. The mirrors are made of Cervit (made by Owens-Illinois) and has a low coefficient of thermal expansion. After polishing, the mirrors are coated with a high reflectivity coating of aluminum which is protected by an overcoat layer of silicon monoxide; this coating is used because of its uniform spectral reflectance in all four channels. Other mechanical features of the telescope are described in Section 4.0.

A unique feature of the AVHRR telescope assembly is the absence of any coma or astigmatism. Thus the angular alignment of the reflective, reimaging optics following the telescope is not critical with respect to the telescope exit beam. A tolerance analysis of all optical elements was performed by Ferson Optics which showed that the only sensitive elements are the primary and secondary mirrors (i.e. the alignment with respect to each other). The optic subcontractor not only fabricates the mirrors (as well as all lens elements) but assembles and aligns the mirrors in the telescope housing assembly shown in Figure 3.3-1. The primary mirror is first potted in place and then the secondary mirror is adjusted by positioning the entire spider support in an annular ring at the front of the telescope). The performance of the completed telescope is checked as a subassembly after potting has cured.

3.4 Channels 1 and 2 Lens Design

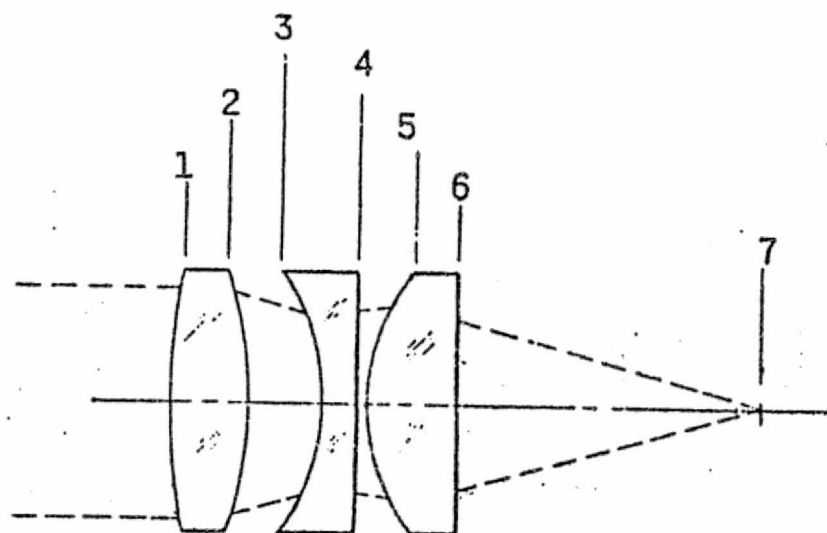
The reimaging optics for Channels 1 and 2 are AR coated lenses consisting of three elements. This triplet design is shown in Figure 3.4-1 which gives the radii of curvatures, axial thickness of each element, axial spacing, minimum half apertures for each lens surface

and the material. The lens materials were selected to control chromatic aberrations over the wide spectral bands, especially channel 1 (0.55 to 0.90 μm). The triplet design has more than adequate MTF performance over the extended FOV and has high transmission and low manufacturing sensitivity. It has been possible to achieve a single design which can be used for both channels 1 and 2 even at the relatively fast effective f/number.

The focal plane is located at position No. 7 in Figure 3.4-1. The field defining aperture (or "field stop") is located at this position; the size of the opening is 0.0238 inch by 0.238 inch and produces the 1.31 mr by 1.31 mr field of view in object space in Channels 1 and 2.

The optical performance data for Channels 1 and 2 is summarized in Table 3.4-1. The optical design was performed by Ferson Optics under subcontract to ITT-A/OD. Preliminary design was carried out using computers at Ferson's plant while the MTF data for the final design was obtained using the Grey Diffraction MTF Program on a CDC 6600 computer. Five wavelengths were used for evaluation for each channel and MTF data was determined for best alignment (on-axis) and worse alignment (at the edge of the extended FOV) for all channels. Note that the calculated MTF for 385 cycles per radian* at the edge of the EFOV is 97.4% for Channel 1 and 96.9% for Channel 2 and is much better on-axis. The required value at this optical

*385 cycles per radian corresponds to 0.831 line pairs per mm in the focal plane and to 0.5 nautical mile target on the earth's surface.



(1)		(2)		
NO	RADIUS MM	THICK MM	HALF APT, MM	MATL.
1	80.24	10.00	17.00	PSK 53
2	-51.04	9.03	16.59	
3	-28.70	4.50	13.33	SF 18
4	420.65	1.00	13.57	
5	26.15	11.38	13.92	PSK 53
6	-1218.2	38.29	12.55	
7	IMAGE			

NOTE: 1) THICKNESS BETWEEN SURFACES ON AXIS
2) HALF APT. SHOWN ARE FOR EFOV EDGE RAY.

DESIGN UNCHANGED BY MODS 6, 7 AND 8.

Figure 3.4-1 AVHRR Triplet Design CH 1 & 2

AVHRR OPTICAL SYSTEM MTF (PERCENT)

ON AXIS

CYCLES/RAD	CH 1		CH 2		CH 3		CH 4	
	SPEC	CALC	SPEC	CALC	SPEC	CALC	SPEC	CALC
19	96	>99	96	>99	96	>99	96	>99
257	93	98.7	91	>99	90	98	91	98.5
385	90	98.2	88	>99	86	97	88	97.7

FIELD EDGE

19	96	>99	96	>99	96	>99	96	>99
257	93	98.4	91	98.2	90	97	91	98
385	90	97.6	88	97.3	86	95	88	97

EFOV EDGE

19	96	>99	96	>99	96	>99	96	>99
257	93	98.2	91	97.9	90	96	91	96
385	90	97.4	88	96.9	86	94	88	94

Table 3.4-1 Calculated MTF Performance

frequency for Channel 2 is 90% and for Channel 1 it is 88% with a design goal of 90% for both channels (see Section 3.1). The high optical performance achieved in the design permits comparatively easy manufacturing tolerances for the lens elements and tolerable mechanical alignment tolerances (see Section 3.6 for tolerance analysis results).

3.5 Channel 3 and 4 Lens Design

The reimaging optics focus the energy coming out of the telescope onto as small a detector as possible. The optics consist of a focus lens assembly (doublet) made of germanium for Channels 3 and 4; the index of refraction of germanium does not change significantly between 4 and 12 μm . The slight difference in index is taken care of by locating each detector at the corresponding focal plane. The focus lenses are axially adjustable to obtain optimum focus by means of an adjustment external to the radiant cooler; this also permits use of a smaller opening in the cooler which lowers the thermal input thereto.

A third germanium lens, called an aplanat, is used just in front of each detector to do the final focusing of the beam (an aplanat introduces no additional coma or spherical aberration). The best signal-to-noise ratio is obtained by using the smallest possible detector area since detector noise depends somewhat on area in Channels 3 and 4. The detector area can be found from the Abbe sine law (see for example, R. C. Jones, Applied Optics, Vol. 1, p. 607, 1962 or D. Marcuse, Applied Optics, Vol. 10, p. 499, 1971).

$$A_o \theta^2 = A_d \pi \sin^2 \mu$$

where A_o = area of collecting optics = $\frac{\pi}{4} D_o^2$

θ = width of square IFOV

A_d = area of square detector = w_d^2

μ = maximum incidence angle of an axial ray at the detector.

This can be simplified to $D_o \theta = 2 w_d \sin \mu$. Using the sine definition of f-number, i.e., $f_n = \frac{1}{2 \sin \mu}$ this becomes $w_d = f_n D_o \theta$. Since θ has been specified ($\theta = 1.31 \text{ m r}$) and we have chosen $D_o = 8.0$ inches, we can only minimize f_n (maximize μ). About the maximum feasible value of μ is 50° ; this gives $f_n = 0.653$ and $w_d = 0.0068$ inch. The sensitive area of the infrared detector is the field defining "stop" in Channels 3 and 4; in both infrared channels the edge width of the square detector is nominally $0.0068 \text{ inch} \pm 0.0004 \text{ inch}$. If we note that $w_d/\theta = \text{EFL}$ (effective system focal length), then

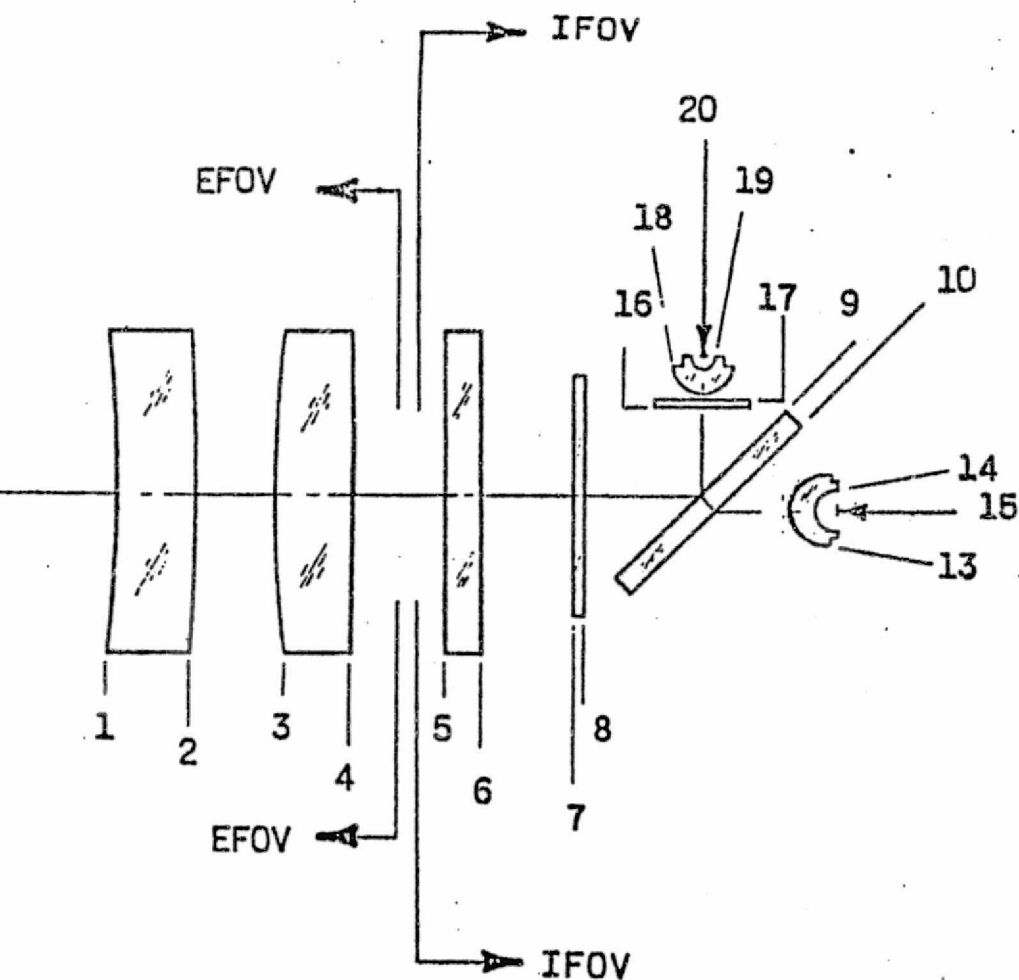
$$f_n = \frac{\text{EFL}}{D_o}$$

which is the common definition of f-number.

The aplanat has the effect of optically magnifying the size of the detector by the refractive index (about 4.0 for germanium at $12 \mu\text{m}$) so that the focus lens "sees" a detector image 0.0272 inch on an edge. Since the focus lens sees an angular field spread of 10.48×10^{-3} radians from the telescope (Channel 3), it has a focal length of about 2.6 inches. The speed of the focus lens is also about 2.6 since the beam is 1.0 inch in diameter (neglecting field spread); the actual clear aperture diameter of the focus lens is large enough to accept the beam spread plus some allowance for mechanical tolerance.

The detail design information for the Channel 3 and 4 re-imaging optics is given in Figure 3.5-1. An enlarged scale drawing of the optical elements mounted inside the radiant cooler is shown in Figure 3.5-2. The sensitive area of the Channel 3 infrared detector is located at position 15 and that of the Channel 4 detector at position 20. The position of the aplanat lens is held very accurately with respect to the detector sensitive area by mounting the aplanat directly to the detector housing. This is shown in Figure 2.2-2 (ITT-A/OD Drawing 8008791), the housing for the Channel 3 infrared detector. The aplanat lens also serves as the window for the housing since it is hermetically bonded in place. The same type of construction has been successfully used by the same detector vendor on the infrared detectors for other programs.

The MTF performance of the infrared bands for both on-axis and edge of the EFOV is given in Table 3.1-1. The MTF data given in the table includes the effects of diffraction. Since Channel 3 is used as the reference channel for registration, the detector-aplanat assembly for this channel is positioned on-axis. Achievement of the 86% MTF requirement for this channel is therefore not expected to present a problem. The calculated MTF values for both infrared channels is appreciably higher than the required values imposed on the optical vendor by ITT-A/OD. Tolerance analysis studies indicate that the required performance is achievable without undue difficulty. The axial astigmatism in Channel 3 which is caused by the tilted dichroic (D2) was analyzed and was found to be masked by diffraction effects at these long wavelengths.



AVHRR CH 3 & 4
ELEMENT PRESCRIPTION

NO.	RADIUS M M	THICK MM ON AXIS	HALF APT MM	MA: L
1	-185.15	10.00	19.66	G E
2	-294.56	10.00	20.54	
3	166.29	10.00	22.15	G E
4	-3238.3	4.32	21.53	
5	--	4.78	15.87	IRTRAN
6	--	17.40	15.35	2
7	--	1.57	11.10	IRTRAN
8	--	15.77	10.93	2
9	--	2.54	--	G E
10	--	7.60	--	
11				FILTER
12				DELETED
13	4.58	3.00	4.43	G E
14	2.80	2.48	2.42	
15	IMAGE PLANE CH 3			
9	--	11.5	--	
16	--	1.01	4.13	G E
17	--	0.25	4.12	
18	3.90	3.00	3.52	G E
19	1.93	1.57	1.51	
20	IMAGE PLANE CH 4			

Figure 3.5-1 Infrared Reimaging Optics Data

REPRODUCIBILITY OF THIS
ORIGINAL PAGE IS POOR

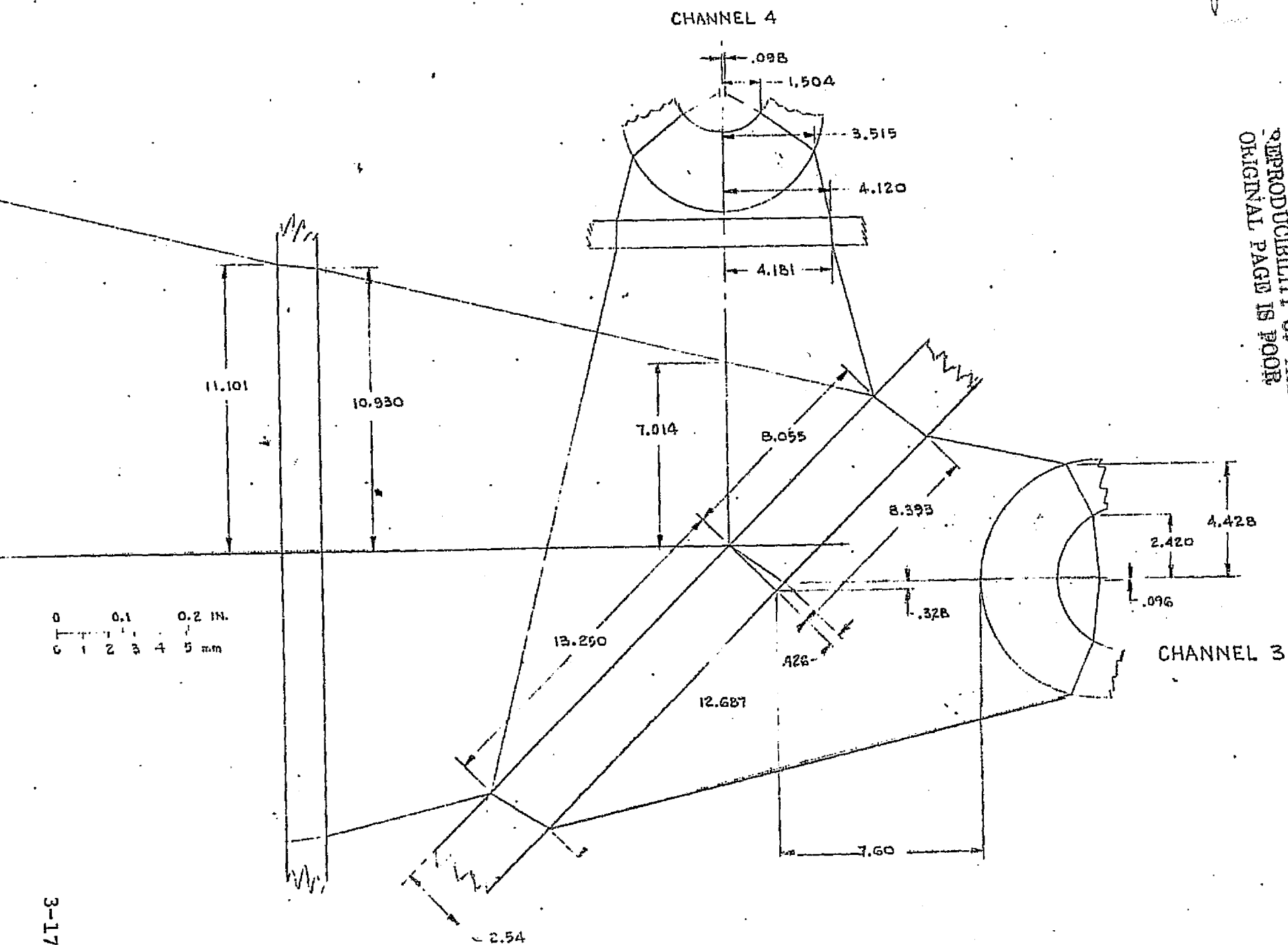


Figure 3.5-2 Cooler Optics Configuration

3.6 AVHRR Tolerance Analysis

A tolerance analysis was run on the AVHRR Optical Design using a Ferson Optics computer program. The program provides information of changes in the OPD* (in Raleigh units) due to perturbation of optical design parameters about their nominal values. From the OPD variations due to perturbations, the mechanical tolerances for manufacture can be determined. The data presented here is for individual elements as well as groups of elements which are mounted on subassemblies. Figures 3.6-1 and 3.6-2 show concentricity and parallelism for group data in schematic presentation. Mirrors and dichroics are not shown but must be considered when distributing the parallelism and concentricity tolerances. A summary of the recommended tolerances follows.

3.6.1 Summary of Mechanical Tolerances**

Channel 1 and 2 - Focus Lens

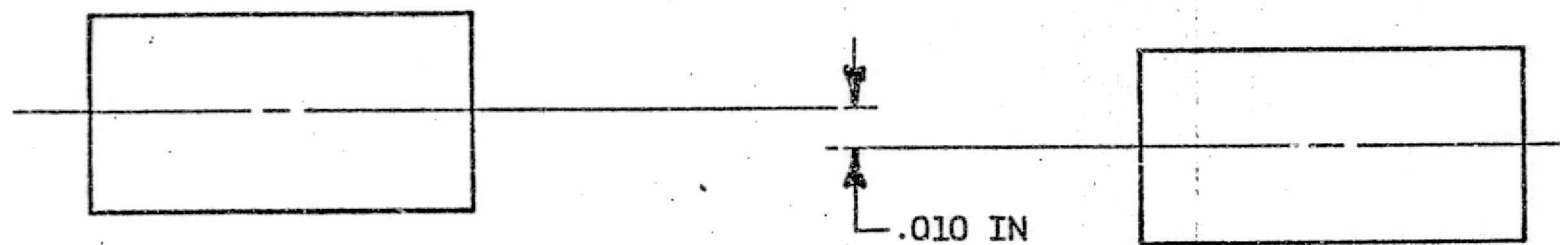
- a. Focus Lens Diameter - OD + 0.000 -0.002
- b. Focus Lens Cell - ID +0.002 -0.000
- c. Minimum Clearance for Thermal Expansion - 0.001
- d. Triplet concentricity relative to telescope optical axis - 0.010
- e. Triplet parallelism relative to telescope optical axis - 4 mr

* OPD = Optical path difference.

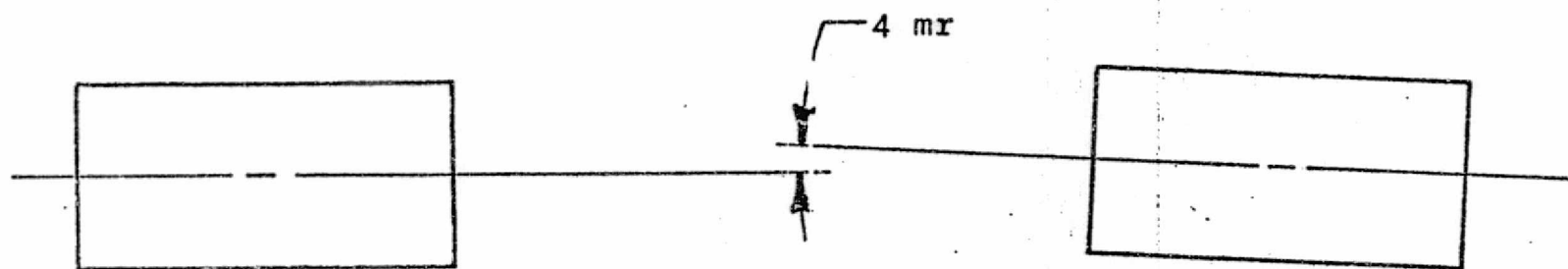
** Linear dimensions in inches, angles in milliradians (mr).

TELESCOPE

TRIPLET



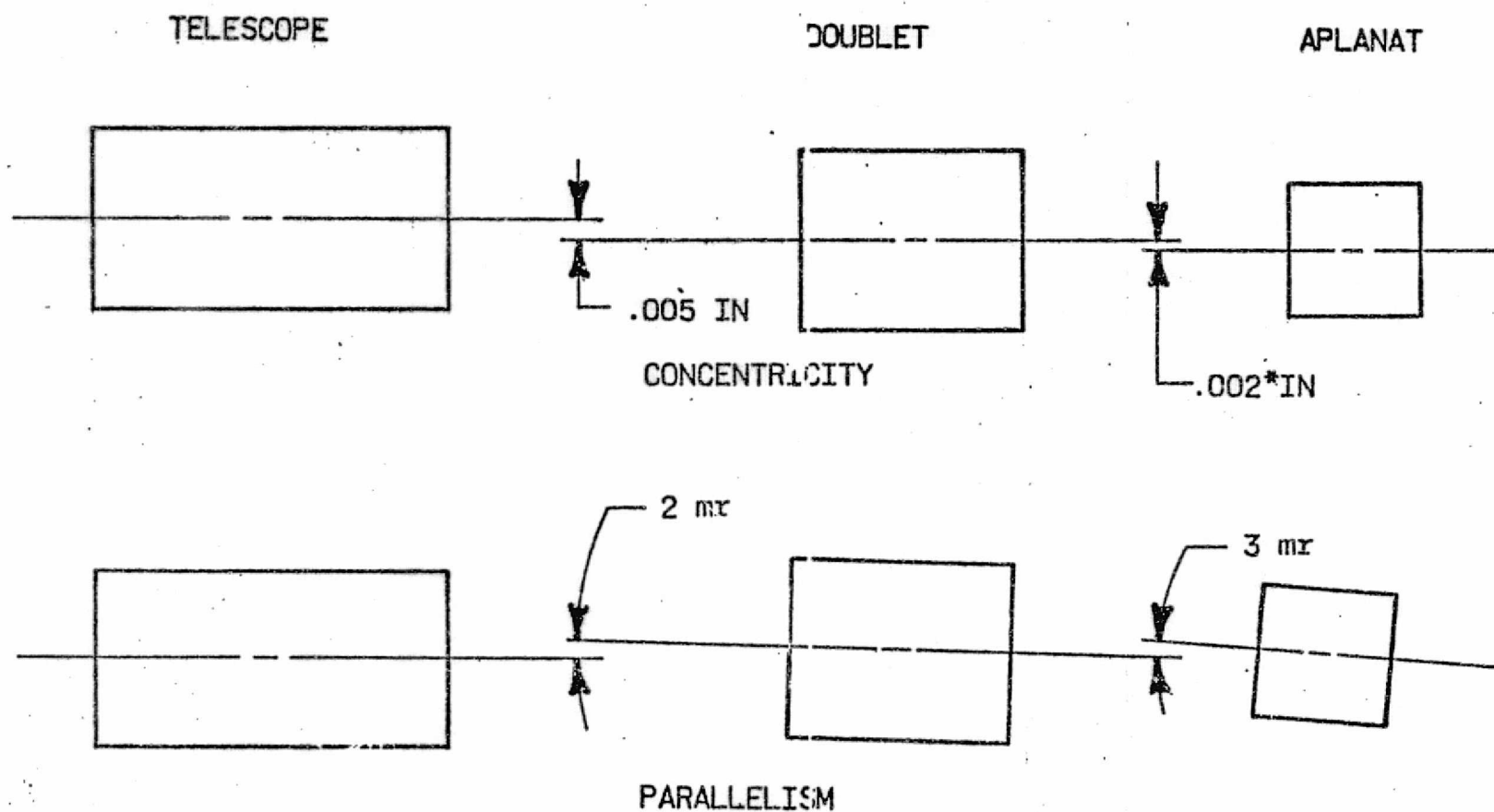
CONCENTRICITY



PARALLELISM

CHANNEL 1 & 2 TOLERANCE DATA
FOR ELEMENT GROUPS

FIGURE 3.6-1



*0.002 INCH IS TOL. OF APLANAT WITH RESPECT
TO DETECTOR CENTER; TOLERANCE INDICATED
SHOULD BE 0.015 INCH.

CHANNEL 3 & 4 TOLERANCE DATA
FOR ELEMENT GROUPS

FIGURE 3.6-2

f. Spacer Data

Lenses	16-17*	17-18*
Length	± 0.002	± 0.003
ID	± 0.001	± 0.001
OD	$+0.000 -0.002$	$+0.000 -0.002$

*See Figure 3.4-1.

Channels 3 and 4 - Focus Lens

- a. Focus Lens Dia. - OD $+0.000 -0.002$
- b. Focus Lens Cell - ID $+0.002 -0.000$
- c. Minimum clearance for thermal expansion - 0.001
- d. Doublet concentricity relative to telescope optical axis - 0.005
- e. Spacer Data
 - Length - ± 0.003
 - ID - ± 0.002
 - OD - $+0.000 -0.002$

Channels 3 and 4 - Aplanat

- a. Outsider Diameter Aplanat - $+0.000 -0.002$
- b. Diameter aplanat cell - $+0.002 -0.000$
- c. Concentricity of cell diameter relative to detector axis - 0.002
- d. Mounting Surface deviation relative to detector surface - ± 0.001

3.6.2 Surface Quality for Filters, Beamsplitters

	Ch. 1 and 2	Ch. 3 and 4
a. Scratch	60	80
b. Dig	40	50
c. Flatness	10 fr	2 fr
d. Irregularity	1 fr	2 fr
e. Wedge	1 mr	1 mr

3.6.3 Mechanical Adjustment Data (Inches)

	Back Focus	Focus Adjust	X-Y Adjust
Channel 1	1.512	± 0.050	± 0.040
Channel 2	1.515	± 0.050	± 0.040
Channel 3	0.0976 ± 0.002	$\pm 0.050^*$	± 0.040
Channel 4	0.062 ± 0.002	$\pm 0.050^*$	± 0.040

*An additional adjustment of 0.0606 for Channel 3 and 0.0343 for Channel 4 toward the focus lens is required for room temperature testing.

Position of Channel 4 aplanat relative to Channel 3 aplanat - ± 0.002 .

3.7 Dichroics, Beamsplitters and Cooler Windows

Dichroics D1 and D2, Beamsplitter D3, the Irtran cooler windows and the Channel 3 filter are being obtained from OCLI (Optical Coating Labs, Inc., Santa Rosa, Calif.). The function of the two dichroics and the beamsplitter is to separate the optical beam exiting the telescope into four separate beams before final focussing in each of the four channels. Dichroic D1 consists of a thin "Transparent" coating of gold evaporated onto a flat glass substrate. This type dichroic reflects

radiation in Channels 3 and 4 with approximately 82% efficiency and transmits Channels 1 and 2 with approximately 75% and 70% efficiency, respectively. It does polarize the energy in Channels 1 and 2 and is the reason why an additional folding mirror (M3) is used. More complete details of this dichroic are given in ITT-A/OD Spec. No. 8009262.

Dichroic D2 reflects Channel 4 radiation and transmits Channel 3. This dichroic is the bandpass filter for Channel 3 which is designed for a 45° incidence angle and the focused optical beam when cooled to 105 Kelvin. The "filter-dichroic" reflects energy in the 3.5 to 4.0 μ m spectral band. The reflectance for Channel 4 radiation is 90% minimum and the transmittance for Channel 3 radiation is 75% minimum. The substrate material for the dichroic is optical grade germanium; the thickness was made as large as feasible to minimize bending when it is cooled to operating temperature. More complete details of this dichroic are given in ITT-A/OD Spec. No. 8008792.

A detail layout drawing showing the extreme optical rays at Dichroic D1, Beamsplitter D3 and folding mirrors M3 and M4 is shown in Figure 3.7-1. The angle of beamsplitter D3 with respect to the optical axis was minimized in order to reduce polarization effects. Since the spectral bands of Channels 1 and 2 overlap each other, D3 cannot be a dichroic beamsplitter but must be a neutral density separator. The neutral density beamsplitter consists of a thin evaporated coating of inconel on an optically-polished, flat glass substrate. The minimum average reflectance is 22% for Channel 1 energy and the minimum average transmittance is 34% for Channel 2. Complete details for beamsplitter D3 are given in ITT-A/OD Spec. No. 8007932.

REPRODUCIBILITY OF THE
ORIGINAL PAGE IS POOR

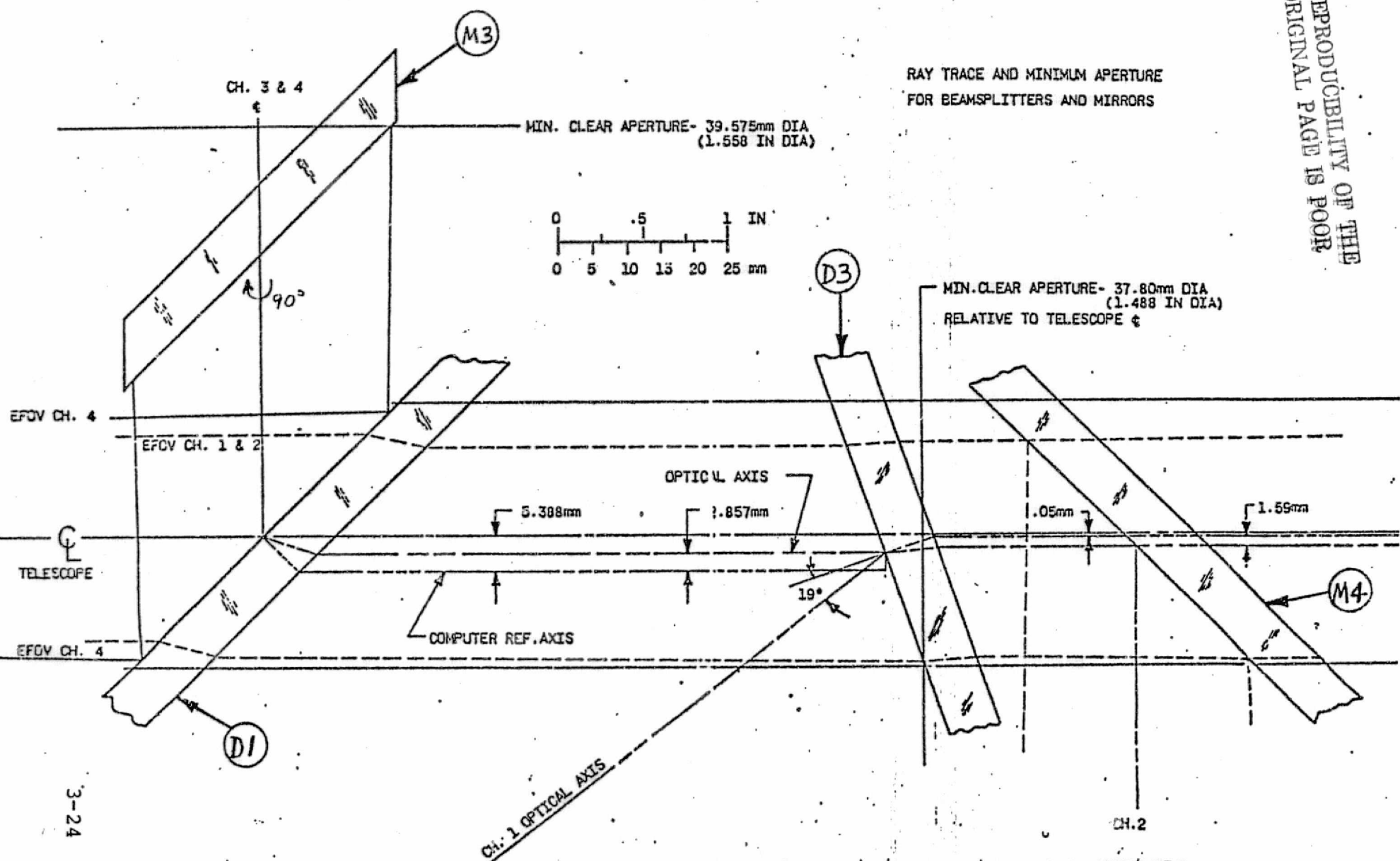


FIGURE 3.7-1 RAY TRACE AND MINIMUM APERTURE FOR BEAMSPLITTERS AND MIRRORS

The cooler windows are optically-polished, flat circular discs of Irtran 2 material (Eastman Kodak trade name). They are antireflection coated by OCLI to give a minimum transmission of 85% in both Channels 3 and 4. The coated windows meet standard military specifications for adherence, hardness and humidity. The outer cooler window (W1) is comparatively thick since it must withstand atmospheric pressure when the cooler is evacuated for bench cooling tests.

The Channel 4 bandpass filter is a conventional multilayer coating on a polished germanium substrate. The bandpass characteristics such as cuton and cutoff slopes, tolerances on location of the 50% transmission wavelength, etc., are given in Section 3.8.2.

3.8 Spectral Definition

3.8.1 Spectral Definition of Solar Channels

In order to determine the AVHRR system spectral response in Channels 1 and 2, it is necessary to determine the effects of those elements having a varying spectral characteristic. These elements are:

- a. Mirror Coatings
- b. Gold Beamsplitter
- c. Lens AR Coatings
- d. Silicon Detectors
- e. Spectral Bandpass Filters

Since the relative spectral response of the above elements affects the system spectral response in the given bands, and since their absolute response affects the signal to noise ratio, both requirements (spectral and sensitivity) must be considered together. The spectral

characteristics of the above five groups will be discussed individually below, followed by their combined effects.

3.8.1.1 Mirror Coatings

A complete study of the various potential mirror coatings was done in the preliminary design of the AVHRR. It was decided that to achieve maximum sensitivity in Channel 2 (where overcoated aluminum mirrors have a dip in their reflectivity) silver mirrors would be used for the telescope mirrors. For polarization compensation, however, the scan mirror and the folding mirror behind the solar channel beam-splitter were aluminized. The silver coating chosen was the Muffelleto Optics "low pit" coating which was supposed to survive the required humidity and temperature extremes.

In the process of building the Breadboard and Engineering Model telescopes, no silver coating was found (at reasonable cost) which passed the humidity test. In all cases the mirrors degraded extensively when placed in the humidity test. Therefore, the decision was made to use aluminum mirrors which have a reflectivity equal to or greater than that shown in Figures 3.8-1 and 3.8-2. The coating after which the reflectivity curves were fashioned is the Evaporated Metal Films Corp. "enhanced aluminum" coating.

3.8.1.2 Gold Beamsplitter

The dichroic to split Channels 1 and 2 from Channels 3 and 4 is the thin gold film type at 45° to the incident beam with the near IR and visible energy being transmitted. Figure 3.8-3 shows the measured solar channel reflectivity of the gold dichroic used in the PTM.

REV
DRAWING NUMBER
8008787

"EXCEPT AS MAY BE OTHERWISE PROVIDED BY CONTRACT, THESE DRAWINGS AND SPECIFICATIONS ARE THE PROPERTY OF ITT AEROSPACE/OPTICAL DIVISION, ARE ISSUED IN STRICT CONFIDENCE, AND SHALL NOT BE REPRODUCED, OR COPIED, OR USED AS THE BASIS FOR THE MANUFACTURE OR SALE OF APPARATUS WITHOUT PERMISSION."

ITT AEROSPACE/OPTICAL DIVISION
FORT WAYNE, INDIANA, U.S.A.
INTERNATIONAL TELEPHONE AND TELEGRAPH CORPORATION

NOTE: 90% MINIMUM @ 525 n.m.

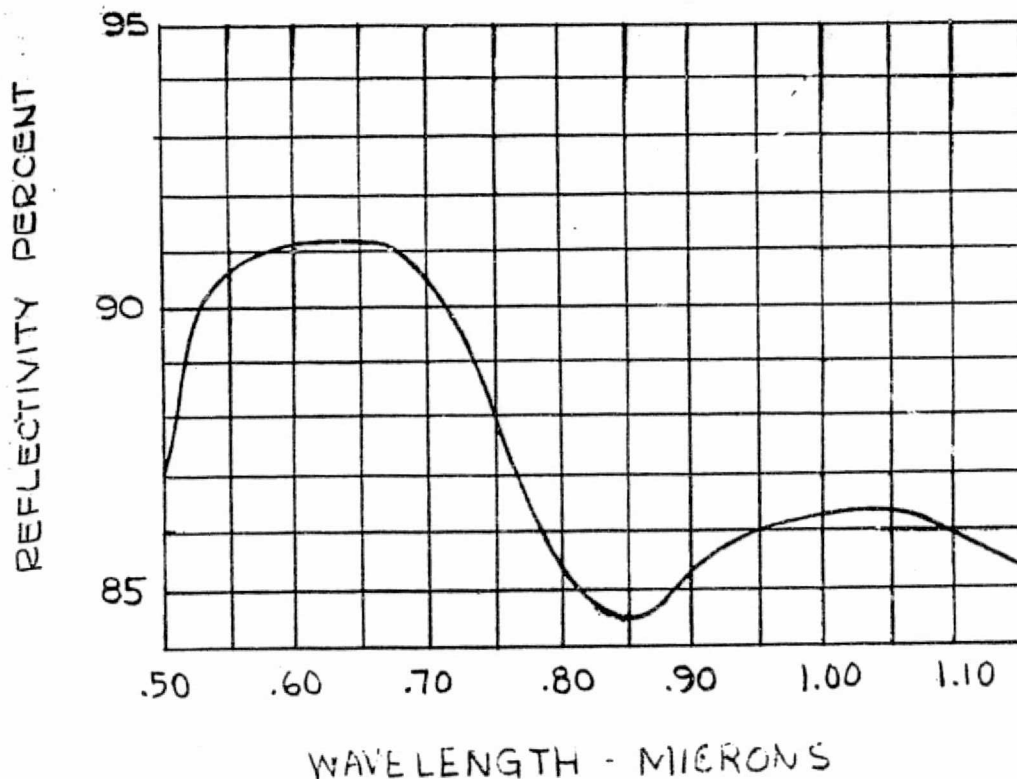


FIG 3.8-I ABSOLUTE SPECTRAL
REFLECTIVITY REQUIREMENT
(ALL MIRRORS EXCEPT CHAN 2 FOLDING)

DWG
A
SIZE

CODE IDENT NO.
31550

8008787

SCALE

SHEET

3-27

REV B
DRAWING NUMBER
800878

"EXCEPT AS MAY BE OTHERWISE PROVIDED BY CONTRACT, THESE DRAWINGS AND SPECIFICATIONS ARE THE PROPERTY OF ITT AEROSPACE/OPTICAL DIVISION, ARE ISSUED IN STRICT CONFIDENCE, AND SHALL NOT BE REPRODUCED, OR COPIED, OR USED AS THE BASIS FOR THE MANUFACTURE OR SALE OF APPARATUS WITHOUT PERMISSION."

ITT AEROSPACE/OPTICAL DIVISION
FORT WAYNE, INDIANA, U.S.A.
INTERNATIONAL TELEPHONE AND TELEGRAPH CORPORATION

REFLECTIVITY PERCENT

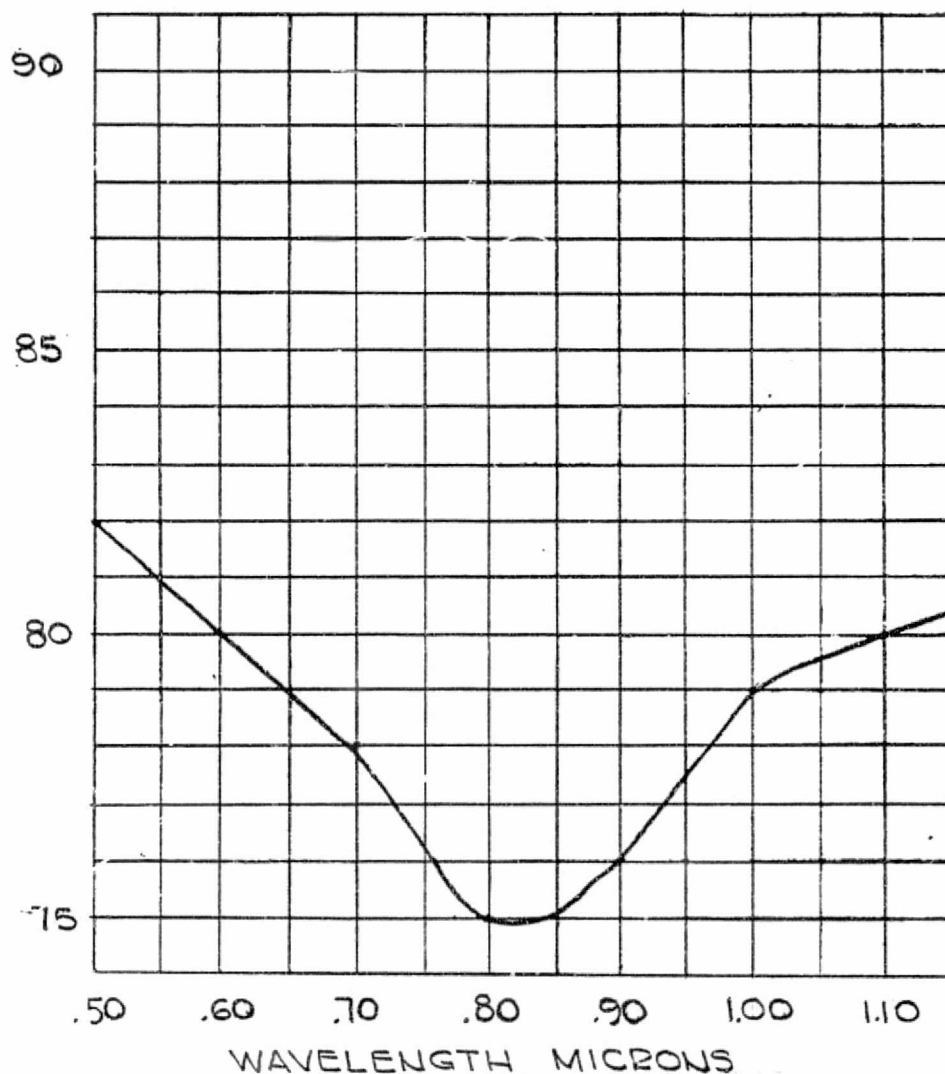


FIG 3.8-2 ABSOLUTE SPECTRAL
REFLECTIVITY REQUIREMENT
(CHAN 2 FOLDING MIRROR)

DWG CODE IDENT NO.

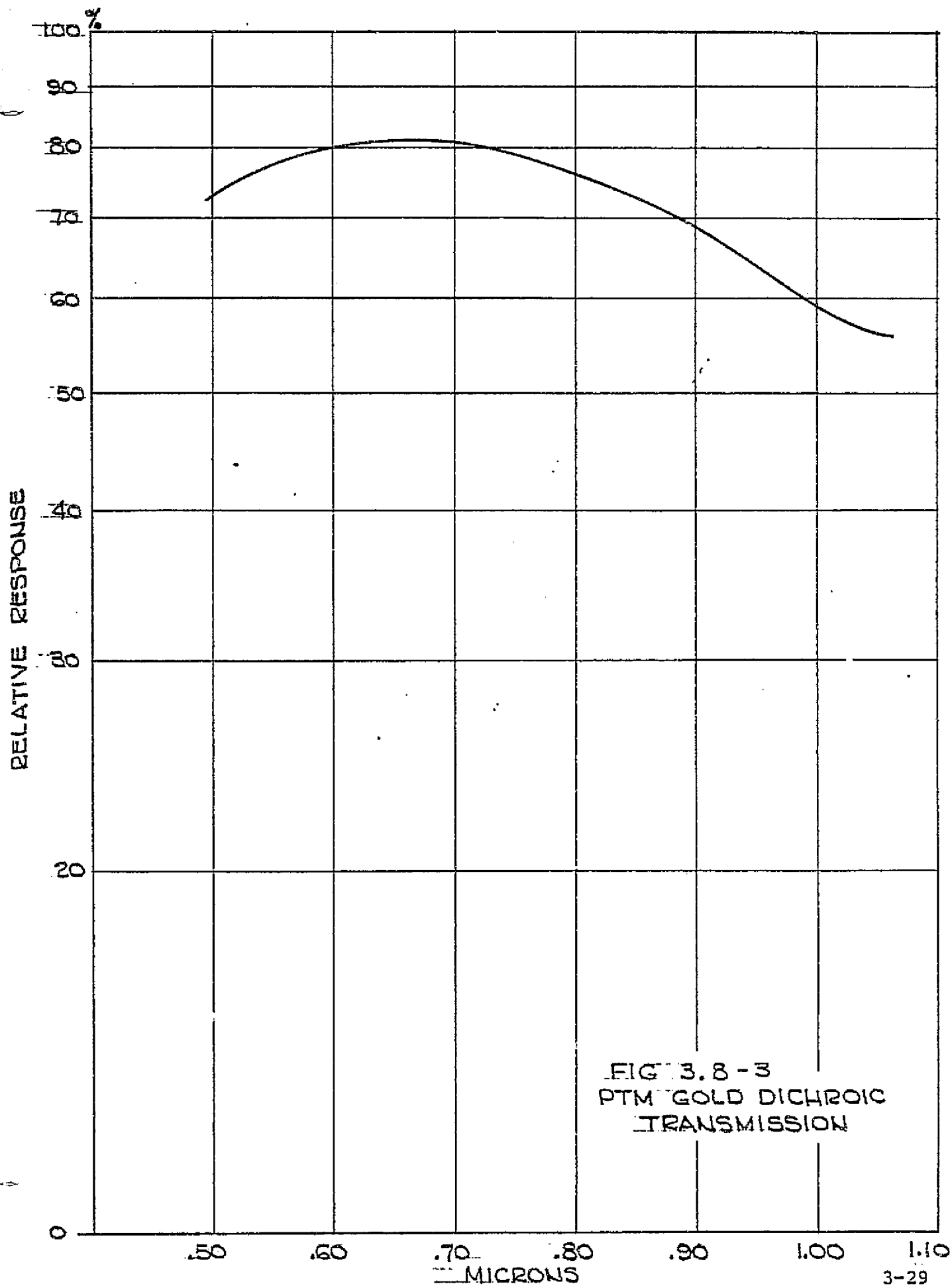
A 31550

8008787

SIZE

SCALE

SHEET 3-28



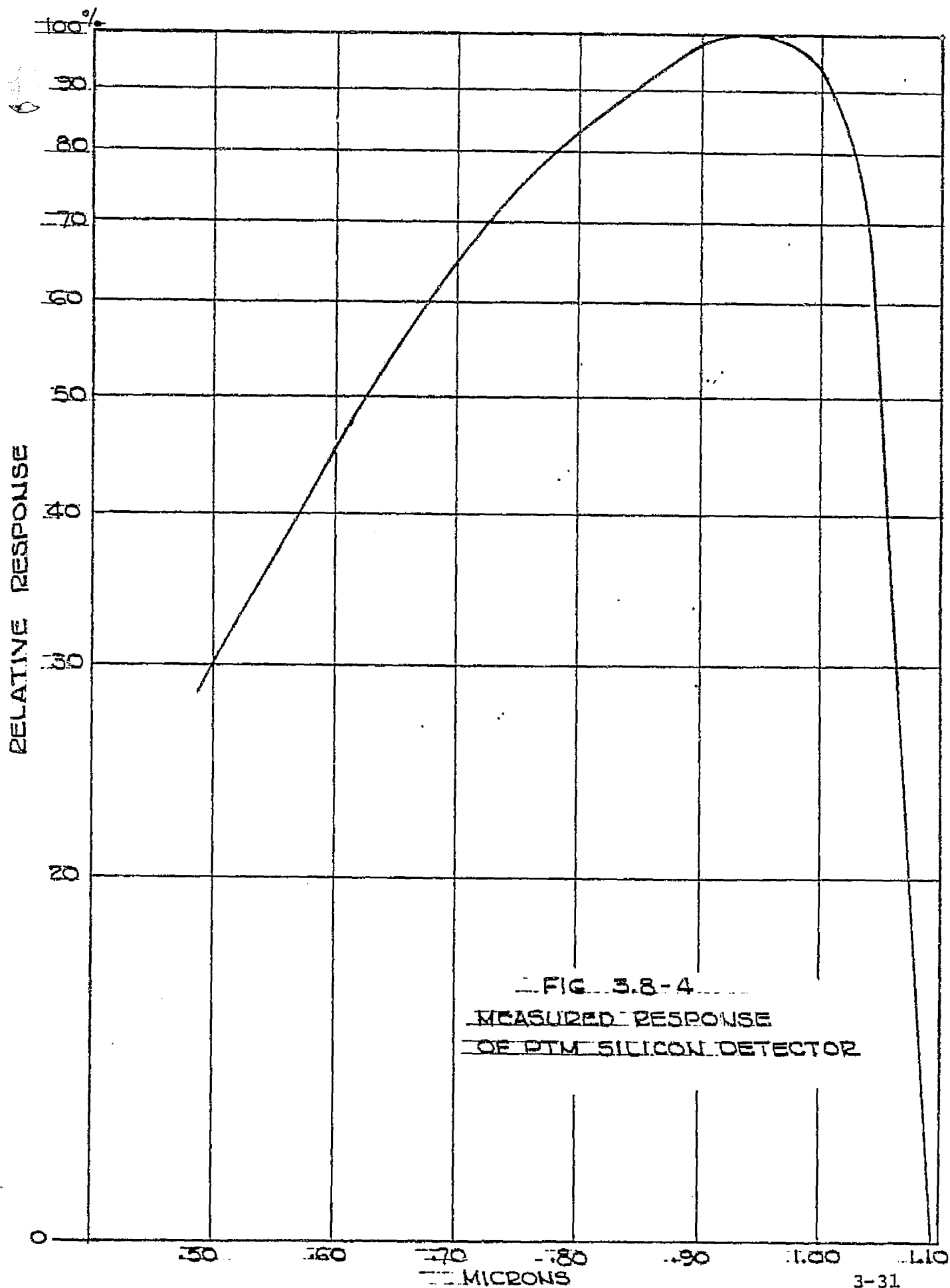
3.8.1.3 Lens AR Coatings

The anti-reflection coatings on the three relay optic lenses used in each channel do not materially affect the relative spectral response of the solar channels. A MgF_2 type single layer coating is used and the total lens transmission will change from about 97% near the band center to 95% near the edges. Even for three lenses, the effect is insignificant.

3.8.1.4 Silicon Detectors

Because of the wide spectral bands covered by Channels 1 and 2, the detector in each is an important factor in defining the band edges. Quotes were solicited from six different companies, and all were requested to define the spectral characteristics of their proposed device. Selection of the vendor was based on both the relative spectral response and the absolute sensitivity. The definition of the Channel 1 spectral band edges is complicated by the fact that the silicon detector relative response is down to about 30% at 0.50 micron. This means that above some relative transmission value (about 40%) the spectral bandpass filter does not define the system response. The response is basically defined by the detectors and the other spectrally variant elements. This effect could have been reduced by cutting the detector peak spectral response and lowering the system signal-to-noise ratio; however, it was decided that the slow cuton of the system spectral response is more acceptable than a reduced signal-to-noise ratio.

As stated previously, one detector design is used for both solar channels. This approach provides excellent sensitivity in both channels and simplifies (and so reduces the cost of) the detector. The measured spectral response of one of the detectors is shown in Figure 3.8-4.



3. 8.1.5 Spectral Bandpass Filters

The spectral filters were purchased from Fish-Schurman Corp. and have the responses shown in Figures 3.8-5 through 3.8-7. The Channel 1 filter consists of a two piece laminated sandwich with one piece being a 3 mm thick Schott glass filter and the other being a 2 mm thick clear substrate upon which a multilayer coating is applied. The multilayer is placed inside the sandwich and is sealed by the epoxy sealant from ambient conditions. The problem of spectral variations as a function of absorbed water is eliminated. This approach was used in the ATS-F VHRR solar channel filter. The epoxy sealant is Summers Laboratory C-59 which meets MIL-3920 and has measured outgassing characteristics of 2.94% weight loss and 0.108% condensible materials. (This information was supplied to ITT by NASA/GSFC.) This is the same sealant used to seal and focus lenses in each solar channel of the AVHRR.

The filter generates its spectral bandpass using a Schott glass filter for the short wave cut-on and a multilayer coating for the long wave cut off. The slopes of the filters are all about 6% between the 5% and 80% response points. Short wave out-of-band blocking is defined by the Schott glass and is complete. Long wave out of band blocking is defined by the multilayer and, while not as good as the Schott glass, results in an out of band signal well below that specified as discussed later (the detector has cut off by the time the filter transmission comes back up).

In Channel 2 the spectral filter is simply a 3 mm thick Schott glass RG-715 long pass filter. The long wave cutoff of Channel 2 is defined by the silicon detector.

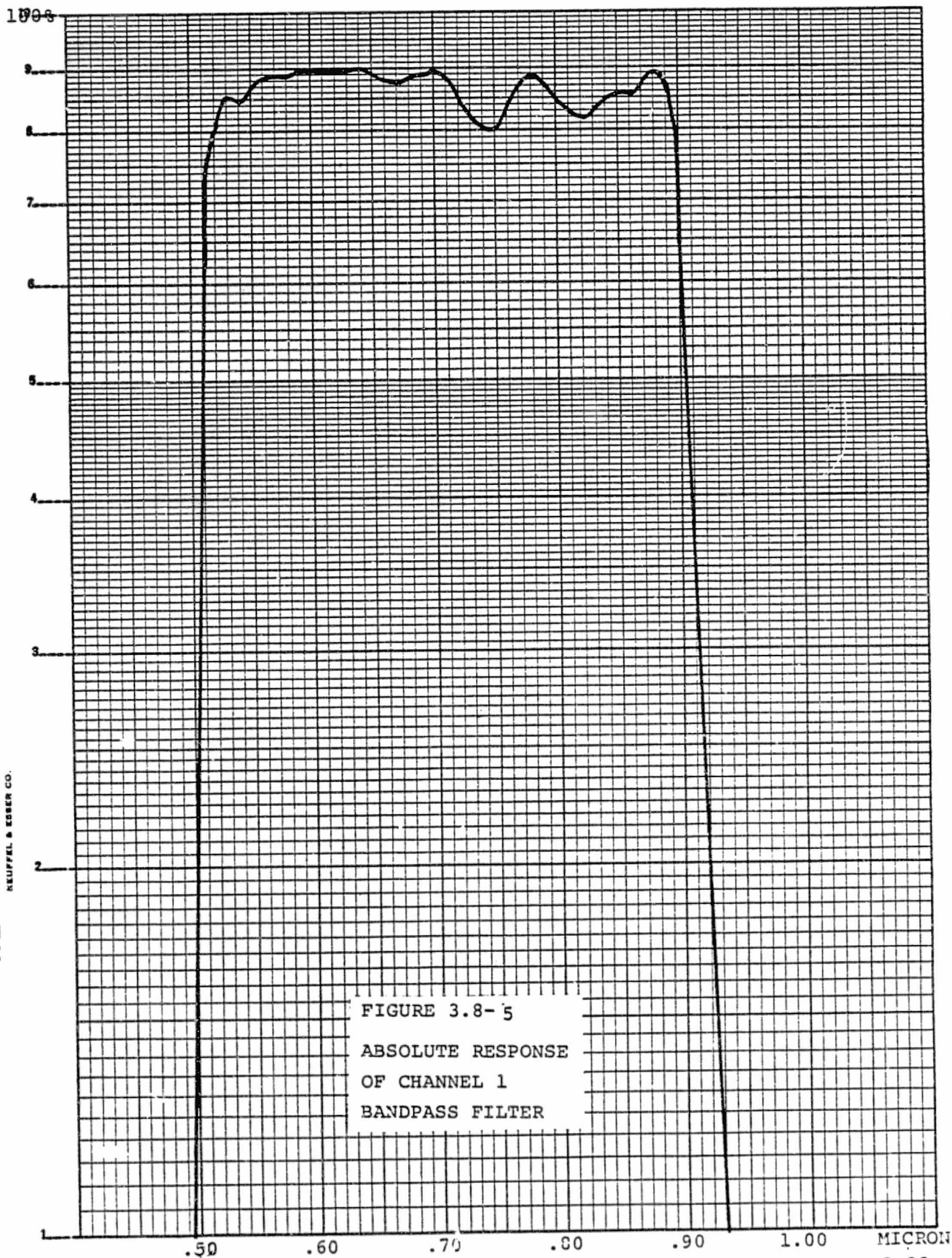
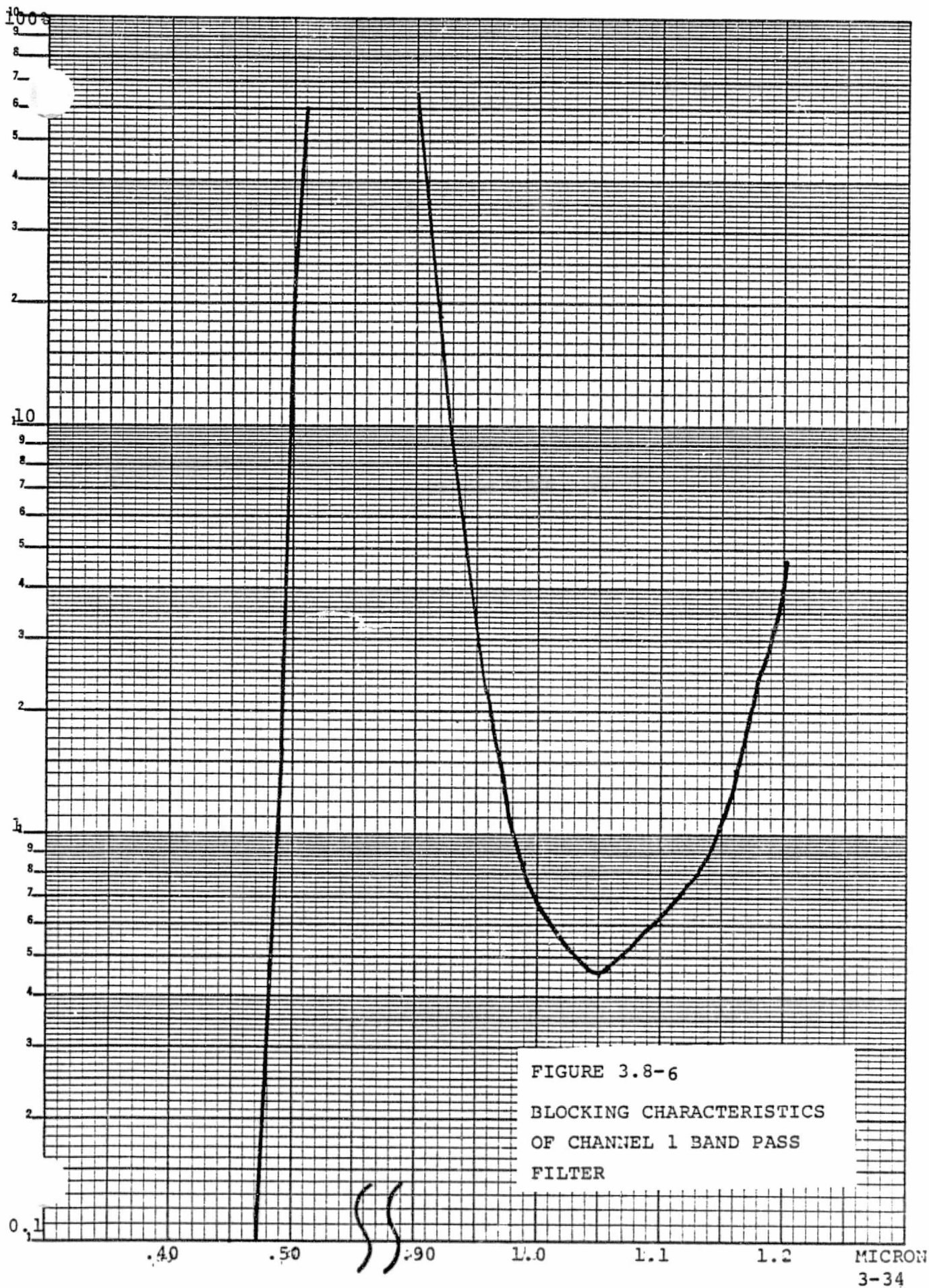


FIGURE 3.8-5
ABSOLUTE RESPONSE
OF CHANNEL 1
BANDPASS FILTER



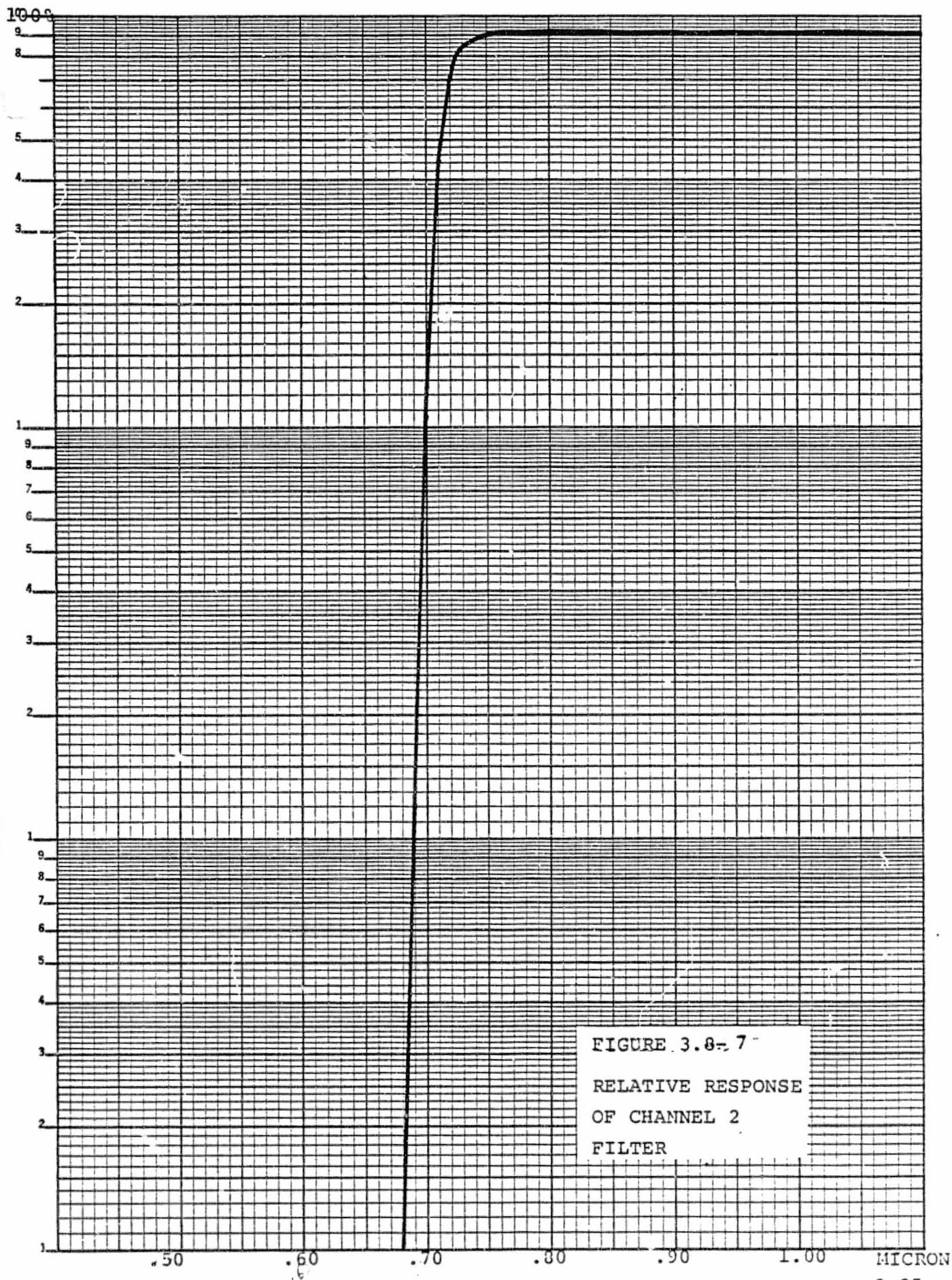


FIGURE 3.8-7
RELATIVE RESPONSE
OF CHANNEL 2
FILTER

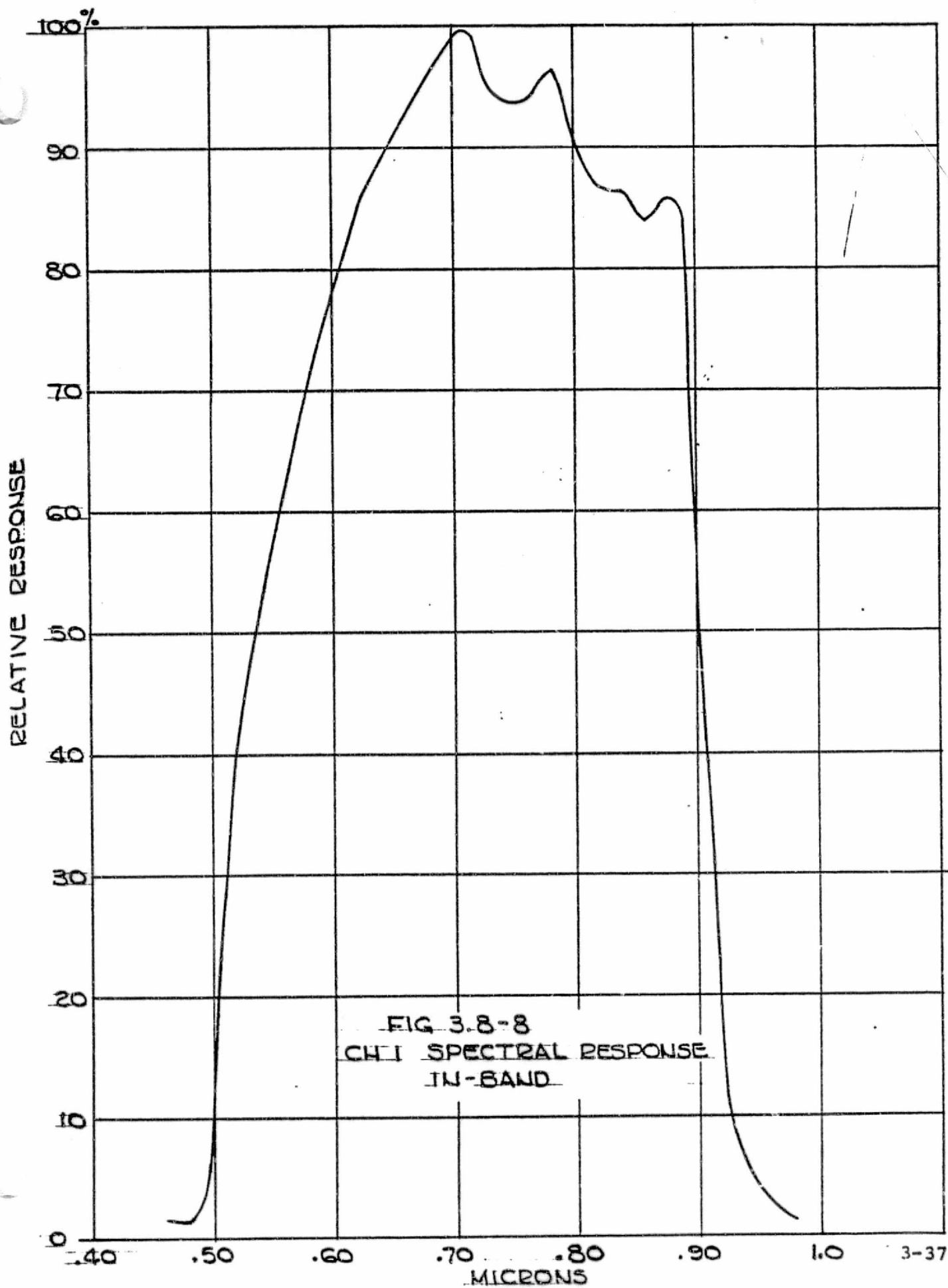
3.8.1.6 System Spectral Response

Figures 3.8-8 and 3.8-9 show the measured PTM AVHRR Spectral responses for Channels 1 and 2.

3.8.1.7 Out-of-Band Signal

Since the bandpass filters have transmission outside of the bands of interest, some of the output signal results from radiation out of the spectral band. The specification requires that the total out of band responses shall be less than 2% of the total integrated response within the passband when viewing a source simulating the solar spectral energy distribution. The Channel 1 passband is defined in the specification as extending from 0.06 micron below the lower 50% response point to 0.04 micron above the higher 50% response point. For Channel 1 then the passband is 0.47 to 0.935 micron. In Channel 2 the passband is from 0.65 micron to the detector response cut off. Since the detector response is about 0.3% at 1.30 microns, this will be taken as the cutoff point for purposes of this analysis.

Using the solar spectral distribution curves generated by Thekaekara and the system response curves we can calculate the amount of signal both in and out of the two spectral bands. In Channel 1, Table 3.8-1 shows that the in-band signal is 3422 while the out of band is 21. Since the in-band transmission of the spectral filter is about 80%, we must reduce the in-band level to 2740. We have then a maximum out of band signal of $\frac{21}{(.80)(3422)} = 0.8\%$.



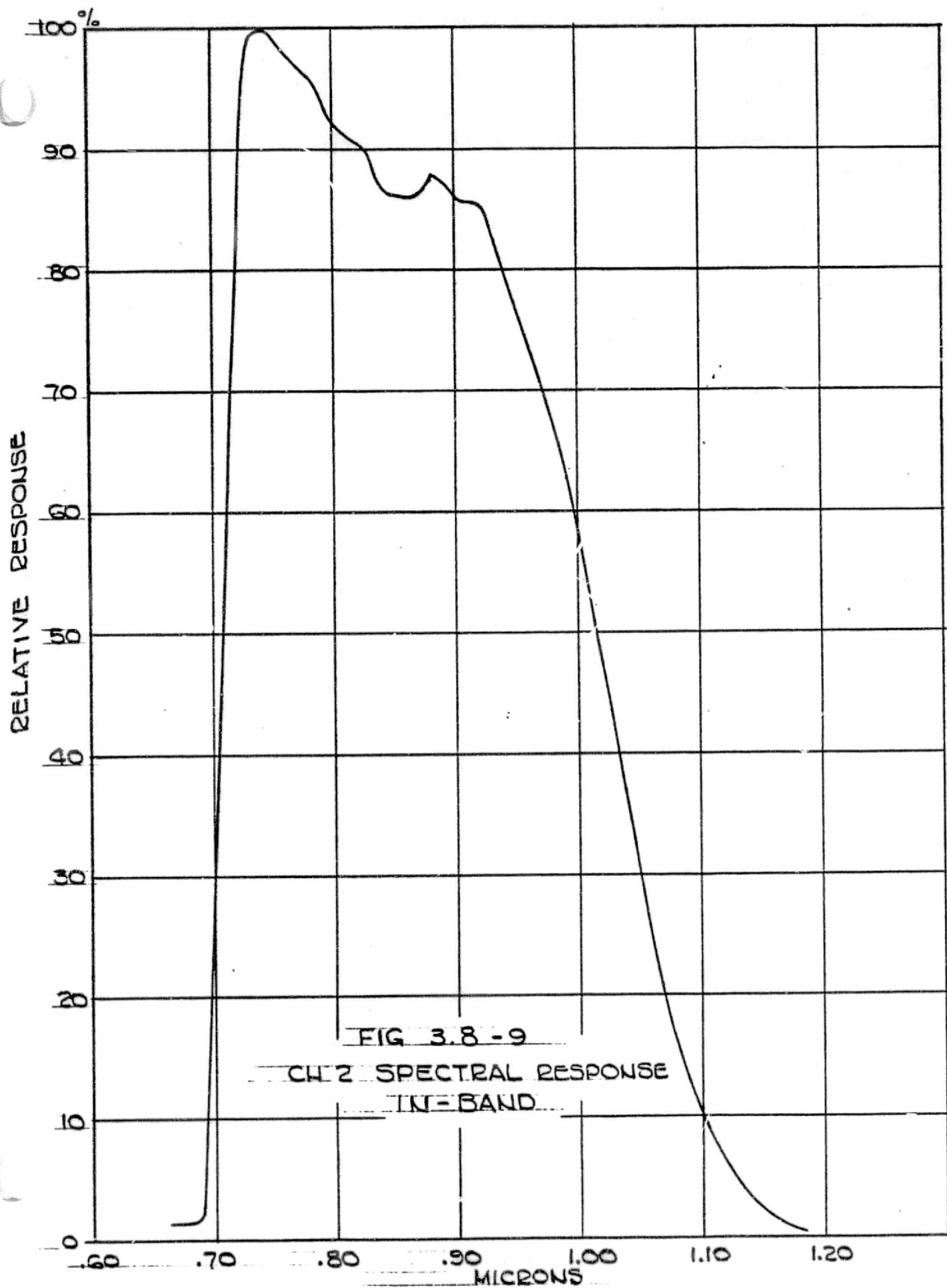


TABLE 3.8-1 IN BAND AND OUT OF BAND SIGNAL FOR CHANNEL 1

<u>SPECTRAL INTERVAL MICRON</u>	<u>CH 1 SYSTEM RESPONSE</u>	<u>SOLAR ENERGY</u>	<u>SUMMATION OF FACTORS</u>
<0.20	0	0.05	
0.20 - 0.47	0.1*	18.2	1.8
0.47 - 0.49	0.5	3.00	1.5
0.49 - 0.50	10	1.44	14.4
0.50 - 0.51	27	1.42	38.3
0.51 - 0.70	75	22.9	17.7
0.70 - 0.89	97	15.8	1534
0.89 - 0.92	56	1.97	110
0.92 - 0.93	13	0.64	8.3
0.93 - 0.95	6	1.89	11.3
0.95 - 1.00	1.8	2.94	5.3
1.00 - 1.10	0.55	4.95	2.7
1.10 - 1.20	0.06	3.97	.24
>1.20	0		

*Maximum specified allowable transmission.
Actual filters are less.

TABLE 3.8-2 IN BAND AND OUT OF BAND SIGNAL FOR CHANNEL 2

<u>SPECTRAL INTERVAL MICRON</u>	<u>CH 2 SYSTEM RESPONSE</u>	<u>SOLAR ENERGY</u>	<u>SUMMATION OF FACTORS</u>
<0.65	0.1*	41.6	4.2
0.65 - 0.68	0.1	3.3	0.3
0.68 - 0.69	0.5	1.04	.52
0.69 - 0.70	5.0	1.02	5.1
0.70 - 0.72	45	1.99	89.6
0.72 - 1.00	90	2062	1856
1.00 - 1.05	72	261	188
1.05 - 1.20	25	6.30	157
1.20 - 1.30	1.0	3.25	3.2
1.30 - 1.40	.16	2.68	.43
>1.40	0	15.7	0

*.1% is maximum specified allowable transmission of
filter. Actual filter much less than this.

Similarly in Channel 2, the in-band signal from Table 3.8-2 is 80% of 2300 while the out of band is 4.6. The ratio of out of band to in-band signal is $\frac{4.6}{(.80)(2300)} = 0.25\%$.

Measurements on both the ETM and PTM verify that the out-of-band response is well below the 2% maximum allowed in both channels.

3.8.2 Spectral Definition of Thermal Channels

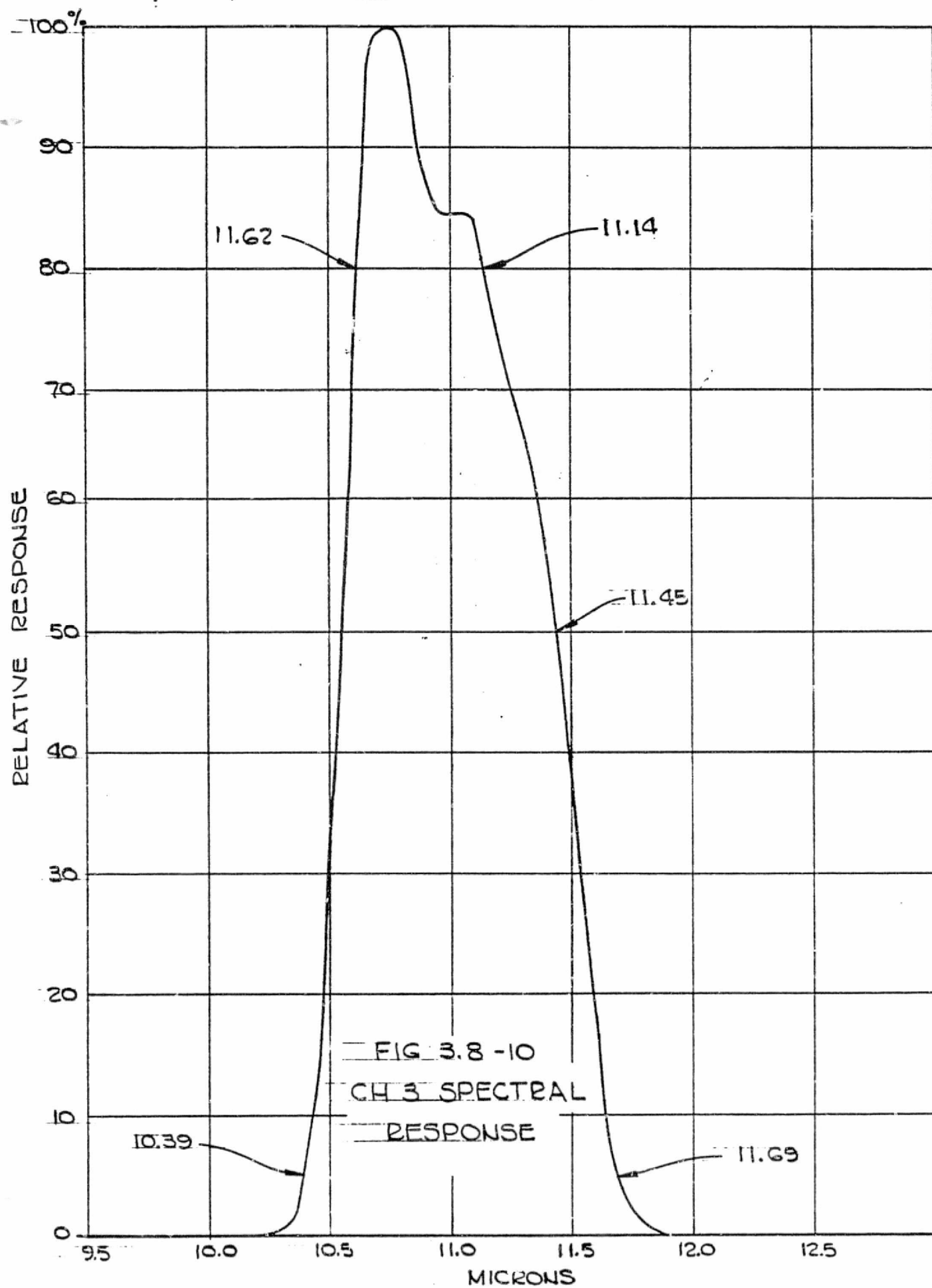
The spectral characteristics of the bandpass filters for Channels 3 and 4 are summarized in Table 3.8-3. The filters are the dominant element in defining the spectral response of the AVHRR instrument. The response of the indium antimonide detector varies smoothly from 3.5 to 4.0 μm , being about 5% less at the shorter wavelength side of the band. The Hg Cd Te detector procurement specification contains a requirement that the response at any wavelength between 10.5 and 11.5 μm be no less than 80% of the maximum in-band response. Therefore, the detectors should not appreciably affect the system response. The complete procurement specifications for the bandpass filters are contained in ITT-A/OD Specifications 8008790 (Channel 4) and 8008792 (Channel 3).

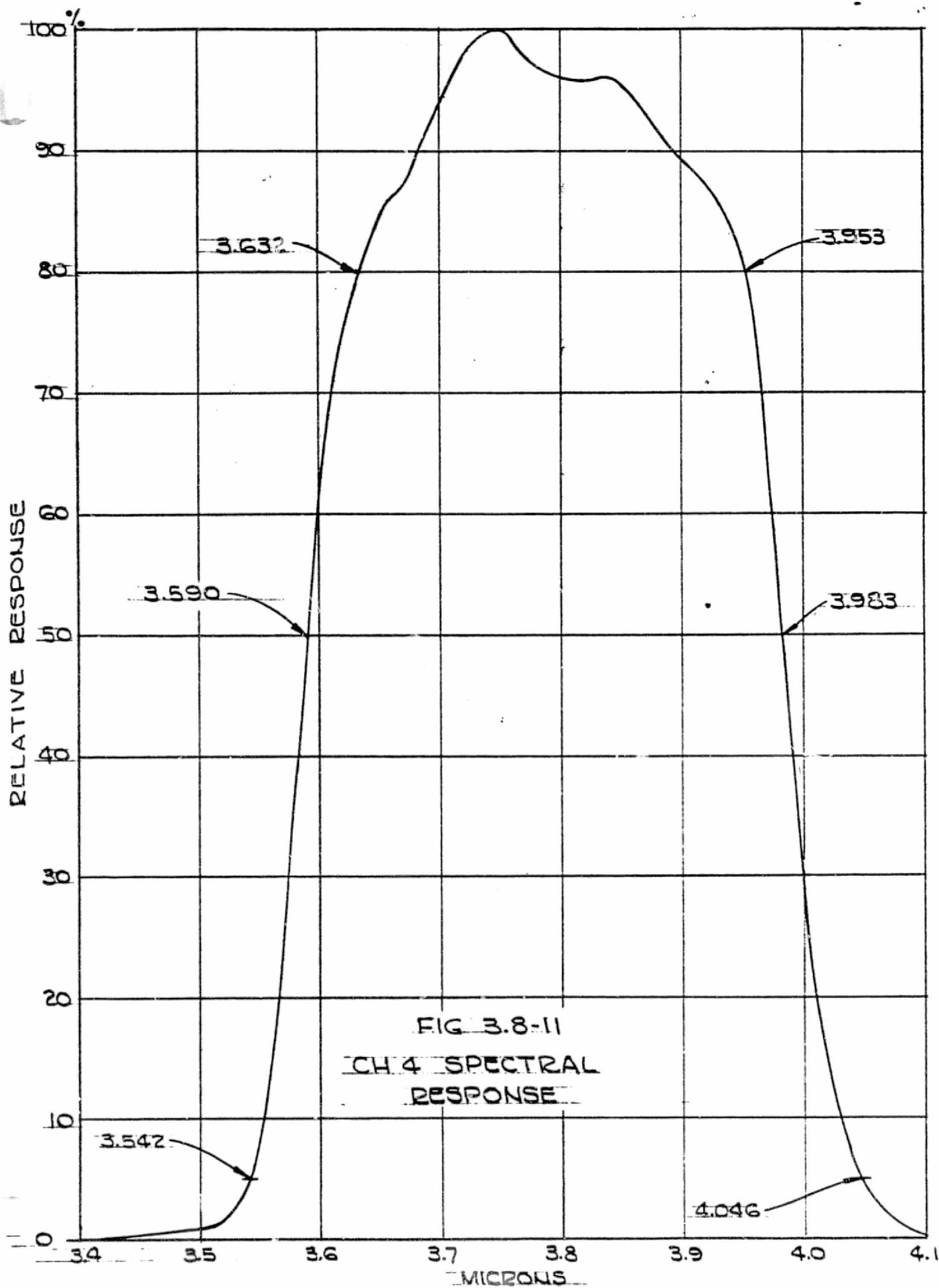
The germanium lenses have some effect on the response of Channel 3 due to their increased absorption toward longer wavelengths. This effect causes the Channel 3 response to be somewhat skewed to shorter wavelengths in the band. Figures 3.8-10 and 3.8-11 show the measured PTM channels 3 and 4 spectral response.

The out-of-band response for both channels was analyzed by graphing the product of the detector response and the 300 Kelvin emission as a function of wavelength. The area under the curves was then measured with a planimeter and the in-band value multiplied by the

TABLE 3.8-3
FILTER CHARACTERISTICS

<u>CHARACTERISTIC</u>	<u>CHANNEL 3</u>	<u>CHANNEL 4</u>
50%-of-Peak Cuton Wavelength	10.5±0.09μm	3.55±.06μm
50%-of-Peak Cutoff Wavelength	11.5±0.09μm	3.93±.06μm
Cuton and Cutoff Slopes	≤ 3%	≤ 3%
Response at 10.0 and 12.0μm	≤ 1%	N.A.
Response at 3.40 and 4.12μm	N.A.	≤ 1%
Transmission less than 0.1%	From 1.8 to 9.8μm and from 12.2 to 18.0μm	From 1.8 to 3.2μm and from 4.3 to 7.0μm
In-Band Transmission	≥ 75% Avg.	≥ 75% Avg.





expected in-band transmission (80% average) and the out-of-band value by 0.1%. The ratios of out-of-band response to in-band response were 1.6% for Channel 4 and 0.74% for Channel 3.

Measurements on the ETM and PTM verify that the response in both channels is below the 2% maximum allowed.

3.9 Channel Registration

The approach used to register the AVHRR channels consists of first registering the two thermal channels at a subassembly level. The patch, with both detectors mounted, is placed in a test vacuum dewar and illuminated through the relay optics, by a collimated beam. The collimator is a germanium lens which has a slit target and chopped radiation source. The slit is moved while the outputs of the two channels are recorded. The difference between the 50% response points is the misregistration. This is repeated with a slit rotated 90° so that the distance that each detector must move is measured. The patch is then removed from the dewar, the adjustment made, and the patch retested to verify alignment.

The following procedure is used for channel registration.

- a. Determine the physical location of the focal points for Channels 3 and 4 with reference to the optics subassembly during optics acceptance tests.
- b. Place the subassembly into the AVHRR and mount the cooler to place the detectors in their proper position.

- c. With the solar channels centered in their EFOV, determine the misregistration between all the channels. If the error is more than can be corrected by moving the solar channels, reposition the cooler to place the IR detectors in the correct location.
- d. Remeasure the misregistration and move the solar channel detectors to complete the registration procedure.

Step c. essentially eliminates the tolerance buildup problem in the instrument by actually measuring the positions and correcting accordingly. If the initial placement of the cooler is sufficiently close to place the IR detectors within the solar channel EFOV, then no cooler repositioning will be required.

The procedure has been used to register both the ETM and PTM instruments well within the specified value.

3.10 Polarization Sensitivity

An analysis was made of the polarization sensitivity of Channels 1 and 2 with the object of meeting the requirements of the GSFC Specification.

$$P = \frac{T_1 - T_2}{T_1 + T_2} \leq .053$$

This equation holds at nadir (or at 90° from nadir) as a result of the orientation of the optical elements that contribute to the polarization. (On the Flight Model instruments, the maximum allowed polarization sensitivity is .07.) The transmittances obtained for the parallel and perpendicular polarizations are the extremes for any linearly polarized wave that travels through the optical train.

The theoretical and measured polarizations of the elements are given in the tables contained in the DIR's. The channel transmittances were calculated by giving a weight of 1/2 to the spectral end points (i.e., originally 0.5 and 0.9 μm in Channel 1 and 0.75 and 1.00 μm in Channel 2; revised to 0.55 to 0.9 μm in Channel 1 and 0.725 and 1.1 μm (silicon detector cutoff) in Channel 2).

The analysis performed during the design phase of the AVHRR program considered several options including the angular position of the dichroics and beamsplitters, the addition of reflecting surfaces for compensation, and the types of coatings on reflective surfaces. The complete analysis is detailed in AVHRR D.I.R. #6 and 7.

Several changes have been made to the original polarization sensitivity design of the AVHRR. In particular, the gold dichroic has been made by OCLI so that the percent polarization of that element is considerably less than originally thought. The scan mirror coating is the major compensating element for the polarization of the gold dichroic. The high reflectivity coating used on the PTM and Flight Models also has less polarization (because the reflectivity dip around 0.86 micron is minimal). The combination results in a measured PTM polarization sensitivity as listed in Table 3.10-1. The Polarization sensitivity as a function of scan mirror position was measured on the PTM as a matter of interest. As can be seen the instrument performs quite well and it can be expected that the Flight Model units will be well within the 0.07 allowed.

TABLE 3.10-1

MEASURED PTM AVHRR POLARIZATION
SENSITIVITY

SCAN MIRROR <u>POSITION</u>	CHANNEL 1 <u>P.S.</u>	CHANNEL 2 <u>P.S.</u>
50° (Sunside)	.032	.047
25° (Sunside	.039	.049
Nadir	.037	.053
25° (Antisunside)	.038	.047
50° (Antisunside)	.030	.049

3.11 Scattered Sunlight

We have studied the following effects of direct sunlight:

- a. The temperature gradient it produces across the honeycomb of the in-flight target.
- b. Its reflection from the in-flight target and the resultant calibration errors.
- c. Scattering and the resultant signal contamination.

Because the above occurs only during the nighttime portion of the orbit, we need to consider only Channel 3 (10.5 to 11.5 μm) and Channel 4 (3.55 to 3.93 μm).

From our studies to date, we conclude that:

- a. The honeycomb gradient is not sensibly changed from its value in the 906 n mi orbit.
- b. Under the worst conditions, reflection of sunlight from the in-flight target introduces a significant error (0.65K) in Channel 4. As a result, it may be desirable to restrict the Channel 4 calibration period, e.g., to the portions of the orbit when the target is shaded by the earth, spacecraft, instruments, or sunshields (if added). The corresponding error in Channel 3 is negligible (0.002K).

The temperature errors quoted in b are for the preliminary TIROS-N instrument/spacecraft layout shown in NASA/GSFC Drawing GDSK-4799. Two separate instrument orientations are of interest, for scattering from the telescope and from the scan mirror.

3.11.1 Honeycomb Temperature Gradient

This problem was analyzed in DIR #18 (Worst Case Honeycomb Temperature Gradient in the In-Flight Thermal Calibration Target, May 9, 1974; included in Section 7.1). The analysis was revised for the new altitude of 450 n mi and the new range of sun angle β (memo of May 2, 1974). The results are:

$$\text{For } \beta \leq 27.83^\circ, \text{ min. } \theta = 62.17^\circ \text{ at } \beta = 27.83^\circ$$

$$\text{For } \beta \geq 27.83^\circ, \text{ min. } \theta = 62.17^\circ$$

$$(T_o - T_\ell)_1 = 2.513^\circ$$

$$(T_o - T_\ell)_2 = 0.639^\circ\text{C}$$

$$\text{Effective cell gradient} = (T_o - T_\ell) = 0.95^\circ\text{C}$$

$$\text{Effective calibration gradient} = 0.079 (T_o - T_\ell) = 0.075^\circ\text{C}.$$

The effective calibration gradient is not sensibly changed from its previous value of 0.077°C .

3.11.2 Sunlight Reflections from In-Flight Target

Sunlight reflected from the in-flight target introduces a calibration error in addition to those errors we have previously considered. The error is negligible in Channel 3, but can be significant in Channel 4.

The solar exitance reflected from the target is given by

$$M_s = E_s \rho \frac{A_s}{A_T}$$

- where
- E_s = direct solar incidence (irradiance) in the wavelength band and perpendicular to the sun's rays.
 - ρ = diffuse hemispherical reflectivity of the in-flight target
 - A_s = exposed target area projected perpendicular to the sun's rays
 - A_T = effective target area viewed by radiometer
= $\pi (8)^2 / 4 \text{ in}^2$.

The values of solar incidence were calculated from the table given by Thekaekara (Optical Spectra, March 1972, p. 32); the results are

$$\text{Channel 3 (10.5 - 11.5 } \mu\text{m)}, E_s = 1.71 \times 10^{-5} \text{ Wcm}^{-2}$$

$$\text{Channel 4 (3.55 - 3.93 } \mu\text{m)}, E_s = 2.52 \times 10^{-4} \text{ Wcm}^{-2}$$

The reflectivity ρ can be calculated from the limiting formula of Treuenfels (J. Opt. Soc. Am. 53, 1162, 1963) or by interpolation from the graph of Sparrow and Cess (Radiation Heat Transfer, Brooks/Cole, 1966 p. 165). In either case, an assumed paint emissivity of 0.92 (3M 401 black) results in a hemispherical cavity emissivity of 0.980 and a reflectivity of 0.020. As shown in the graph of Sparrow and Cess, the limiting emissivity of a cylindrical cavity is reached at a length to radius ratio of about 2:1 when the paint emissivity exceeds 0.7. The length to radius ratio of a honeycomb cavity is 8:1. The ratio of flat to total target area is 0.045, so that the hemispherical reflectivity is 0.0227. It would be desirable to have spectral emissivity (or reflectivity) data on the 3M 401 in the bands of interest. However, data could only be found for 3M 101 and; therefore, an average 401 value of approximately 0.92 was used.

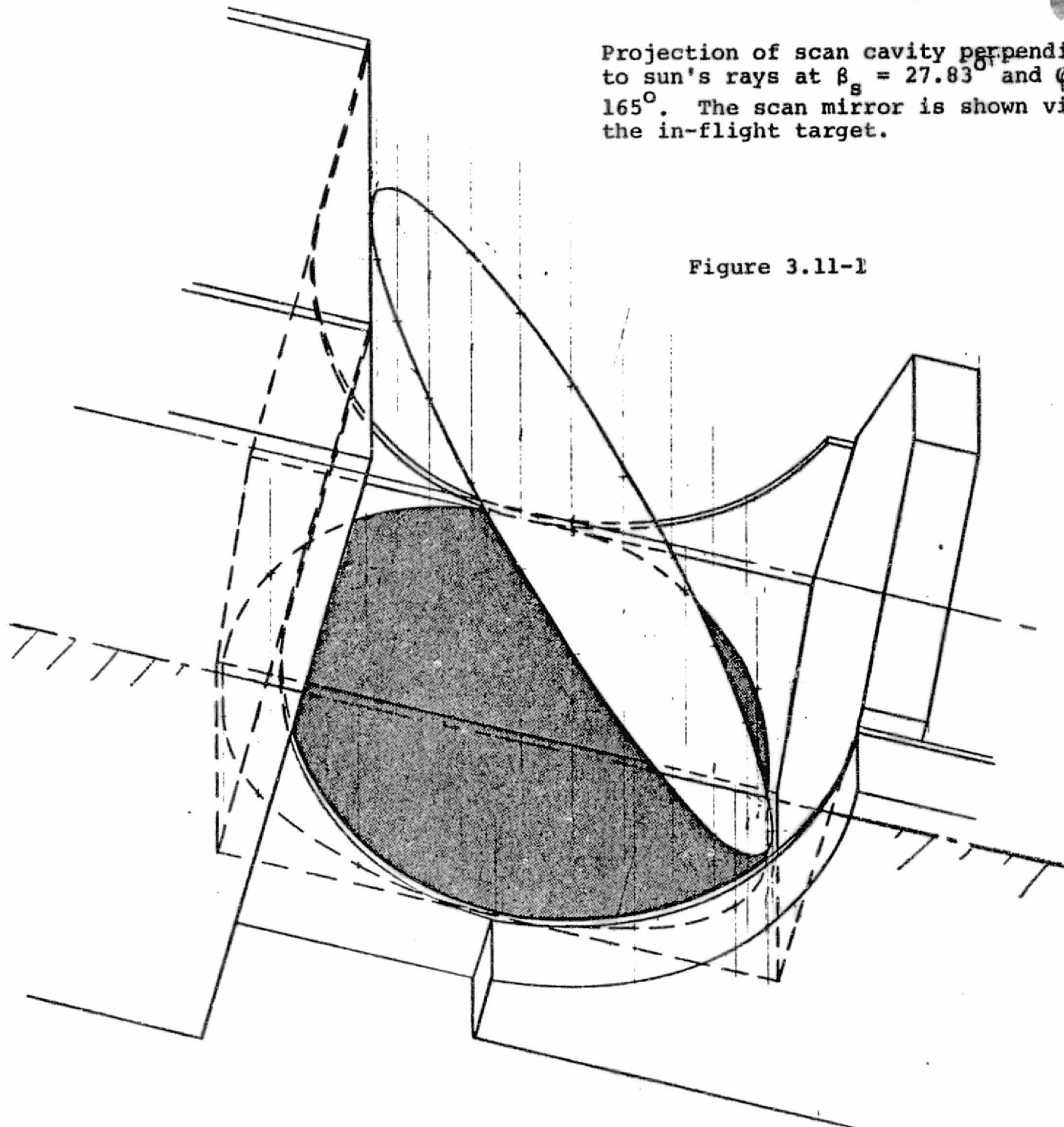
The exposed area A_s normal to the sun's rays was determined from scan cavity projections supplied by J. D. Crawford. The worst case situation is shown in Figure 3.11-1. It occurs at a β angle of 27.83° , when the spacecraft leaves the earth's shadow, and an orbital position 15° north of the plane of the ecliptic in the night-time part of the orbit. The value of A is 10.9 square inches when shading from the anticipated spacecraft is included. We then have (in the absence of any sun shield)

$$M_s \text{ (Ch. 3)} = 8.43 \times 10^{-8} \text{ Wcm}^{-2}$$

$$M_s \text{ (Ch. 4)} = 1.24 \times 10^{-6} \text{ Wcm}^{-2}$$

Projection of scan cavity perpendicular
to sun's rays at $\beta_s = 27.83^\circ$ and $\phi_s =$
 165° . The scan mirror is shown viewing
the in-flight target.

Figure 3.11-1



The comparative effect of the reflected sunlight is shown in Figure 3.11-2. In Channel 3, the sunlight produces an exitance level that is more than 4 orders of magnitude below that of the 295K self-emission. On the other hand, the reflected sunlight in Channel 4 is only about an order of magnitude below the self-emission.

The calibration error introduced by reflected sunlight may be expressed as an effective temperature increase; it is given by

$$\delta T_s = \frac{M_s}{dM/dT}$$

where dM/dT is the rate of change of in-band blackbody exitance at the nominal target temperature of 295K (22°C). For the bands of interest, we have

$$\frac{dM}{dT} \text{ (Ch. 3)} = 4.263 \times 10^{-5} \text{ Wcm}^{-2} \text{ K}^{-1} \text{ at } T = 295\text{K}$$

$$\frac{dM}{dT} \text{ (Ch. 4)} = 1.905 \times 10^{-6} \text{ Wcm}^{-2} \text{ K}^{-1} \text{ at } T = 295\text{K}$$

The calibration errors for the worst case are then

$$\delta T_s \text{ (Ch. 3)} = 0.002^\circ\text{C}$$

$$\delta T_s \text{ (Ch. 4)} = 0.65^\circ\text{C}$$

3.11.3 Signal Contamination

With the AVHRR mounted as shown in Figure 2 of GSFC Specification S-731-P-118 (Rev. C), there is a large effective sunshield (i.e., the spacecraft itself) that limits direct solar exposure of the instrument to the night-time portion of the orbit. During this time, of course, Channels 1 and 2 are not used. As a result, we need to consider the effect of scattered sunlight only in Channels 3 and 4. In common with the reflections from the in-flight target, the larger effect is in Channel 4.

REPRODUCIBILITY OF THE
ORIGINAL PAGE IS POOR

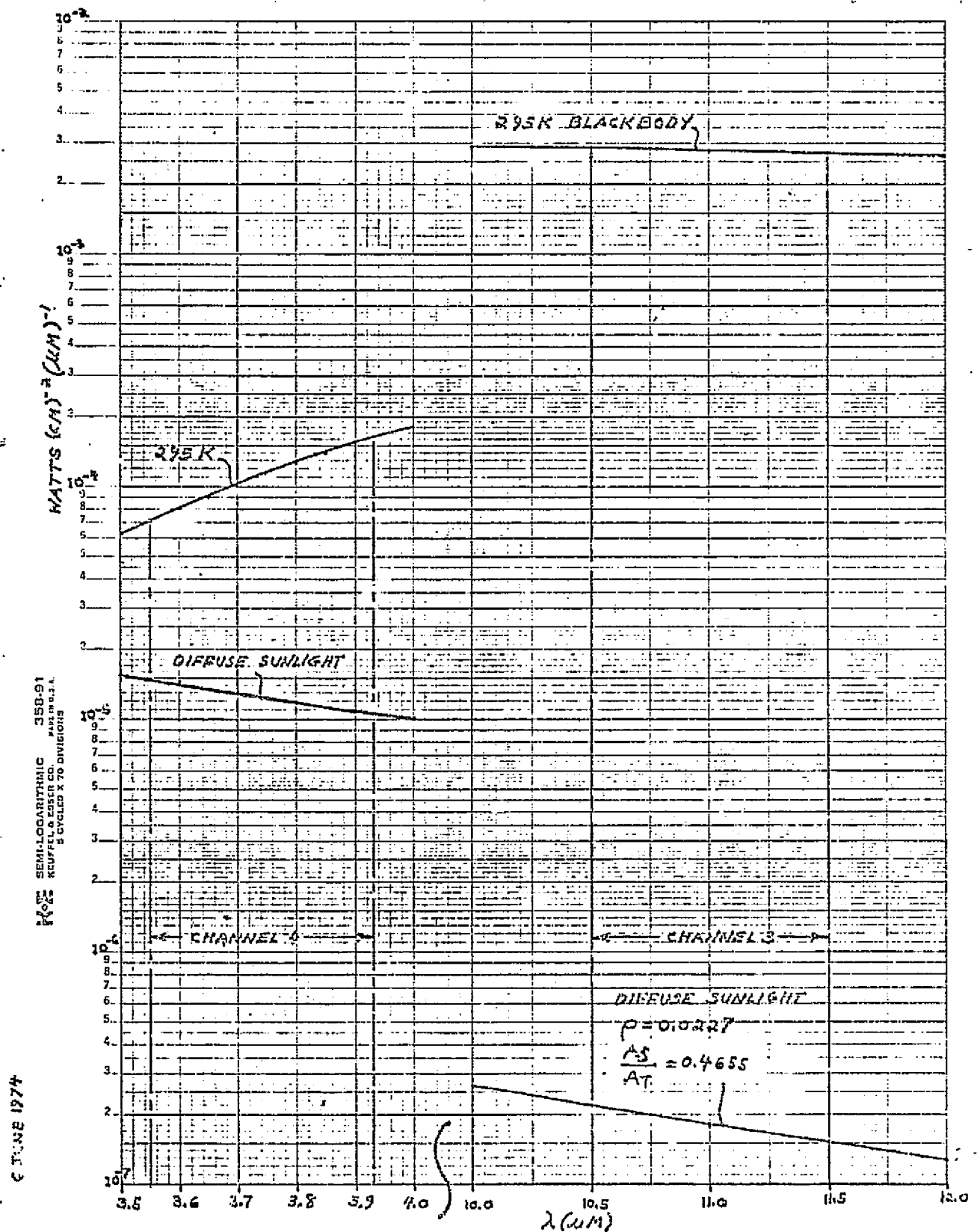


Figure 3.11-2 Comparative Effect of Reflected Sunlight

We may define the required attenuation coefficient for scattered sunlight as the normal solar incidence (irradiance) outside the earth's atmosphere divided by one-third of the minimum radiant signal,

$$a = \frac{E_s}{(1/3) (NER) A\Omega}$$

where NER = noise equivalent radiance = 1.6×10^{-6}

$\text{Wcm}^{-2} \text{ster}^{-1}$ (Ch. 3), 8.0×10^{-8}

$\text{Wcm}^{-2} \text{ster}^{-1}$ (Ch. 4)

$A\Omega$ = throughput of optics = $5.43 \times 10^{-4} \text{ cm}^2 \text{ster}$.

The NER values were supplied by R. J. Koczor for the nominal spectral bands and a 0.12K NETD. We therefore require

$$a(\text{Ch. 3}) = 5.87 \times 10^4 \text{ cm}^{-2} = 3.79 \times 10^5 \text{ in}^{-2}$$

$$a(\text{Ch. 4}) = 1.74 \times 10^7 \text{ cm}^{-2} = 1.12 \times 10^8 \text{ in}^{-2}$$

Attenuation coefficients for scattered sunlight were measured as part of an earlier study on the HRIR (Final Technical Report, Solar Sun Shield Study for the HRIR on TIROS-M Satellite, Feb. 6, 1967, ITT-A/OD Report No. 14-16400). The HRIR had a $3.7 \mu\text{m}$ band channel and was to operate in a 750 to 900 n mi sun-synchronous orbit over a sun angle range from 37.5° to 50° . The instrument had a modest external shield and simple internal baffles with a Cassegrain telescope and a reflective secondary optic. With the scan mirror looking 45° from nadir on the sun side, attenuation coefficients of $0.6 \times 10^8 \text{ in}^{-2}$ and higher were measured, the value depending on the sun angle and orbital position.

3.11.4 Sun Scatter Test Results

The BBM AVHRR was tested to determine the level of scattered light getting into Channels 1, 2 and 4. The tests for Channels 1 and 2 were run together while that for Channel 4 required a modified set up.

3.11.4.1 Channel 1 & 2 Test Setup

The BBM was placed on a 2-axis rotary table which rotated the instrument about its pitch and yaw axes. A 9 inch aperture Astrola telescope was used to illuminate the scan cavity. A 24 Hz chopper and a tungsten iodide lamp (with a Lucalox diffuser) were used as the radiation source at the Astrola focal plane.

Signals were taken out of the Channels 1 and 2 preamplifiers (to reduce system noise) and fed to an electrical bandpass filter (20 to 31 Hz) then to a Ballantine True RMS voltmeter. The BBM was operated from the P.T.E.

3.11.4.2 Test Procedure

As discussed in Section 3.11.3 the procedure is to calculate an attenuation factor for the scattered light at various angles of irradiance. The detectors in the BBM were used for the test. They were removed from the unit (mechanically not electrically) and illuminated directly by the chopped collimator signal, thru the appropriate spectral filter. They were then placed back in the unit in their proper location to measure any scattered signal.

The collimator is used to irradiate the scan cavity at sun angles θ of 0° to 67° and orbit angles μ_s of 280° to 230° . Initial readings were taken with the scan mirror positioned at nadir and $\pm 45^\circ$ from nadir; however, no change was observed and so further testing was done with a nadir-looking scan mirror only.

3.11.4.3 Test Results Channel 1 & 2

The data obtained in this phase of the test is given in Table 3.11-1. The data is given as a function of sun angle then orbit angle. The irradiance level signal measured at the scan cavity was 6.40 volts in Channel 2 and 4.00 volts in Channel 1. As can be

Measured Irradiance Onto Scan Cavity

Channel 1 4.0 volts

Channel 2 6.4 volts

SUN ANGLE	ORBIT ANGLE	CHANNEL 1 SIGNAL			CHANNEL 2 SIGNAL		
		.58 mv	NADIR	-45°	+45°	NADIR	-45°
67°	280°	.58 mv	.58 mv	.60 mv	.53 mv	.55 mv	.53 mv
	270	.56	.58	.61	.52	.53	.54
	260	.62	.63	.62	.51	.53	.53
	250	.60	.60	.63	.52	.53	.55
	240	.63	.60	.62	.54	.52	.57
	230	.66	.63	.66	.56	.57	.58
58°	280	.65	.60	.60	.55	.50	.52
	270	.65	.65	.65	.50	.50	.50
	260	.58	.60	.60	.53	.46	.53
	250	.56	.57	.57	.45	.48	.52
	240	.58	.62	.57	.51	.50	.50
	230	.57	.57	.58	.55	.53	.53
50°	280	.62	.56	.60	.52	.54	.62
	270	.60	.61	.59	.54	.53	.52
	260	.60	.60	.58	.52	.51	.51
	250	.65	.63	.62	.54	.50	.53
	240	.65	.62	.64	.55	.54	.54
	230	.64	.67	.65	.63	.62	.64
41°	280		.62			.55	
	270		.58			.52	
	260		.58			.52	
	250		.60			.56	
	240		.62			.60	
	230		.63			.60	
29°	280°		.55 mv			.58 mv	
	270		.56			.59	
	260		.62			.58	
	250		.65			.58	
	240		.63			.61	
	230		.63			.60	
18°	280		.58			.55	
	270		.60			.57	
	260		.63			.57	
	250		.60			.60	
	240		.60			.60	
	230		.56			.56	
9°	280		.63			.56	
	270		.61			.57	
	260		.61			.59	
	250		.62			.61	
	240		.60			.60	
	230		.61			.62	

TABLE 3.11-1

CHANNELS 1 & 2 SCATTERED SIGNAL AND NOISE LEVEL

seen in Table 3.11-1, the measured signal and noise level Channel 1 was on the order of 0.65 m volts. This is a ratio of

$$\frac{4000}{.65} = 6150:1$$

Similarly in Channel 2 the ratio is

$$\frac{6400}{.58} = 11000:1$$

There was no evidence of a measurable scattered light signal in either channel at any of the measurement points. This was verified by blocking off the source. The numbers given in the Table are only the noise in the test setup.

Using the formula given earlier, we have

$$a = \frac{E_s}{E_{s/\pi} \times .005 \times 1/3 \times \Omega A}$$

In the above case the coefficient gives the attenuation required for the scatter to be equal to the specified noise equivalent albedo ($1/3$ of $1/2^*$). Using the coefficient we can calculate the required ratio of S_1 (collimator irradiance) to S_2 (scatter signal measured in system) as

$$S_1/S_2 = A_d \times A$$

Where A_d is the test detector area. In our case AVHRR thruput is $5.43 \times 10^{-4} \text{ cm}^2 \text{ ster}$ (including secondary obscuration) so that

$$a = 2.24 \times 10^7 \text{ in}^{-2}$$

The test detector has a 0.010" square aperture so that the ratio that would be measured in the test set up if the scattered signal were equivalent to the specified Noise Equivalent Albedo is

$$S_1/S_2 = (.01)^2 \times 2.24 \times 10^7 = 2240:1$$

In both channels our test ratio was at least 3x better than this. Therefore, we conclude that if there is any scattered signal in the orbits and at the angles measured (which are the computer-projected "worst cases"), they are at least three times less than the Noise Equivalent Albedo specified.

3.11.4.4 Channel 4 Test Set Up

The BBM AVHRR was in place on the two axis table with the collimator in position as for Ch 1 and 2. However, an .027" square active area InSb detector was placed at the focus of the IR Relay lenses. A Channel 4 filter is set in place in front of the detector so that only the spectral band of interest is viewed. This detector-filter combination is placed at the scan cavity for incidence measurement as above. The radiance source is a 900°C blackbody source chopped as before at 24 Hz.

The scan mirror was checked at several angles on various sun positions, but no measurable effect was observed. All recorded data is for the scan mirror at nadir.

The procedure was basically identical to that previously described; however, since Channel 4 can be used at night, the orbital angles which were checked were extended to a range of 230° to 310°. Table 3.11-2 gives the measured results.

3.11.4.5 Test Results Channel 4

The maximum measured scattered signal plus noise was 85 microvolts. With an incidence signal of .636 volts, we have a ratio of

$$\frac{636000}{85} = 7480:1$$

ORBIT
ANGLE
S

SUN ANGLE β_s

	<u>7°</u>	<u>18°</u>	<u>29°</u>	<u>38°</u>	<u>48°</u>	<u>54°</u>	<u>67°</u>
230°	20	20	15	15	20	15	25
240	20	20	15	15	25	20	30
250	20	15	15	15	15	30	25
260	15	25	20	20	25	20	30
270	25	30	20	25	45	50	85
280	15	25	25	20	25	35	30
290	20	20	30	15	20	20	15
300	20	15	15	15	30	25	25
310	25	15	15	30	20	25	20

Readings are in microvolts

MEASURED IRRADIANCE ONTO SCAN CAVITY IS .636 volt rms

1 NER = 24 microvolts

TABLE 3.11-2

CHANNEL 4 SCATTERED SIGNAL PLUS NOISE LEVELS

The required attenuation coefficient for Channel 4 has been calculated to be $1.12 \times 10^8 \text{ in}^{-2}$ for a scattered signal equal to 1/3 NER. The ratio S_1/S_2 for this channel is

$$S_1/S_2 = (1.12 \times 10^8) (.027 \text{ in})^2 = 81650$$

where .027" is the InSb detector width. This means that the maximum scattered signal found is equivalent to

$$\frac{81650}{3 \times 7480} = 3.6 \text{ NER}$$

SUMMARY

Measurements in the solar channels indicate that no measurable scattering exists in these channels at solar incidence angles which computer projections indicate are worst case conditions. In Channel 4, the measured scattered signal is less than two NER's for orbits with sun angles below about 48° and at all orbit angles except 270° . The maximum measured anywhere is 3.6 NER's.

It is apparent that no sun shield is required for the solar channels. Further because of the low level and limited extent of the scattered signal in Channel 4, it is probable that no sun shield is required in that channel. Further, assuming a reasonably sized shield attached to the AVHRR, it is not possible to eliminate the scattered signal completely since the irradiance is reaching the telescope through the shield area which would be cut out to allow an earth view at the maximum scan angle.

4.0 MECHANICAL DESCRIPTION

4.1 Overall Instrument Configuration

The AVHRR instrument design provides for a basically modular configuration. An exploded view of the instrument which depicts the various modules is shown in Figure 4.1-1. The basic modules are:

1. Base plate with related cover plates
2. Scanner
3. Optics
4. Radiant Cooler
5. Electronics

An outline drawing of the assembled instrument is shown in ITT Drawing No. 8008778 which is reproduced in Figure 4.1-2.

4.1.1 Structure

The baseplate can be seen in Figure 4.1-1. Provision is made for locating the scanner and optics on the base plate by means of dowel pins. The radiant cooler is positioned by means of shims in order to align the Channel 3 and 4 detectors to the optical axis. The electronics package attaches to the side of the instrument by means of machine screws and dowel pins for rigidity.

The structural integrity of the instrument was proven during the extensive vibration testing given both the Mechanical Structural Model and the Engineering Model. The Engineering Model successfully passed vibration tests per ITT Procedure No. 8120266 and acceleration tests per ITT No. 8120267 with the exception of

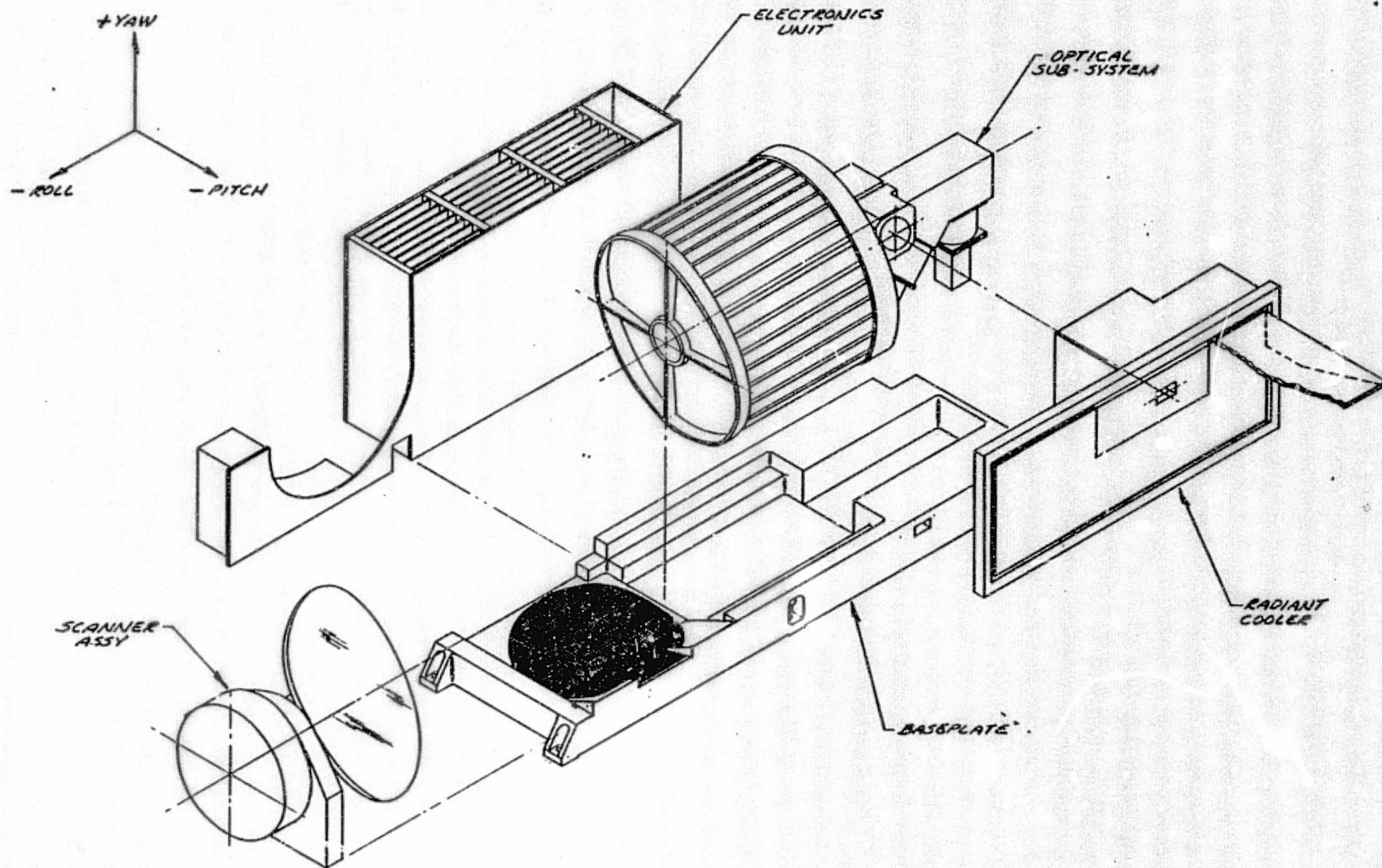


Figure 4.1-1 AVHRR Modules

NOTES (CONTINUED)

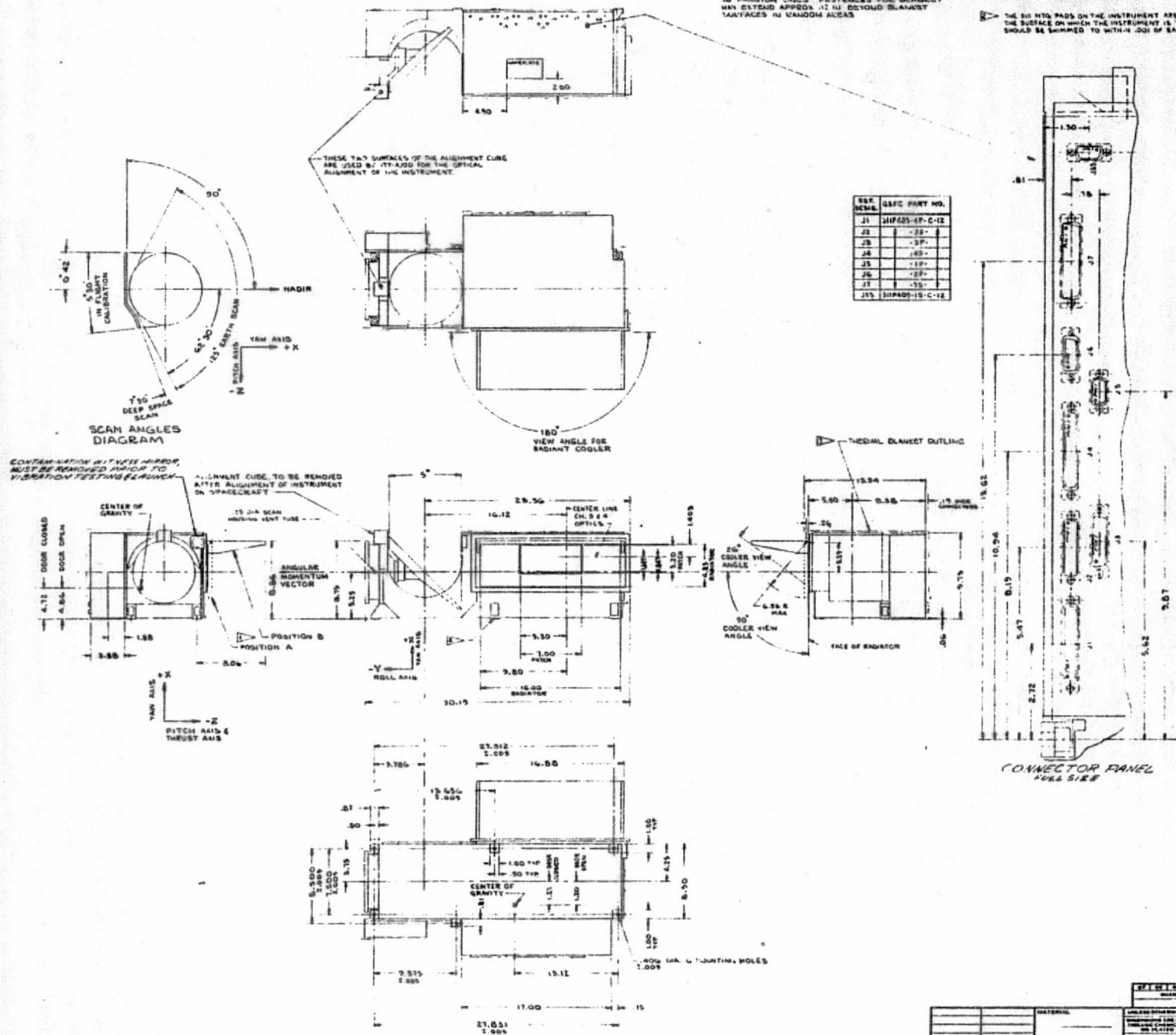
OVERALL DIMENSIONS DO NOT INCLUDE THERMAL BLANKET. THERMAL BLANKET EXTENDS APPROX 25 INCHES OVER OUTSIDE SURFACES AS SHOWN IN DIMENSION LINES. FASTENERS FOR BLANKET MAY EXTEND APPROX 12 IN BEYOND BLANKET SURFACES IN RANDOM AREAS.

NOTES:

RADIANT COOLER SHIELD TO BE IN POSITION A DURING LAUNCH AND IN POSITION B FOR NORMAL COOLER OPERATION IN ORBIT.

THE SIX HTA PADS ON THE INSTRUMENT ARE PLACED WITHIN 20% OF THE SURFACE ON WHICH THE INSTRUMENT IS TO BE MOUNTED SHOULD BE SHIPPED TO WITHIN 30% OF EACH HTA PAD.

REV	DESCRIPTION	DATE	BY	CHKD
1	REVISED CONNECTOR PANEL	1-2-74	WJ	WJ
2	ADDED CONNECTOR LOCATION SHY	8-21-74	WJ	WJ
3	ADDED CENTER OF GRAVITY	9-1-74	WJ	WJ
4	REVISED CENTER OF GRAVITY	10-1-74	WJ	WJ
5	ADDED CENTER OF GRAVITY	10-1-74	WJ	WJ
6	ADDED CENTER OF GRAVITY	10-1-74	WJ	WJ
7	ADDED CENTER OF GRAVITY	10-1-74	WJ	WJ
8	ADDED CENTER OF GRAVITY	10-1-74	WJ	WJ
9	ADDED CENTER OF GRAVITY	10-1-74	WJ	WJ
10	ADDED CENTER OF GRAVITY	10-1-74	WJ	WJ
11	ADDED CENTER OF GRAVITY	10-1-74	WJ	WJ
12	ADDED CENTER OF GRAVITY	10-1-74	WJ	WJ
13	ADDED CENTER OF GRAVITY	10-1-74	WJ	WJ
14	ADDED CENTER OF GRAVITY	10-1-74	WJ	WJ
15	ADDED CENTER OF GRAVITY	10-1-74	WJ	WJ
16	ADDED CENTER OF GRAVITY	10-1-74	WJ	WJ
17	ADDED CENTER OF GRAVITY	10-1-74	WJ	WJ
18	ADDED CENTER OF GRAVITY	10-1-74	WJ	WJ
19	ADDED CENTER OF GRAVITY	10-1-74	WJ	WJ
20	ADDED CENTER OF GRAVITY	10-1-74	WJ	WJ
21	ADDED CENTER OF GRAVITY	10-1-74	WJ	WJ
22	ADDED CENTER OF GRAVITY	10-1-74	WJ	WJ
23	ADDED CENTER OF GRAVITY	10-1-74	WJ	WJ
24	ADDED CENTER OF GRAVITY	10-1-74	WJ	WJ
25	ADDED CENTER OF GRAVITY	10-1-74	WJ	WJ
26	ADDED CENTER OF GRAVITY	10-1-74	WJ	WJ
27	ADDED CENTER OF GRAVITY	10-1-74	WJ	WJ
28	ADDED CENTER OF GRAVITY	10-1-74	WJ	WJ
29	ADDED CENTER OF GRAVITY	10-1-74	WJ	WJ
30	ADDED CENTER OF GRAVITY	10-1-74	WJ	WJ
31	ADDED CENTER OF GRAVITY	10-1-74	WJ	WJ
32	ADDED CENTER OF GRAVITY	10-1-74	WJ	WJ
33	ADDED CENTER OF GRAVITY	10-1-74	WJ	WJ
34	ADDED CENTER OF GRAVITY	10-1-74	WJ	WJ
35	ADDED CENTER OF GRAVITY	10-1-74	WJ	WJ
36	ADDED CENTER OF GRAVITY	10-1-74	WJ	WJ
37	ADDED CENTER OF GRAVITY	10-1-74	WJ	WJ
38	ADDED CENTER OF GRAVITY	10-1-74	WJ	WJ
39	ADDED CENTER OF GRAVITY	10-1-74	WJ	WJ
40	ADDED CENTER OF GRAVITY	10-1-74	WJ	WJ
41	ADDED CENTER OF GRAVITY	10-1-74	WJ	WJ
42	ADDED CENTER OF GRAVITY	10-1-74	WJ	WJ
43	ADDED CENTER OF GRAVITY	10-1-74	WJ	WJ
44	ADDED CENTER OF GRAVITY	10-1-74	WJ	WJ
45	ADDED CENTER OF GRAVITY	10-1-74	WJ	WJ
46	ADDED CENTER OF GRAVITY	10-1-74	WJ	WJ
47	ADDED CENTER OF GRAVITY	10-1-74	WJ	WJ
48	ADDED CENTER OF GRAVITY	10-1-74	WJ	WJ
49	ADDED CENTER OF GRAVITY	10-1-74	WJ	WJ
50	ADDED CENTER OF GRAVITY	10-1-74	WJ	WJ
51	ADDED CENTER OF GRAVITY	10-1-74	WJ	WJ
52	ADDED CENTER OF GRAVITY	10-1-74	WJ	WJ
53	ADDED CENTER OF GRAVITY	10-1-74	WJ	WJ
54	ADDED CENTER OF GRAVITY	10-1-74	WJ	WJ
55	ADDED CENTER OF GRAVITY	10-1-74	WJ	WJ
56	ADDED CENTER OF GRAVITY	10-1-74	WJ	WJ
57	ADDED CENTER OF GRAVITY	10-1-74	WJ	WJ
58	ADDED CENTER OF GRAVITY	10-1-74	WJ	WJ
59	ADDED CENTER OF GRAVITY	10-1-74	WJ	WJ
60	ADDED CENTER OF GRAVITY	10-1-74	WJ	WJ
61	ADDED CENTER OF GRAVITY	10-1-74	WJ	WJ
62	ADDED CENTER OF GRAVITY	10-1-74	WJ	WJ
63	ADDED CENTER OF GRAVITY	10-1-74	WJ	WJ
64	ADDED CENTER OF GRAVITY	10-1-74	WJ	WJ
65	ADDED CENTER OF GRAVITY	10-1-74	WJ	WJ
66	ADDED CENTER OF GRAVITY	10-1-74	WJ	WJ
67	ADDED CENTER OF GRAVITY	10-1-74	WJ	WJ
68	ADDED CENTER OF GRAVITY	10-1-74	WJ	WJ
69	ADDED CENTER OF GRAVITY	10-1-74	WJ	WJ
70	ADDED CENTER OF GRAVITY	10-1-74	WJ	WJ
71	ADDED CENTER OF GRAVITY	10-1-74	WJ	WJ
72	ADDED CENTER OF GRAVITY	10-1-74	WJ	WJ
73	ADDED CENTER OF GRAVITY	10-1-74	WJ	WJ
74	ADDED CENTER OF GRAVITY	10-1-74	WJ	WJ
75	ADDED CENTER OF GRAVITY	10-1-74	WJ	WJ
76	ADDED CENTER OF GRAVITY	10-1-74	WJ	WJ
77	ADDED CENTER OF GRAVITY	10-1-74	WJ	WJ
78	ADDED CENTER OF GRAVITY	10-1-74	WJ	WJ
79	ADDED CENTER OF GRAVITY	10-1-74	WJ	WJ
80	ADDED CENTER OF GRAVITY	10-1-74	WJ	WJ
81	ADDED CENTER OF GRAVITY	10-1-74	WJ	WJ
82	ADDED CENTER OF GRAVITY	10-1-74	WJ	WJ
83	ADDED CENTER OF GRAVITY	10-1-74	WJ	WJ
84	ADDED CENTER OF GRAVITY	10-1-74	WJ	WJ
85	ADDED CENTER OF GRAVITY	10-1-74	WJ	WJ
86	ADDED CENTER OF GRAVITY	10-1-74	WJ	WJ
87	ADDED CENTER OF GRAVITY	10-1-74	WJ	WJ
88	ADDED CENTER OF GRAVITY	10-1-74	WJ	WJ
89	ADDED CENTER OF GRAVITY	10-1-74	WJ	WJ
90	ADDED CENTER OF GRAVITY	10-1-74	WJ	WJ
91	ADDED CENTER OF GRAVITY	10-1-74	WJ	WJ
92	ADDED CENTER OF GRAVITY	10-1-74	WJ	WJ
93	ADDED CENTER OF GRAVITY	10-1-74	WJ	WJ
94	ADDED CENTER OF GRAVITY	10-1-74	WJ	WJ
95	ADDED CENTER OF GRAVITY	10-1-74	WJ	WJ
96	ADDED CENTER OF GRAVITY	10-1-74	WJ	WJ
97	ADDED CENTER OF GRAVITY	10-1-74	WJ	WJ
98	ADDED CENTER OF GRAVITY	10-1-74	WJ	WJ
99	ADDED CENTER OF GRAVITY	10-1-74	WJ	WJ
100	ADDED CENTER OF GRAVITY	10-1-74	WJ	WJ



REPRODUCIBILITY OF THE ORIGINAL PAGE IS POOR

FIG 4.1-2

AVHRR INSTRUMENT INSTRUMENT SPECIFICATIONS INSTRUMENT NO. 31550 INSTRUMENT NAME AVHRR INSTRUMENT TYPE AVHRR INSTRUMENT WEIGHT 1.000 INSTRUMENT LENGTH 1.000 INSTRUMENT WIDTH 1.000 INSTRUMENT HEIGHT 1.000 INSTRUMENT DENSITY 1.000 INSTRUMENT MATERIAL 1.000 INSTRUMENT FINISH 1.000 INSTRUMENT TOLERANCE 1.000 INSTRUMENT SURFACE 1.000 INSTRUMENT COATING 1.000 INSTRUMENT PAINT 1.000 INSTRUMENT LABEL 1.000 INSTRUMENT MARKING 1.000 INSTRUMENT IDENTIFICATION 1.000 INSTRUMENT RECORDING 1.000 INSTRUMENT STORAGE 1.000 INSTRUMENT TRANSPORT 1.000 INSTRUMENT USE 1.000		LIST OF MATERIALS OR PARTS LIST MATERIAL QUANTITY PART NO. DESCRIPTION UNIT TOTAL COMMENTS		AVHRR INSTRUMENT INSTRUMENT NO. 31550 INSTRUMENT NAME AVHRR INSTRUMENT TYPE AVHRR INSTRUMENT WEIGHT 1.000 INSTRUMENT LENGTH 1.000 INSTRUMENT WIDTH 1.000 INSTRUMENT HEIGHT 1.000 INSTRUMENT DENSITY 1.000 INSTRUMENT MATERIAL 1.000 INSTRUMENT FINISH 1.000 INSTRUMENT TOLERANCE 1.000 INSTRUMENT SURFACE 1.000 INSTRUMENT COATING 1.000 INSTRUMENT PAINT 1.000 INSTRUMENT LABEL 1.000 INSTRUMENT MARKING 1.000 INSTRUMENT IDENTIFICATION 1.000 INSTRUMENT RECORDING 1.000 INSTRUMENT STORAGE 1.000 INSTRUMENT TRANSPORT 1.000 INSTRUMENT USE 1.000	
--	--	--	--	---	--

channel registration. The required registration stability was achieved on the PFM after improved methods of securing certain optical elements were incorporated into the design and pinning and staking procedures were improved.

In order to prove the structural integrity of the radiant cooler prior to vibration, a computer analysis of the configuration was conducted by Computer Sciences Corp. and Butler Analyses, Inc., under NASA Contract NAS 5-24012 Mod. 10. Copies of the Final Report of this analysis were reviewed and are on file.

4.1.2 Materials in Structure

The primary structural material is 6061-T6 Aluminum tooling plate (Alcoa Type 200). The scanner housing is fabricated from HP-20 grade Beryllium or equivalent. In some low stress areas structural parts are fabricated from AZ31B magnesium.

The magnesium surfaces are finished with DOW-7, and the aluminum is finished with Alodine 600. Where thermal control is required, the surfaces are painted.

Beryllium is electroless nickel plated.

4.2 Scanner Subassembly

An assembly drawing of the scanner is shown in ITT Drawing No. 8009201 which is reproduced in Figure 4.2-1.

4.2.1 Scan Motor

The 80 pole hysteresis synchronous scan motor was procured from Schaeffer Magnetics, Inc., Chatsworth, California. The motor is described in ITT Specification No. 8007929. Typical performance test curves for the scanner motors are shown in Figures 4.2-2 through 4.2-5.

LTM MOTOR 5/1004
KRYTOX LUBE
2-6-74

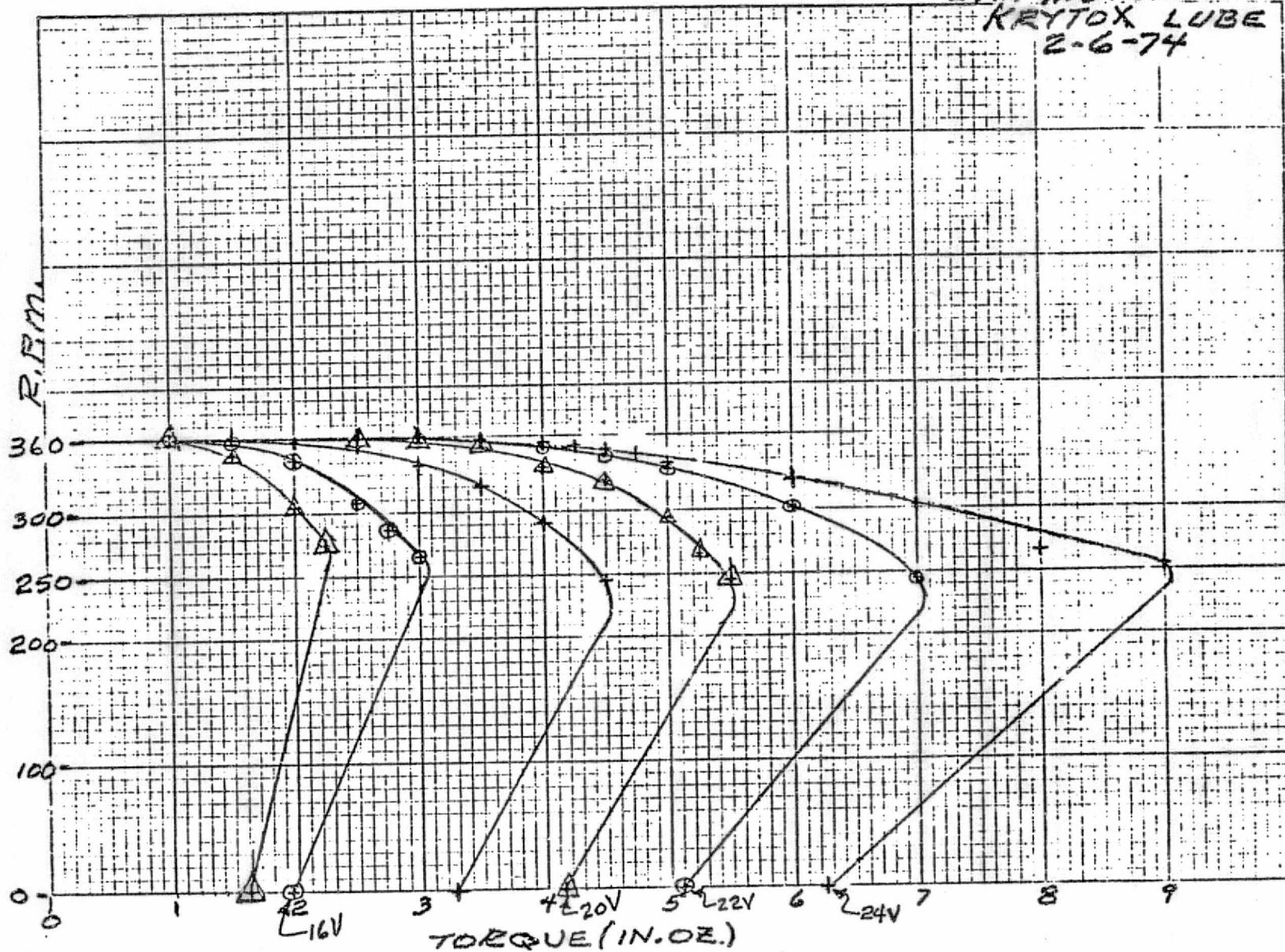


Figure 4.2-2

ETM MOTOR (9N002)
 KRYTOX LUBE
 2-5-74

REPRODUCIBILITY OF THE
 ORIGINAL PAGE IS POOR

R.P.M.

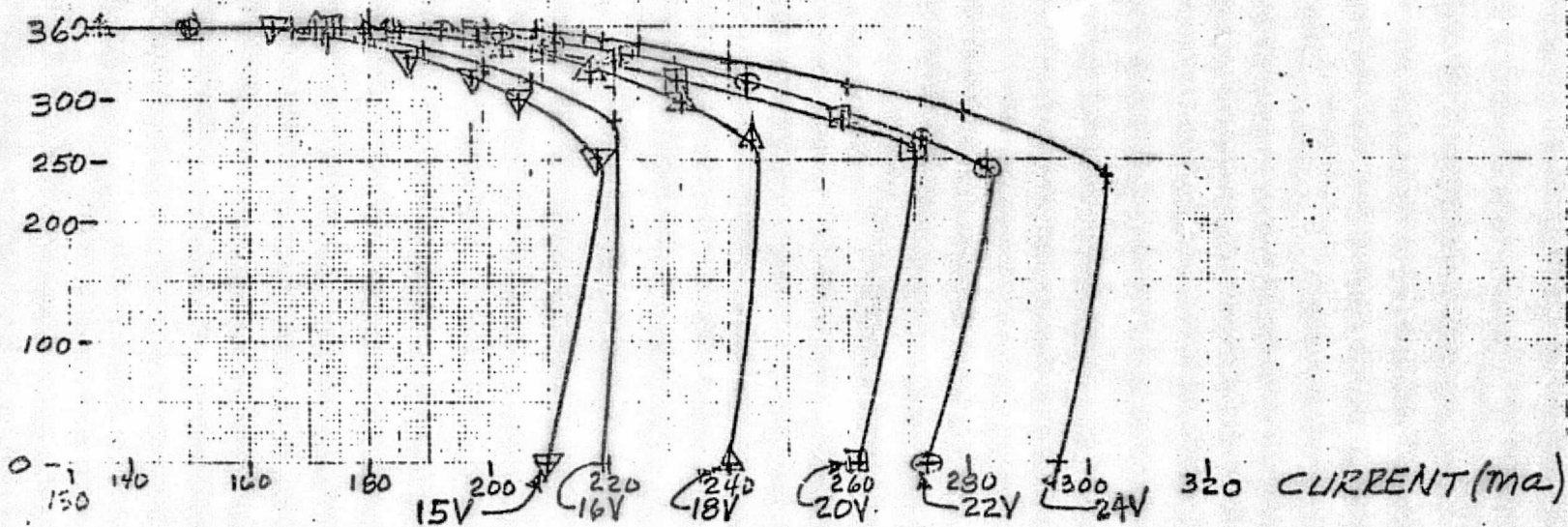


Figure 4.2-3

REPRODUCIBILITY OF THE
ORIGINAL PAGE IS POOR

K&E 10 X 10 TO THE INCH 46 0703
7 X 10 INCHES
KUFFEL & EDDER CO.

ETM MOTOR 3/4N002
KRYTOX LUBE
2-5-74

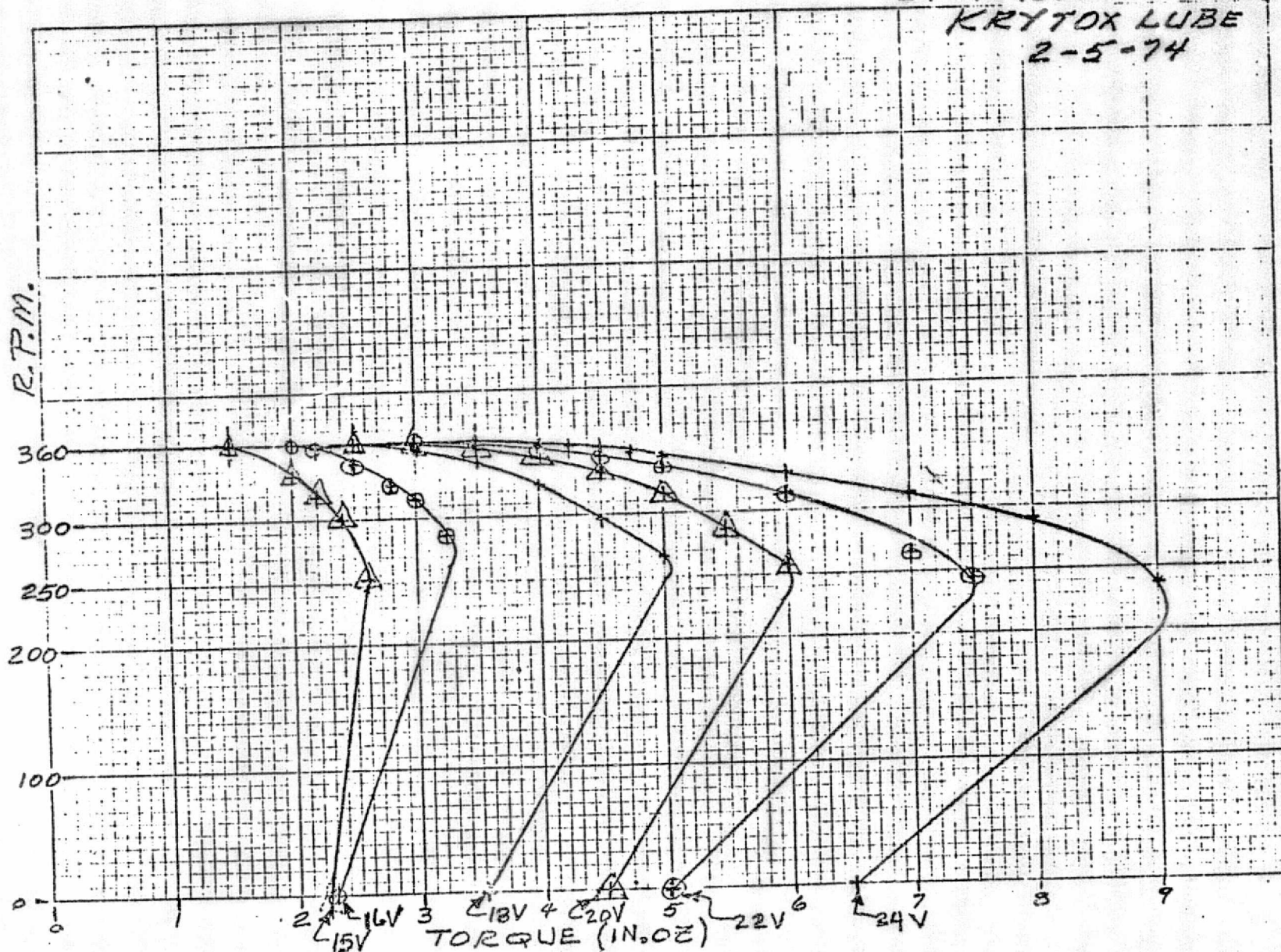
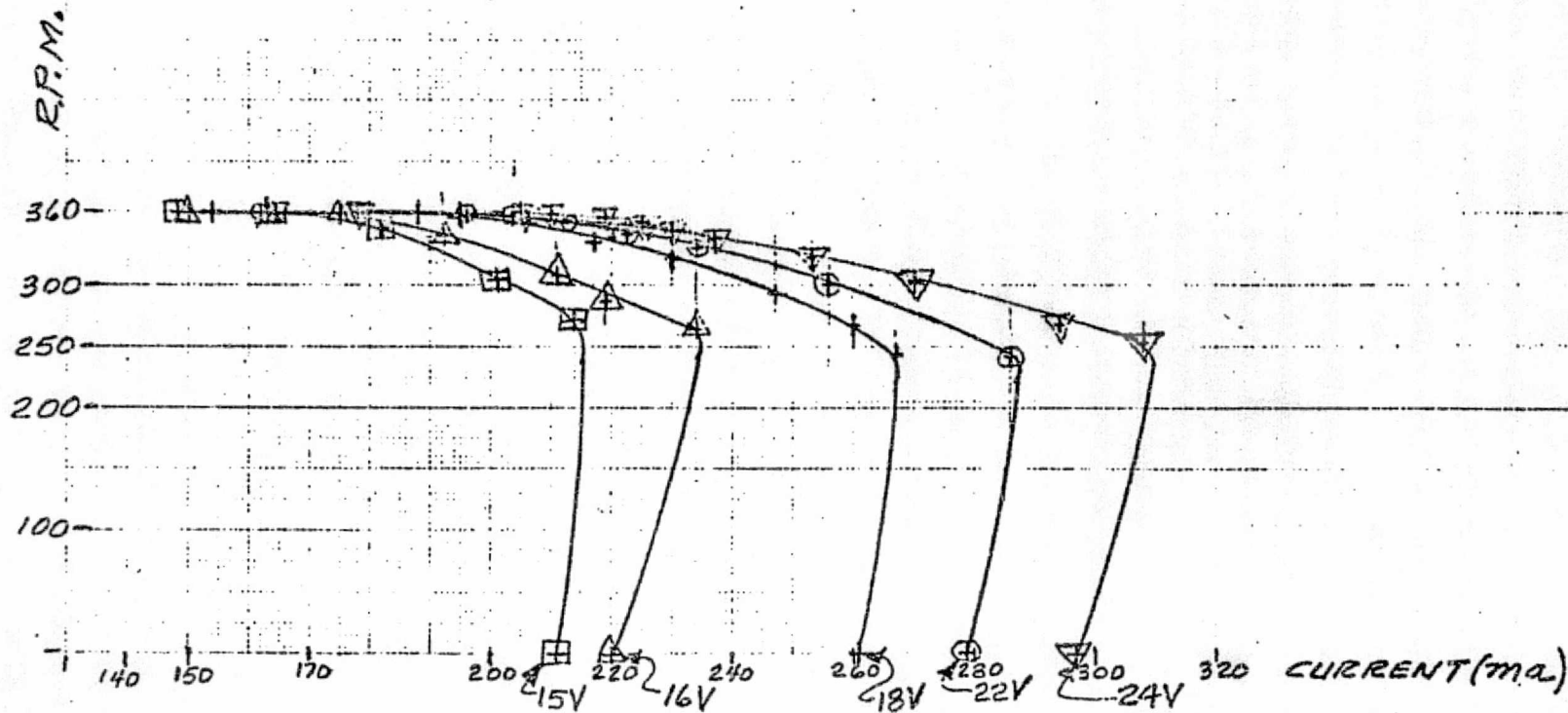


Figure 4.2-4

REPRODUCIBILITY OF THE
ORIGINAL PAGE IS POOR

10 X 10 TO THE CENTIMETER - 46 1513
17 X 25 CM
KODAK SAFETY FILM

LTIM MOTOR (S/N 004)
KRYTOX LUBE
2-6-74



4.2.2 Bearings

The motor shaft bearings are a set of DB duplex bearings separated by 2 inch spacers. The bearings are specified in ITT Drawing #8007937. Each bearing has a static radial non-brinell load capacity of 602 lb. and a dynamic radial load capacity of 125 lb. for 17,500 hours of operation at 360 rpm.

An unusual feature of this bearing is the square ball pockets in the retainer. It was determined during the SCMR program that the shape of retainer ball pocket is a major factor influencing jitter. Square ball pocket bearings exhibited less jitter than round pockets. Based upon that, the AVHRR bearings were procured with square ball pockets.

Tests have shown that bearings with improved surface finish on the races (achieved both by diamond honing by the manufacturer and running in at ITT) can perform within specification when lubricated with the proper amount of lubricant. Tests have also shown that performance is appreciably degraded when too much lubricant is used.

4.2.3 Bearing Fits

Table 4.2-1 shows the shaft and housing fits for the AVHRR.

4.2.3.1 Thermal Consideration of Bearing Fit

Bearing, shaft and housing materials and coefficients of thermal expansion are noted in Table 4.2-2. The deviation from nominal bearing fit over the temperature range, 0 to +40°C, is considered negligible.

TABLE 4.2-1

SHAFT, BEARING, AND HOUSING DIMENSIONS

ID		OD	
Bearing	Shaft	Bearing	Housing
$\frac{1.0623}{1.0625}$	$\frac{1.0622}{1.0620}$	$\frac{1.5000}{1.4998}$	$\frac{1.5000}{1.5002}$

SHAFT, BEARING AND HOUSING FITS

ID		OD	
Loose	Loose	Tight	Loose
0.0001	0.0005	0.0000	0.0004

TABLE 4.2-2

THERMAL EXPANSION CHARACTERISTICS
OF BEARINGS

<u>Item</u>	<u>Material</u>	<u>Coefficient of Thermal Expansion</u>
Bearing	440 C SS	$5.6(10)^{-6} / ^\circ\text{F}$
Shaft	Inconel X750	$6.96(10)^{-6} / ^\circ\text{F}$
Housing	Beryllium	$6.4(10)^{-6} / ^\circ\text{F}$

With all parts measuring nominal dimensions at 20°C , the total changes in fit at $\pm 20^\circ\text{C}$ from nominal will be:

Change in Bearing to Housing Fit	$-4.32(10)^{-5}$ IN	$+4.32(10)^{-5}$ IN
Change in Bearing to Shaft Fit	$-6.13(10)^{-5}$ IN	$+6.13(10)^{-5}$ IN

4.2.4 Lubrication

The bearings of the scanner are lubricated with Krytox 143AB. This lubricant was selected after evaluating a number of lubricants and upon the recommendation of GSFC.

A summary of the pertinent characteristics of KRYTOX 143AB is shown in the following:

Weight loss % - 30 days at 50°C & 10 ⁻⁶ mm Hg	.023%
Lubricity - cycles - A151550 Block 150 lb. @ 100 RPM	10 ⁶ + cycles
Viscosity 32F	140 CS
Viscosity 77F	49 CS
Viscosity 100F	36 CS
Radiation Resistance - min. safe dosage	10 ⁸ rads

The amount of lubricant in each bearing is critical for achieving proper scanner performance. Nominally, 7 ⁺¹₋₀ mg of KRYTOX 143AB is used in each bearing. To achieve this level, ITT Procedure No. 8008007 is followed for cleaning and lubricating each bearing.

4.2.5 Jitter

The current jitter spec calls for:

"scan line to scan line jitter as measured on the leading edge of the synchronization pulse shall be less than 1/2 of an IFOV for 98% of the data points when data is taken every scan line for a 20 minute period.

"The jitter of the synchronization pulse between any two scan lines within a 20 minute period shall be within an IFOV (34 microseconds)."

Jitter characteristics of Engineering Model, Life Test Model and Protoflight Model instruments were all within this spec as noted below:

	Vertical Jitter <u>TP 8121091</u>	Line/Line Jitter <u>TP 8120888</u>	Line/Line Jitter <u>TP 8121133</u>
ETM	99.9%	--	--
LTM	--	99.9%	--
PFM	--	--	99.8%

4.2.6 Life Test

A nominal one year life test was run at ITT on the Life Test Model Scanner. The motor survived the life test as indicated by its end-of-test performance characteristics. As of this writing, a complete teardown of the LTM had not yet been accomplished.

LTM performance characteristics are noted below.

	<u>Start-of-Test</u>	<u>End-of-Test</u>
Coast Down	1.21 min.	2.25 min.
Jitter-Line/Line	78.7% (within 8μsec)	99.9% (within 8 & 16μsec)
Torque	3.3 in oz at Drop Out	4.0 in oz at Drop Out

4.2.7 Angular Momentum

Angular momentum of the ETM scanner is calculated to be 35.8 in. oz sec based upon a measured moment of inertia of .9502 in. oz sec². Momentum vector direction is along y axis.

Moment of inertia was measured with a Model XR50 moment of inertia tester manufactured by Space Electronics, Inc.

4.2.8 Venting of the Scanner Housing

Because of the limited torque margin of the scanner motor, shaft seals are not used. A close clearance labyrinth cap does cover the shaft clearance through the housing for the purpose of limiting the outgassing toward the scan mirror and optics. Details of the cap are shown in Figure 4.2-8.

A vent hole is included in the motor housing to allow an escape path for air during decompression to preclude large volumes of air from rushing through the bearings and causing contamination. Some concern has been expressed because open vent holes could allow lubricant vapor to escape after the instrument is in orbit. While this does not appear to be a problem when Krytox is used provision has been made for a fitting to be attached to the vent hole as requested by NASA/GSFC.

4.3 Radiant Cooler Subassembly

An exploded view of the radiant cooler is shown in Figure 4.3-1.

4.3.1 Support Body

The radiator is supported by nine support rods fabricated of glass epoxy composite tubing (G10 Synthane) and stainless steel inserts, or end caps:

2 pcs .25" O.D. x .19" I.D. x 1.31" total length or .98" thermal length

2 pcs .25" O.D. x .19" I.D. x 0.82" total length or .52" thermal length

5 pcs .38" O.D. x .28" I.D. x 3.40" total length or 3.15" thermal length

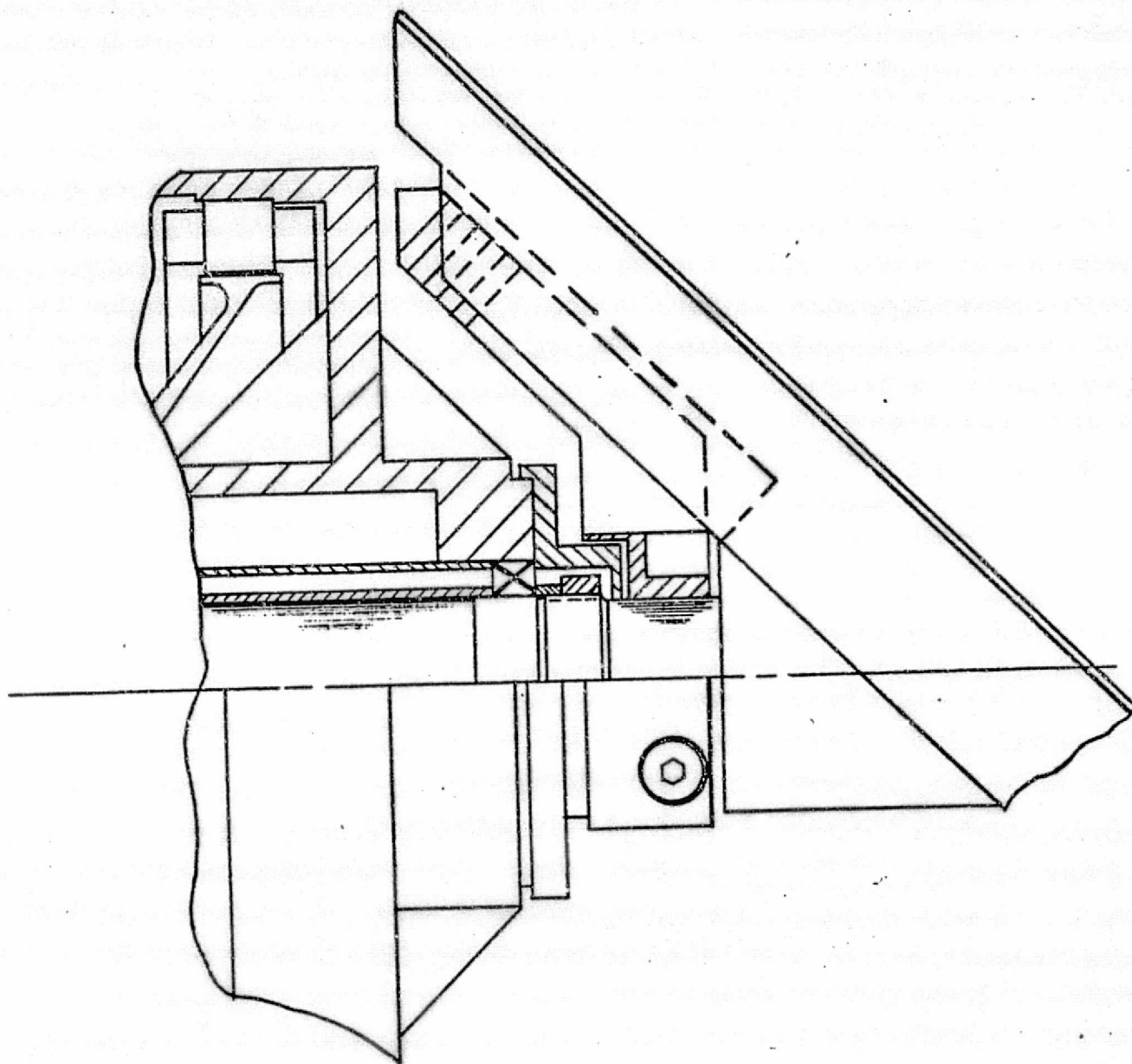
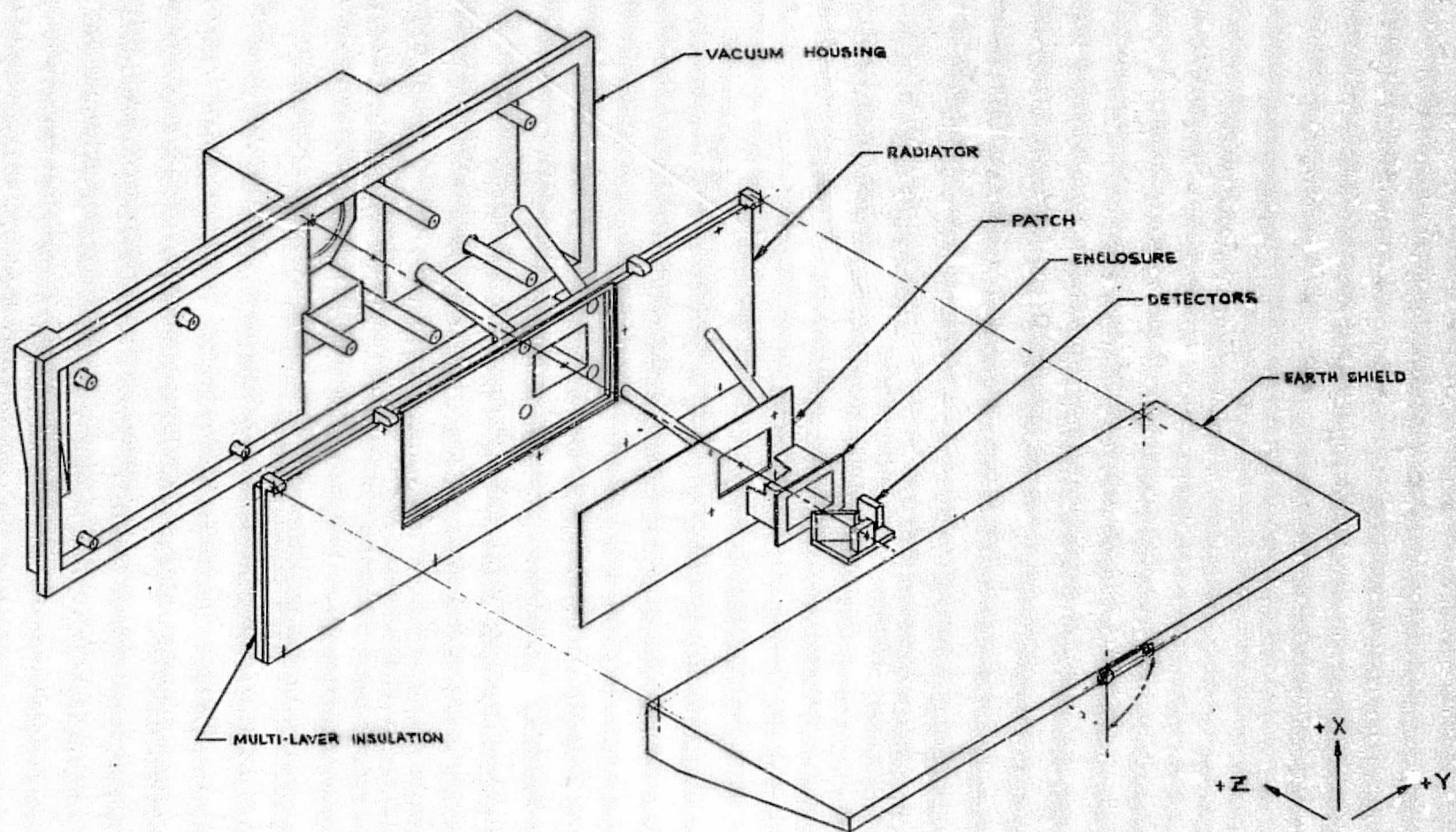


Figure 4.2-8 Shaft Clearance Cap



Exploded View Radiant Cooler

FIG 4.3-1

The patch is supported by four rods of the same materials as above:

.19" O.D. x .16" I.D. x 3.06" total length or 2.70" thermal length

4.3.2 Detector Location

The detectors for Channels 3 and 4 are located on the patch. A layout of the detectors on the patch is shown in Figure 4.3-2.

4.3.3 Deployable Earth Shield

The radiant cooler Earth shield is a "one-shot" device which will be deployed by torsion springs located at the hinge pins. A mechanical latch holds the shield in the closed (undeployed) position. Two rotary solenoids are utilized to release the latch. Each is independent of the other and each capable of unlatching the shield.

Switches located at both the open and closed positions will indicate shield position.

A positive mechanical stop which is an integral part of the radiator will stop the shield in the open position.

Hinges consist of music wire torsion springs rotating in polyimide bushings. No lubricant is required.

The shield can be manually closed without the aid of special tools.

In order to deploy the shield in a 1g gravity field for test, the torsion springs develop 162 in. oz of torque of which 40 in. oz are required to lift the weight of the shield and 2 in. oz are required to overcome friction in the bearings. With torsion springs designed to produce 162 in. oz torque, the torque margin in orbit is greater than 80:1.

An analysis of the earth shield door motion was made and reported in DIR #36.

REPRODUCIBILITY OF THE
ORIGINAL PAGE IS POOR

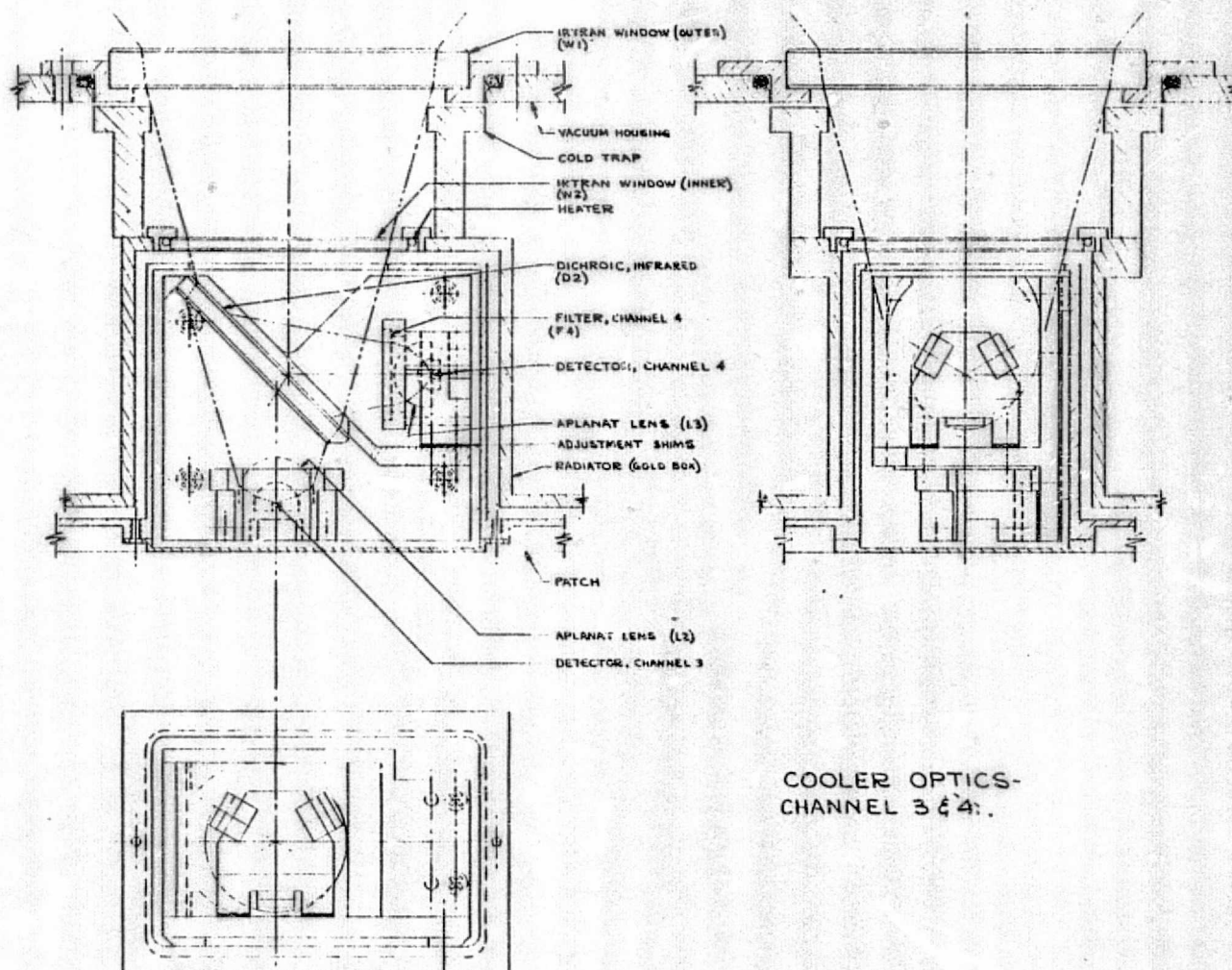


Figure 4.3-2

4.3.4 Materials and Finishes in Cooler

Generally, the major cooler components are fabricated from 6061 T6 aluminum. Radiator surfaces are electroplated gold and painted black with 3M401. The back of the patch and the surfaces of the gold box are electroplated gold. The earth shield is electroless nickel plated and polished optically. Then it is coated with evaporated aluminum. Aluminized polyester film multi-layer insulation is used inside the cooler with polyester mesh separators.

4.4 Optics Subassembly

4.4.1 Optics Outline

The optics assembly is shown in ITT Drawing No. 8008030 - Figure 4.4-1.

4.4.2 Materials and Finishes Used in Optics

Generally, 6061 Aluminum is used as the main structural material. The corrugated tube in the telescope is invar. Graphite filled polyimide is used as the separator material for lens elements.

4.5 Electronics Package

4.5.1 Electronics Package Layout

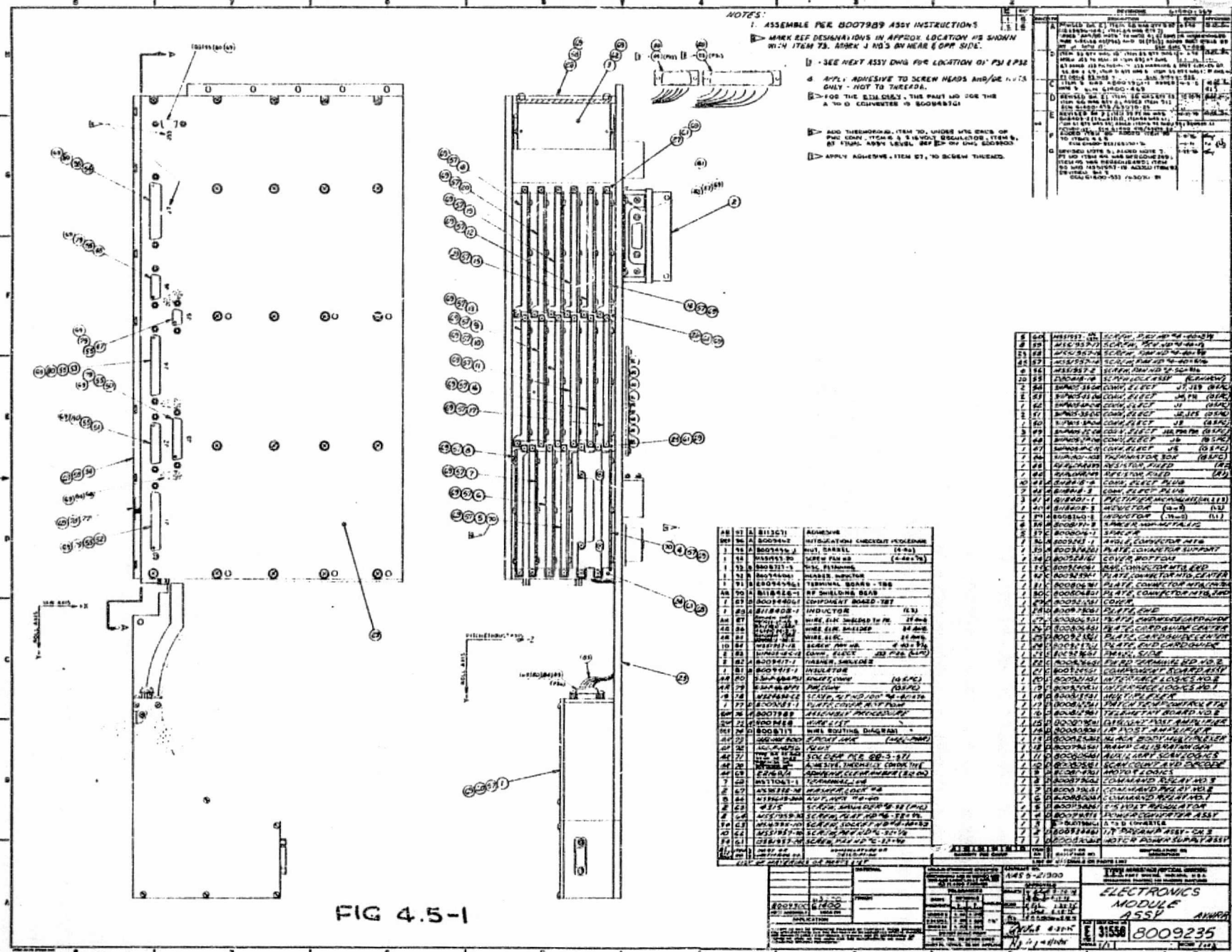
The Assembly Drawing No. 8009235 of the electronics package is shown in Figure 4.5-1.

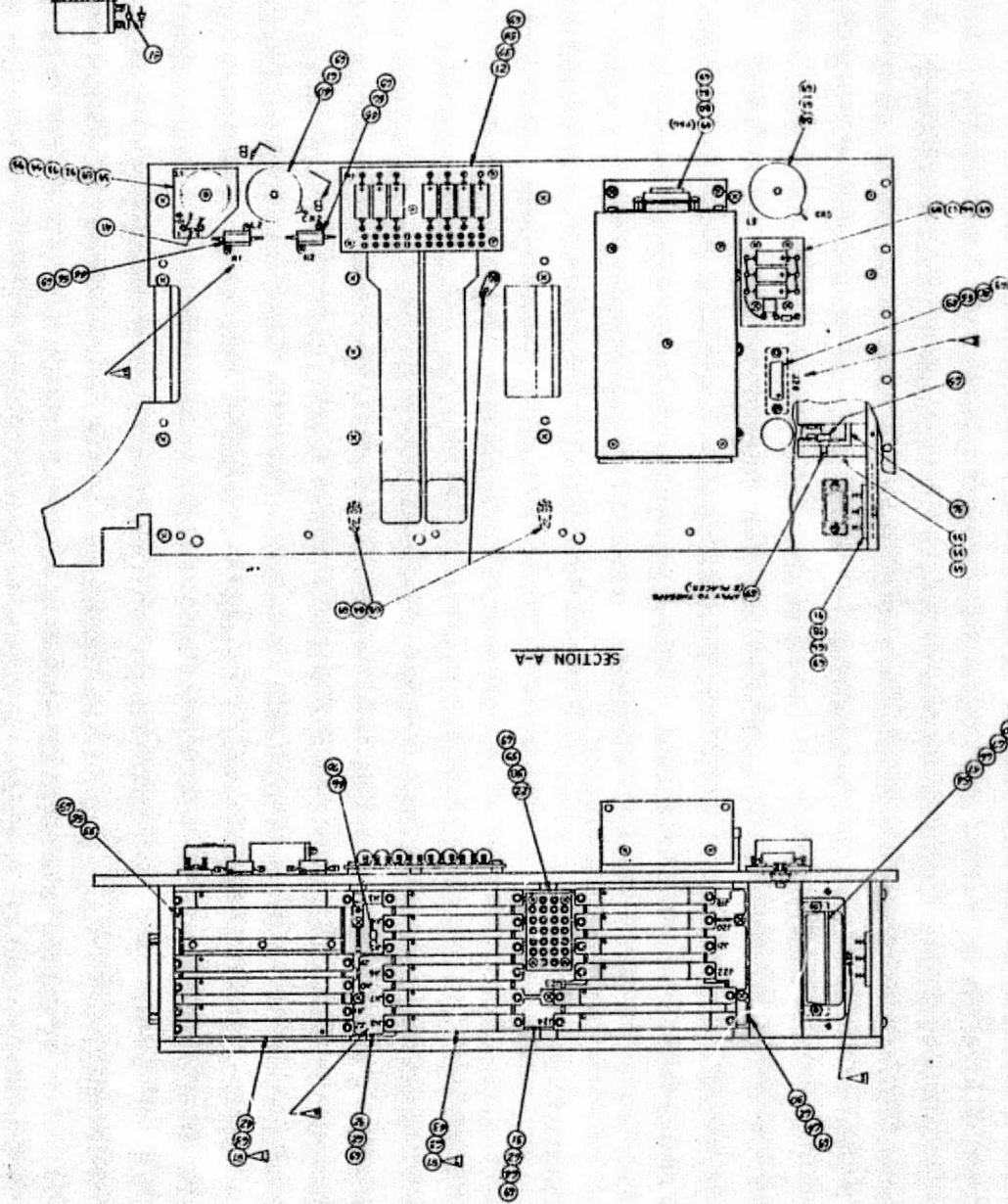
4.5.2 Accessibility

All electronics modules are accessible from the Earth side of the instrument when it is mounted on the spacecraft with the exception of Channels 1 and 2 preamps.

[illegible][illegible]

FIG 4.4-1





VIEW B-B
TYP 2 PLACES

1 VP 2 PLACES

FIG. 4.5-1

[illegible][illegible]

4.5.3 Thermal Considerations

Louvers on the spacecraft platform are used for thermal control. Heat sinks on each PC board conducts the heat into the structure of the electronics package.

4.5.4 Radiation Considerations

Nominally 1/8 inch thick magnesium plates are used for all external walls of the electronics package. This thickness will provide adequate radiation shielding.

4.5.5 Materials and Finishes in Electronics

The entire electronics package is fabricated from AZ31B magnesium with Dow 7 finish.

4.6 Weight Breakdown

A weight breakdown is shown in Table 4.6-1.

4.7 Materials

The Materials List has been issued as ITT Drawing No. 8009466.

MASS PROFILE

ITEM	WEIGHT
STRUCTURE	6,200 GMS
SCANNER	4,370 GMS
OPTICS	4,200 GMS
COOLER	2,575 GMS
ELECTRONICS	9,433 GMS
THERMAL BLANKET	425 GMS
	<hr/>
TOTAL IN GRAMS (GMS)	27,198
EQUIVALENT IN PDS (LBS)	59.96

TABLE 4.6-1

5.0 ELECTRICAL SYSTEM

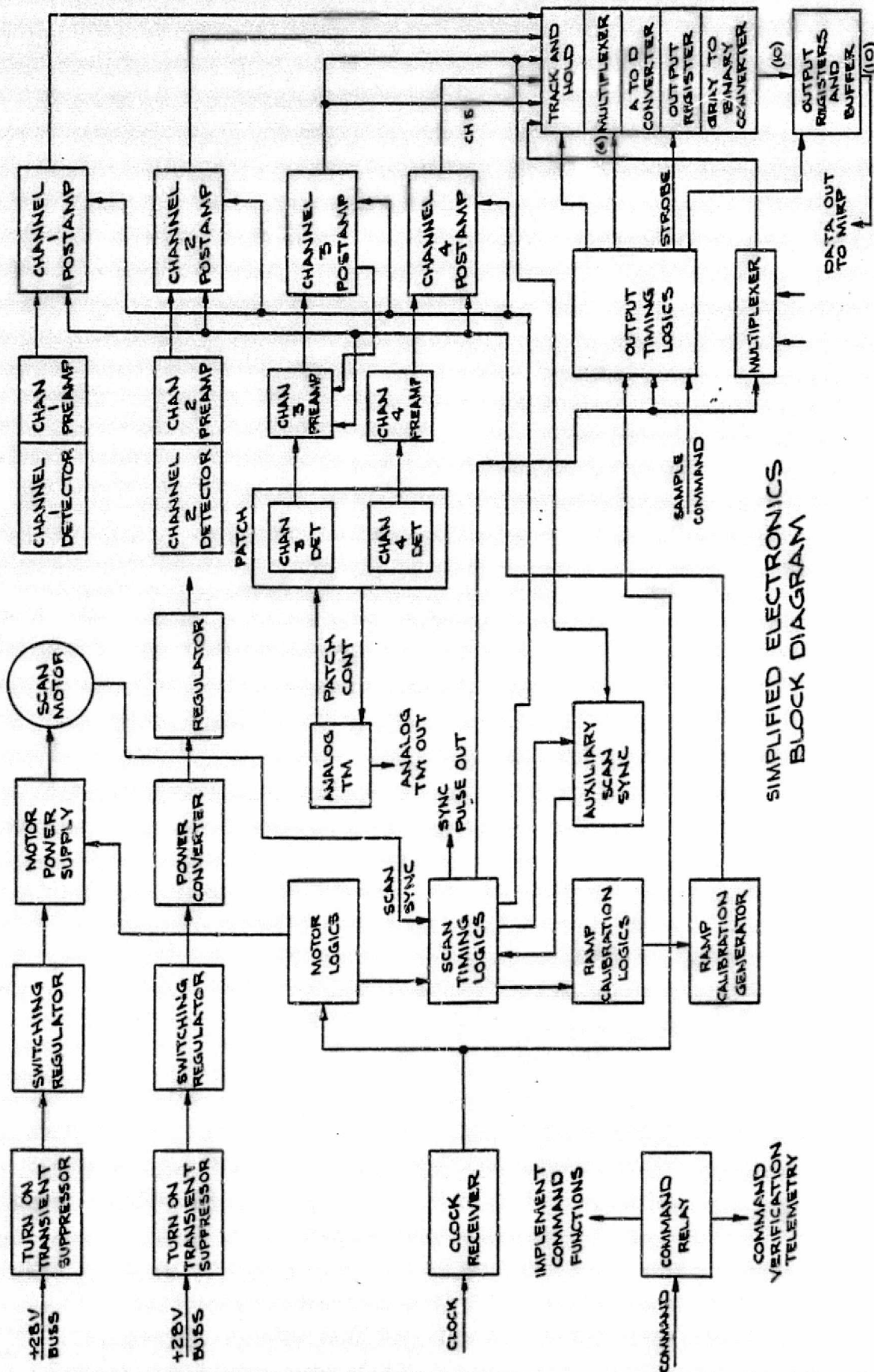
The basic function of the AVHRR electronics is to provide outputs of four data channels in digital form and supporting telemetry signals. Given inputs of power, a reference clock, and commands, the AVHRR electronics provides the command storage, power conversion and regulation, timing and control signal generation, a signal amplification, and analog-to-digital conversion necessary to perform its function.

A simplified block diagram of the AVHRR electronics is shown in Figure 5-1. This diagram shows the basic functions and interconnections of the electronics.

5.1 Electronic Packaging

The majority of the AVHRR electronics are mounted on printed circuit boards. The following is a list of the AVHRR boards:

1. Power Converter Assembly in a metal can
consisting of:
 - a. Power Converter and Switching Regulator
 - b. Logic Regulators
2. ± 15 Volt Regulators
3. Command Relay No. 1
4. Command Relay No. 2
5. Command Relay No. 3
6. Scan Count and Decode Logics
7. Motor Logics
8. Auxiliary Scan
9. Patch Temperature Control and Telemetry
10. Telemetry Board No. 2
11. Interface Logics No. 1
12. Interface Logics No. 2



SIMPLIFIED ELECTRONICS
BLOCK DIAGRAM

Figure 5-1

13. IR Post Amplifier
14. Daylight Post Amplifier
15. Multiplexer
16. Ramp Calibration
17. Blackbody Mux
18. Motor Power Supply
19. Switching Regulator
20. Ch 3 IR Preamplifier
21. Ch 4 IR Preamplifier
22. Daylight Preamplifier

The first 17 cards listed are mounted as plug-in units in the electronics assembly.

Items 18 and 19 are mounted in a metal can which is located between the electronics assembly and the scan motor. These two cards are hard-wired inside the can. The entire can assembly is a plug-in unit with two connectors, one to the electronics assembly, the second to the scan motor.

The Ch 3 IR Preamplifier (Item 20) is mounted in a metal can. The assembly is mounted outboard of the electronics package.

The Ch 4 IR Preamplifier (Item 21) is located on the cooler vacuum housing in the proximity of the cooler interface headers. The preamplifier board is mounted in a metal can.

Two daylight preamplifiers (Item 22) are located within the optics package with the silicon detectors connected directly to the PC board. The board is hard-wired within the optics module and is provided with copper shielding.

Break connectors are provided between the electronics package and the wiring required in the remainder of the instrument making the electronics package in its entirety a plug-in unit.

The final major assembly of the AVHRR electronics is the analog-to-digital converter. This unit is located in the electronics package with short connections to the post amplifiers and output connectors.

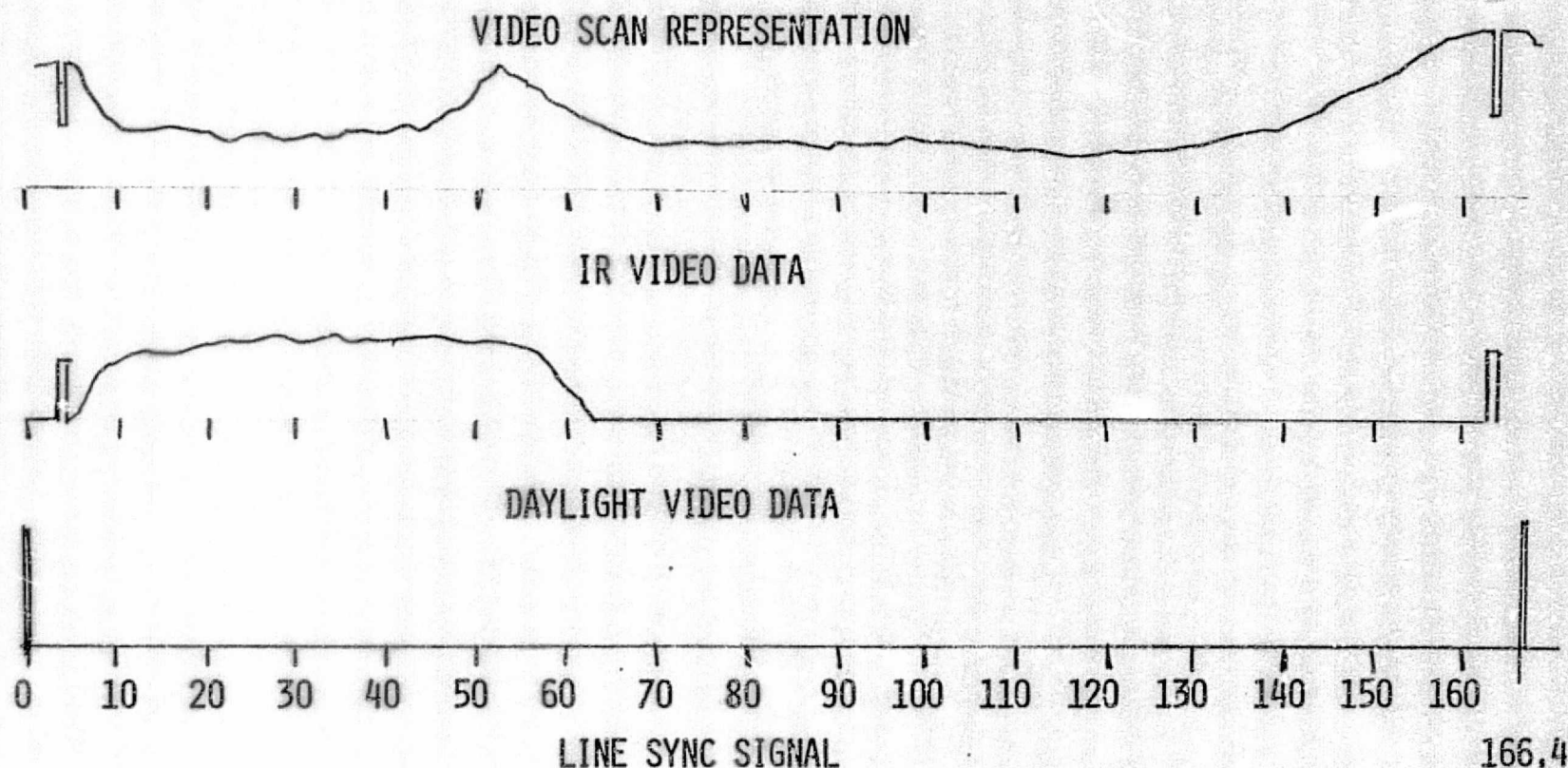
5.2 Electrical Design Considerations

The electrical design is to the extent possible based upon existing designs used on space qualified instruments. Parts selection criteria include the use of parts on the NASA/GSFC Preferred Parts List where possible and the use of previously approved parts where the PPL parts are not suitable. Derating of parts is in accordance with the requirements of the PPL and consideration of the special environment of the AVHRR.

5.3 Video Scan Timing

Figure 5-2 shows the timing relationship of the scene as viewed by the scan mirror and the sync pulse which is the time reference point. Time intervals of 1 millisecond before and after the sync pulse have been provided by insertion by the MIRP of coded pre-cursor signals. The tolerance of the viewing times due to spacecraft attitude control tolerance are indicated.

The times indicated on this drawing and times and frequencies listed on all other timing diagrams and schematics are based on a normal 1 MHz clock. To obtain actual times the numbers must be multiplied by 1.0016. To obtain actual frequencies multiply numbers of 0.9984.



0-0.1	LINE SYNC	34.2	NADIR NOMINAL
0.5-1.5	MIRP PRE-CURSOR TIME	62.6	SPACE START WORST CASE - EARLY S/C ATTITUDE
1.8	RADIOMETER SPACE VIEW START	63.1	SPACE START NOMINAL
1.9-3.5	RADIOMETER SPACE SAMPLE	63.6	SPACE START WORST CASE - LATE
3.5-4.0	RAMP CALIBRATION	65.6-65.8	IR TARGET TEMPERATURE
4.13	SPACE END WORST CASE - EARLY	65.8-66.0	PATCH TEMPERATURE
		117.1	IR TARGET FULL VIEW START
5.3	SPACE END NOMINAL	117.6-118.4	IR TARGET SAMPLE
5.8	SPACE END WORST CASE - LATE S/C ATTITUDE	119.0	IR TARGET FULL VIEW END
		165.0-166.0	MIRP PRECURSOR TIME

FIGURE 5-2

5.4 Power Subsystem

5.4.1 General

The +28V DC input from the spacecraft is regulated to obtain isolation from spacecraft voltage variations, converted to develop a system ground, and re-regulated to obtain noise rejection and precision.

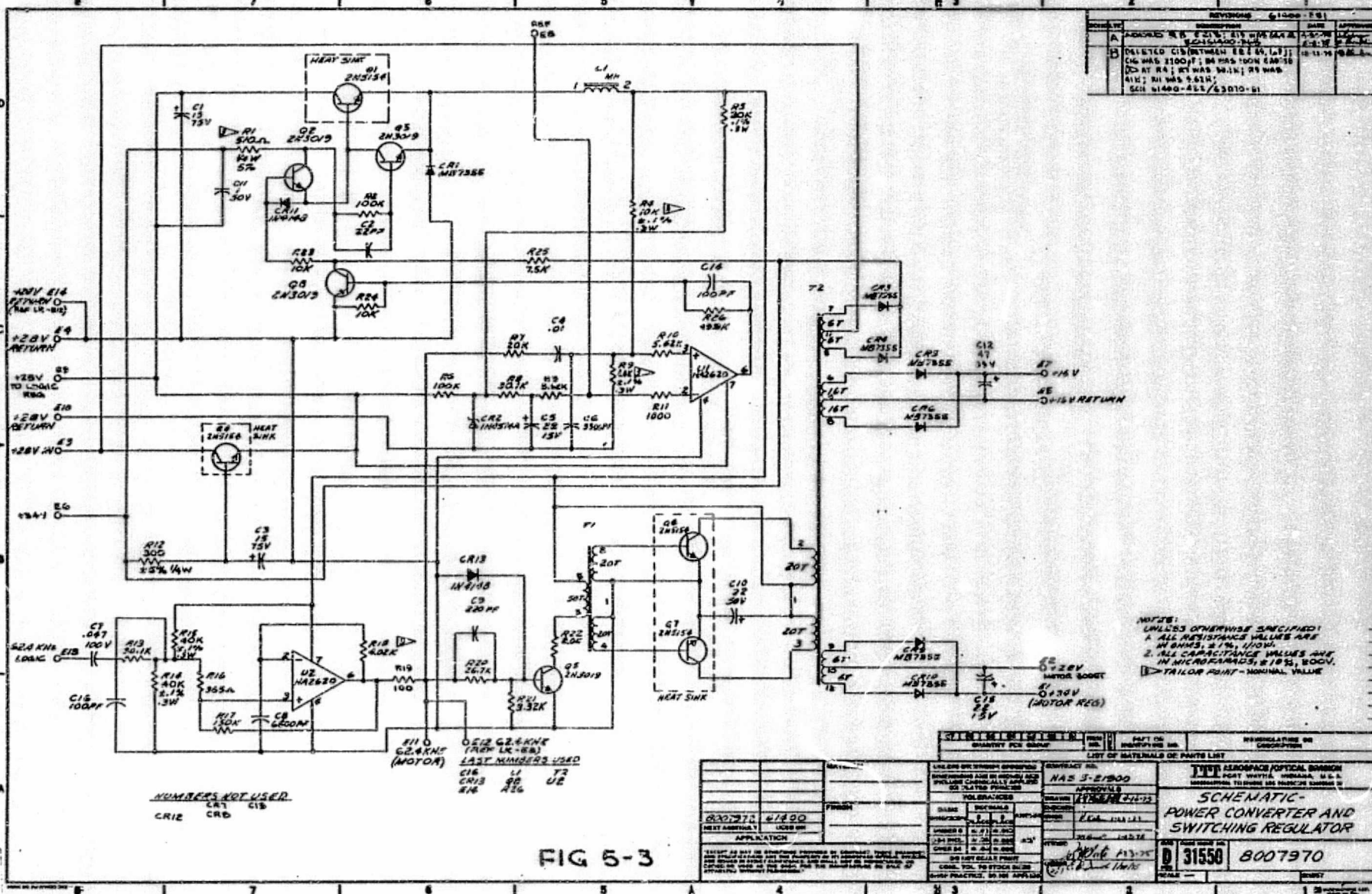
The schematic for the Power Converter and Switching Regulator Board is shown in Figure 5-3. The schematic for the Logic Regulator is shown in Figure 5-4. Both boards are assembled in a conetic can with LC EMI filters on all inputs and outputs with the exception of the clock signals.

5.4.2 Turn on Transient

Turn on transients are suppressed by limiting the base voltage rise time of the input pass transistor Q4 of the PC & SR. The changing path is through T2 and R17. This circuit limits the surge current into the input filtering. The input switching regulators have long time constants on the reference inputs which slows the build-up of all the circuits beyond that point.

5.4.3 Electronics Switching Regulator

Two input switching regulators are provided using Harris HA2620 amplifiers as comparators: The circuits are self starting and driven by a 62.4 Kh signal for synchronization with the spacecraft clock. A +34V boost voltage derived from the Power Converter provides the drive voltage for the pass transistor to provide good saturation for minimum dissipation.



5.4.4 Power Converter

Two DC/DC Converters are provided, one powered from each Switching Regulator. These circuits establish signal ground for the AVHRR and provide the proper voltage inputs to the electronics regulators. They are driven converters being synchronized with the same 62.4 Kh clock signal as the switching regulators. The converters operate from switching regulator outputs and therefore the maximum VCE on the converter transistors is limited to 44V.

5.4.5 +5V Regulators

A switching regulator is used to provide +5 volts for logic circuits. The output of the switching regulator directly feeds the logic circuits required for motor frequency countdown and the input clock circuits. The major portion of the logics is powered through a switching transistor from the regulator output. This transistor is turned on with the Electronics ON command.

5.4.6 ± 15V Regulators

The 15 volt regulators are linear circuits utilizing the Harris HA2620 I.C. as the voltage comparator. The schematic for the ± 15V Regulators is shown in Figure 5-5.

Also on this board are the pass transistors for the channel enable/disable commands and Electronics ON command.

The +15 volt regulator uses a +20 volt "boost" voltage from the power converter to enable a low input/output differential and minimize the pass transistor power loss. The circuit will regulate under full load with an input/output differential equal to the collector/emitter saturation voltage of the pass transistor which is typically 0.2 volt.

5.4.7 Motor Power Supply Switching Regulator

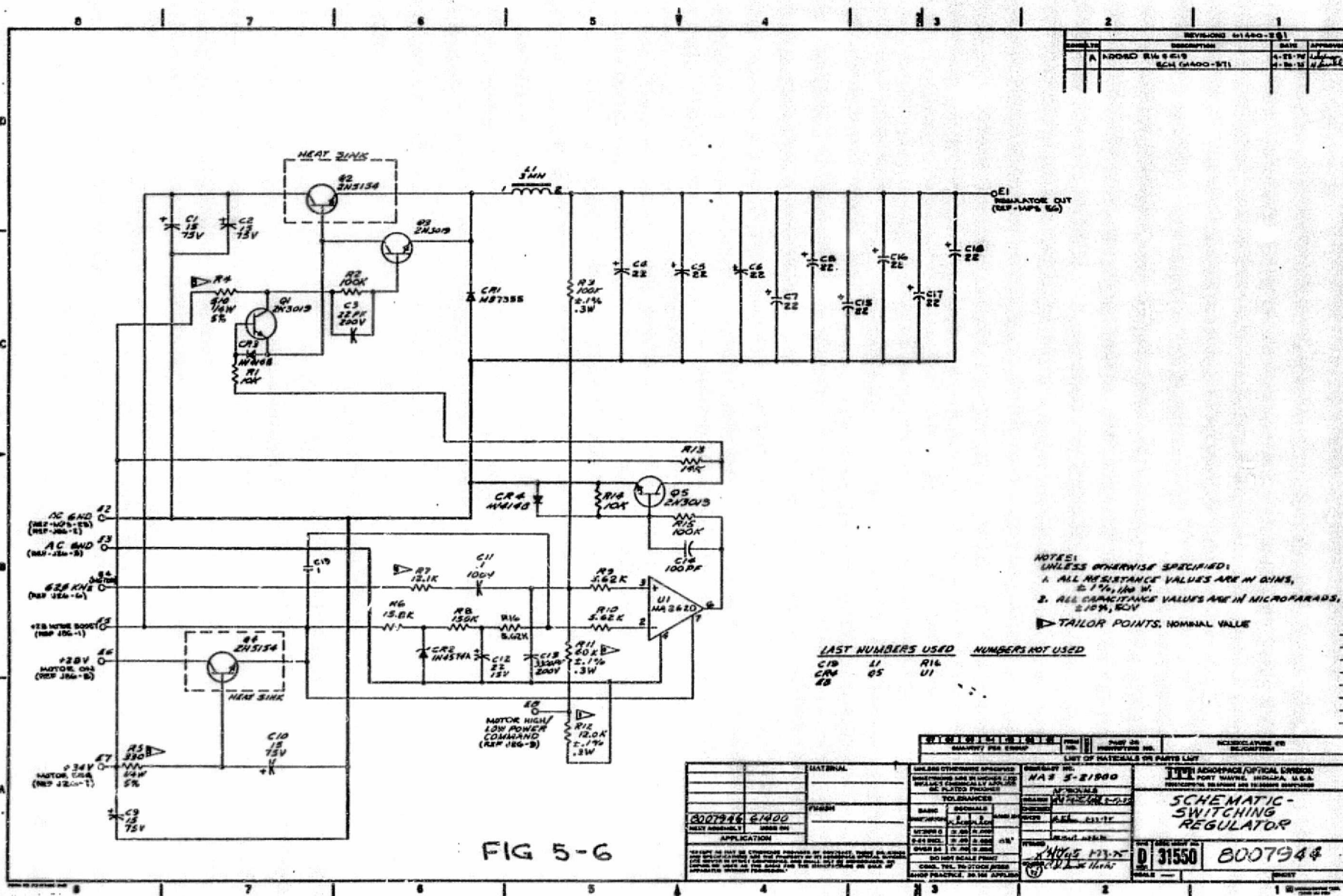
The schematic for the motor power supply switching regulator is shown in Figure 5-6.

The circuitry is similar to the electronics switching regulator, the exception being that the motor switching regulator will regulate at one of two voltage levels selected upon command.

5.5 Commands and Digital TM

The following is a list of the presently planned commands for the AVHRR:

1. Scan Motor/Telemetry ON
2. Scan Motor/Telemetry OFF
3. Electronics/Telemetry ON
4. Electronics/Telemetry OFF
5. Ch 1 Enable
6. Ch 1 Disable
7. Ch 2 Enable
8. Ch 2 Disable
9. Ch 3 Enable
10. Ch 3 Disable
11. Ch 4 Enable
12. Ch 4 Disable
13. Voltage Calibrate ON
14. Voltage Calibrate OFF
15. Patch Control High Mode
16. Patch Control Low Mode



NOTES:
 1. ALL RESISTANCE VALUES ARE IN OHMS, UNLESS OTHERWISE SPECIFIED.
 2. ALL CAPACITANCE VALUES ARE IN MICROFARADS, UNLESS OTHERWISE SPECIFIED.
 3. TAILOR POINTS, NOMINAL VALUE

LAST NUMBERS USED	NUMBERS NOT USED
CR1 11	R14
CR2 05	U1
CR3 10	

WIREWORTH WIREWORTH, INC. 1000 W. 10TH ST. PORT WAINWRIGHT, PA. 15127		SCHEMATIC SWITCHING REGULATOR D 31550 8007944	
REVISIONS REVISION NO. 1 DATE 10-1-77 BY J. H. H.		LIST OF MATERIALS OR PARTS LIST PART NO. DESCRIPTION QTY. REQUIRED	
UNLESS OTHERWISE SPECIFIED DIMENSIONS ARE IN INCHES DIMENSIONS ARE IN MILLIMETERS DIMENSIONS ARE IN METERS		UNLESS OTHERWISE SPECIFIED DIMENSIONS ARE IN INCHES DIMENSIONS ARE IN MILLIMETERS DIMENSIONS ARE IN METERS	
UNLESS OTHERWISE SPECIFIED DIMENSIONS ARE IN INCHES DIMENSIONS ARE IN MILLIMETERS DIMENSIONS ARE IN METERS		UNLESS OTHERWISE SPECIFIED DIMENSIONS ARE IN INCHES DIMENSIONS ARE IN MILLIMETERS DIMENSIONS ARE IN METERS	

17. Cooler Heat ON
18. Cooler Heat OFF
19. Scan Motor High Mode
20. Scan Motor Low Mode
21. Telemetry Locked ON
22. Telemetry Unlocked
23. Earth Shield Deploy
24. Earth Shield Disable
25. Patch Control ON
26. Patch Control OFF

The following is a list of the functions performed by executing the listed commands.

<u>Command No.</u>	<u>Function</u>
1. Scan Motor/Telemetry ON	Applies Power to: <ol style="list-style-type: none"> 1. Electronics sw. regulator 2. Motor sw. regulator 3. Power converter 4. $\pm 15V$ regulators 5. +5V logic reg. 6. Clock receiver 7. Motor logic 8. Analog telemetry circuits 9. Patch temp. control
2. Electronics/Telemetry	Applies Power to: <ol style="list-style-type: none"> 1. Electronics sw. regulator 2. Power converter 3. $\pm 15V$ regulators

2. Electronics/Telemetry - Continued

4. +5V logic regulator
5. +5V electronics circuits
6. Analog telemetry circuits
7. A/D Converter
8. Scan timing logic
9. Clock receiver
10. Motor logic
11. Patch temp. control

5. Ch 1 Enable

If "Electronics ON" has been executed - Applies Power to:

1. Ch 1 preamplifier
2. Ch 1 Post Amplifier

7. Ch 2 Enable

If "Electronics ON" has been executed - Applies Power to:

1. Ch 2 Preamplifier
2. Ch 2 Post Amplifier

9. Ch 3 Enable

If "Electronics ON" has been executed - Applies Power to:

1. Ch 3 Preamplifier
2. Ch 3 Post Amplifier

11. Ch 4 Enable

If "Electronics ON" has been executed - Applies Power to:

1. Ch 4 Preamplifier
2. Ch 4 Post Amplifier

13. Voltage Calibrate

If "Electronics ON" has been executed -

1. Deactivate IR & Daylight detectors.

13.

2. Provides simulated earth scene and backscan video.

15. Patch Control High Mode

If "Telemetry ON" has been executed

1. Sets patch temp control point to 107°K

16. Patch Control Low Mode

If "Telemetry ON" has been executed

1. Sets patch temp control point to 105°K

17. Cooler Heat ON

If "Electronics ON", "Motor ON" or "Telemetry ON" has been executed - Applied Power to:

1. Radiator Decontamination Heater
2. Patch Decontamination Heater

19. Scan Motor High Mode

If "Motor ON" has been executed -

1. Sets motor sw. regulator voltage to HIGH LEVEL

20. Scan Motor Low Mode

If "Motor ON" has been executed -

1. Sets motor sw. regulator voltage to LOW LEVEL

21. Telemetry Locked ON

Applies Power to:

1. Electronics sw. regulator
2. Power converter
3. ±15V regulators
4. +5V logic regulator
5. Clock Receiver
6. Motor Logic

21.

23. Earth Shield Deploy

24. Earth Shield Disable

25. Patch Control ON

7. Analog Telemetry Circuits

8. Patch control circuitry

Applies Power to:

1. Earth Shield Circuitry

Removes Power from:

1. Earth Shield Circuitry

If "Telemetry ON" has been executed -

1. Applies Controlled Heat to Patch

Digital T/M

The following is a list of the Digital T/M functions:

1. Scan Motor Status	"1"	ON
	"0"	OFF
2. Electronics Status	"1"	ON
	"0"	OFF
3. Ch 1 Status	"1"	ON
	"0"	OFF
4. Ch 2 Status	"1"	ON
	"0"	OFF
5. Ch 3 Status	"1"	ON
	"0"	OFF
6. Ch 4 Status	"1"	ON
	"0"	OFF
7. Voltage Calibrate Status	"1"	ON
	"0"	OFF
8. Patch Control Mode	"1"	107°K
	"0"	105°K
9. Cooler Heat Status	"1"	ON
	"0"	OFF
10. Scan Motor Mode	"1"	HIGH POWER
	"0"	LOW POWER

11. Telemetry Status	"1"	ON
	"0"	OFF
12. Earth Shield Status	"1"	DEPLOY
	"0"	DISABLE
13. Patch Control	"1"	ON
	"0"	OFF

The schematics for Command Relay #1, 2 and 3 are shown in Figures 5-7, 5-8 and 5-9. Command Relay's are P&B HL11D 12VDC Latching Type. For Commands and Digital T/M "1" true or 0.0V Level "0" = False or +5.0V Level.

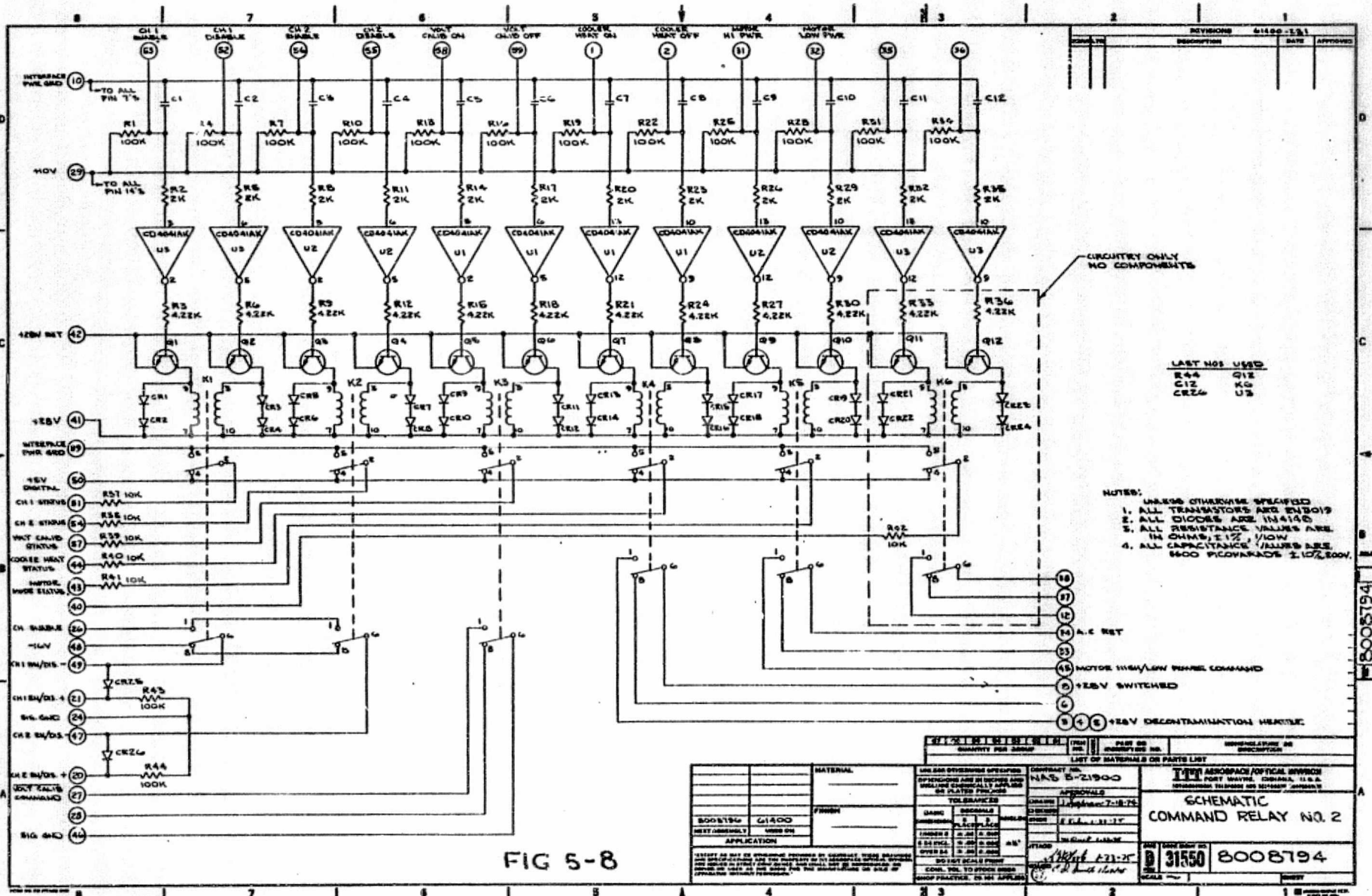
5.6 Analog TM and Patch Control

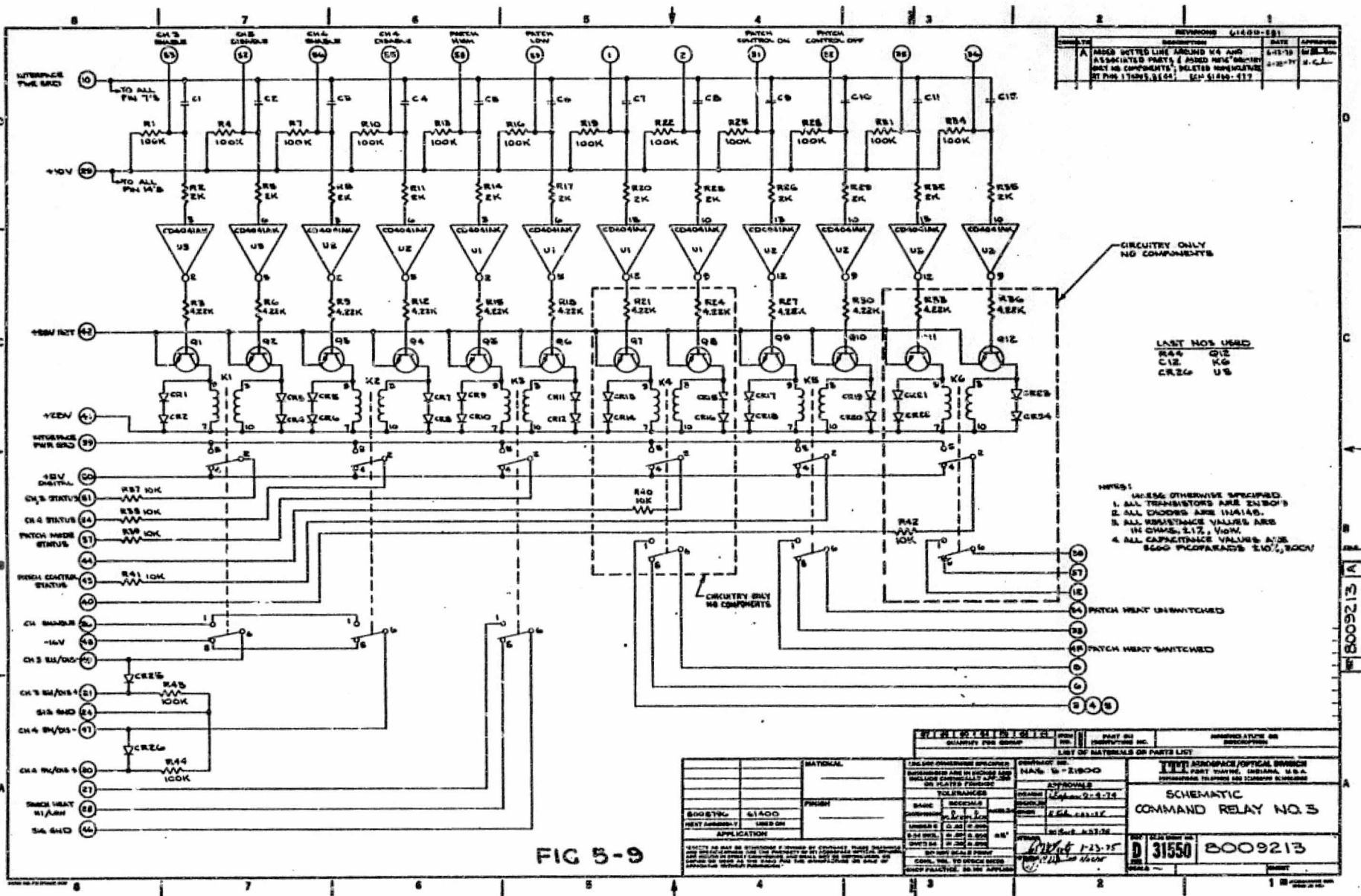
5.6.1 Analog Telemetry

The following is a list of the presently planned analog telemetry points.

1. Patch Temperature
2. Patch Temperature Extended
3. Patch Power
4. Radiator Temperature
5. Blackbody No. 1 Temperature
6. Blackbody No. 2 Temperature
7. Blackbody No. 3 Temperature
8. Blackbody No. 4 Temperature
9. Electronics Current
10. Motor Current
11. Earth Shield Position
12. Electronics Temperature
13. Cooler Housing Temperature
14. Baseplate Temperature







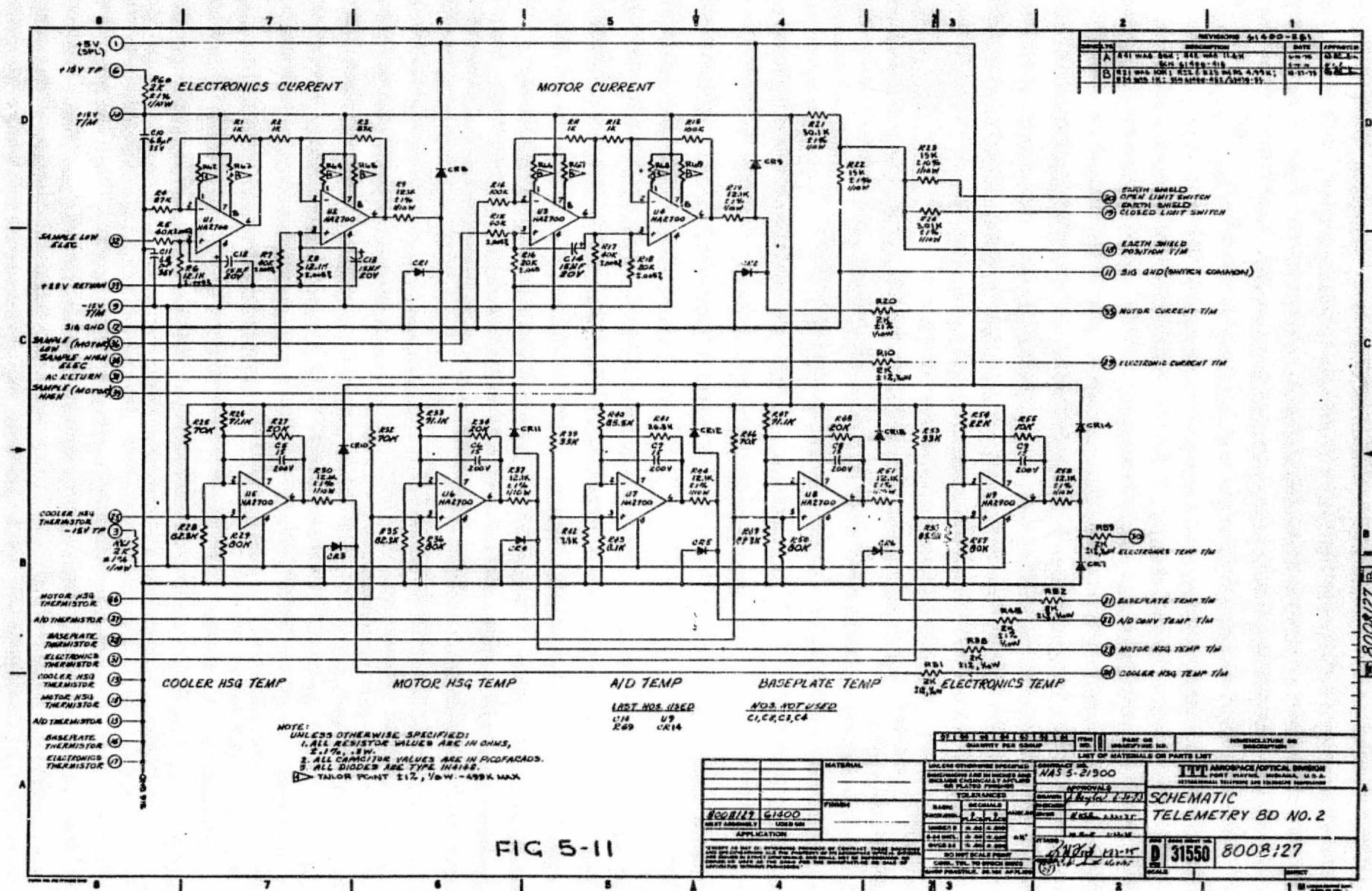
15. Motor Housing Temperature
16. A/D Converter Temperature
17. Detector No. 3 Bias Voltage
18. Blackbody Temperature IR Ch 3
19. Blackbody Temperature IR Ch 4
20. Reference Voltage

The circuitry for telemetry points 1-16 is located on the Patch Temperature Control and Telemetry Board shown schematically in Figure 5-10 and the Telemetry #2 Board shown schematically in Figure 5-11.

The following is a list of the range and resolution of the analog telemetry points.

	<u>Range</u>	<u>Resolution</u>
1. Patch Temperature	+0.2V = 90.7 [°] K +5.0V = 115.5 [°] K	0.1935V/Degree
2. Patch Temperature Extended	+0.2V = 99.4 [°] K +5.0V = 316.0 [°] K	0.02216V/Degree
3. Patch Power	+0.2V = 0.08 MW +5.0V = 50.0 MW	0.067V/mm at 32 mw out.
4. Radiator Temperature	+0.2V = 148.7 [°] K +5.0V = 317.3 [°] K	0.0285V/Degree
5, 6, 7, 8. Blackbody Temp 1, 2, 3 & 4	+0.2V = 5.086 [°] C +5.0V = 44.974 [°] C	0.1203V/Degree
9. Electronics Current	+0.2V = 39.3 MA +5.0V = 982.5 MA	5.088MV/Milliamp.
10. Motor Current	+0.2V = 12 MA +5.0V = 300 MA	16.6 MV/Milliamp
11. Earth Shield Position	3 Levels	+5.0V Open +3.0V In Between +1.0V Closed
12. Electronics Temperature	+0.2V = 38.73 [°] C +5.0V = 10.8 [°] C	0.171735V/ [°] C
13, 14, 15. Cooler Housing Temperature Baseplate Temperature Motor Housing Temperature	+0.2V = 33.24 [°] C +5.0V = 3.95 [°] C	0.129V/ [°] C





REV	DESCRIPTION	DATE	APPROVED
A	REV 1 WAS 504; REV 1 WAS 11.4N	11-76	0.5.1
B	REV 1 WAS 504; REV 1 WAS 11.4N	11-76	0.5.1
C	REV 1 WAS 504; REV 1 WAS 11.4N	11-76	0.5.1

- 20 EARTH SHIELD
- 21 OPEN LIMIT SWITCH
- 22 EARTH SHIELD
- 23 CLOSED LIMIT SWITCH
- 24 EARTH SHIELD
- 25 POSITION T/M
- 26 SIG GND (SWITCH COMMON)
- 27 MOTOR CURRENT T/M
- 28 ELECTRONIC CURRENT T/M

- 29 COOLER HSQ TEMP T/M
- 30 BASEPLATE TEMP T/M
- 31 A/D CONV TEMP T/M
- 32 MOTOR HSQ TEMP T/M
- 33 COOLER HSQ TEMP T/M

REVISIONS REV. NO. 1 DATE 11-76 BY 0.5.1		QUANTITY PER GROUP 1		PART OR SUBPART NO. 1		DESCRIPTION 1	
LIST OF MATERIALS OR PARTS LIST 1		UNLESS OTHERWISE SPECIFIED: 1		ASSEMBLY 1		TEST 1	
REVISIONS 1		REVISIONS 1		REVISIONS 1		REVISIONS 1	
REVISIONS 1		REVISIONS 1		REVISIONS 1		REVISIONS 1	
REVISIONS 1		REVISIONS 1		REVISIONS 1		REVISIONS 1	

16.	A/D Converter Temperature	+0.2V = 84.49°C +5.0V = 44.51°C	0.12V/°C
17.	Detector #3 Bias Volt.	1.923 = -13V 2.384 = -11V	0.23/V/V
18.	Blackbody Temp IR Ch 3	To be Calibrated*	
19.	Blackbody Temp. IR Ch 4	To be Calibrated*	
20.	Reference Voltage	+0.2V = 0.266V +5.0V = 6.657V	0.750V/V

*Range and value of calibration dependent on individual instrument calibration. Equations derived from EM matched to Calibration from 0°C to 40°C are

$$\text{Ch 3} - ^\circ\text{C} = 1.1\text{V}^2 - 13.2 \text{ V} + 330.2$$

$$\text{C 4} - ^\circ\text{C} = -3\text{V}^2 + 11\text{V} + 302.3$$

2000 Ohm ice Point Platinum sensors are used for the following telemetry.

1. Patch Temperature
2. Radiator Temperature
3. BB No. 1
4. BB No. 2
5. BB No. 3
6. BB No. 4

30K ohm Y.S.I. Thermistors, 0.1°C interchangeability, are used for the following telemetry.

1. Baseplate Temperature
2. A/D Converter Temperature
3. Electronics Temperature
4. Cooler Hsg. Temperature
5. Motor Hsg. Temperature.

Diodes have been provided on all operational amplifier outputs to limit analog telemetry points voltage range to -0.7V to +6.0.

5.6.2 Patch Temperature Control

The circuitry for temp. control is shown on the Patch Temp Control and Telemetry schematic, Figure 5-10.

It is a proportional control with a DC output (steady state) to eliminate transients.

The temperature sensor is a platinum resistance unit, Rosemount Model. No. 164MA with an ice point resistance of 2000 ohms. This will provide the input amplifier with a low impedance, stable, and linear source with a resistance change of approximately 8.6 ohms/degree.

The heating unit on the patch is a high rel. RNR55 2000 ohm resistor.

The operational amplifiers are Harris devices, HA-2700. They were selected for the low offset voltage, typically 0.5 mv and offset voltage as a function of temperature typ. 0.25 mv from 0 to 50°C.

5.6.2.1 Theory and Operation

The R3, R4 resistors are used to zero the 1st stage amplifier offset voltage at +25°C.

The R6, R7, R8, combination is tailored to match the platinum sensor resistance at 105 and 107 Kelvin. R-2 limits the sensor dissipation to the values in the following table and establishes the input voltage change to the 1st stage amplifier at 12.5 mv/degree.

<u>Sensor Power Dissipation</u>	<u>Sensor Dissipation/mw</u>
95°	1.31
100°	1.41
105°	1.50
110°	1.59
323°	3.15

R-5 is selected for a first stage gain of approximately 70 and the amplifier output is 0.0 volts at the selected control point.

With the 0.0 volt inverting input on the second stage and 0.134 volt established by R11, R12 on the non-inverting input, the second stage amplifier output = $(0.34 \times 67.6) = 9.07$ VDC. With a 0.6 volt drop across CR1 the patch control output is 8.4 volts at the selected temp. control point. With the 2.0K heating unit on the patch, the patch control circuitry provides 35 milliwatts at 105.0 or 107.0 degree Kelvin.

Figure 5-12 indicates the deviation in temperature of the control point with variations in control heat requirements (35 mw nominal).

5.6.2.2 Circuit Stability

The resistor types used in the patch control are Vishay S202 high rel units with shelf life and load life data available. Calculations from these data indicate that the resistor stability is a negligible factor.

The operational amplifier stability can be related to a millivolt/degree factor at the first amplifier input. The typical initial offset voltage for the HA2700 is 0.5 millivolts which is compensated for at board test. With the loop gain indicated on the schematic, a long term offset voltage change of 1.25 millivolts would be required to result in an error in temperature control of 0.1 degree.

The relative location of the detectors, temperature sensor and heater is shown on ITT Dwg. #8008799 Detector/Frame Assembly, Channel 3 and 4 Figure 5-13.

PATCH TEMPERATURE - DEGREES KELVIN

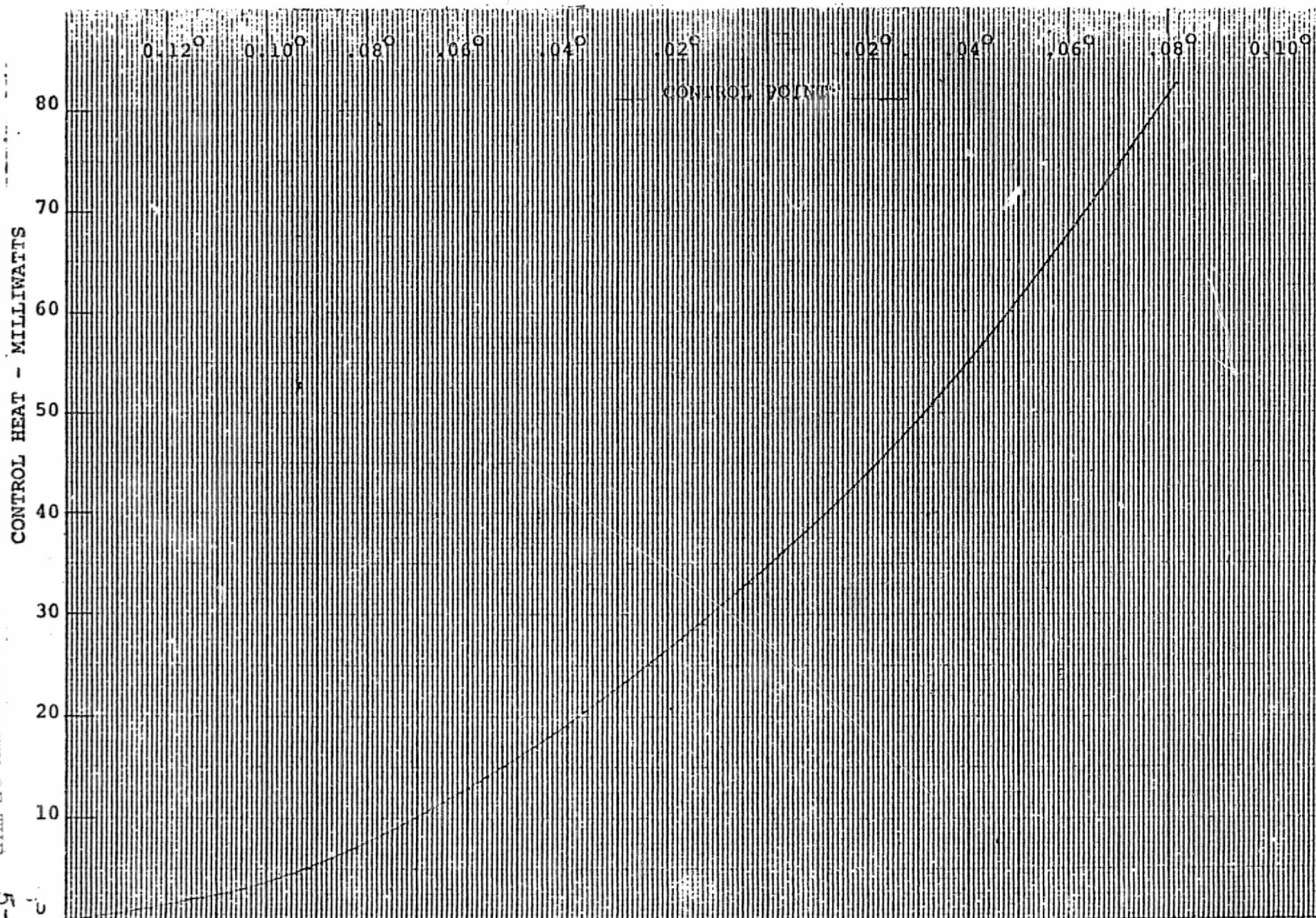


Figure 5-12

1

1

The sensor and heater is located as close as possible to the detectors to minimize sensor/detector/heater gradients and provide the input circuitry with feedback which is a monitor of detector temperature as opposed to the patch temperature.

5.7 Motor Logics

The clock receiver arrangement utilizing the Texas Instruments, Inc. SN55107 clock receiver, as specified in the GFSC specification for an Advanced Very High Resolution Radiometer, is located on the motor logics printed circuit board. An output of the clock receiver is available on a connector pin for use in the interface logics.

The motor countdown logics convert the 0.9984 MHz clock receiver signal into 62.4 KHz for use in the switching regulators and 240 Hz 2Ø for use in the motor power supply.

The 0.9984 MHz input signal is first divided by 16 in a ripple counter to achieve the 62.4 KHz signal at pin 9 of A7. This signal is then buffered and is available for use in the switching regulators.

To obtain the 240 Hz 2Ø signal, the 62.4 KHz signal is divided in a series of counters. The first is a divide by thirteen counter which produces a 4.8 KHz signal at pin 9 of A4. This signal is then divided by 10 to obtain a 480 Hz signal at pin 9 of A1. The inverted and non-inverted forms of this signal are further divided by 2 in their respective J-K flip flops, and the 240 Hz 1Ø signal is present at pins 9 and 12 of B1. A reset circuit acts as a monostable and supplies a pulse to the clear

input of one of the J-K flip flops, B1 pin 2. The reset pulse insures the proper 90° phase relationship between the 2Ø 240 Hz output.

A portion of the scan count logics is also included in the motor logics circuit. The time base for scan counting is the spacecraft 0.9984 MHz clock. A divide by 100 counter provides a 100 µsecond (10 KHz) time base for the remainder of the counter and decoding.

The counter is designed to count continuously and be reset by the pick-up sync pulse. The reset logics for the entire scan count circuit are on this circuit.

The final circuit on this board is the sync pick-up circuit. There are two magnetic pick-ups in the motor housing which provide the inputs to the sync pick-up circuit.

The HA-2700 operational amplifiers act as level detectors and provide logic level pulses to the logic circuitry. The circuit is designed for redundant operation such that if either pick-up fails, a sync pick-up pulse will still be present at the output.

Drawing No. 8008045 is the schematic diagram of the motor logics (Figure 5-14). The motor logics timing diagram is shown in Figure 5-15.

5.8 Scan Count and Decode

The scan count and decode board provides the basic count-down of the scan period and the decoding of gating signals for the AVHRR electronics. The schematic diagram is given on Drawing 8008049 (Figure 5-16).

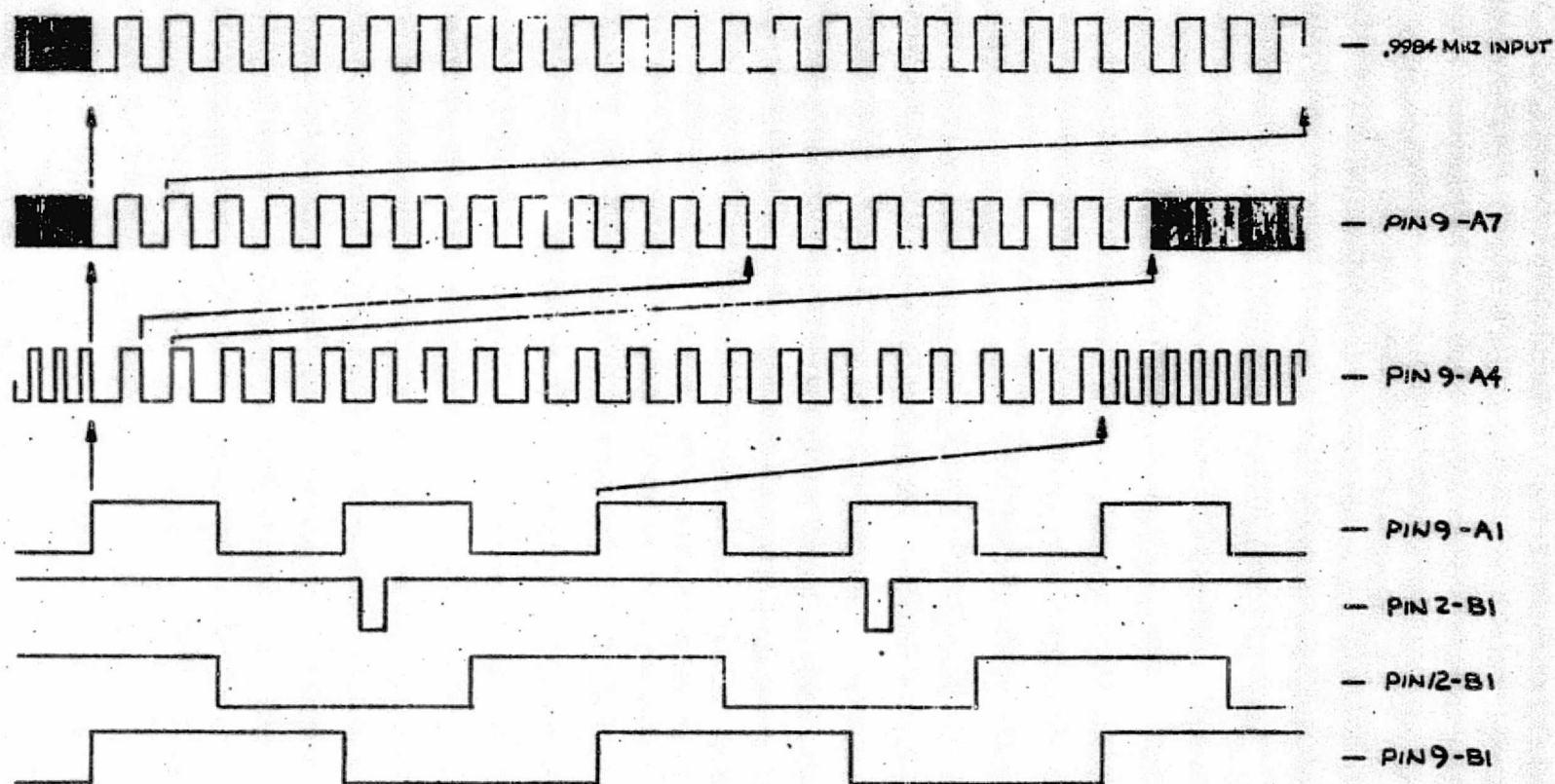


Figure 5-15 Motor Logic Circuit - Timing Diagram

A 10 KHz clock from the motor logics is the time base for the counter. The first six flip flops are a conventional binary ripple counter. The last four counting stages are a divide by 13 ripple counter. The counter is designed to repeat the scan period automatically but is normally reset by magnetic pick-up initiated reset pulse.

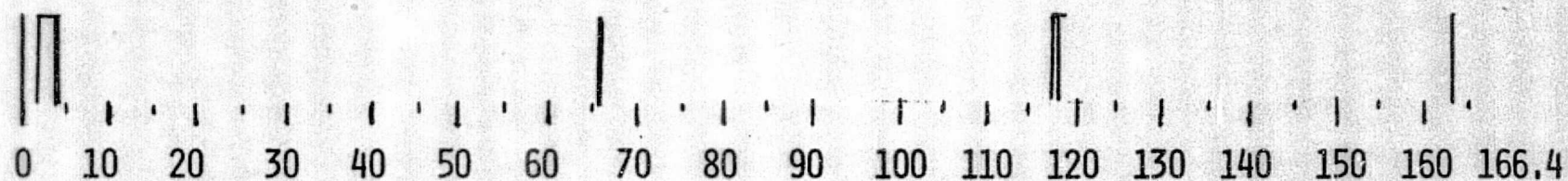
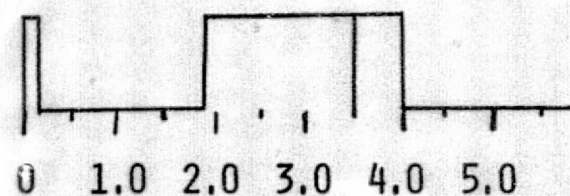
The method of decoding is setting flip-flops at the beginning and end of the desired time interval and decoding the set condition of the first and the reset condition of the second. The clock input is always the highest frequency of the decoded time, which arrangement when used with a ripple counter, provides unambiguous decoding.

The timing of the normal operation signals is shown in Figure 5-17. Timing for the voltage calibration signals is on Figure 5-18.

5.9 Output Data Control

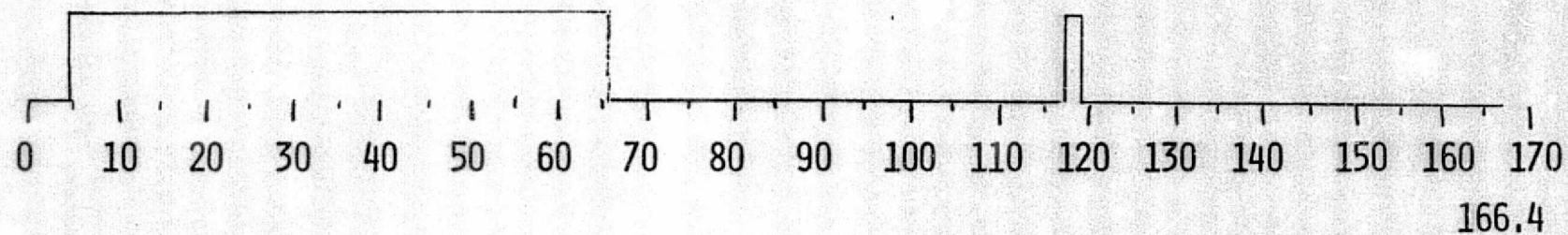
The logics for controlling the conversion of Analog to Digital Data and the transmission to the MIRP is shown on Schematic-Interface Logic No. 1 - 8009206 Figure 5-19 and Schematic Interface Logic No. 2 - 8009209 Figure 5-20. The timing for the output Data Control is shown in Figure 5-21.

By specification, the minimum time between samples from the MIRP can be 25 micro-seconds. With minimum timing, the A to D converter operates in the hold or convert mode for 16 microseconds and in the track or sample mode for 9 microseconds. For longer



0.0-0.1 SYNC PULSE
 1.9-3.5 AMPLIFIER SPACE REFERENCE SAMPLE
 3.5-4.0 RAMP CALIBRATION
 65.6-65.8 IR TARGET TEMPERATURE
 65.8-66.0 PATCH TEMPERATURE
 117.6-118.4 BLACK BODY TEMP - IR SAMPLE

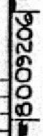
FIGURE 5-17 SCAN TIMING SIGNALS

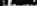


4.0-65.6 SIMULATED EARTH SCENE

117.6-118.4 SIMULATED BACK SCAN TARGET

FIGURE 5-18 SCAN TIMING SIMULATED CALIBRATION



MATERIAL		LARGEST DIMENSION SPECIFIED N/A S-21900		CONTRACT NO. N/A S-21900		 ITT MICROFILM OPTICAL SYSTEMS 201 PARKWAY, WARREN, U.S.A. TELEPHONE AND TELETYPE DEPARTMENTS	
FINISH		TOLERANCES		APPROVALS		SCHEMATIC INTERFACE LOGIC NO. 1	
8009206 61400 BEST AVAILABLE APPLICATION		SIZE DIMENSIONS UNDER 1/8 IN. TO .001 OVER 1/8 IN. TO .002 OVER 1/4 IN. TO .003		DRAWN BY CHECKED BY DATE 7-14-77		APPROVED BY DATE 7-14-77	
REVISIONS 1. 7-14-77 2. 7-14-77		NO SCALE PRINT CORR. NO. TO BRUSH BROS.		ITMS 7-14-77		D 8009206 61400	

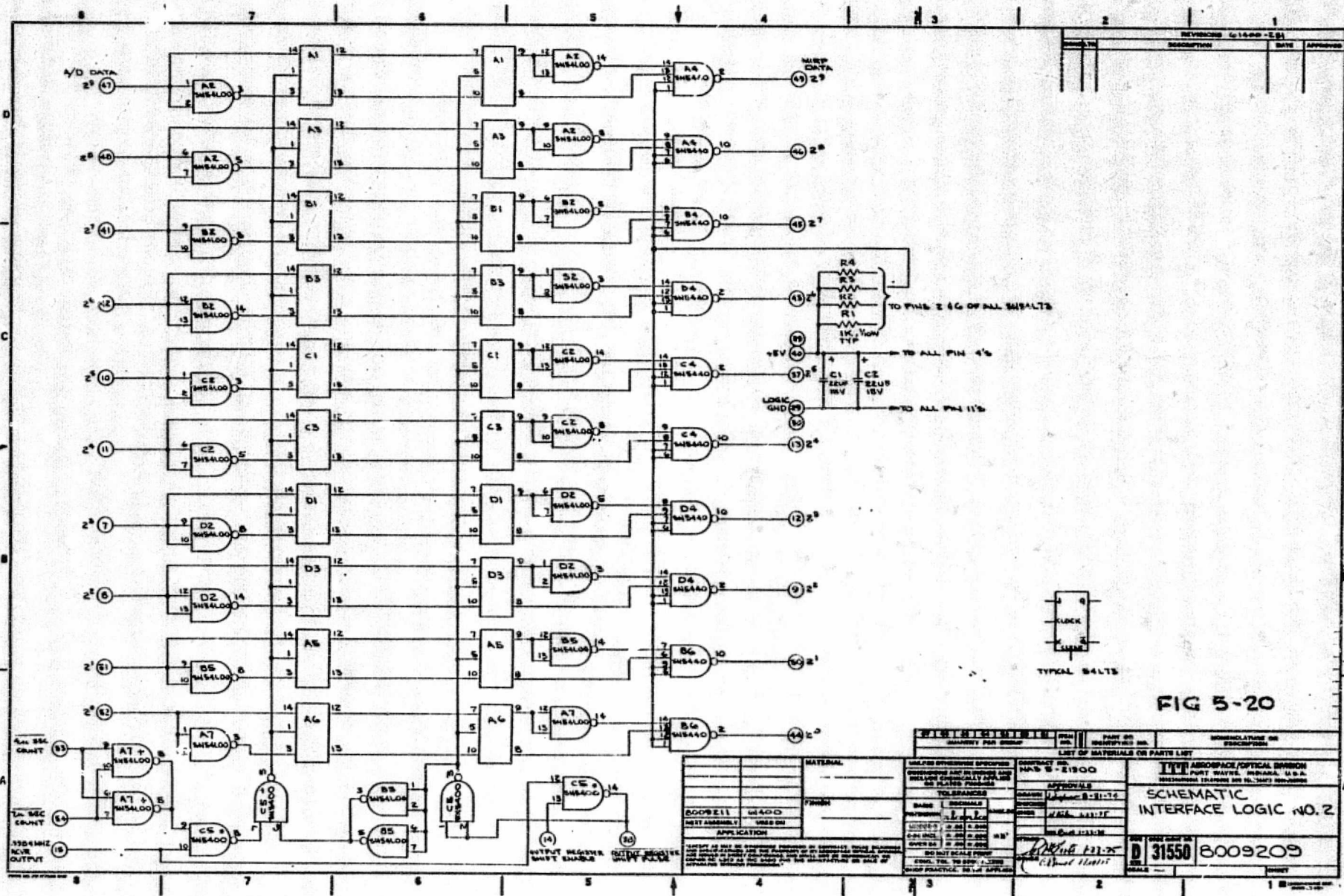


FIG 5-20

REVISIONS REVISION NO. 1 DESCRIPTION DATE APPROVED	
LIST OF MATERIALS OR PARTS LIST PART NO. 1 PART DESCRIPTION QUANTITY PER DRAWING	
CONTRACT NO. 31550 WAS 5-21300 APPROVALS DESIGNER: [Signature] CHECKER: [Signature] DATE: 11-17-76 SCALE: 1:1	
SCHEMATIC INTERFACE LOGIC NO. 2 D 31550 8009209	

SPACECRAFT DATA PROCESSOR/AVHRR INTERFACE TIMING

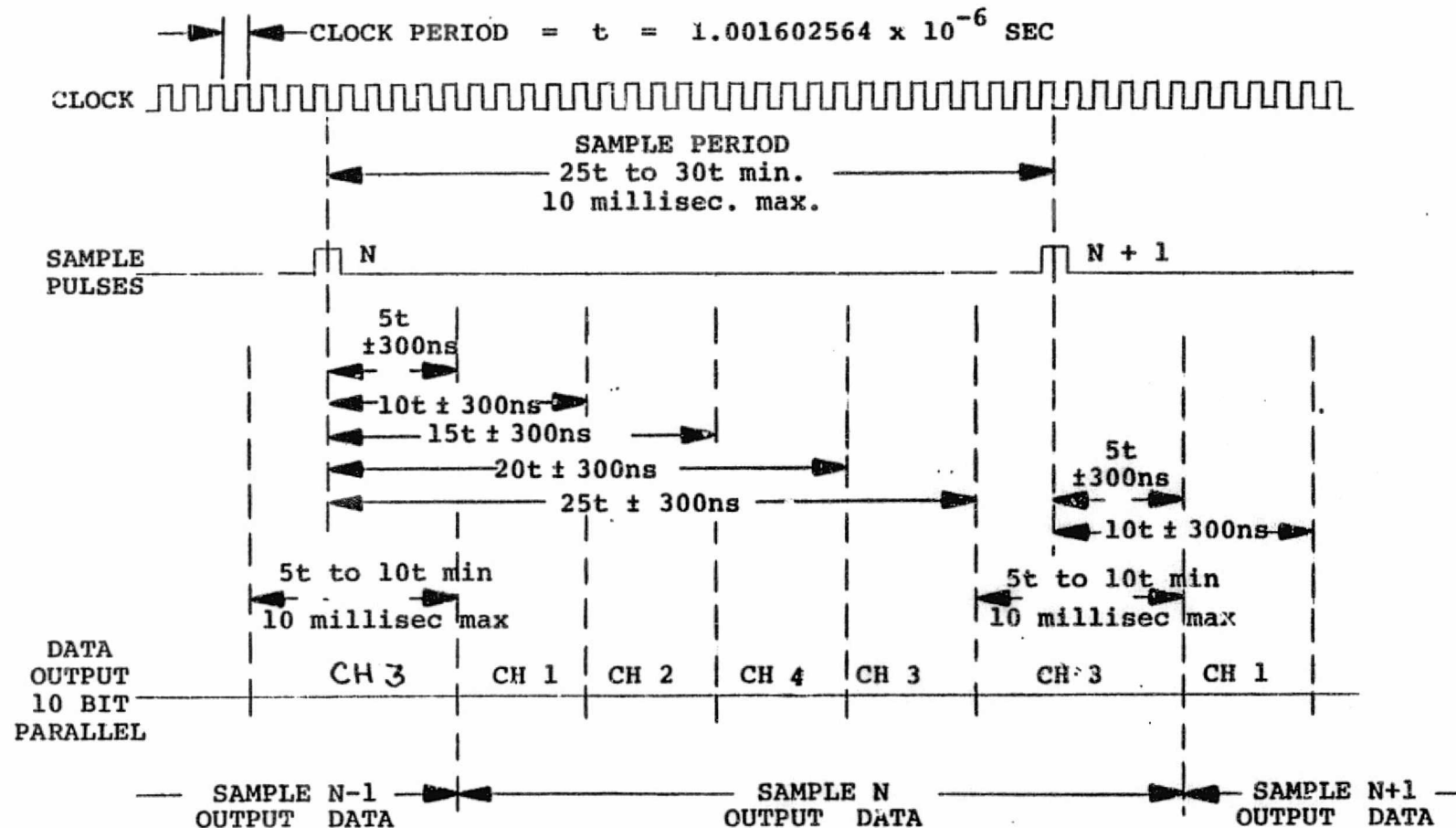


Figure 5-21

intervals between sample pulses, the track time is increased. The sample signal from the MIRP determines the transition from track to hold.

The A to D converter operates on a basic 3 microsecond conversion time. The time allowed for Channel 5 conversion is increased to 4 microseconds to minimize the data storage and gating circuits required.

The A to D converter provides for six input data channels. The target five channels correspond to the five channels of the specification. The sixth channel has multiplexed telemetry data and is switched in under logic control in place of channels 3, 4, and 5 of the appropriate time in the line scan.

Three microseconds (4 microseconds for channel 5) after a channel is selected a strobe signal is sent to the A to D which stores the digitized data in the A to D internal register. The data of this point is in Grey code. Within 0.5 microseconds the Grey to binary conversion is completed and valid binary data is present on the A to D output lines.

The data is later strobed into an intermediate storage register and in sequence to the output register whose outputs directly connect to the output drivers for the MIRP lines.

The following chart gives the timing data for the sequence in microseconds with respect to the MIRP select pulse.

	CH 1	CH 2	CH 4	CH 3	CH 5 **
Analog to Digital Conversion	0-3	3-6	6-9	9-12	12-16
Data in A to D internal register (Grey Code)	3-6	6-9	9-12	12-16	16-3*
A to D output (binary)	3.5-6	6.5-9	9.5-12	12.5-16	16.5-3*
Data in Intermediate register (Reg. 1)	4-7	7-10	10-15	15-20	20-4*
Data in output register (MIRP Signals)	5-10	10-15	15-20	20-25	25-5*

* Time of next conversion cycle.

** Channel 5 input is connected to the Output Data Amplifier of Channel 3.

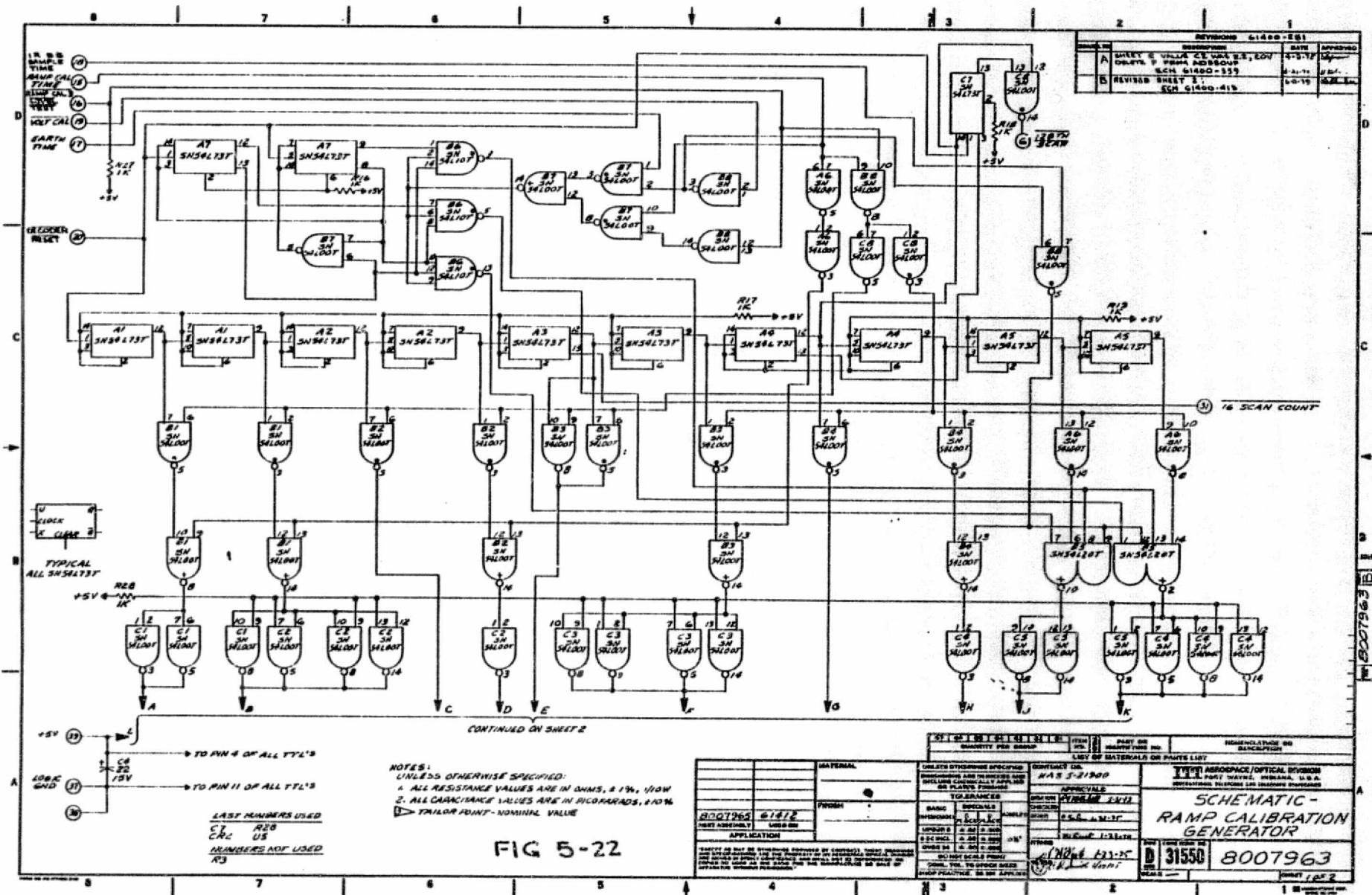
5.10 Ramp Calibration Generator

The ramp calibration and simulated calibration functions have been combined to have the same digital to analog converter be the signal source for both and have the signal control and switching only a logic function. Drawing No. 8007963 sheets 1 and 2 is a schematic diagram of the ramp calibration generator (Figure 5-22).

The counter for the ramp calibration is a conventional 10-bit ripple counter. The outputs are gated to the D to A converter. The system is connected such that each successive scan will give a one-step voltage change in the direction of increasing radiance. This means that the signal will be increasing in voltage in channels 1 and 2 and be decreasing in voltage in channels 3 and 4.

Since ramp calibration signals of both polarities with respect to zero radiance are required, a digital offset (Binary Number 43) is maintained at all times other than ramp calibration time. During space look, the data amplifiers will re-zero on this offset allowing ramp calibration signals of both polarities from zero radiance. The following tables will illustrate this further.

Since the zero radiance voltages were specified at different intervals from the limits of the ramp calibration voltage (+0.25 volts and -0.1 volt) and +6.2 volts and +6.4 volts) the difference was split maintaining the 6.5 volt ramp calibration range giving a 0.275 volt excursion below minimum radiance. This gives a binary value of $1023/6.5 \text{ volts} \times 0.275 \text{ volt} = 43 \text{ bits}$.



The earth scene during simulated calibration is derived from a divide-by-3 counter. The three states are decoded and gated through the two most significant bits giving signals of 1.626, 3.253, and 4.879 volts above minimum radiance.

A test connection has been added to allow three known values of ramp calibration signal to be sequentially gated out when calibrating. This signal must be matched to the amplifier gain which is a function of detector sensitivity.

The clock signal for both counters is derived from the scan timing logics.

The D/A Converter is a 10-bit current switching type converter. The output of the converter is a positive going 0 to 10.23 volt ramp consisting of 1023 steps. The output of the D/A converter is sent to a unity gain inverting amplifier located on the multiplexer board. These two outputs provide both polarity ramp signal for insertion into the data channels as required by circuit configuration.

The ramp calibration generator also provides ± 6.2 volt outputs for use as a stable reference voltage.

<u>VOLTAGE</u>	<u>CHANNELS 1 and 2</u>
+6.475	Channel Ramp Calibration Limit - Binary 1023
6.39375	A/D Converter Signal Limit
6.1	Maximum Scene Radiance
0.25	Zero Radiance - Binary 43
0	A/D Converter Signal Limit
-0.025	Channel Ramp calibration Limit - Binary 0

CHANNELS 3 and 4

+6.475	Channel Ramp Calibration Limit - Binary 0
6.39375	A/D Converter Signal Limit
6.2	Zero Radiance - Binary 43
0.3	Maximum Scene Radiance
0	A/D Converter Signal Limit
-0.025	Channel Ramp Calibration Limit - Binary 1023

5.11 Auxiliary Scan Timing

The auxiliary scan timing circuitry is added to provide continued operation of the AVHRR in the event of the loss of the pick-up signal which synchronizes the scan timing with the scan mirror position.

A block diagram of these circuits is given in Figure 5-23. The complete schematic is shown on Drawing 8008052 (Figure 5-24). The timing for auxiliary scan operation is shown in Figure 5-25. Timing signals are generated on the Scan Count and Decode Board.

The circuit operation is based on the fact that the minimum output signal on Channel 3 occurs when the radiometer views space. With the loss of the synchronizing pulse, the scan counter period is the same as the mirror rotational time but not in synchronism. Two samples of the output voltage are taken at time the scan counter timing indicates that the instrument is viewing space. From this point two different modes of operation ensue. If in the remainder of the scan a signal level lower than the average of the two samples is detected, the scan counter is reset. When the cold target

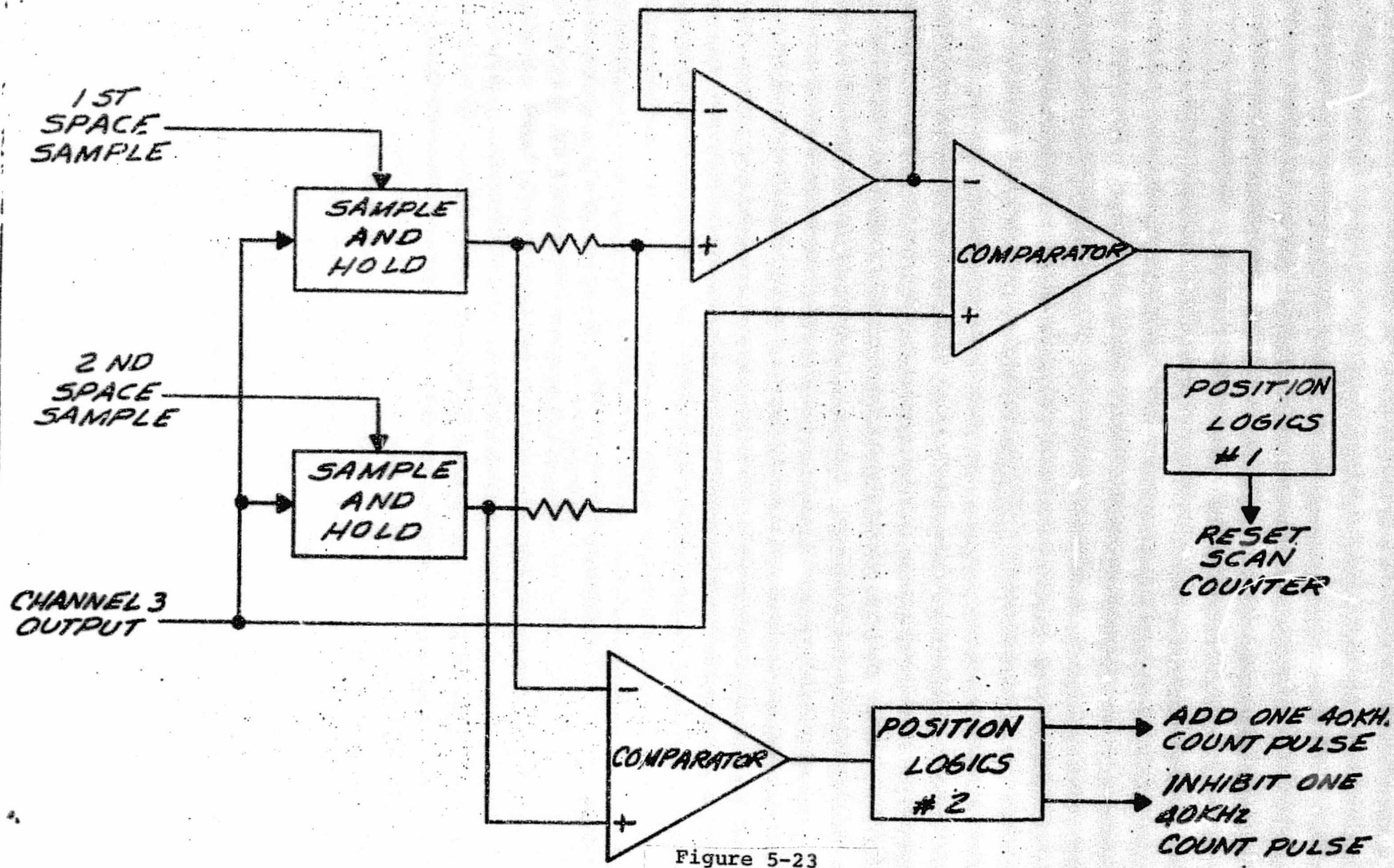
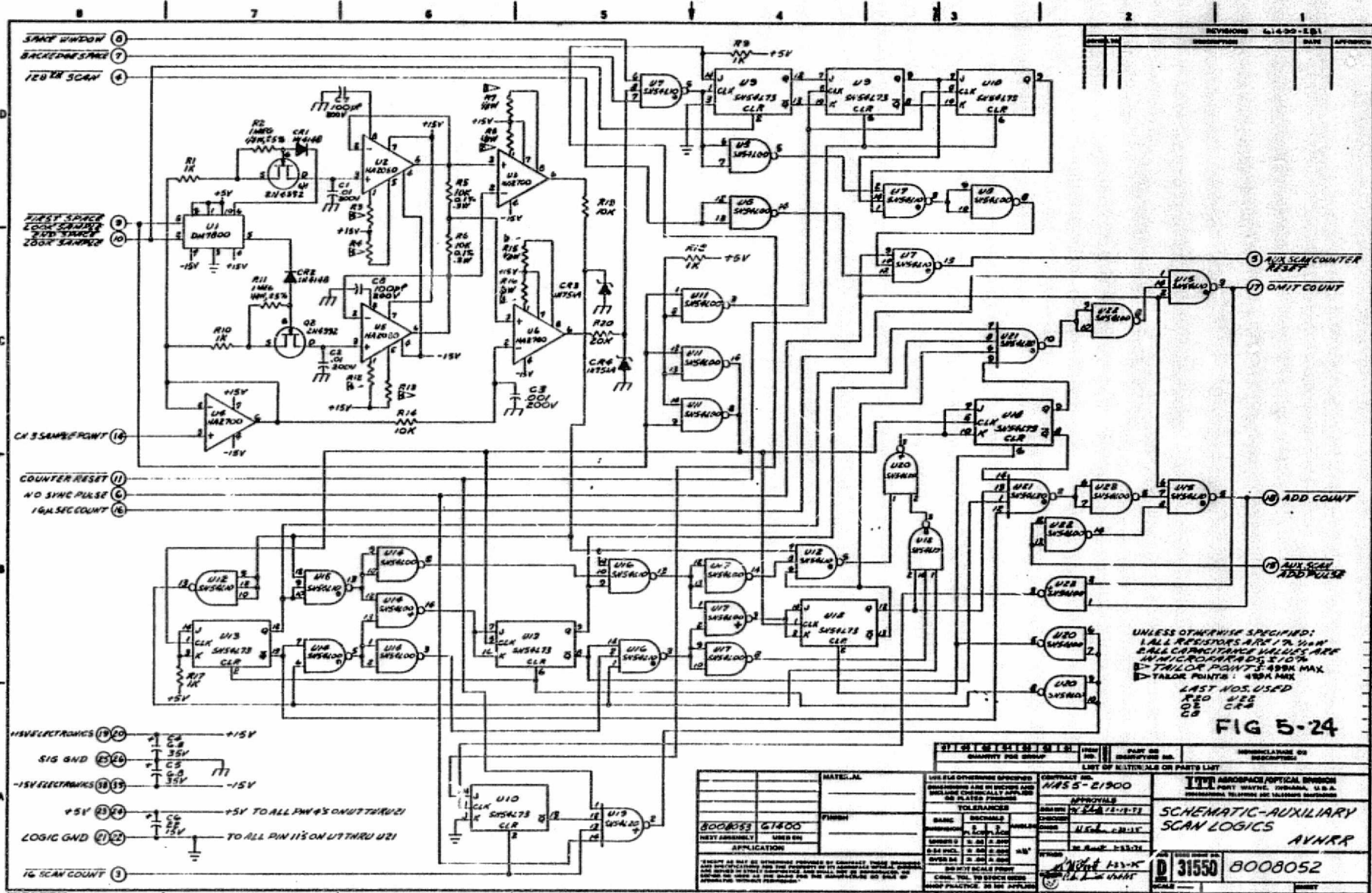
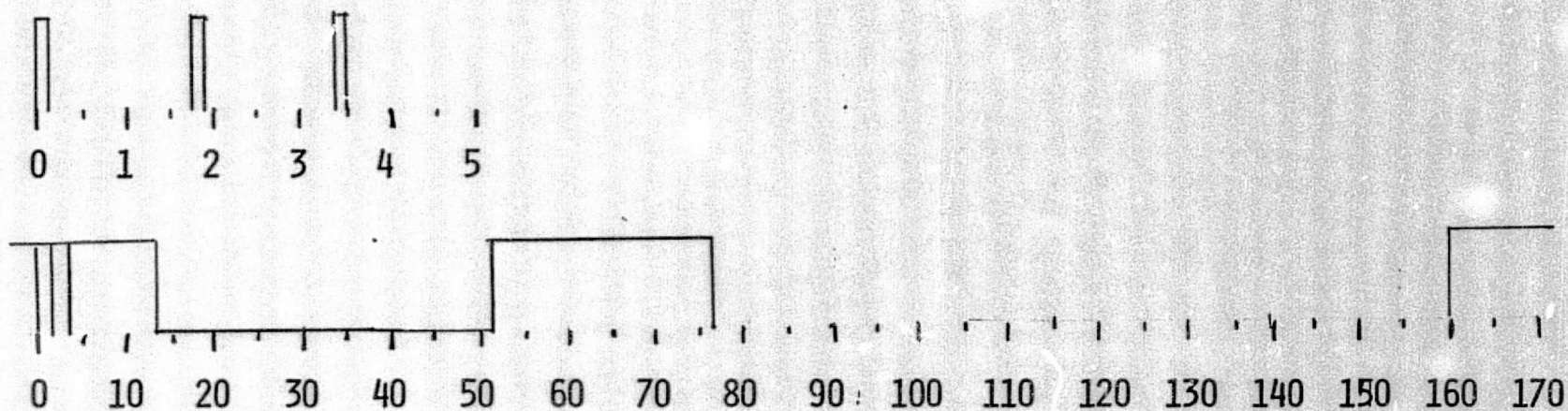


Figure 5-23

BLOCK DIAGRAM AUXILIARY SCAN TIMING





0-0.1	SYNC PULSE
1.8-1.9	FIRST SPACE SAMPLE
3.4-3.5	SECOND SPACE SAMPLE
51.2-76.8	TRAILING EDGE SPACE WINDOW
160.0-170.0	SPACE WINDOW

FIGURE 5-25 AUXILIARY SCAN TIMING

which causes the reset is space, the reset places the counter within a few milliseconds of the correct point. This operation is performed only every 128th scan to allow the data amplifier to settle with the new reference. When the scan counter is near synchronism, a logic gate inhibits this circuit while the mirror is viewing space on the trailing edge of the earth view.

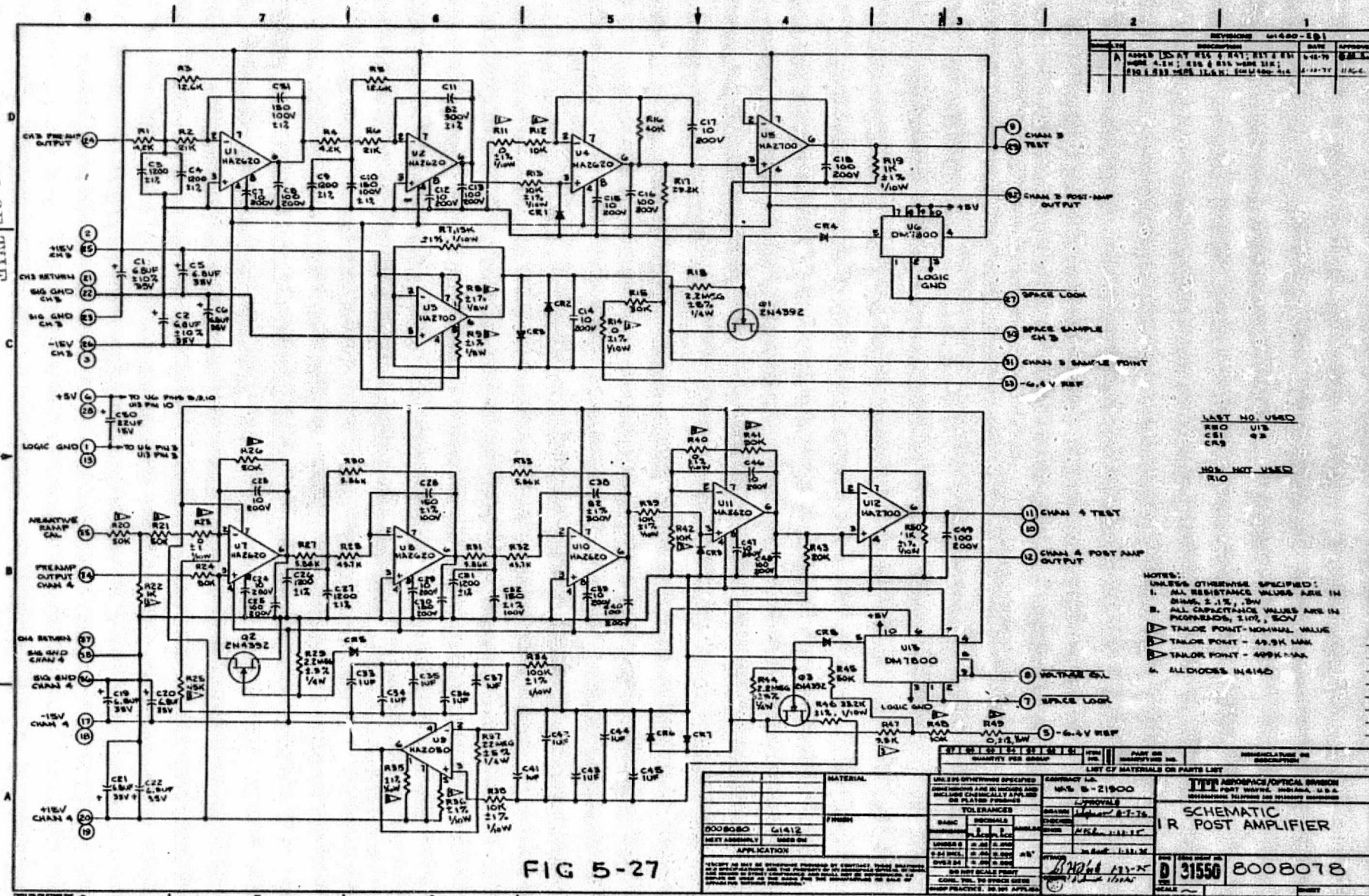
For finer positioning, the relative amplitudes of the two samples are compared. An up-down counter sums the net number of differences over sixteen scans. If a sufficient unbalance exists, the logic will cause a 40 KHz clock signal to be added or omitted, depending on the direction of unbalance. The counter limits are unbalanced in an attempt to cause the samples to go to the early portion of the space view as in the normal scan cycle.

5.12 Ch 3 Data Amplifier

The schematics depicting the Channel 3 amplifier chain are shown on Drawing 8008101 (Figure 5-26) and Drawing 8008078 (Figure 5-27).

The preamplifier has a positive and negative voltage regulator to provide additional regulation for the detector bias and to provide power supply isolation from the remaining electronics for these low level signals.

The input stage of the preamplifier is a differential pair consisting of transistors Q5 and Q7. Transistor Q4 provides a constant current source for Q5 and Q7. The detector signal is inserted at the base of Q5. Stage feed-back, zero-reference feedback, ramp calibration signals, and a DC offset signal are all summed at the base of Q7. This transistor circuit provides an open loop gain of approximately 2500. Amplifier U3 is included in the first stage to provide a single ended output for the signal.



LIST NO. USED
R20 U13
C81 93
C85

NOT USED
R10

- NOTES:
1. UNLESS OTHERWISE SPECIFIED:
A. ALL RESISTANCE VALUES ARE IN OHMS, 5% TOL., 1/4W.
B. ALL CAPACITANCE VALUES ARE IN PICOSECONDS, 5% TOL., 50V.
C. TAILOR POINT - NOMINAL VALUE
D. TAILOR POINT - 49.5K MAX.
E. TAILOR POINT - 495K MAX.
F. ALL DIODES IN4140

MATERIAL		UNLESS OTHERWISE SPECIFIED		CONTRACT NO.		ITP AEROSPACE/OPTICAL DIVISION	
8008078		C1412		NAVS 5-21900		PORT WAREHOUSE, INDIANAPOLIS, U.S.A.	
NEXT ASSEMBLY		USED ON		APPROVALS		SCHEMATIC	
APPLICATION		FRONT		DESIGNED BY		IR POST AMPLIFIER	
QUANTITY		1		CHECKED BY		31550 8008078	
DATE		11/1/77		APPROVED BY		31550 8008078	
REVISION		1		DATE		11/1/77	

Amplifier U4 is an additional stage of voltage gain.

Transistors Q3 and Q6 perform the function of shorting out the detector bias and the offset bias when operating in the Voltage Calibration mode. The removal of bias from the detector effectively eliminates the detector signal. The offset bias is simultaneously removed to allow the zeroing reference circuit to operate at close to normal operating conditions.

The first two post-amplifier stages comprise the pre-sampling filter. This filter is a four pole transitional Butterworth Thomas filter. The relative frequency response curve for the filter is shown in Figure 5-28. The two filter stages give a DC gain of approximately 9 to the chain. An additional stage provides additional gain and a relatively wide band output stage. A unity gain amplifier is used to provide a buffered output to the test connector.

The final amplifier output (inverted) is sampled through a FET and fed back to the preamplifier. This signal is stored in capacitors C14 through C18. This signal is fed back to the preamplifier input stage through amplifier U5 which is an FET input amplifier operating as a low pass amplifier. This amplifier is operated as a non-inverting amplifier providing feedback to the input during the sampling interval.

Sampling time constants are selected such that the amplifier output can be restored to zero during the 2 millisecond sampling time. The DC gain of the U5 amplifier stage allows correction

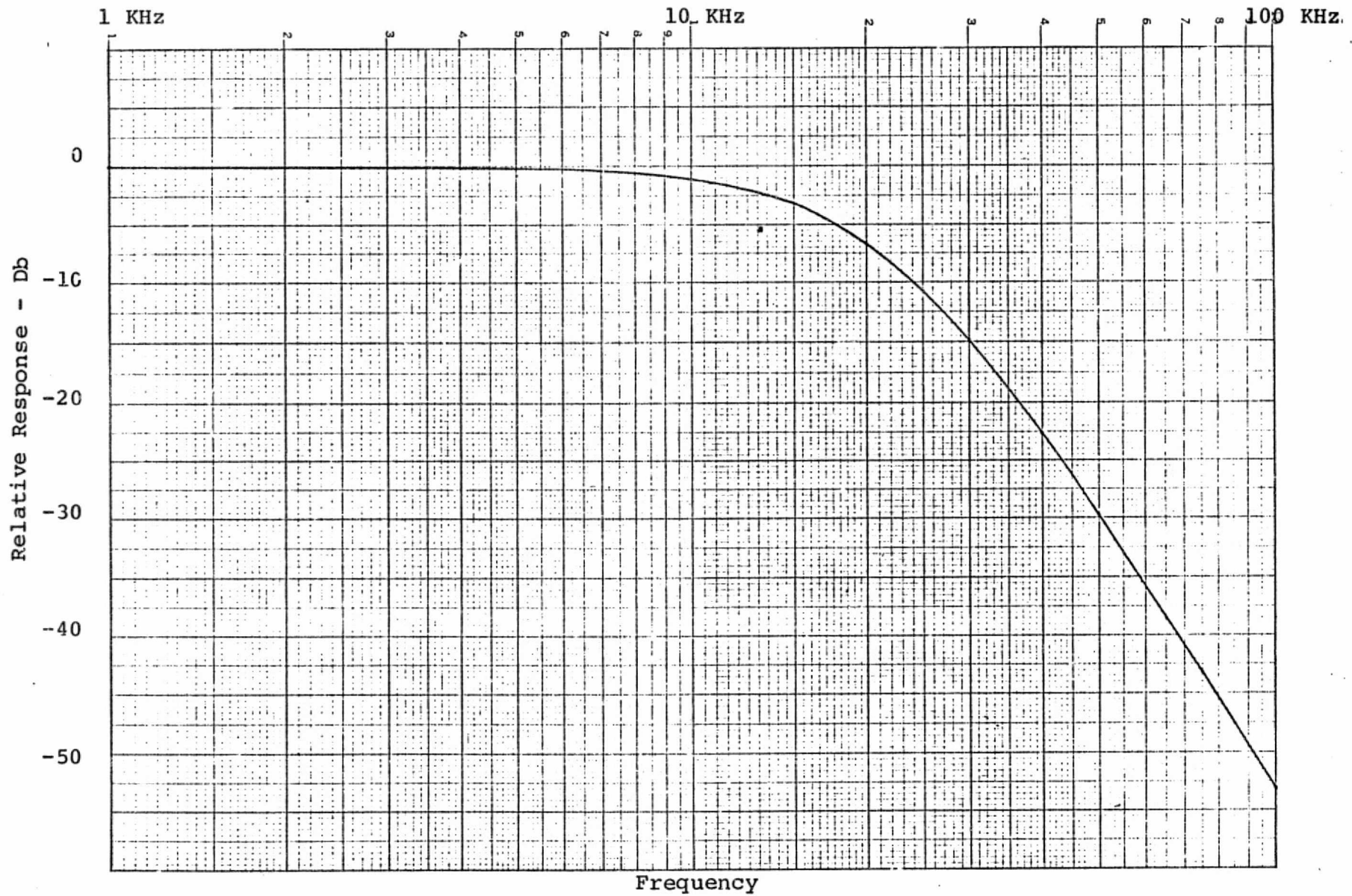


Figure 5-28 Four Pole Transitional Butterworth Thompson Filter Response

of DC offsets with very low DC shifts in the output signal.

A significant amount of tailoring is required in the Ch 3 amplifier to match the possible detector responsivity and bias currents. Provisions are made in several of the amplifier stages for a systematic adjustment by tailoring of gain with fixed resistors. The ramp calibration signal must then be tailored inversely to the overall amplifier gain.

Individual amplifier stages are designed for essentially flat frequency response (except for the filter stages) through the cut-off frequency. For board test the combined gain of the preamplifier and post amplifier will be set at approximately 50,000 which is more than any anticipated requirement. Any tailoring will then be a gain reduction which will not have an adverse affect on frequency response.

5.13 Channel 4 Amplifier

The schematic for the channel 4 preamplifier is shown on 8009217 (Figure 5-31). The channel 4 post amplifier is physically located with the channel 3 post amplifier (Figure 5-27).

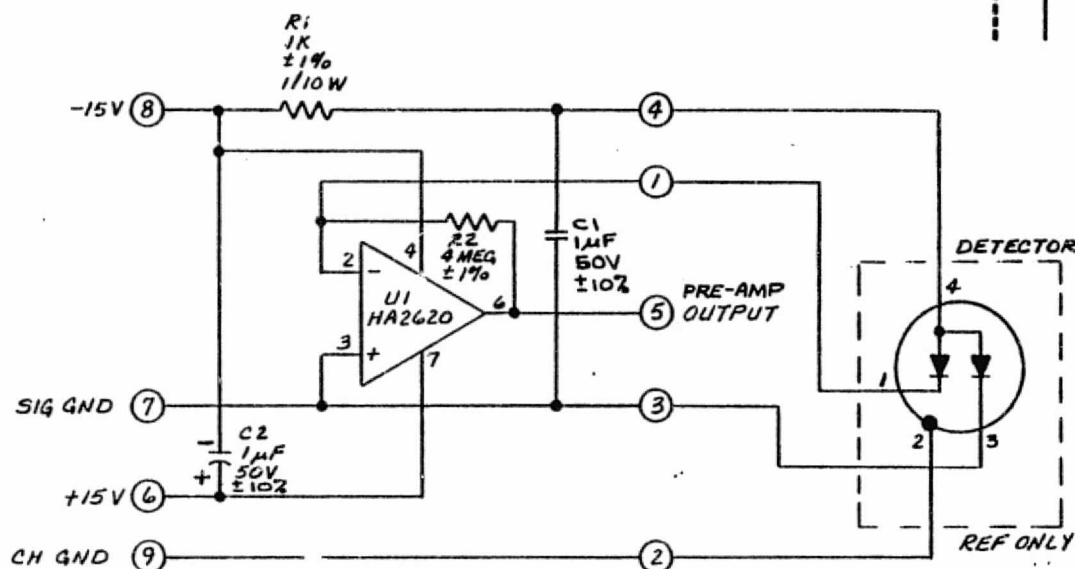
The channel 4 preamplifier is a current to voltage converter with a high (16 meg) feedback resistor for low noise operation. The detector is maintained with a low back bias for minimum detector noise output. This bias is tailored to match each detector.

The Post Amplifier is identical to the Daylight Post Amplifier.

5.14 Daylight Amplifiers

The schematics of the daylight amplifier system are shown in Drawing 8008130 (Figure 5-29) and Drawing 8008096 (Figure 5-30). The amplifiers for channel 1 and channel 2 are identical except for the tailoring required to match detector responsivity.

The preamplifiers are located in the optics module with the detectors directly connected to the preamplifier terminals.



REVISIONS 61400-2B1				
ZONE	LYR	DESCRIPTION	DATE	APPROVED

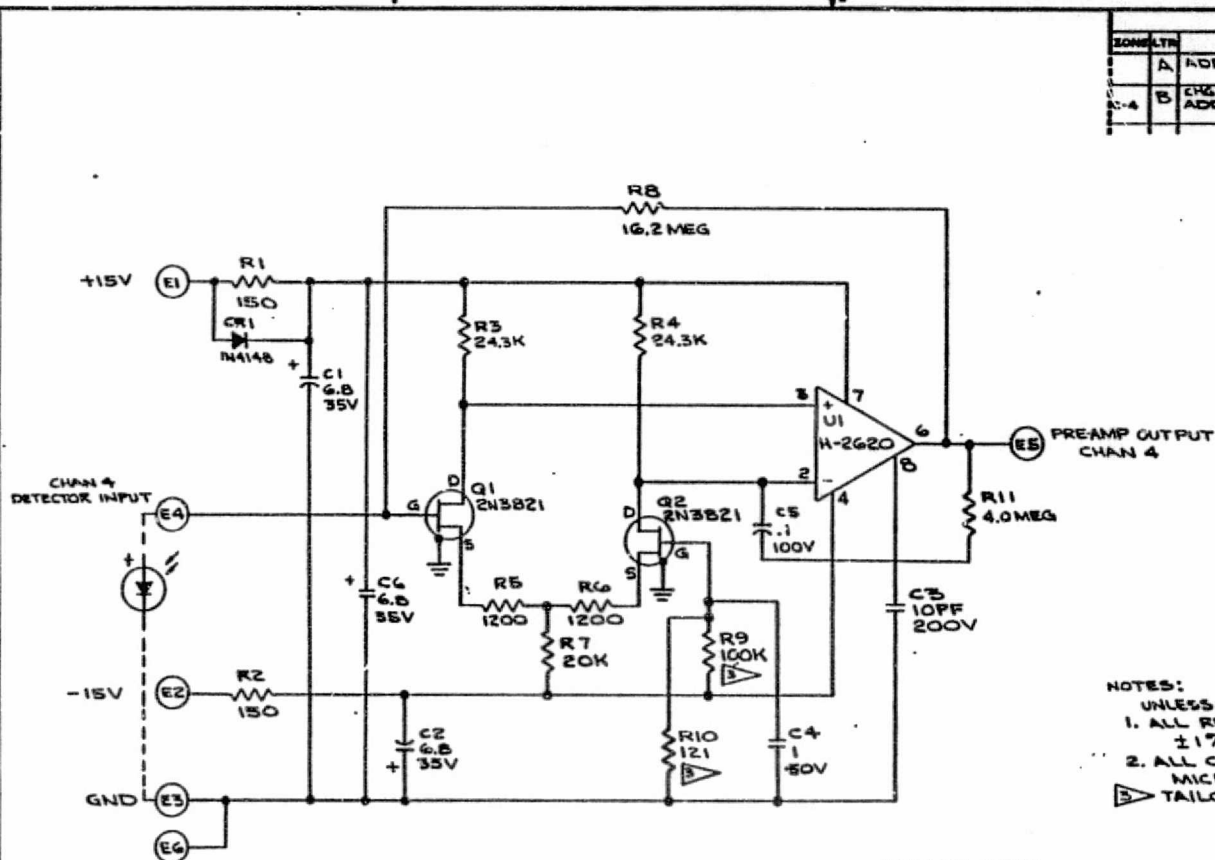
LAST NO'S. USED

R2
C2
U1

FIG 5-29

Q7	Q6	Q5	Q4	Q3	Q2	Q1	ITEM NO.	PART OR IDENTIFYING NO.	NOMENCLATURE OR DESCRIPTION
QUANTITY PER GROUP									
LIST OF MATERIALS OR PARTS LIST									
CONTRACT NO. NAS 5-21900		ITV AEROSPACE/OPTICAL DIVISION FORT WAYNE, INDIANA, U.S.A. INTERNATIONAL TELEPHONE AND TELEGRAPH REGISTRATION							
APPROVALS		SCHEMATIC DAYLIGHT PREAMP							
DRAWN <i>V. Douglas 6/1/73</i>									
CHECKED									
ENGR <i>H. G. 1-22-73</i>									
ITTAOD <i>1-23-73</i>									
OTHER <i>1-23-73</i>									
UNLESS OTHERWISE SPECIFIED DIMENSIONS ARE IN INCHES AND INCLUDE CHEMICALLY APPLIED OR PLATED FINISHES									
TOLERANCES									
2 PLACE DECIMALS ±.02									
3 PLACE DECIMALS ±.010									
ANGLES ±1/2°									
COML TOL TO STOCK SIZES									
SHOP PRACTICE, 39.101 APPLIES									
MATERIAL									
FINISH									
APPLICATION									
NEXT ASSEMBLY USED ON									
HCMR									
8008132 AVHRR									
SIZE B		CODE IDENT NO. 31550		8008130					
SCALE ~				SHEET					





REVISIONS L1400-251			
NO.	DESCRIPTION	DATE	APPROVED
A	ADDED CR1 & C6 ECN 61400-303	2-12-75	Shannon
B	CHG VALUE R8 WAS 22.4MEG ADD DETECTOR ECN 61400-352	4-8-75	Shannon

- NOTES:
UNLESS OTHERWISE SPECIFIED:
1. ALL RESISTANCE VALUES ARE IN OHMS,
±1%, 1/10W.
2. ALL CAPACITANCE VALUES ARE IN
MICROFARADS ±10%
▷ TAILOR POINT - NOMINAL VALUE

LAST NO. USED
R11 U1
C6 Q2
CR1

FIG 5-31

87 86 85 84 83 82 81		ITEM NO.	PART OR IDENTIFYING NO.	NOMENCLATURE OR DESCRIPTION
QUANTITY PER GROUP		LIST OF MATERIALS OR PARTS LIST		
MATERIAL		CONTRACT NO. NA 5-21900		ITT AEROSPACE/OPTICAL DIVISION FORT WAYNE, INDIANA, U.S.A. INTERNATIONAL TELEPHONE AND TELEGRAPH CORPORATION
FINISH		APPROVALS		
8009219 61400		DRAWN CHECKED ENGR		SCHEMATIC CHANNEL 4 PREAMPLIFIER
NEXT ASSEMBLY USED ON		DATE 1-21-75		
APPLICATION		DATE 1-11-78		C 31550 8009217
*EXCEPT AS MAY BE OTHERWISE PROVIDED BY CONTRACT, THESE DRAWINGS AND SPECIFICATIONS ARE THE PROPERTY OF ITT AEROSPACE/OPTICAL DIVISION, AND SHALL BE KEPT IN STRICT CONFIDENCE, AND SHALL NOT BE REPRODUCED OR COPIED OR USED AS THE BASIS FOR THE MANUFACTURE OR SALE OF APPARATUS WITHOUT PERMISSION.		ITTACOR 1-23-75 1-23-75		
		DO NOT SCALE PRINT		SCALE
		CONV. TOL. TO STOCK SIZES		SHEET
		SHOP PRACTICE, 30.101 APPLIES		

The detectors are operated in biased mode as a current source. A 4 megohm feedback resistor is used to minimize noise current.

The post amplifiers for the daylight channels are essentially the same as the post amplifier for channel 3. The space sample for the zero reference is fed back to the input stage of the post amplifier. The ramp calibration signal is summed in at first post amplifier stage. A FET is used to short out the preamplifier signal during the Voltage calibration mode of operation.

5.15 Multiplexer Board

This printed circuit board contains the multiplexer for the 6th input channel of the analog-to-digital converter, the blackbody temp. IR TM circuits, and over-temperature monitor circuits for the patch and radiator.

The multiplexer consists of five FET switches feeding amplifier U3. The logic timing signals for control of the FET's are generated on Black Body Mux board. The four Black Body TM signals are sequenced in the same time position on a line scan basis. During the fifth line scan, none of the signals are gated providing a 0 volt marker in that time position. The low range patch temperature is the other multiplexed signal.

The blackbody temp - IR telemetry signals are two identical sample and hold circuits (amplifiers U12 and U13). The sample logic signal is generated on the Scan Count and Decode board and is to provide a sample of the two IR channel outputs at the time the scan mirror has a full view of the internal calibration target (internal blackbody).

The patch and radiator temperature TM voltages are fed to amplifiers U6 and U8 operating as comparators with a reference voltage. The amplifier outputs drive switching transistors in the patch and radiator heater circuits to remove power if the temperature exceeds the allowable figure (currently 40°C).

The schematic diagram for this board is shown in Figure 5-32.

5.16 Black Body Mux

A logic divide by five counter of the BB Temp (logic) signal with four of the counter states decoded provide the logic control signals for the time multiplexing of the four Black Body TM signals. The fifth undecoded state provides the marker scan.

Individual transistor Q2 and Q4 are used to drive each Earth Shield deploy solenoid. Feedback from the shield position switches remove transistor drive current through amplifier U6. The Earth Shield Disable removes all power from these circuits. An R-C delay in the base circuit limits the input current surge. See Figure 5-33.

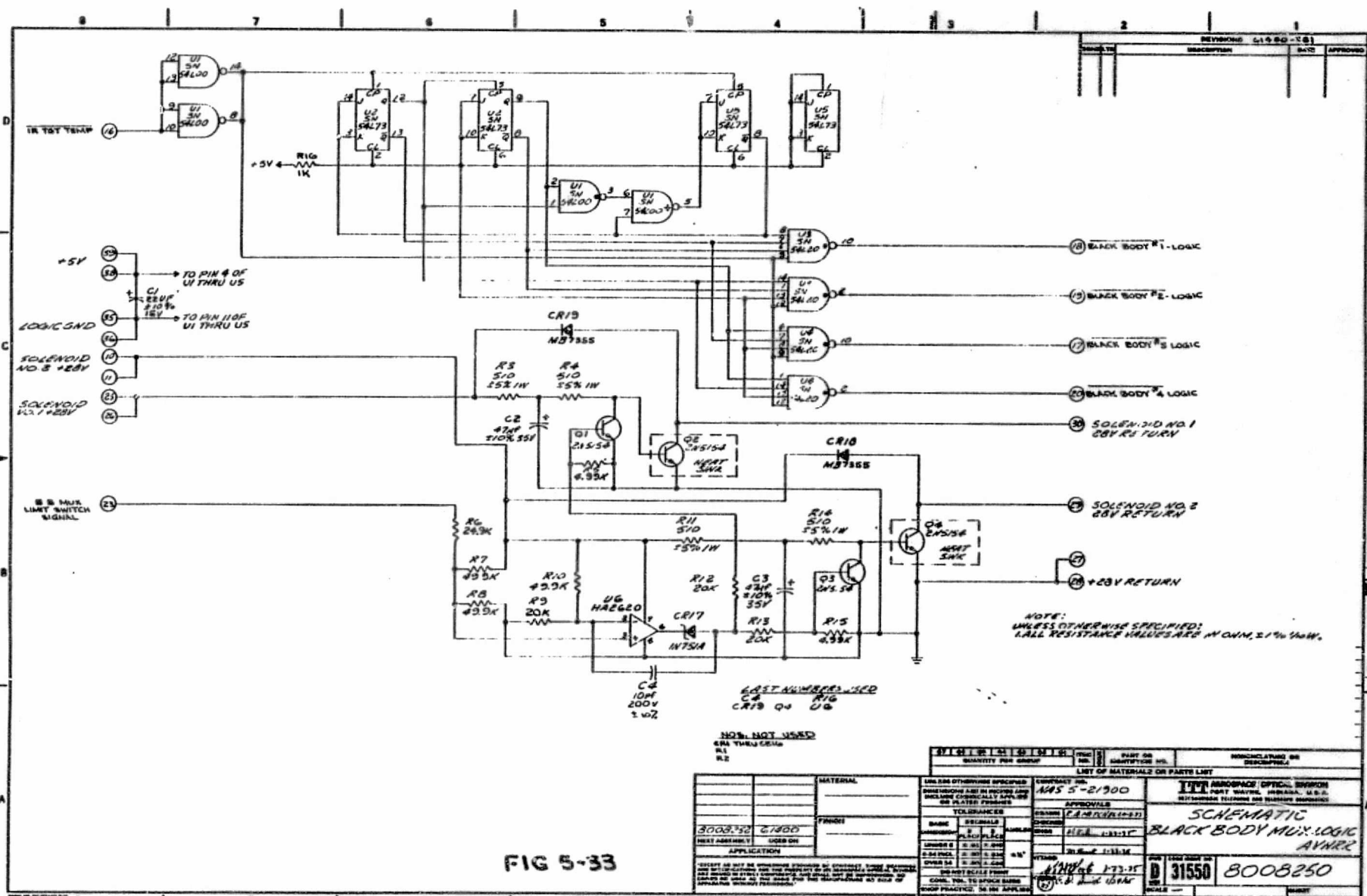
5.17 Motor Power Supply

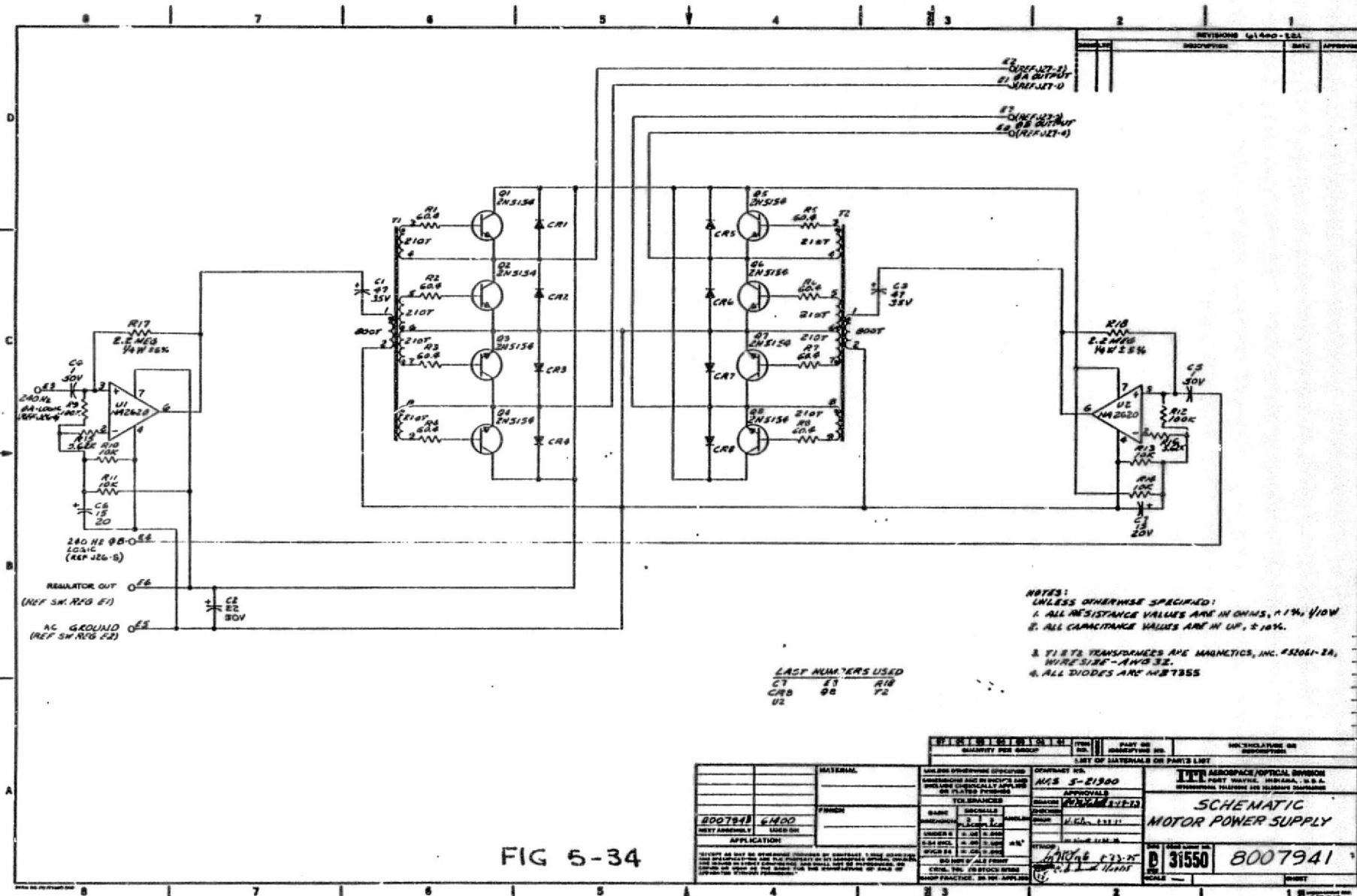
The motor power supply converts +22 volts DC (high power mode) or +18 volts DC (low power mode) into a two-phase 240 Hz square wave to drive the 80 pole scan mirror motor. The circuit is a conventional bridge switching inverter. Drawing No. 8007941 is the schematic diagram of the motor power supply (Figure 5-34).

The input signals from the Motor Logics circuit are AC coupled for ground isolation. The HA2620 operational amplifiers act as comparators and provide sufficient drive for the primary circuit to insure saturation of the inverter transistors.



FIG 5-32





- NOTES:
UNLESS OTHERWISE SPECIFIED:
1. ALL RESISTANCE VALUES ARE IN OHMS, 1% 1/10W
2. ALL CAPACITANCE VALUES ARE IN UF, 5%
3. T1 & T2 TRANSFORMERS ARE MAGNETICS, INC. #31061-2A,
WIRE SIZE #14-32
4. ALL DIODES ARE M7355

LAST NUMBERS USED
C7 E3 R10
C8 E2 F2
U2

8007941 PART NO. QUANTITY PER GROUP		5-21900 PART NO. QUANTITY PER GROUP		31550 PART NO. QUANTITY PER GROUP	
8007941 PART NO. QUANTITY PER GROUP		5-21900 PART NO. QUANTITY PER GROUP		31550 PART NO. QUANTITY PER GROUP	
8007941 PART NO. QUANTITY PER GROUP		5-21900 PART NO. QUANTITY PER GROUP		31550 PART NO. QUANTITY PER GROUP	
8007941 PART NO. QUANTITY PER GROUP		5-21900 PART NO. QUANTITY PER GROUP		31550 PART NO. QUANTITY PER GROUP	

5.18 Power Profile

Figure 5-35 depicts the power usage under the mode of operation indicated.

5.19 Interface Connectors

Table 5-1 lists the connections and type of connectors for the AVHRR Electrical Interface.

5.20 Electronics Drawings

Table 5-2 is a list of the drawings for the electronics printed circuit boards.

POWER PROFILE

FUNCTION	POWER	NORMAL OPERATION	TELEMETRY ONLY	MOTOR ON	COOLER HEATER	INSTRUMENT OFF
ANALOG TELEMETRY	1.89W	X	X	X	X	
A-D & ELECTRONICS **	12.91W	X				
SCAN MOTOR HIGH	4.48W	X		X		
SCAN MOTOR LOW	3.67W			X		
MOTOR LOGIC	1.3W	X	X	X	X	
CHANNEL 1	.84W	X				
CHANNEL 2	.84W	X				
CHANNEL 3	1.5W	X				
CHANNEL 4	1.16W	X				
COOLER HEATER	24.6W				X	
COOLER COVER DEPLOY	56.9W*					
STANDBY HEATER	22.8W***					X
		24.92W	3.19W	6.86W or 7.67W	27.79W	22.8W*

* Required only once for a period of approximately 1 sec.

** Measured PFM values. ETM total was 25.51W.

*** Supplied from TCE - not from +28V buss.

Table 5-1 Interface Connectors

<u>NO.</u>	<u>FUNCTION</u>	<u>GSFC STYLE</u>	<u>DESCRIPTION</u>
J1	Command	311P405-4P-C-12	37 Pin Male
J2	Digital TM	311P405-3S-C-12	25 Pin Female
J3	Power	311P405-3P-C-12	25 Pin Male
J4	Analog TM	311P405-4S-C-12	37 Pin Female
J5	Clock	311P405-1P-C-12	9 Pin Male
J6	Data Processor	311P405-2P-C-12	15 Pin Male
J7	Test	311P405-5S-C-12	50 Pin Female
J33	Pulse Load Heater	311P405-18-C-12	9 Pin Female

J1 COMMAND

<u>PIN NO.</u>	<u>FUNCTION</u>
1	Elec/Telemetry On
2	Elec/Telemetry Off
3	Motor/Telemetry On
4	Motor/Telemetry Off
5	Telemetry Not Locked On
6	Telemetry Locked On
7	Channel 1 Enable
8	Channel 1 Disable
9	Channel 2 Enable
10	Channel 2 Disable
11	Channel 3 Enable
12	Channel 3 Disable
13	Channel 4 Enable
14	Channel 4 Disable
15	Motor Low Power
16	Motor High Power
17	Patch Low
18	Patch High
19	
20	Patch Control Off
21	Patch Control On
22	Earth Shield Disable
23	Earth Shield Deploy
24	Cooler Heat Off
25	Cooler Heat On
26	Voltage Calibrate Off
27	Voltage Calibrate On

J1 COMMAND (Continued)

PIN NO.

FUNCTION

28

29

37

Chassis Ground

J2 DIGITAL TM

PIN NO.

FUNCTION

1	Earth Shield Status
2	Patch Control Status
3	Patch Mode Status
4	Motor Mode Status
5	Voltage Calibrate Status
6	Cooler Heat Status
7	Electronics/Telemetry Status
8	Motor/Telemetry Status
9	Telemetry Lock Status
10	Channel 1 Status
11	Channel 2 Status
12	Channel 3 Status
13	Channel 4 Status
14	
25	Chassis Ground

J3 POWER

<u>PIN NO.</u>	<u>FUNCTION</u>
1	+28V Buss
2	+28V Buss
3	+28V Buss (Motor)
4	+28V Buss (Motor)
5	Power Ground
6	Power Ground
7	AC 28V Return
8	AC 28V Return
9	+10V Buss
10	+10V Buss
11	+5V Buss
12	+5V Buss
13	Interface Power Ground
14	Interface Power Ground
15	Signal Ground
16	Signal Ground
17	Chassis Ground
18	Chassis Ground

J4 ANALOG TM

<u>PIN NO.</u>	<u>FUNCTION</u>
1	Radiator Temp. TM
2	Patch Power TM
3	Patch Temp TM Low Range
4	Patch Temp TM Ext Range
5	Black Body #1 TM
6	Black Body #2 TM
7	Black Body #3 TM
8	Black Body #4 TM
9	Motor Current TM
10	Elect. Current TM
11	Earth Shield Position TM
12	Electronics Temp. TM
13	Base Plate Temp. TM
14	A/D Conv. Temp. TM
15	Motor Hsg. Temp TM
16	Cooler Hsg. Temp. TM
17	Detector Bias Volt Ch. 3 TM
18	
19	BB Temp. IR Ch. 3 TM
20	BB Temp. IR Ch. 4 TM
21	Offset Voltage TM
37	Chassis Ground

J5 CLOCK

PIN NO.

FUNCTION

1	Clock ~ Ref
2	Clock
3	Clock Shield
4	Chassis Ground

J6 DATA PROCESSOR

<u>PIN NO.</u>	<u>FUNCTION</u>
1	2^9 MIRP Data
2	2^8 MIRP Data
3	2^7 MIRP Data
4	2^6 MIRP Data
5	2^5 MIRP Data
6	2^4 MIRP Data
7	2^3 MIRP Data
8	2^2 MIRP Data
9	2^1 MIRP Data
10	2^0 MIRP Data
11	Chassis Ground
12	Sample Pulse From MIRP
13	Chassis Ground
14	Sync Pulse
15	Chassis Ground

J7 TESTPIN NO.FUNCTION

1	Test - Pick-up loss sim.
2	Ramp Cal. 3 level
3	Ch. 3 Test
4	Ch. 4 Test
5	Ch. 1 Test
6	Ch. 2 Test
7	Ref. V Test Point
8	Pick-up #1 Test
9	Pick-up #2 Test
10	-15V Test
11	+15V Test
12	Clock Rcvr Test
13	Solenoid +28
14	Solenoid +28
15	+5V Test
17	Sync Pulse
50	Chassis Ground

J33 - PULSE LOAD HEATER

PIN NO.

FUNCTION

1	Pulse Load Heater
2	Pulse Load Heater Ret.
3	Temp. Control Sensor
4	Temp. Control Sensor
5	
6	
7	Chassis Ground
8	
9	

Table 5-2 AVHRR DRAWING NUMBERS

CIRCUIT NAME	SCHEMATIC	BOARD #	ASSEMBLY DRAWING	ASSEMBLY PROCEDURE	TEST PROCEDURE
POWER CONV. & SW. REG.	8007970	8007971	8007972	8008230	8008278
LOGICS REGULATORS	8007975	8007976	8007977	8008231	8008279
±15V REGULATORS	8007980	8007981	8007982	8008232	8008282
MOTOR SW. REG.	8007944	8007945	8007946	8008233	8008297
COMMAND RELAY #1	8008800	8008801	8008802	8008234	8008280
COMMAND RELAY #2	8008794	8008795	8008796	8008235	8008281
COMMAND RELAY #3	8009213	8008795	8008796	8009224	8009227
PATCH TEMP CONT. & T/M	8008120	8008121	8008122	8008236	8008290
T/M BOARD #2	8008127	8008128	8008129	8008237	8008291
MOTOR LOGICS	8008045	8008046	8008047	8008238	8008283
SCAN COUNT & DEC.	8008049	8008050	8008051	8008239	8008284
INTERFACE LOGICS #1	8009206	8009207	8009208	8008240	8008293
INTERFACE LOGICS #2	8009209	8009210	8009211	8009225	8009228
RAMP CAL. GEN.	8007963	8007964	8007965	8008241	8008285
AUX SCAN LOGICS	8008052	8008053	8008054	8008242	8008286
CH. 3 PREAMP	8008101	8008102	8008103	8008243	8008294
CH. 4 PREAMP	8009217	8009218	8009219	8009226	8009229
IR POST AMP	8008078	8008079	8008080	8008244	8008288
DAYLIGHT PREAMP	8008130	8008131	8008132	8008245	8008295
DAYLIGHT POST AMP	8008096	8008097	8008098	8008246	8008289
MULTIPLEXER	8008133	8008134	8008135	8008247	8008292
MOTOR POWER SUPPLY	8007941	8007942	8007943	8008248	8008296
BLACK BODY MUX	8008250	8008251	8008252	8008249	8008287

6.0 RADIANT COOLER

The radiant cooler has a simplicity of design (Figure 6.0-1) that reflects the advantageous orbit and the absence of spacecraft extensions in the anti-sun direction. It is a conservative design that employs proven hardware and techniques; there is ample cooling margin for both temperature control and possible thermal degradation. The specific requirements imposed on the detector cooler are as follows:

- a. The cooler shall be mounted on the anti-sun side of the space vehicle and shall look into a hemisphere (of cold space) except for the solid angle subtended by the earth. The cooler must be shaded from earth radiation.
- b. The nominal temperature of the infrared detectors shall be actively controlled at either 105K or 110K (selectable by command). At the beginning of orbital life, the uncontrolled temperature shall be 95K or less.
- c. During acquisition, the cooler field of view can sweep through the sun at a rate of 0.5 rpm for an undeterminate period. The cooler must operate with no degradation after this exposure.

We have assumed the earth shading requirement (a) applies to the patch or second stage of cooling and that the margin requirement (b) applies to the nominal orbit (450 n mi altitude and

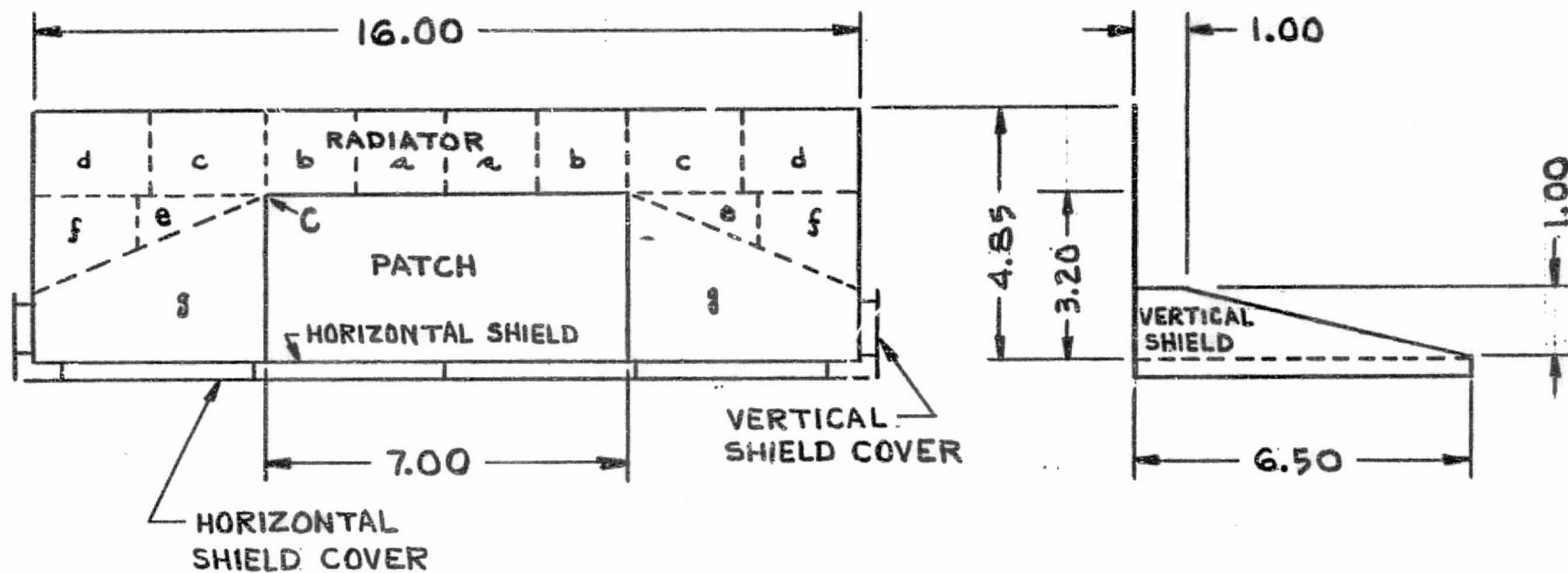


FIG. 6.0-1 BASIC DESIGN OF RADIANT COOLER (DIMENSIONS IN INCHES)

37.5° orbit normal to sun angle). The earth shield will be used as a protective cover during acquisition; exposure is limited to the shield cover, which reaches a maximum temperature of about 0°C during a continuous 0.5 rpm sweep through the sun (Section 6.5).

The design of the radiant cooler is described in detail in Sections 6.1 through 6.4. The performance is analyzed for the nominal condition and for variations in the orbital parameters. The anticontamination provisions to protect both thermal and optical surfaces are described in Section 6.6. Because of the relatively large amount of thermal loading through the optical port to the cooler, we have established detailed models that have been verified by thermal tests (Section 6.7).

The nominal in orbit characteristics of the cooler are summarized in Table 6.0-1 and 6.0-2.

6.1 Field of View

The hemisphere above the cooler patch is cold space except for the earth. As a result, any point on the patch can be shaded by a semicircular shield that matches the angle subtended by the earth and any vertical line by the semicircular shield for its top point. The smallest shield for the entire patch is then obtained by translating the latter shield along the horizontal dimension of the patch. We have modified this shield and increased the shading of the radiator by the use of small vertical sides. The maximum angle subtended by the earth is the solution to \sin

$\beta_m = R_m/R_m + h$, where R_m is the equatorial earth radius (3444.3 n mi) plus the tropical atmospheric height (9.1 n mi) and h is

Table 6.0-1 Nominal Characteristics of the Radiator

Temperature (a)	170.6 K	
Power radiated (a)	1.66 W	
Radiating area	55.2 in ²	
Conductive input (a)	0.195 W	11.7%
Insulation input (a)	0.592	35.6
Earth input	0.210	12.7
Covers input	0.388	23.4
Optical port input (a)	0.275	16.6
dT/dφ (b)	2.05 K (0.1 W) ⁻¹	

(a) For housing at 25°C

(b) Rate of change of temperature with input power at temperature shown.

Table 6.0-2 Nominal Characteristics of the Patch

Temperature (a)	105 K	
Power radiated	96.6 mW	
Radiating area	22.4 in ²	
Conductive input (b)	10.0 mW	10.4%
Insulation input (c)	15.4 mW	15.9
Joule heat input	2.3 mW	2.4
Optical port input	25.3 mW	26.2
Shield input	9.1 mW	9.4
Control power	34.5 mW	35.7
dT/dφ	0.31 K (mW) ⁻¹	

(a) Nominal control point.

(b) Including effect of support shields

(c) Radiative decoupling

the spacecraft altitude (450 n mi). The solution is $\beta_m = 62.20^\circ$. The actual shield completely covers 63.79° , which leaves a margin of 1.59° for spacecraft wobble (1°) and cooler alignment.

6.2 Shield

Figure 6.0-1 shows the radiant cooler shielded designed for use at an altitude of 450 n mi. The shield completely shades the patch (second stage of cooling) from the earth.

6.2.1 Cover Temperatures

Both the vertical and horizontal earth shields are insulated from external inputs by shield covers. The three optically polished shields are thermally and mechanically connected. However, the two vertical covers are not connected to the horizontal cover. The cover temperatures are listed in Table 6.2-1 for the range of sun angles (β_s) at the 450 n mi altitude (see memorandum of May 2, 1974).

The thermal balance equation that determines the temperature T_c of a cover is given by

$$\epsilon_c \sigma T_c^4 = F_{ce} (\epsilon_c W_e + \alpha_c W_r) + \alpha_c S_o < \sin i >$$

where ϵ_c = emissivity = 0.72 (silvered Teflon)

α_c = solar absorptivity = 0.08

F_{cs} = view factor from cover to earth; $\sin^2 \beta_e$ for a horizontal cover and $\frac{1}{\pi} (\beta_e \cos \beta_e)$ for a vertical cover, where β_e (62.17°) is the mean angle from nadir to the earth-tangent line.

Table 6.2-1 Shield Cover Temperatures

β_s	Vertical	Horizontal
0°	167.8K	232.0K
27.83	187.4	241.9
37.5	190.1	238.6
67	195.6	238.7

Table 6.2-2 View Factors from Radiator to Earth

Element	Weight*	F_{ie}	
a	0.1046	0.011	832
b	0.1046	0.012	734
c	0.1345	0.013	825
d	0.1345	0.075	471
e	0.05575	0.002	673
f	0.12485	0.037	845
g	0.3412	0	
Radiator	1	0.019	454

*Relative area.

$\langle \sin i \rangle$ = orbital average of the solar incidence angle, taken to be zero when the cover is shaded from direct sunlight; $\frac{1}{\pi} \sin \beta_s (1 + \cos \Delta\mu_e)$ for a horizontal surface and $\frac{1}{2\pi} \sin \beta_s (1 + \cos \Delta\mu_e)$ for a vertical surface.

$\Delta\mu_e$ = $\arccos (\cos \beta_e / \sin \beta_s)$; zero when $\sin \beta_s \leq \cos \beta_e$, i.e., when the spacecraft is in direct sunlight throughout its orbit.

W_e = infrared exitance of earth = $2.1 \times 10^{-2} \text{ Wcm}^{-2}$

W_r = reflected solar exitance of earth = $1.68 \times 10^{-2} \sin \beta_s \text{ Wcm}^{-2}$

s_o = solar constant = 0.14 Wcm^{-2}

The equation for W_r is derived in Appendix I to Part I of the Final Report on Contract NAS5-10113 (Dec. 1967).

6.2.2 Shielding and View Factors

Figure 6.2-1 shows the projection of the shielded onto the scan earth disk as seen from an upper corner of the patch (i.e., from the most difficult point to shield). The shading from the earth is complete up to a disk angular radius of 63.79° .

The view factor F_{re} from the black radiator to the earth was determined by dividing the radiator into 14 elements, as shown in Figure 6.0-1. By symmetry, there are seven elements are shown in Figure 6.2-2. The view factors were calculated by means of the contour integral technique (R. V. Annable, Applied Optics, Jan. 1970 and July 1972). The results are given in Table 6.2-2.

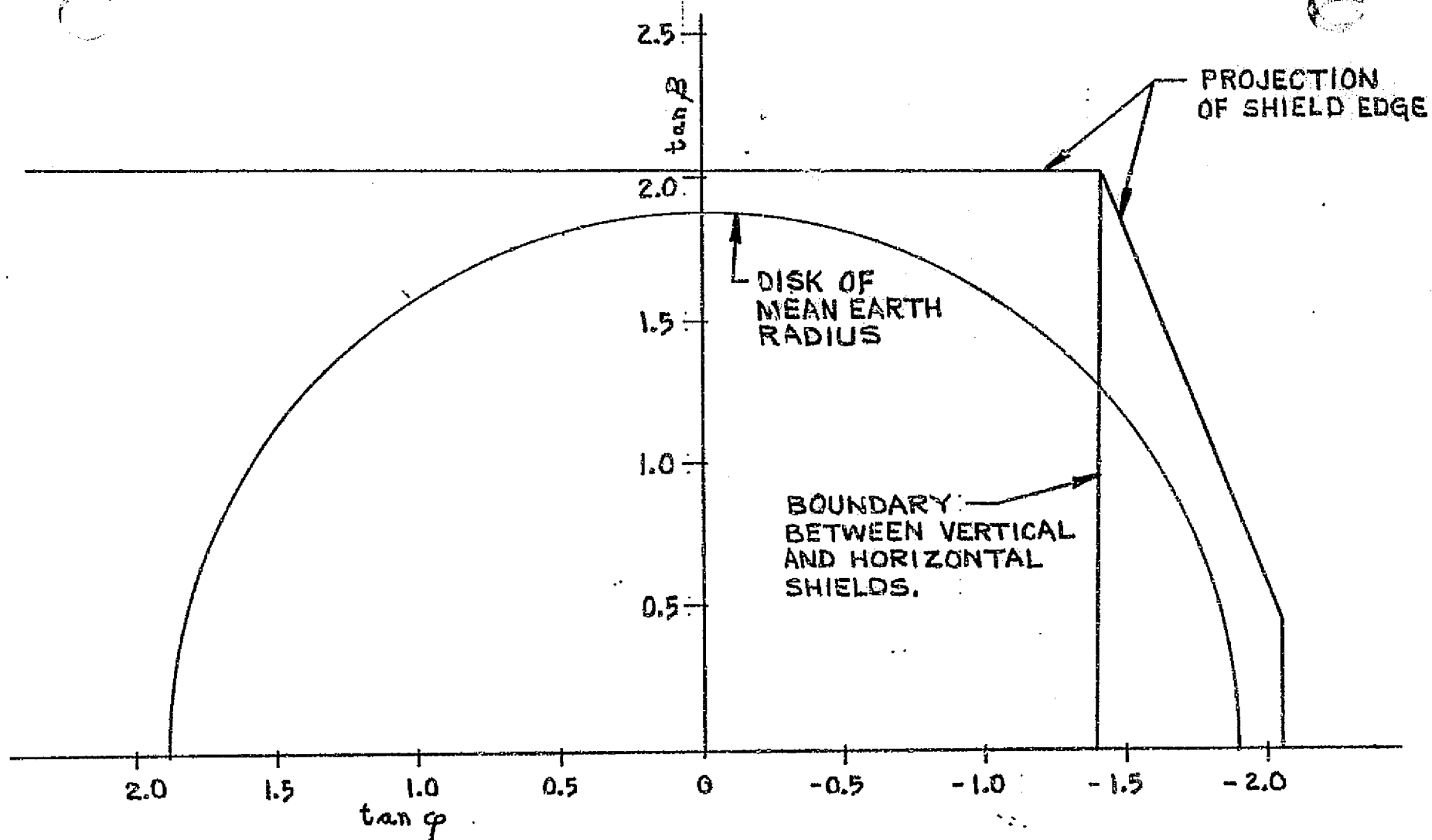


FIG. 6.2-1 PROJECTION OF SHIELD ONTO MEAN EARTH DISK AS SEEN FROM UPPER PATCH CORNER (POINT C IN FIGURE 6.0-1)

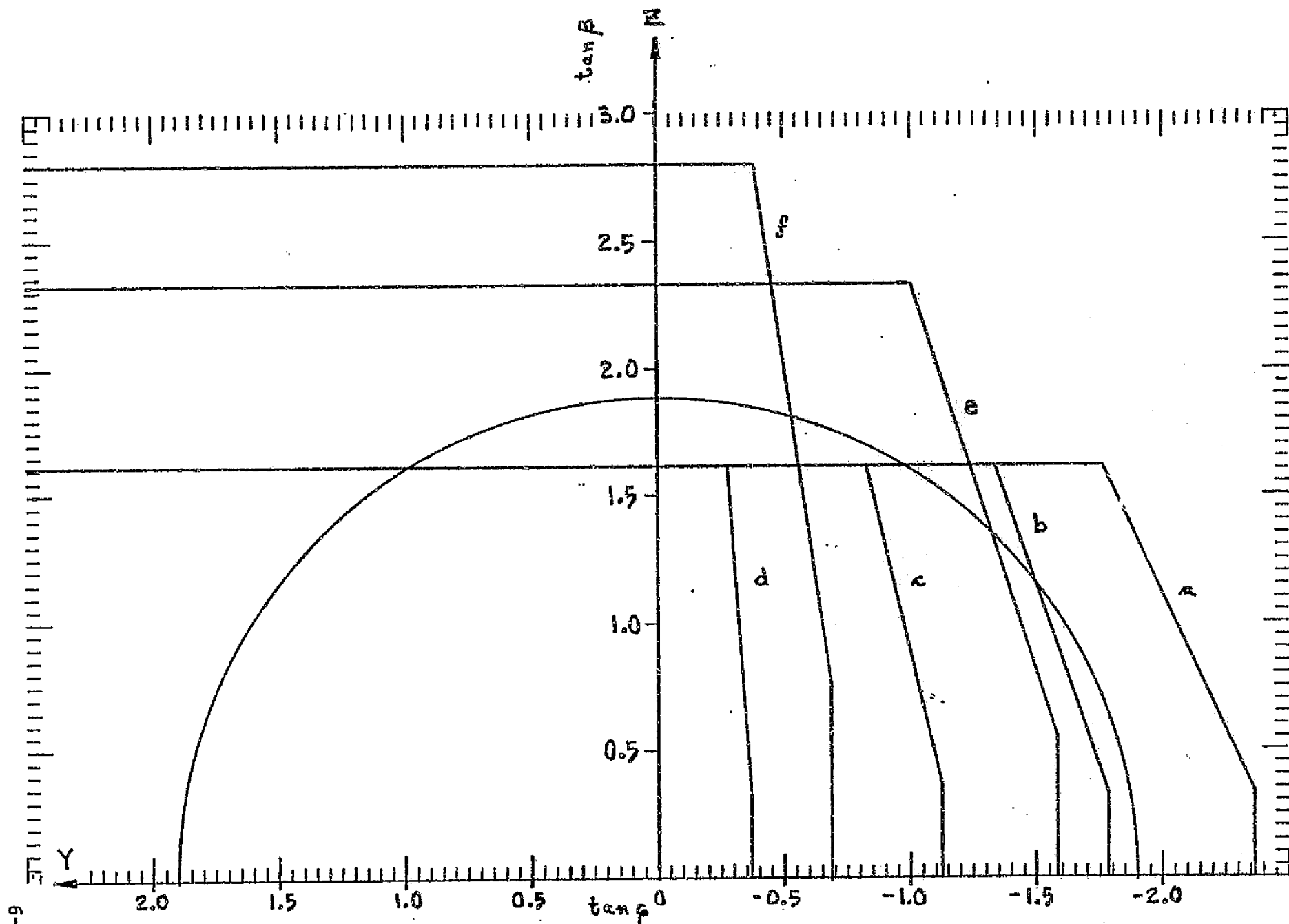


FIG. 6.2-2 PROJECTIONS OF SHIELD ON EARTH DISK AS SEEN FROM RADIATOR ELEMENTS.

The view factor F_{ps} from the patch to the shield was calculated in two parts. First, the view factor to the horizontal shielded was calculated using view factor algebra and the formula for two perpendicular rectangles with a common boundary (E. M. Sparrow and R. C. Cess, Radiation Heat Transfer, Brooks/Cole, 1966, Section 4-3). The result is

$$F_{ps1} = 0.37161$$

Secondly, the view factors to the vertical shields and their specular images in the horizontal were calculated from the center of the patch by the contour integral technique. As shown in Figure 6.2-3, each vertical shield and its complete specular image can be seen from the patch center. By symmetry, the view factors are the same to either vertical shield. The results are

$$F_{ps2} = 0.00359 \text{ to shield}$$

$$F_{ps2} = 0.00339 \text{ to shield image}$$

Finally we determine an effective view factor that can be used directly in the design equations. It is given by

$$F_{ps} = F_{ps1} + 2F_{ps2} + 2(1 - \epsilon_s) F_{ps2}^1,$$

where $(1 - \epsilon_s) = 0.965$ is the reflectivity of the horizontal shield.

The result is

$$F_{ps} = 0.3853$$

6.3 Radiator

The radiator and earth shield have a temperature T_r that is the solution to:

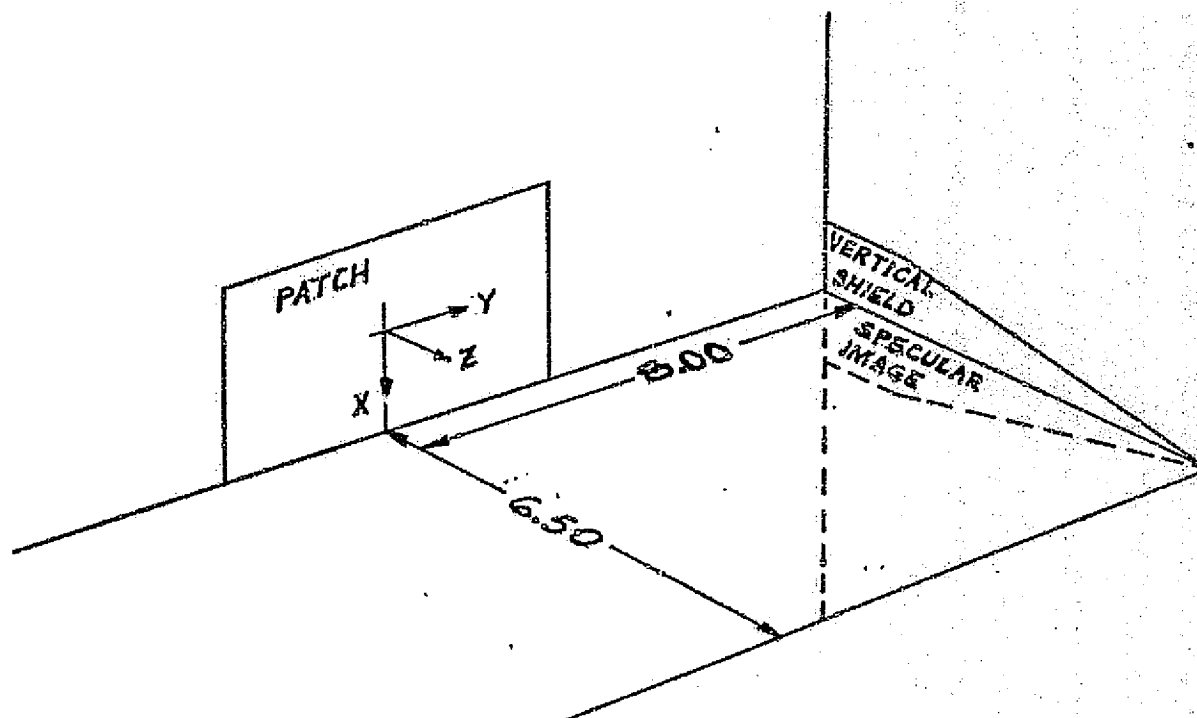


FIG. 6.2-3 GEOMETRY FOR CALCULATION OF VIEW FACTOR TO VERTICAL SHIELD AND ITS IMAGE.

$$\epsilon_r \sigma A_r T_r^4 = \Phi_{er} + \Phi_{cr} + \Phi_i + \Phi_k + \Phi_o$$

where Φ_{ab} = radiant power from a that is absorbed in b

e = earth (infrared and reflected sunlight)

r = black radiator, c - shield covers

Φ_a = input from instrument through a

i = multilayer insulation; k = supports and wires;

o = optical port

$$\Phi_{er} = F_{re} (e_r W_e + \alpha_r W_r) A_r$$

$$\Phi_{cr} = \frac{\sigma A_c}{A_c} (T_c^4 - T_r^4) + K_c (T_c - T_r), \text{ for each cover}$$

F_{ab} = view factor from a to b; A_a = area of a

ϵ_a = emissivity of a; α = solar absorptivity of a

W_e = earth infrared exitance = $2.1 \times 10^{-2} \text{ Wcm}^{-2}$

W_r = earth reflected sunlight exitance

$$= 1.68 \times 10^{-2} \sin \beta_s \text{ Wcm}^{-2}; \beta_s = \text{orbit normal to sun angle}$$

A_c (horizontal) = 104 in^2 ; A_c (2 vertical) = 7.5 in^2

A_r = 55.2 in^2 ;

F_{re} = 0.01945 (Section 6.2)

ϵ_r = $\alpha_r = 0.97$ (honeycomb cavity array covered with black paint)

$s_c = \frac{2}{\epsilon_c} - 1$; ϵ_c = emissivity of gold plating on facing surfaces of shield and cover = 0.035.

K_c = thermal conductance of supports between shield and cover

$$= 2.88 \times 10^{-3} \text{ WK}^{-1} \text{ (horizontal),}$$

$$= 1.44 \times 10^{-3} \text{ WK}^{-1} \text{ (2 vertical)}$$

$$\phi_i = \frac{\sigma A_i}{S_i} (T_h^4 - T_r^4); A_i = 115 \text{ in}^2; S_i = 50$$

T_h = instrument temperature

$$\phi_k = K_r (T_h - T_r); K_r = \text{thermal conductance between h and r} = 1.14 \times 10^{-3} \text{ WK}^{-1}$$

$$\phi_o = 0.257 (T_h = 20^\circ\text{C}) \quad 0.275\text{W} (25^\circ\text{C}), \quad 0.313 \text{ W} (35^\circ\text{C});$$

Because the thermal time constant of the radiator-shield is much greater than an orbital period, orbital averages are used for the earth inputs. The insulation factor of 50 is the minimum expected and was achieved on the ETM.

The thermal conductance K_x between the housing (main instrument) and the first stage of cooling consists of $1.35 \times 10^{-3} \text{ WK}^{-1}$ from the synthane support tubes and $0.18 \times 10^{-3} \text{ WK}^{-1}$ from the following electrical connections:

<u>Quantity</u>	<u>Diameter (inch)</u>	<u>Material</u>	
2	3.9×10^{-3}	Copper	To radiator components
4	3.0×10^{-3}	Chromel	
2	5.0×10^{-3}	Chromel	
4	3.0×10^{-3}	Chromel	To patch components
2	3.9×10^{-3}	Copper	
4	2.0×10^{-3}	Nickel	

All the electrical connections have a conductance length of 3.15 inches.

Table 6.3-1 shows the radiator temperature range of the 450 n mi altitude. The housing temperatures (T_h) are estimates based on the thermal analysis.

Table 6.3-1 Radiator Temperature Range

β_s	T_h	T_r
0°	20°C	165.6K
27.83	35	173.7
37.5*	25	170.6
67	20	170.1

* Nominal orbit (8:30 AM or 3:30 PM).

6.4 Patch

The thermal balance equation for the patch is

$$\sigma \epsilon_p A_p T_p^4 = \phi_s + \phi_k + \phi_i + \phi_j + \phi_o$$

where p = patch

s = earth shield (upper side)

k = thermal conductance including the influence of radiative inputs from the support shields

i = gold-to-gold radiative insulation

j = joule heat of detectors and temperature sensor

o = optical port

$$\phi_s = \sigma \epsilon_p \epsilon_s A_{p ps} T_r^4$$

$$\phi_k = M K_p (T_r - T_p); M = \text{dual mode multiplier}$$

$$\phi_i = \frac{\sigma A_i}{S_i} (T_r^4 - T_p^4); S_i = \frac{2}{\epsilon_i} - 1$$

$$\begin{aligned}
\phi_j &= 2.3 \times 10^{-3} \text{ W} \\
\phi_o &= 2.30 \times 10^{-2} \text{ W } (\beta_s = 0^\circ); 2.83 \times 10^{-2} \text{ W } (27.83^\circ); \\
&\quad 2.53 \times 10^{-2} \text{ W } (37.5^\circ); 2.41 \times 10^{-2} \text{ W } (67^\circ); \\
\epsilon_p &= 0.97 \text{ (black paint on honeycomb cavity array)} \\
\epsilon_s &= 0.035 \text{ (vacuum deposited aluminum)} \\
\epsilon_i &= 0.035 \text{ (gold plate)} \\
A_p &= 22.4 \text{ in}^2; A_i = 32.6 \text{ in}^2 \\
F_{ps} &= 0.3853 \text{ (Section 6.2)} \\
K_p &= 1.1875 \times 10^{-4} \text{ WK}^{-1}; M = 1.28
\end{aligned}$$

The thermal conductance K_p between the radiator and patch consists of the following connections:

Quantity	Diameter (inch)	Length (inch)	Material
4	3/16 x 5/32	2.70	G-10 synthane
4	0.002	2.70	nickel
4	0.003	2.70	chromel
2	0.005	2.70	chromel

The dual heat mode multiplier M was calculated using the approach described in the memorandum "Combined Radiative and Conductive Heat Transfer in the Patch Supports", from Contract 5-21651. A shield emissivity ϵ_s of 0.035 was used in the calculation; and the analysis was carried out for the case $T_s = T_r$ (i.e., the thermal gradient was evaluated at $x = \ell$).

The above equation does not include the input present during chamber testing as a result of reflection of the radiator power from the cold space target. Based on thermal tests and

their analyses, we estimate this input to be given by

$$7.5 \times 10^{-3} \frac{T_r^4}{164} W$$

for the 22.4 in² black radiating area.

The solutions to the patch thermal balance equation are listed in Table 6.4-1. In the nominal orbit, the temperature margin is 10.1K at the 105K control point. The corresponding control power is 35.7% of the total patch load. Or, stated another way, all other thermal inputs would have to increase by 55.5% in order to use up the margin.

6.5 Solar Exposure

If the cooler sweeps through the sun during acquisition, both the patch and radiator will be protected by the shield/cover. The exposure is therefore limited to the (horizontal) shield cover (which is in a vertical position during storage). The worst case is when the sun sweeps through a plane perpendicular to the plane of the shield cover. Even then, as shown by the following analysis, the shield cover has a worst case average temperature of only -0.5°C and a worst case maximum of -0.2°C. During this period, the cooler temperature will then be regulated at 40°C by the outgassing power circuit.

We may treat the shield cover as thermally isolated from the instrument. Its thermal balance equation is then

$$\sigma T^4 + \frac{\delta p_c}{\epsilon} \frac{dT}{dt} = \frac{\alpha}{\epsilon} H_s(t) + W_e + \frac{\alpha}{\epsilon} W_{rm}$$

Table 6.4-1 Patch Temperature Range

β_s	T_p (space)	T_p (chamber)
0°	92.8K	95.5K
27.83	96.7	99.6
37.5*	94.9	97.8
67	94.3	97.2

* Nominal orbit.

Table 6.4-2 Other Patch Parameters

$\Delta T_p / \Delta \phi$	0.34K/mW @ 94.9K,	0.31K/mW @ 105K
Nominal margin	10.1K, space;	7.2K, chamber
Maximum margin	12.2K, space;	9.5K, chamber
Minimum margin	8.3K, space;	5.4K, chamber

where $\epsilon = 0.72$ is the emissivity of the cover and $\alpha = 0.08$ the solar absorptivity. The cover is treated as a plate of thickness δ , density ρ , and specific heat c . $H_s(t)$ is the solar irradiation as a function of time. For the sun in a plane perpendicular to the radiator, $H_s(t)$ is a train of cosine pulses given by

$$H_s(t) = \frac{2}{\pi} S_o \left[1/2 + \operatorname{Re} \sum_{n=1}^{\infty} c_n \exp(j\omega_n t) \right]$$

where S_o is the solar constant, Re is real part of, and

$$c_1 = \pi/4, \quad c_n = \frac{-1(-1)^{n/2}}{n^2 - 1}, \quad n = 2, 4, 6 \dots$$

$$\omega_n = \frac{2\pi n}{P}, \quad \frac{1}{P} = \text{frequency of rotation (0.5 rpm)}.$$

W_e is the infrared exitance of the earth (Section 6.2.1), and W_{rm} is the maximum reflected solar exitance. W_{rm} is given by (Appendix I to part I of the Final Report on Contract NAS 5-10113, Dec. 1967)

$$W_{rm} = \frac{\cos^2 \beta_e}{1 - \sin \beta_e} \sin \beta_s S_o A,$$

where $A = 0.4$ is the average solar reflection factor for the earth.

The worst case orbit is then $\beta_s = 67^\circ$, so that we have

$$W_{rm} = 4.86 \times 10^{-2} W_{cm}^{-2}$$

The steady state solution to the above differential equation is $\sigma T_o^4 = \frac{\alpha}{\pi \epsilon} S_o$ and yields the average radiator temperature of $T_o = 272.7K - -0.5^\circ C$. For small temperature changes about T_o we may now linearize the equation by means of $T = T_o + \Delta T$

and extract the equation of the transient solution

$$4\sigma T_o^3 \Delta T + a \frac{d(\Delta T)}{dt} = \frac{2\alpha}{\pi\epsilon} S_o \operatorname{Re} \sum C_n \exp(j\omega_n t)$$

where $a = \delta_{pc}/\epsilon$. The solution is

$$\Delta T(t) = \frac{\alpha S_o}{2\pi\sigma\epsilon T_o^3} \operatorname{Re} \sum \frac{C_n \exp(j\omega_n t)}{1 + j\omega_n \tau}$$

where $\tau = a/4\sigma\epsilon T_o^3$ is the thermal time constant. For a 0.03 inch aluminum plate ($\rho = 2.7 \text{ gms/cm}^3$, $c = 0.895 \text{ joules/gm}^\circ\text{C}$), we obtain $\tau = 10.34 \text{ mins}$. Taking the real part of the sum, we obtain

$$\Delta T(t) = \frac{S_o}{4\pi\sigma\epsilon T_o^3} \sum_{n=1}^{\infty} \frac{C_n}{1 + \omega_n^2 \tau^2} (\cos \omega_n t + \omega_n \tau \sin \omega_n t).$$

The maximum value of $\Delta T(t)$ occurs at $t = 0.19 \text{ P}$ when $t = 0$ is the point of zero solar incidence angle. The resultant value is

$$\Delta T = 0.29^\circ\text{C}$$

The peak difference from average is reached about 55° of rotation after normal incidence and is very small compared with the average temperature. The maximum temperature, in fact, is only -0.2°C .

6.6 Anti-Contamination Provisions

The radiant cooler is designed to prevent optical or thermal contamination by either the cooler components themselves or by the instrument/spacecraft atmosphere. Specific provisions are (1) conditioning and de-contamination, (2) elimination of internal outgassing paths, and (3) positive protection of sensitive areas.

To outgas the cooler and prevent condensation of external contaminants from the instrument and spacecraft, the cooler will be heated to approximately 40°C for an extended period after acquisition. The same heaters will be used for any subsequent decontamination. The times required for a complete decontamination and for the cool down to operating temperatures are estimated in DIR No. 19. The cooler will be outgassed with the shield/cover closed and decontaminated with it open. In the open position, we require a power level of 14.0 watts on the radiator and 6.4 watts on the patch to achieve a 25°C temperature.

Internal outgassing paths are eliminated by windows that seal the openings between the instrument and radiator and between the radiator and patch. The volumes within the cooler can outgas only by paths that lead directly to space.

To provide positive protection for sensitive areas, the window on the radiator is heated a nominal 8K above the radiator temperature and protected by a cold trap at the radiator temperature. The design and analysis of the window heater is covered in DIR. No. 15. The optical elements on the patch and the low emissivity rear areas of the patch are protected by a cold trap at the patch temperature.

6.7 Optical Port Loading

Three thermal tests were run on a feasibility model cooler and two tests run on the BBM. These tests were used to establish a mathematical model for the loading from the optical port opening onto the radiator and the patch. The opening is shown schematically in Figure 6.7-1. This is the configuration of the instrument final design.

6.7.1 Optical Loading on the Radiator

The optical loading on the radiator is

$$\phi_{or} = \epsilon_1 \sigma T_h^4 A_1 F_{12} (1 - P_2) + (1 - F_{12})$$

where A_1 equals πr_1^2 and P_2 is the fraction of room temperature radiation passed by the inner window. For an inner window of Irtran 2, P_2 is about 0.5 (corresponding to a cutoff wavelength of 14 μ m). The emissivity of the opening is 0.9 in the instrument, where an outer germanium window is added. Using the data given in Figures 6.7-1 and 6.7-2 plus Table 6.7-1 and 6.7-2, we obtain the calculated optical port loadings on the radiator in the final instrument design are then:

$$\phi_{or} (T_h = 20^\circ\text{C}) = 0.257\text{W}$$

$$\phi_{or} (T_h = 25^\circ\text{C}) = 0.275\text{W}$$

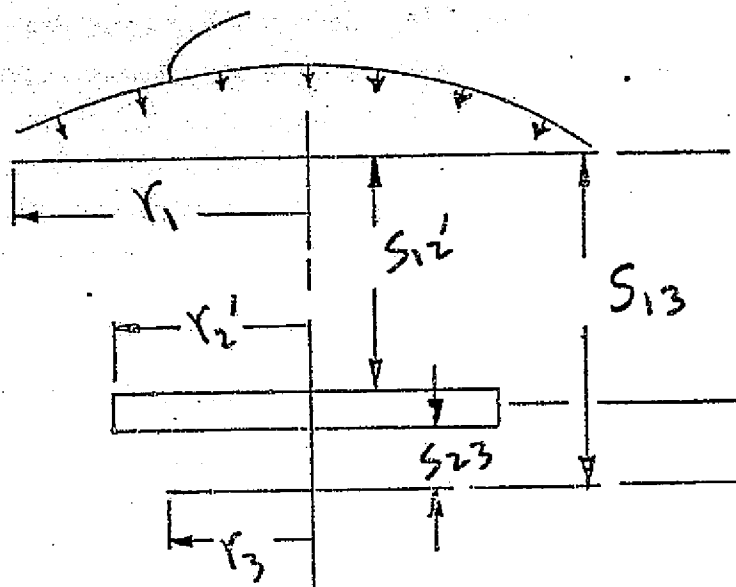
$$\phi_{or} (T_h = 35^\circ\text{C}) = 0.313\text{W}$$

6.7.2 Optical Loading on the Patch

The optical port loading on the patch consists of inputs from the instrument and the radiator. We will restrict the radiator input to that from the inner window itself; radiation at the radiator temperature (ie., the cold trap) is efficiently absorbed in the window. The input from the instrument to the patch is given by

$$\phi_{13} = \epsilon_1 \sigma T_h^4 P_2 \tau_2 F_{31} \gamma_3 A_3$$

where τ_2 is the transmittance of the inner window for greybody radiation at the temperature T_h , γ_3 is the effective absorptivity of the patch opening.



	r_1	r_2'	r_3	S_{13}	S_{23}	S_{12}'
Instrument	0.630	0.570	0.415	0.855	0.07	0.685

Instrument
Opening

Radiator
Opening

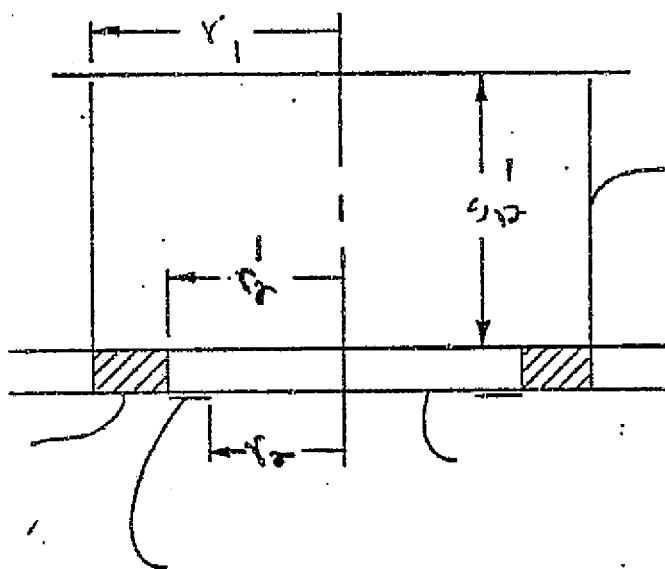
Patch
Opening

Germanium

Irtran 2

Optical elements
& gold baffle

Figure 6.7-1 Characteristics of the Optical Opening to the Radiant Cooler (Dimensions in Inches)



r_1	r_2	r_2'	s_{12}'	F_{12}'
0.630	0.430	0.570	0.685	0.303

Figure 6.7-2 Optical Opening to the Radiator
in the Instrument (Dimensions in Inches)

Table 6.7-1 View Factors and Blockage Within the Optical Opening

$$\begin{aligned} F_{32} &= 0.875 \\ F_{31} &= 0.319 \\ F_{12} &= 0.303 \end{aligned}$$

Table 6.7-2 Temperatures Within the Optical Opening
(Instrument Test)

Instrument	Radiator	Patch
20°C, 35°C	173.6K 181.7K	105K (b)
25°C, 20°C	178.6K 178.1K	

(a)

(a) Heated Window

(b) Control Point

The effective absorptivity γ_3 is given by

$$\gamma_3 = \alpha_3 + (1 - \alpha_3) \rho_2 F_{33'} + \alpha_3 + (1 - \alpha_3)^2 \times \\ \rho_2^2 (F_{33'})^2 \alpha_3 + \dots$$

$$\gamma_3 = \frac{\alpha_3}{1 - \rho_2 (1 - \alpha_3) F_{33'}}$$

where α_3 is the actual absorptivity of the patch opening, ρ_2 is the (specular) reflectance of the inner window, and $F_{33'}$ is the view factor from the patch opening to its own specular image in the inner surface of the window. The value of γ_3 was experimentally determined from; a theoretical model of α_3 is described in Section 6.7.3.

The input from the inner window attached to the radiator is given by

$$\Phi_{23} = \sigma_{T_w}^4 \epsilon_2 F_{32} \gamma_3 A_3$$

The window temperature T_w is equal to the radiator temperature plus 8K. For an inner window of Irtran 2 and for greybody radiation in the range from 160K to 175K, the window emissivity ϵ_2 is approximately 0.6 and the window reflectance ρ_2 , approximately 0.2. Using the theoretical α_3 value of 0.675 (Section 6.7.3) and test values for ρ_2 (0.1), and $F_{33'}$ (0.743), the theoretical value of γ_3 is 0.692. The experimental γ_3 is 0.773 and is based upon test data from a feasibility model cooler.

Using the experimental value for γ_3 and the instrument parameters listed in Figures 6.7-1 and 6.7-2 and in Tables 6.7-1 and 6.7-2, we calculated Φ_{op} for the final instrument. The results are given in Table 6.7-3.

Table 6.7-3. Calculated Patch Loading from Optical Port (Instrument)

β_s	T_h	ϕ_{op}
0°	20°C	0.0230 W
27.83	35	0.0283
37.5	25	0.0253
67	20	0.0241

6.7.3 Absorptivity of the Instrument Patch Opening (Theoretical Model)

To complete the consideration of optical port loading, we constructed a theoretical model for the absorptivity α_3 of the patch opening in the instrument cooler. A view of the patch opening as seen from the inner window is shown in Figure 6.7-3. The area b_1 occupied by the Channel 3 spectral filter and its specular image b_2 in the infrared dichroic are effectively black. Thus in area b_1 , some radiation is absorbed in the Channel 3 filter or transmitted by the filter and absorbed in the cavity below; the remainder is reflect to b_2 , where it is either absorbed or transmitted by the dichroic and absorbed below.

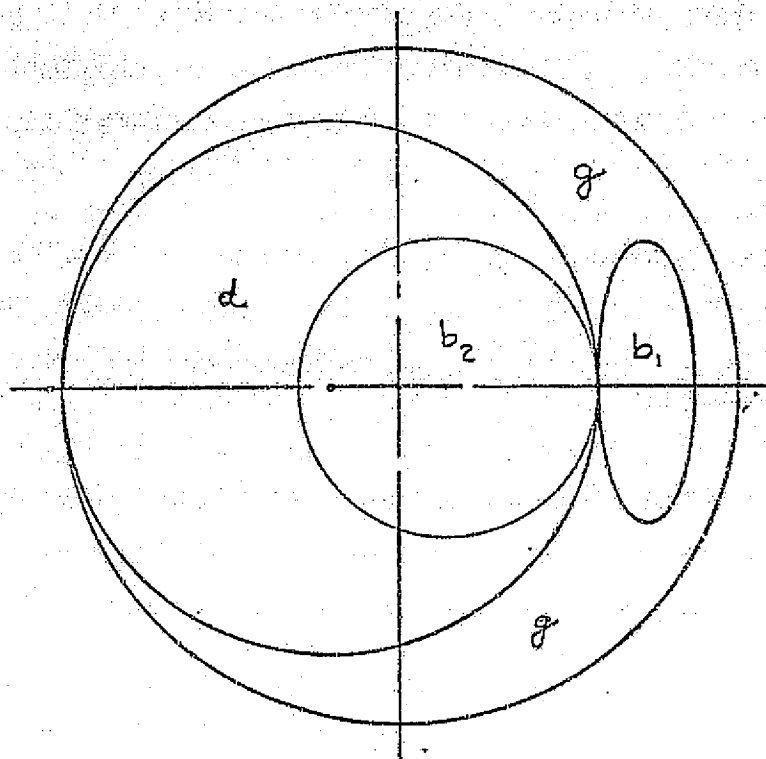
The effective absorptivity of the area d (dichroic minus area b_2) is given by

$$\alpha_d' = \alpha_d + (1 - \alpha_d) \alpha_g'$$

where α_d = actual absorptivity of area $d = 0.4$

α_g' = effective absorptivity of gold baffle g

This equation assumes that radiation not absorbed or transmitted by d (the fraction α_d) is specularly reflected to the gold baffle. The value given for α_d is an estimate for the infrared dichroic on a germanium substrate. Thus for radiation at the instrument temperature, only about 0.5 is transmitted through the inner Intran window. For a dichroic with a separation wavelength of $9.0 \mu\text{m}$, about 0.4 is transmitted and therefore absorbed. For radiation at the radiator temperature, about 0.2 of the total is reflected if the dichroic reflects over the band from $9 \mu\text{m}$ to $16 \mu\text{m}$. If the dichroic has



- g = Gold Baffle
- b_1 = Opening For Channel 3
- b_2 = b_1 Reflected In Dichroic
- d = Dichroic Minus b_2

Figure 6.7-3 Top View of Optical Opening on Patch
(Note that the model applies to the
breadboard model used in Test 4.)

the properties of a germanium substrate beyond 16 μm , the remaining fraction of 0.8 has an absorptivity equal to approximately 0.47, the transmittance of the substrate. The value of α_d for radiator emission is then 0.8×0.47 or about 0.4.

In order to calculate the effective absorptivity α_g' , of the gold baffle, we assumed that the gold is in the form of a diffuse gold plating. We then have

$$\alpha_g' = \alpha_g + (1 - \alpha_g) F_{gg} \alpha_g' + F_{gb1} + F_{gb2}$$

where α_g is the infrared absorptivity (0.035) of the gold plating and F_{ij} is the view factor from area i to area j . This equation can be solved for α_g' ; we then have

$$\alpha_g' = \frac{\alpha_g + (1 - \alpha_g) F_{cb1} + F_{gb2} + F_{gd} (\alpha_d + (1 - \alpha_d) F_{db1})}{1 - (1 - \alpha_g) F_{gg} + F_{gd} (1 - \alpha_d) F_{dg}}$$

The view factors F_{ij} were approximated by

$$F_{ij} = \frac{A_j}{\sum A_j}$$

This equation is strictly true only for a sphere. For the components in the patch opening of the instrument, we have

$$A_3 = 0.636 \text{ in}^2 \text{ (0.9 inch diameter opening)}$$

$$A_{b1} = 0.126 \text{ in}^2 \text{ (0.4 inch diameter)}$$

$$A_{b2} = a A_{b1} = 0.178 \text{ in}^2$$

$$A_d = \pi 0.7 \times 1 - A_{b2} = 2.021 \text{ in}^2$$

$$A_g = \frac{1}{2} \pi \cdot 0.45 \times 0.75 - A_{b1} = 0.404 \text{ in}^2$$

$$\Sigma A_i = 3.365 \text{ in}^2$$

$$F_{ij} = 0.12$$

$$F_{ib1} = 0.04$$

$$F_{ib2} = 0.05$$

$$F_{id} = 0.60$$

$$F_{io} = 0.19$$

We then have for the effective absorptivities

$$\alpha_g' = 0.435$$

$$\alpha_d = 0.66$$

Finally, the value of α_3 can be calculated as the area-weighted average

$$\alpha_3 = \frac{1}{A_3} A_g' \alpha_g' + A_{b1}' + A_{b2}' + A_d' \alpha_d'$$

where the primes on the areas denote projection into the opening A_3

$$A_g' = 0.210 \text{ in}^2$$

$$A_{b1}' = 0.041 \text{ in}^2$$

$$A_{b2}' = 0.126 \text{ in}^2$$

$$A_d' = 0.259 \text{ in}^2$$

For the above values of α_g' and α_d' , we then have

$$\alpha_3 = 0.675.$$

7.0 CALIBRATION

7.1 Thermal Channels Calibration

The infrared calibration signal to the AVHRR is the difference in signals from a calibration blackbody of known temperature and a blackbody of essentially zero exitance. The zero level source is provided by deep space during in-flight calibration and by a liquid nitrogen cooled black cavity during chamber calibration. Other calibration requirements are listed in Table 7.1-1. We have interpreted the temperature calibration accuracy of the chamber targets (B.b.) to mean the equivalent temperature accuracy determined by all error sources.

7.1.1 Calibration Accuracy

The absolute radiometric calibration of the instrument is to have an accuracy of $\pm 0.5K$ throughout the calibration range of each channel. Before we consider how this requirement can be met, let's define some terms. In particular, we can differentiate between precision (or sensitivity) and accuracy by means of the following:

Precision: A measurement is regarded as precise if the dispersion of values, i.e., the standard deviation σ , is small.

Accuracy: A measurement is regarded as accurate if the values cluster closely about the correct value.

By accuracy of an individual measurement or of an average of measurements is usually meant the maximum possible error (constant and/or random) that could influence the observed value. It is frequently thought of in terms of the number of significant figures to which a value can be regarded as correct.

TABLE 7.1-1 Requirements for Thermal Channels Calibration

A. Inflight Blackbody

- a. Measured with platinum resistance thermometers
Appropriately arrayed to adequately define the
temperature.
- b. Temperature sensor instrumentation accuracy of
 $\pm 0.1\text{K}$.
- c. To be compared with the chamber targets during
thermal vacuum calibrations.

B. Chamber (Standard) Blackbodies

- a. Greater emissivity, temperature stability, and
temperature sensor accuracy than inflight target.
- b. Absolute temperature measurement accurate to
 $\pm 0.5\text{K}$.

The precision is limited by the instrument noise, i.e., by the sensitivity. In order to measure the noise of the instrument and to reduce its effect on the absolute radiometric calibration, a set of n measurements will be made at each calibration point. The precision (or sensitivity) is then given by the best estimate of the standard deviation (see for example, D.C. Baird, Experimentation: An Introduction to Measurement Theory and Experiment Design, Prentice - Hall, 1962).

$$\sigma = \left[\sum (x - \bar{x})^2 / (n-1) \right]^{1/2},$$

where x is an individual measurement and \bar{x} the average of n measurements. On the other hand, the standard deviation of the average of n measurements is given by

$$\sigma_n = \sigma / n^{1/2}$$

The influence of the instrument noise and of all other random errors can therefore be reduced to the point where the accuracy of a calibration is determined by the systematic errors in the calibration target itself. This could be done during both the chamber (Section 7.1.2) and in-flight (Section 7.1.3) calibration. There are 10 calibration points (elemental dwell times) during each scan of a target, and so for a 1 minute period, we have $n = 3600$.

Before we consider the errors in the calibration targets, however, let's list all the components and procedures that can limit the accuracy of a calibration. We can identify two major

areas, within which there may be important subareas. They are as follows:

- A. Calibration target
 - a. Temperature: Measurement $\left\{ \begin{array}{l} \text{Sensor} \\ \text{Instrumentation} \end{array} \right.$
Gradients or uniformity
Control (chamber)
 - b. Non-blackness
- B. Electronics
 - a. Noise (NETD)
 - b. Signal processing: Digitization
Recording (In-flight)
Transmission
Ground Processing

We will limit ourselves to errors from sources A and B.a. We are therefore assuming that the experiment is so designed that the errors contributed by B.b. are negligible by comparison.

If the difference in surround between chamber targets can be made zero or very small, the non-blackness errors will be greatly reduced and the accuracy of the calibration limited only by the errors and uncertainties in the calibration target temperature. Accuracy estimates for the chamber calibration are given in Table 7.1-2 and for the in-flight calibration in Table 7.1-3.

We see that we have met our objective of 0.5K for the total channel calibration error throughout the temperature range of both channels.* In addition, the total in-flight error at 295K

* We have arbitrarily set the lower limit in Channel 4 at 250K, where the noise equivalent temperature difference is approximately 1K.

Table 7.1-2 Accuracy of Chamber Calibration

Temperature:

Measurement	Sensor	$\pm 0.05K$
	Instrumentation	± 0.05
	Control	± 0.05
Gradients' base (uniformity)		$\pm 0.10^*$
Honeycomb (1K)*		± 0.06
Wall	Diff from box ($\pm 1K$)*	± 0.0026
	Gradient within (5K)*	± 0.00045
Accuracy (max of errors + uncertainties)		0.32K

Non-blackness

Net from standard-cold space difference

(10K difference in surrounds):

Channel	T	$\delta^2 T$
3	185K	+0.018K
3	320	-0.046
4	250	+0.027
4	320	-0.016

Total accuracy (including noise for $n = 3600$)**

Channel	T	δT
3	185K	0.35K
3	320	0.37
4	250	0.37
4	320	0.34

* Actual value of gradient.

** Based on specified NETD of 0.12K at 300K.

Table 7.1-3 Accuracy of In-flight Calibration For $T = 295K$ *

Temperature:

Measurement	Sensor	$\pm 0.05K$
	Instrumentation	± 0.10
Gradients	Base	± 0.08
	Honeycomb (1K)	± 0.08
		± 0.31

Non-blackness:

Channel	δT
3	-0.080
4	-0.029

Total accuracy (including noise for $n = 3600$)

Channel	δT
3	0.39K
4	0.34

* Exclusive of errors from scattered sunlight (Section 3.11)

has a comparable value when the calibration is made in the absence of direct sunlight (See Section 3.11). In the following sections, we consider in detail how we obtained the estimate listed in Tables 7.1-2 and 7.1-3.

7.1.2 Chamber Calibration Targets

Errors and uncertainties in the exitance (emitted W_{cm}^{-2}) of the calibration target arise from its temperature inaccuracies (Section 7.1.2.1) and its deviation from blackness (Section 7.1.2.2). Because a calibration signal is equal to the difference in signals from a calibration target and a cold space target, the inaccuracy from non-blackness is greatly reduced by making the two targets the same form and exposing them to the same surround.

7.1.2.1 Temperature Uncertainty

The accuracy of the calibration target temperature is limited by measurement errors, control stability, and gradients. The uncertainty in a temperature measurement relative to the international practical temperature scale (ITS-68, which is essentially identical to the absolute thermodynamic temperature scale) is $\pm 0.10K$. About half of this is the calibration accuracy; the remainder is produced by the sensor, bridge, and power supply. The latter produce errors that are largely random in nature, as do the readout device and temperature controller. The readout device introduces an error that can be kept small, about $\pm 0.01K$ for an integrating digital voltmeter. The stability of the controller is about $\pm 0.05K$.

The base gradient or uniformity can be held to $\pm 0.10\text{K}$. We have included this variation as part of the calibration error. In fact, the base temperature will be measured with an array of calibrated platinum sensors. The average of this array should then provide a measurement whose gradient error is less than the actual gradient. The gradient through the honeycomb can be estimated from the measurements on a similar target (A. R. Karoli, J. R. Rickey, and R. E. Nelson, Appl. Opt. 6, 1183, 1967). The honeycomb gradient was 1.6K in a 290K target that had a view factor of about 0.5 to a warm surround at 25°C . If the target temperature were reduced to 210K , the gradient would increase to about 2.5K . However, the view factor to the warm surround is reduced to 0.2 in our design, so the gradient is about 1.0K .

Moreover, the corresponding increase in the radiance temperature is much less than the gradient because most of the normal emission comes from the base and walls near the base. When the instrument views the calibration target at normal incidence during a calibration, the nominal cavity emissivity of 0.999327 (Section 7.1.2.2) may be divided between the base honeycomb and the cavity walls. For the nominal paint emissivity of 0.92, the base has a normal emissivity of 0.996696. Therefore 0.002631 of the normal cavity emissivity arises in the cavity walls (and is seen by reflection in the base). The emissivity of the base may, in turn, be divided among emission from the base bottom, the flat top area of the honeycomb, and the walls

of the honeycomb. The fraction of flat area of 0.025, so that the emissivity from the top is 0.92×0.025 and from the bottom, 0.92×0.975 . The remainder of base emissivity, $0.996\ 696 - 0.92 = 0.076\ 696$ arises in the sides of the honeycomb. We will assume that the walls of the cavity emit at the bottom temperature of the base and that the base honeycomb sides have an exitance equal to the average of the basebottom and honeycomb flats. The effective exitance M_E of the target seen at normal incidence is then

$$0.999\ 327\ M_E = 0.061\ 348\ M_F + 0.937\ 979\ M_B,$$

where F denotes base flats and B base bottom. Now a calibration temperature will be the measured value of the base bottom B. In both Channels 3 and 4, we find that a honeycomb gradient $T_F - T_B = \pm 1B$ results in a calibration error $T_E - T_B = \pm 0.061K$ (see Table 7.1-6 in Section 7.1.2.2).

The temperature errors introduced by deviations in the cavity wall temperature were analyzed for Contract NAS5-21651 (HIRS for Nimbus F)*. This analysis shows that the wall temperature deviations (difference from the base and internal gradient) introduce a temperature uncertainty of only about $\pm 0.003K$. As a result, the total temperature uncertainty in the chamber target is approximately 0.32K.

7.1.2.2 Deviation from a Blackbody

The uncertainties in the calibration of the instrument are expressed as absolute temperature errors in blackbody sources

*Memo from R. V. Annable "Deviations in the Wall Temperature of the Chamber Calibration Target", dated 6-28-72.

within the calibration range of each channel. The principles and practice of absolute radiometry are explored by R. E. Bedford and A. R. Karoli in Volume 14 of Advances in Geophysics (Precision Radiometry, ed. by A. J. Drummond, Academic Press, 1970). We have already covered the uncertainty in the temperature of the calibration target (Section 7.1.2.1). We now wish to consider the uncertainties produced by non-black calibration and cold space targets.

The real problem here is not the small decrease in target emission below that of a blackbody, but the reflection of the higher temperature surround. The calibration target consists of a honeycomb array with a length to width ratio of 4:1 (or its emissivity equivalent in another geometrical form) housed in a tube whose length is equal to the aperture diameter (Figure 7.1-1). The tube is covered on its inner wall with a honeycomb array whose length to width ratio is 2:1. In this way, we obtain a second, large cavity in addition to the array of small cavities. It is also equivalent to controlling a large fraction of the target surround. The tubular enclosure must not be thermally attached to the base calibration target; this would induce significant thermal gradients in the target. In addition, the cavity mouth and base must be sufficiently large that only the base is seen by the instrument during a calibration.

Because a calibration depends on the difference in signals from the calibration and cold space targets, the accuracy can be further increased by making both targets in the same form and exposing them, as nearly as possible, to the same surround. We have an estimate of the residual non-black error based on a

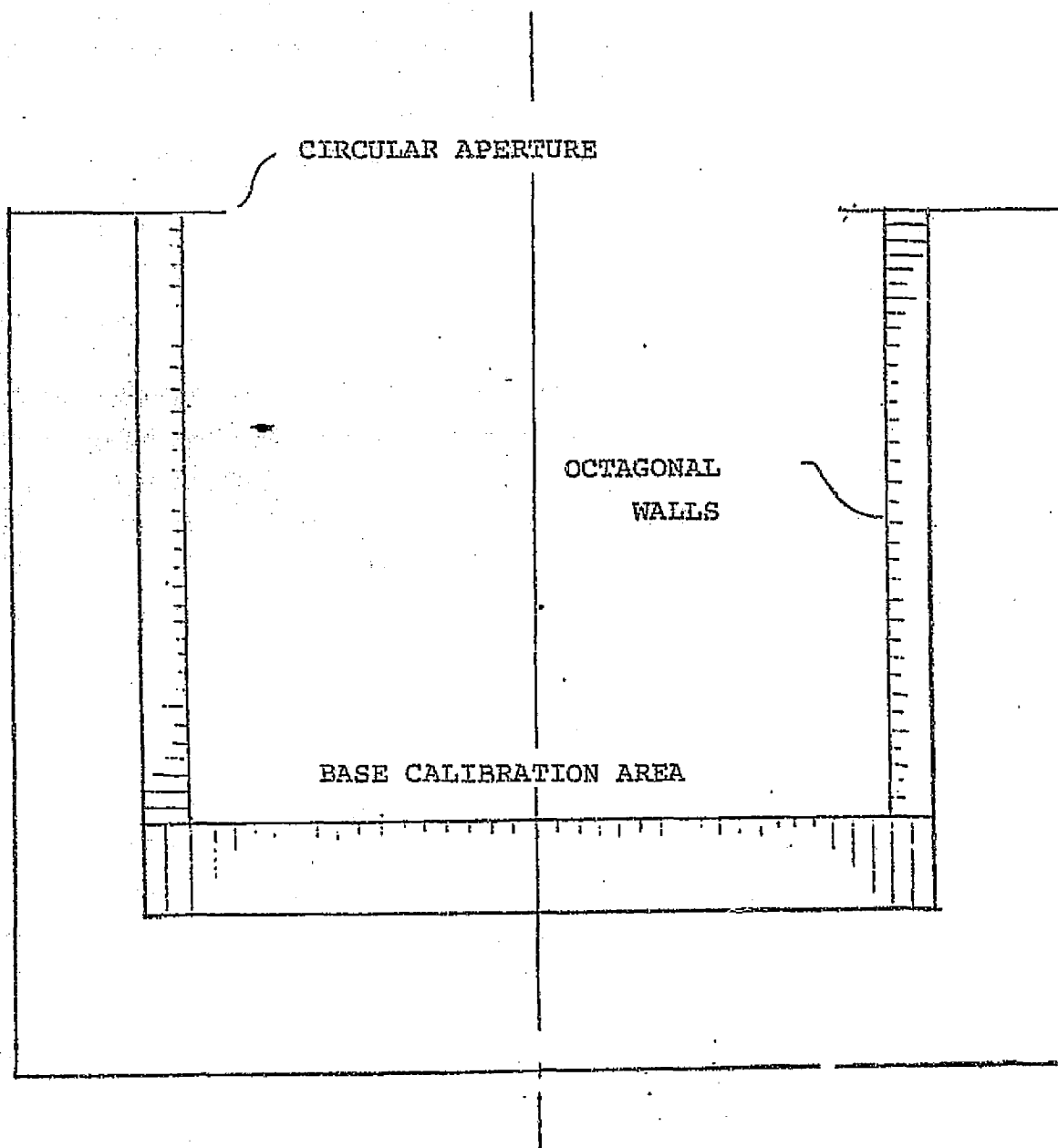


Figure 7.1-1 Chamber Calibration Target

calibration target surround of 293K and a space target surround of 283K; it ranges from +0.018 to -0.046K in Channel 3 and from 0.027 to -0.016K in Channel 4.

The base of the calibration target is in the form of honeycomb cavity array in which the cavities have a length to width ratio of 4:1 (A.R. Karoli, J. R. Hickey, and R. E. Nelson, Appl. Opt. 6, 1183 (1967)). A single cavity may be approximated by a cylinder whose emissivity is given by (P. Campanaro and T. Ricolfi, J. Opt. Soc. Am. 57, 48 (1967).)

$$\epsilon_c = \epsilon + \left[\frac{\rho \alpha^2}{2} \left(1 + \frac{4}{\alpha^2} \right)^{\frac{1}{2}} - 1 \right] - \frac{\rho^2 \alpha^2}{2} \left[\frac{1 + \frac{2}{\alpha^2}}{\left(1 + \frac{4}{\alpha^2} \right)^{\frac{1}{2}}} - 1 \right]$$

where α = ratio of height to radius

ϵ = normal surface emissivity

ρ = hemispherical surface reflectivity

For high emissivity materials, the normal and hemispherical emissivity are nearly equal (m. Jakob, Heat Transfer, Vol. I, Wiley 1949, Sections 4.9 and 7.2) and ρ is nearly equal to $(1 - \epsilon)$.

The flat area of the array is about 2.5 percent of the total source area. The effective normal emissivity of the array is then

$$\epsilon_A = 0.975 \epsilon_c + 0.025 \epsilon$$

The formula of Companaro and Ricolfi for the normal emissivity of a cavity in the array can also be used to calculate the emissivity of the large cylinder (i.e., the complete target). The cavity array normal emissivity becomes the wall emissivity of the cylinder. To use the formula, we also need the hemispherical emissivity of the cavity array. This can be calculated from the limiting value formula of Treuenfels (J. Opt. Soc. Am. 53, 1162, 1963) or interpolated from the results of Sparrow and Cess (Radiation Heat Transfer, Brooks/Cole, 1966, pp. 164-165). However, when the cavity array normal emissivity and hemispherical reflectivity are used in the formula of Companaro and Ricolfi, we find that the normal emissivity of the cylinder exceeds unity even for an initial surface emissivity as low as 0.89.

To overcome this problem, we will use the formula developed by Bauer and Bischoff (Appl. Opt. 10, 2639, 1971). For a cylindrical cavity with a plane bottom perpendicular to the axis, they obtain a normal reflectivity of

$$\rho_c = \rho_o \cdot (1 - \rho_o)^{-1} \cdot 1 + (L/R)^2^{-1}$$

where ρ_o is the normal reflectivity of the inner surface and L/R is the length to radius ratio (α in the formula of Companaro and Ricolfi). According to the nomenclature developed by Nicodemus, et. al. (Appl. Opt. 9, 1474, 1970), ρ_o is the directional-hemispherical reflectance for normally incident flux, that is, the fraction of normally incident flux that is reflected into a hemisphere. It is also equal to the hemispherical-directional

reflectance for normally incident flux, that is, the fraction of normally incident flux that is reflected into a hemisphere. It is also equal to the hemispherical-directional reflectance factor for normally reflected flux, that is, the fraction of hemispherically incident flux that is reflected in the normal direction.

Equation (1) is based on experimental measurements and holds for large value of α , the range of validity depending on the value of ρ_0 . However, it yields a conservative result at all values of α , i.e., the calculated value of ρ_0 is always greater than or equal to the experimental value. To begin with, we applied the equation to the cavity array in which 2.5 percent of the area is flat. The results are given in Table 7.1-4, where they are compared with those from the equation of Companaro and Ricolfi. We will assume the surface emissivity has a nominal value of 0.92.

The normal reflectivity ρ_N of the complete target can now be calculated from equation (1) by setting $\rho_0 = 1 - \epsilon_A$. The space in the chamber limits the α value of the large cylinder to 2:1. The measurements of Bauer and Bischoff (op. cit.) show that the actual reflectivity will be less than that calculated from the formula because of the relatively low value of α . The results of the complete target are given in Table 7.1-5 at four values of the initial surface emissivity ϵ when the walls also have an L/R ratio of 8:1.

Table 7.1-4 Normal Emissivity of the Honeycomb Cavity Array

ϵ Surface	B&B	ϵ_A	C&R
0.89	0.99 6 396		0.99 5 451
0.91	0.99 6 266		0.99 6 304
0.92	0.99 6 696		0.99 6 726
0.93	0.99 7 121		0.99 7 145

Fraction of flat area = 0.025

L/R ratio of cavities = 8.

Table 7.1-5 Normal Reflectivity of In-Chamber Target With
4:1 Honeycomb Array on the Base and Walls

ϵ	ρ_N
0.89	0.000 925
0.91	0.000 750
0.92	0.000 663
0.93	0.000 577

If we neglect multiple reflections between the wall and base of the cavity, we can write the cavity emissivity as

$$\epsilon_N = \epsilon_b + a \epsilon_w,$$

where b = base, w - wall, and a is a constant. For 4:1 cavities on both the base and the wall, we have

$$a = \frac{\epsilon}{\epsilon_b} - 1 = 0.002\ 050$$

If the 4:1 honeycomb on the walls is replaced with 2:1, the wall emissivity is reduced to 0.993013. Using the same value of a, the normal cavity emissivity is then reduced to

$$\epsilon_N = 0.996\ 696 - 0.002650 \times 0.993013 = 0.999\ 327$$

Now the deviation of ϵ_N from unity produces an apparent change in the target radiance given by

$$\delta M = (1 - \epsilon_N) (M_s - M_t)$$

where M is the blackbody exitance and the subscripts s and t denote surround and target, respectively. If the change in exitance is small, the corresponding change in effective blackbody temperature is given by

$$\delta T = \frac{\delta M}{DM/dT}$$

The values of M are given in Table 7.1-6 for Channels 3 (4) at temperatures in the range from 185K (250K) to 321K. The values of δT at representative temperatures are then as follows:

Channel	T	δT
3	185K	0.229K
3	320	-0.0164
4	250	0.0903
4	320	0.0118

Again a calibration depends on the difference between the calibration and space targets, and we can further reduce the non-black errors by constructing the targets in the same geometry and placing them in surrounds as identical as possible. In order to estimate the residual error after taking the difference between targets, we will assume that the calibration target has a surround at 293K and the space target, a surround at 283K. The relative net error in terms of blackbody radiance is then

$$M_{\lambda} = \frac{3.7413 \times 10^4}{\lambda^5} - \frac{1.4388 \times 10^4}{\lambda T} - 1$$

$$\delta^2_M = \epsilon_N M_t + (1 - \epsilon_N) M_{s1} - (1 - \epsilon_N) M_{s2} - M_t$$

$$\delta^2_M = (1 - \epsilon_N) (M_{s1} - M_{s2} - M_t)$$

where s1 denotes the surround the calibration target and s2 the surround of the cold space target. The corresponding errors in blackbody temperature are given in Table 7.1-7 for the representative temperatures.

7.1.2.3 Surround Difference Measurement

In order to verify that the space clamp target and calibration target are exposed to the same surrounds, it was suggested early in the AVHRR program that the two targets be switched in the chamber. This would show if surround reflections were contributing any error to one or the other target. A simpler check can be done by simply comparing the channel 4 signals when it views each target. When the calibration target is run

Table 7.1-6 In-Band Radiant Exitance

	<u>T (K)</u>	<u>(Emitted W cm⁻²)</u>
Channel 3:	185	1.973×10^{-4}
	186	2.047×10^{-4}
	283	2.304×10^{-3}
	293	2.703×10^{-3}
	295	2.787×10^{-3}
	296	2.829×10^{-3}
	300	3.003×10^{-3}
	301	3.048×10^{-3}
	320	3.962×10^{-3}
	321	4.013×10^{-3}
Channel 4:	250	4.174×10^{-6}
	251	4.436×10^{-6}
	283	2.479×10^{-5}
	293	3.931×10^{-5}
	295	4.295×10^{-5}
	296	4.481×10^{-5}
	300	5.331×10^{-5}
	301	5.561×10^{-5}
	320	1.183×10^{-4}
	321	1.228×10^{-4}

Table 7.1-7 Net Non-Black Calibration Error

Channel	T	$\delta^2 T$
3	185K	0.0184 K
3	320	-0.0464
4	250	0.0266
4	320	-0.0156

to 175K, its exitance is below the noise level of the AVHRR in Channel 4. If the output of Channel 4 is then, the same when viewing the cold space target, we can assume that the surrounds are not influencing the accuracy of the calibration in the thermal channels.

Table 7.1-8 shows the calibration data taken in channels 3 and 4 of the ETM on October 6, 1975. The baseplate temperature is $+30^{\circ}\text{C}$. The data shows that in channel 4, the output is identical when viewing the cold space target and the calibration target. As expected the channel 3 output shows some signal from the calibration target at 175K.

From this we conclude that there is no significant calibration error introduced into the thermal channels due to surround differences.

7.1.3 In-Flight Calibration Target

The in-flight calibration is provided by views of the internal blackbody at the housing temperature and of the zero level signal at deep space temperature.

7.1.3.1 Temperature Uncertainty

The temperature measurement error is $\pm 0.05\text{K}$ from the sensor calibration and $\pm 0.10\text{K}$ (specified value) from the instrumentations. Additional temperature uncertainties arise from the gradients within the internal target. The nominal gradient across the base of the target is $\pm 0.08\text{K}$, as determined by the thermal analysis of the instrument. The effective value of this gradient will again be reduced by using an array of

<u>CHANNEL 3 OUTPUT</u>			<u>CHANNEL 4 OUTPUT</u>	
<u>Cal. Target</u> <u>Tamp.</u>	<u>Cal. Target</u> <u>Signal</u>	<u>Space</u> <u>Signal</u>	<u>Cal. Target</u> <u>Signal</u>	<u>Space</u> <u>Signal</u>
K	mvolts	mvolts	mvolts	m volts
320	760.0	6187.5	931.2	6256.8
315	1112.8	6187.5	1879.0	6256.5
305	1769.3	6187.1	3357.1	6257.1
295	2349.6	6187.5	4325.6	6258.1
285	2878.4	6187.5	5035.	6257.1
275	3438.4	6188.1	5495.	6258.1
265	3893.4	6193.7	5822.8	6263.7
255	4284.3	6193.4	6007.1	6264.0
245	4636.2	6193.1	6123.4	6263.7
235	4960.3	6193.7	6189.3	6263.1
225	5225.0	6193.7	6230.0	6264.6
215	5450.6	6193.1	6247.5	6264.0
205	5641.2	6192.8	6254.0	6264.0
195				
185	5906.2	6193.4	6259.0	6263.1
175	5993.7	6193.7	6264.6	6264.6

TABLE 7.1-8

ETM AVHRR CALIBRATION RUN SHOWING
SURROUNDS EFFECT

calibrated platinum sensors to measure the base temperature. The worst case honeycomb gradient is 1.0K (DIR No. 18). Following an analysis similar to that given in Section 7.1.2.1, we find that the corresponding uncertainty in radiance temperature at normal incidence is 0.08K. The total temperature uncertainty of the internal inflight target is then 0.31K.

7.1.3.2 Deviation from a Blackbody

The internal target has a normal emissivity of 0.995 when coated with a black paint whose emissivity is 0.92. The deviation from a blackbody reduces the signal from the target itself but introduces an additional signal from the surround. To obtain the most accurate calibration of the internal target, we would have to compare its signal with that of the more accurate chamber target when the internal target is in the range of surrounds encountered in orbit. The worst case non-blackness errors is shown below to be about 0.08K in Channel 3 and -0.03K in Channel 4.

The internal calibration target is in the form of a honeycomb cavity array in which the length to width ratio is 4:1. Specifically, the basic material has a thickness of 0.001 inch and a cavity width (distance between flats) of 0.060 inch. Each cavity has two walls of its own (where the joined material has a double thickness) and four shared walls or a total of four. The ratio of flat to total target area is then

$$\frac{4 A_W}{A_C + 4 A_W}$$

where A_w is the top area of a wall and A_c the area of a cavity. If w is the distance between flats and t the thickness, we then have

$$A_w = \frac{t}{\sqrt{3}} (w - t)$$

$$A_c = 2 \sqrt{3} \left(\frac{1}{2} w - t \right)^2$$

when the cavity openings are in the form of hexagons. For the above dimensions, the ratio of flat to total surface area is 0.045, and the normal emissivity is given by

$$\epsilon_N = 0.045\epsilon + 0.955 \epsilon_c$$

where ϵ is the emissivity of the black paint and ϵ_c the normal emissivity of the cavity.

The value of ϵ_c can be calculated from the formula of Bauer and Bischoff (Section 7.1.2.2). The results are listed in Table 7.1-9; the paint emissivity is 0.92.

In the case of the in-flight target, the non-black temperature error is given by

$$\delta T = \frac{\delta M}{dM/dT}$$

where $dM/dT = 4.263 \times 10^{-5} \text{ Wcm}^{-2} \text{ K}^{-1}$ in Channel 3 and $1.859 \times 10^{-6} \text{ Wcm}^{-2} \text{ K}^{-1}$ in Channel 4 for a target at $T = 295\text{K}$. The apparent change in target radiance δM is given by

$$\delta M = (1 - \epsilon_N) F_{te} M_e - (1 - F_{ti}) M_t$$

ϵ	0.89	0.998 099	0.994 584
	0.91	0.998 478	0.994 947
	0.92	0.998 662	0.995 122
	0.93	0.998 842	0.995 294
ϵ_c			
ϵ_N			

Table 7.1-9 Normal Emissivities of the Internal
Inflight Calibration Target

where F_{te} = view factor from target to earth = 0.21
 F_{ti} = view factor from target to instrument = 0.741
 M_e = infrared exitance of earth
 M_t = infrared exitance of the target and instrument

The view factors are taken from the thermal analysis of the instrument; they are the values when the instrument is viewing the internal target. As a worst case, we will assume the earth is at its minimum temperature of 185K.* Using the exitance values from Table 7.1-6 and the target emissivity of 0.995 122, we obtain

$$\delta T (\text{Channel 3}) = -0.080K$$

$$\delta T (\text{Channel 4}) = -0.029K$$

for the non-blackness errors in the inflight calibration at $T = 295K$.

7.1.3.3 Scattered Sunlight Error

Depending on its location on the spacecraft and the orbit normal to sun angle (β_s), the in-flight target may be exposed to direct sunlight during the nighttime portion of the orbit. The diffuse reflection of direct sunlight from the target can produce a significant error in the calibration of Channel 4; this subject is covered in Section 3.11.

* The corresponding exitance in Channel 4 is $1.944 \times 10^{-8} \text{ Wcm}^{-2}$.

8.0 THERMAL DESIGN

The thermal design of the AVHRR Instrument was described in Dir #38 on the pages which follow. The validity of the thermal design was established during Solar Simulation Tests performed at NASA/GSFC using the ETM.

The Thermal Interface Drawing for AVHRR is given in Figure 8-1 (page 8-19).



AEROSPACE/OPTICAL
DIVISION
3700 E. Pontiac Street
Fort Wayne, Ind. 46803
(219) 423-9636 - TWX 810-332-1413

To: R. H. Foote

From: J. D. Crawford, *JC*

Date: April 13, 1976

Subject: DIR #38 Final Thermal Model Analysis

CC: R. Annable, T. Diederich, C. Soest, J. Stark

Summary

The analysis of the AVHRR thermal model has been completed. This analysis has included orbit normal to sun angles of 0° , 28° , and 68° which correspond to the warmest, coolest, and extreme orbits. Worst case studies were made within each orbit with the warmest orbit being analyzed with maximum solar, earth IR and albedo inputs; surface finish maximum alpha and minimum ϵ ; and good attainable insulation blanket. The coolest orbit was the 68° orbit which was analyzed with minimum solar, earth IR and albedo inputs; surface finish minimum alpha and maximum ϵ and a not too good insulation blanket. Studies were made with the instrument electronics "on", "Off" and "off - with make-up heaters."

The radiating area of the baseplate, node 50, was trimmed to $.35 \text{ ft}^2$ resulting in an effective louver ϵ of $.44$ for the warmest nominal orbit. This same area resulted in an effective louver ϵ of between $.32$ and $.26$ for both the nominal 0° and 68° orbit. Worst case studies for the hot orbit indicated that the maximum louver ϵ would be $.45$; while the worst case study for the coldest orbit indicated that the louver effective ϵ would be $.16$.

Analysis of the worst case off instrument for heater size indicated that for the coldest orbit 22.8 watts were required to maintain an instrument baseplate temperature of 14.6°C .

Procedure

The thermal analysis for the TIROS-N AVHRR has been performed with the 100 node BAN program supported by view factor, projected area, flux calculations and summation programs. A preprocessor was also used to prepare the data formats for the view factor and projected area programs and also to be data for computer plots. A list of the nodal designations is included in Table I and Figures A and B show the relative node location.

The solar input and albedo inputs were calculated for 10° orbital steps throughout the 0° , 28° and 68° orbits. Those values were then summed and averaged to get the steady state orbital average value. The solar constant used was 429 B/hr Ft^2 , the IR flux value was 75.15 B/hr Ft^2 and the albedo used was $.30$. Values for α and ϵ are listed in Table IIA and Table IIB and include the range of values expected for the listed materials and nodes. The values for the internal power are measured values and will not change by any significant amount.

Conduction Couplings

All conductive couplings are calculated from dimensions taken from detail drawings. The value for the conductivity of the couplings is listed in Table III. Conductance through joints is used for all applicable joints and assumed to be a nominal 72 B/hr Ft².

Radiative Couplings

The radiative couplings were obtained from calculated and estimated view factors and calculated areas. Where the configuration was repetitive, a view factor calculation program was run to get the necessary factors; if a particular shape appeared only once, its value was estimated from a shape factor graph. Block F's were used in this simulation program. Since all of the internal emissivities were relatively high, a product was used rather than the effective emissivities.

Scan Mirror Modeling

The view factors for the scan mirror and cavity areas were obtained by calculating the view factors for ten mirror positions and averaging these values. Solar, albedo and Earth IR inputs to the scan cavity area were calculated with no mirror blockage and then 50% of the flux was assigned to the mirror (25% each to front and back) and 50% to the scan cavity area in question. While these assignments are rather arbitrary, they are better than assuming no mirror as in previous models.

Nominal Case Analysis

The AVHRR instrument was thermally designed to the nominal solar input and surface finish values of the 0, 28 and 68 degree orbits (orbit normal to sun angle). Active thermal control is maintained by using louvers to maintain a nominal TMP temperature of 15°C with an effective emissivity of between .26 and .45. This range of effective louver emissivity was obtained by using a silver teflon surface on the plus velocity electronics surface and trimming the base radiating area - node 50 - to .35 ft². All other exposed surfaces, except insulation surfaces, have black surfaces to minimize scattered light. The insulation surfaces consist of an aluminized Kapton outer layer with 10 layers of multilayer insulation.

Table IV is a listing of the nodal temperatures and emissivities for the nominal case orbits and a radiating area of 1.26 ft². In the 28° orbit the warmest instrument node temperature in the 15 volt regulator board which is 37°C and the remainder of the instrument temperatures range down to 7°C in the electronics baseplate area. The insulation blanket ranges from -99°C to 40°C. These temperatures are maintained with an effective emissivity through the louver of .44.

In the colder orbits (0° and 68°) the warmest electronic temperature is again the 15 volt regulator and the coolest temperature is $.6^\circ\text{C}$ in the electronic baseplate area. Two temperatures to note are the 57°C on the scan mirror when in the 0° orbit and the telescope temperature of 21°C when in the 68° orbit. The scan mirror scans through the sun each rotation and receives maximum solar illumination with no blockage. The temperature of the mirror will be reduced rapidly at about a 4° orbit angle due to S/C blockage. The telescope temperature changes very slowly the incidence angle and area change are offset by the increase in exposure time. Emissivity for the cold orbits is between .25 and .31.

Worst Case Analysis

The AVHRR instrument was modeled for the worst case hot and cold orbits using the radiation area established in the steady state run. Worst case is defined as the range of values that could be expected at launch - surfaces were not degraded by the space environment. The following list defines the worst case condition:

<u>Variable</u>	<u>Warmest</u>	<u>Coldest</u>
Emissivity	Minimum	Maximum
Solar Radiation	Maximum	Minimum
Absorbtivity	Maximum	Minimum
Earth IR	Maximum	Minimum
Albedo	Maximum	Minimum
Blanket Conductance	Best Expected	Worst Expected
Power	Nominal	Nominal

Simulations were run to determine if the worst case equivalent insulation conductance was the best or worst conductance. For the cold orbit the worst case is the worst expected blanket conductance, which leaks more heat to space, and the best expected blanket conductance in worst case for the warmest orbit, which leaks least heat to space. Table V lists the temperatures and emissivities for the worst case hot (28°) and cold (0° and 68°) orbits. The hot orbit ϵ is .05 below the maximum and the cold ϵ is .01 above the minimum.

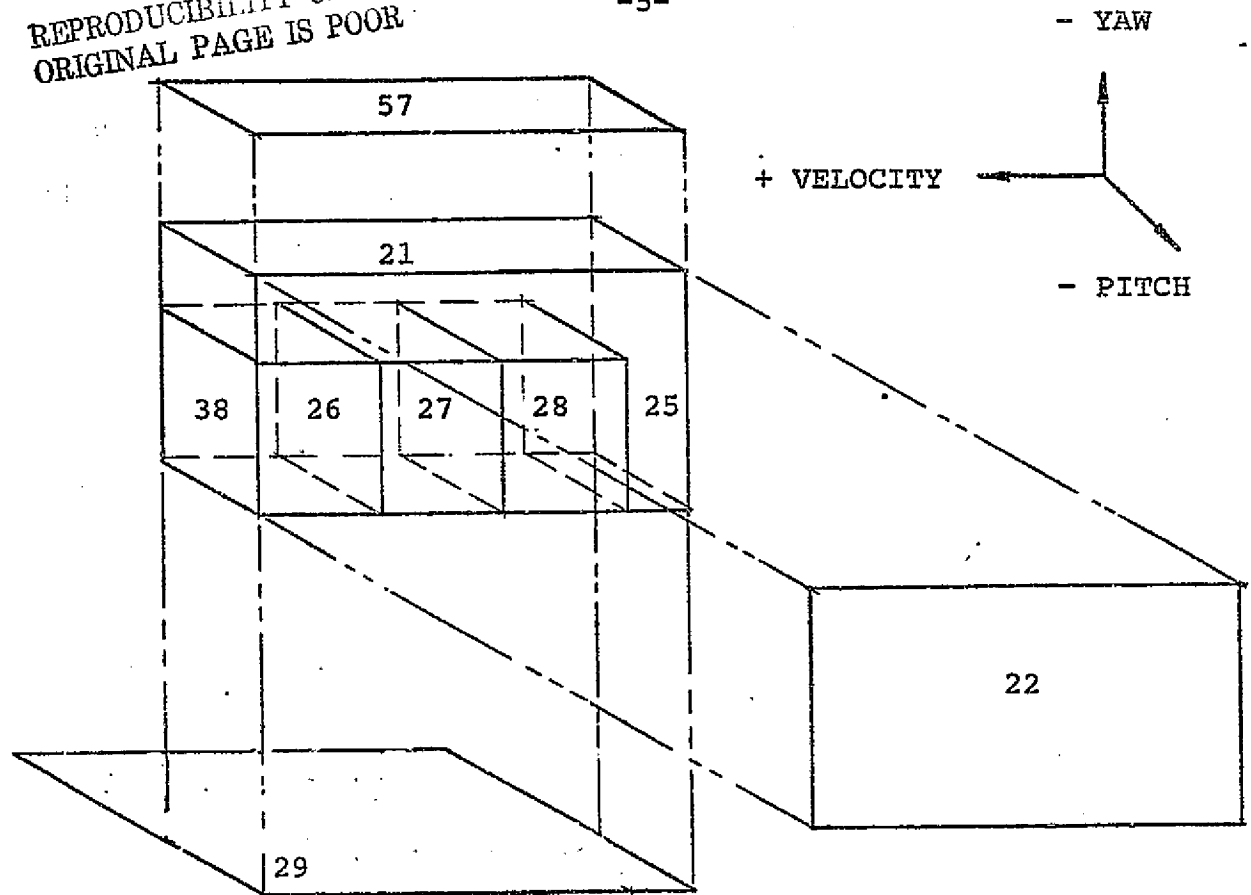
Both the warmest and coldest nodes occur in the 0° degree orbit, the telescope receives no solar heating and the scan mirror is in the sun during the entire orbit with no S/C blockage. In the 68° degree orbit the scan mirror and scan cavity are the coldest nodes - running at 12°C .

Off Instrument Worst Case

When the instrument is turned off, make-up heaters must be turned on to maintain a baseplate temperature of 14°C. Table V. indicates the temperatures expected with 22.84 watts of heater power. Heaters rated at 15.8 and 7.0 watts are mounted on the baseplate and scan motor respectively. These heaters will maintain the scan mirror at 11°C and the telescope at 16°C.

REPRODUCIBILITY OF THE
ORIGINAL PAGE IS POOR

-5-



23 CONNECTORS

24 HARNESS

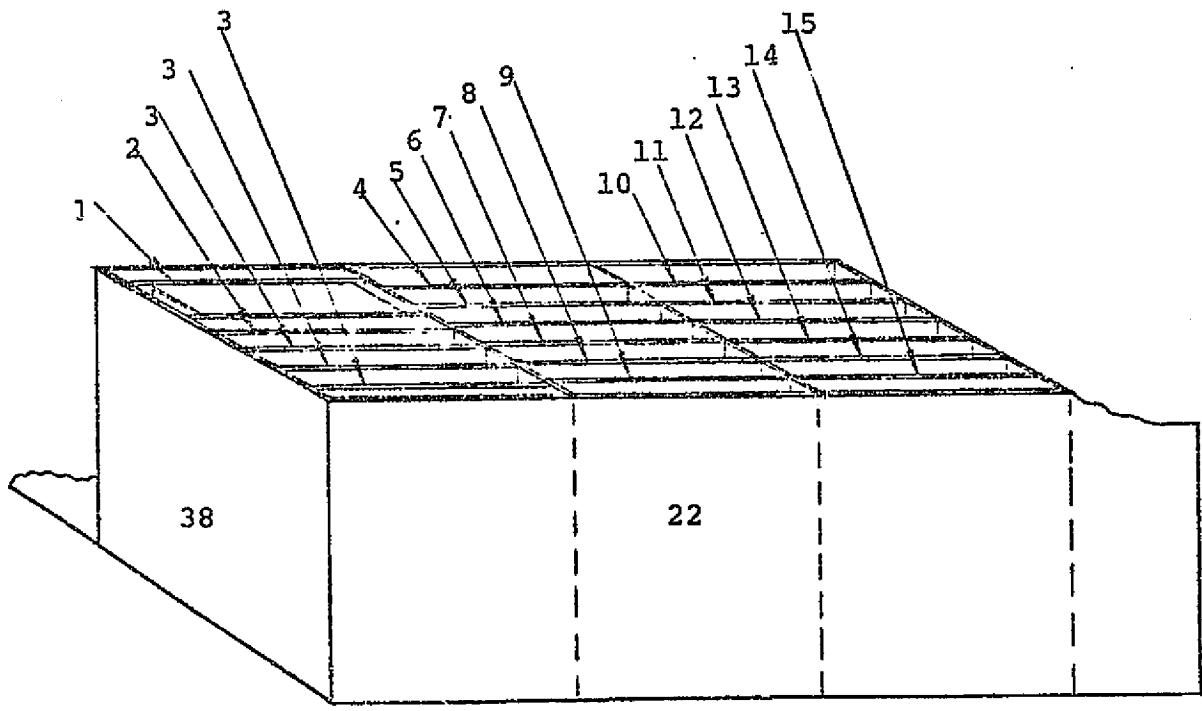


FIGURE A PICTORIAL NODE IDENTIFICATION - ELECTRONIC NODULE

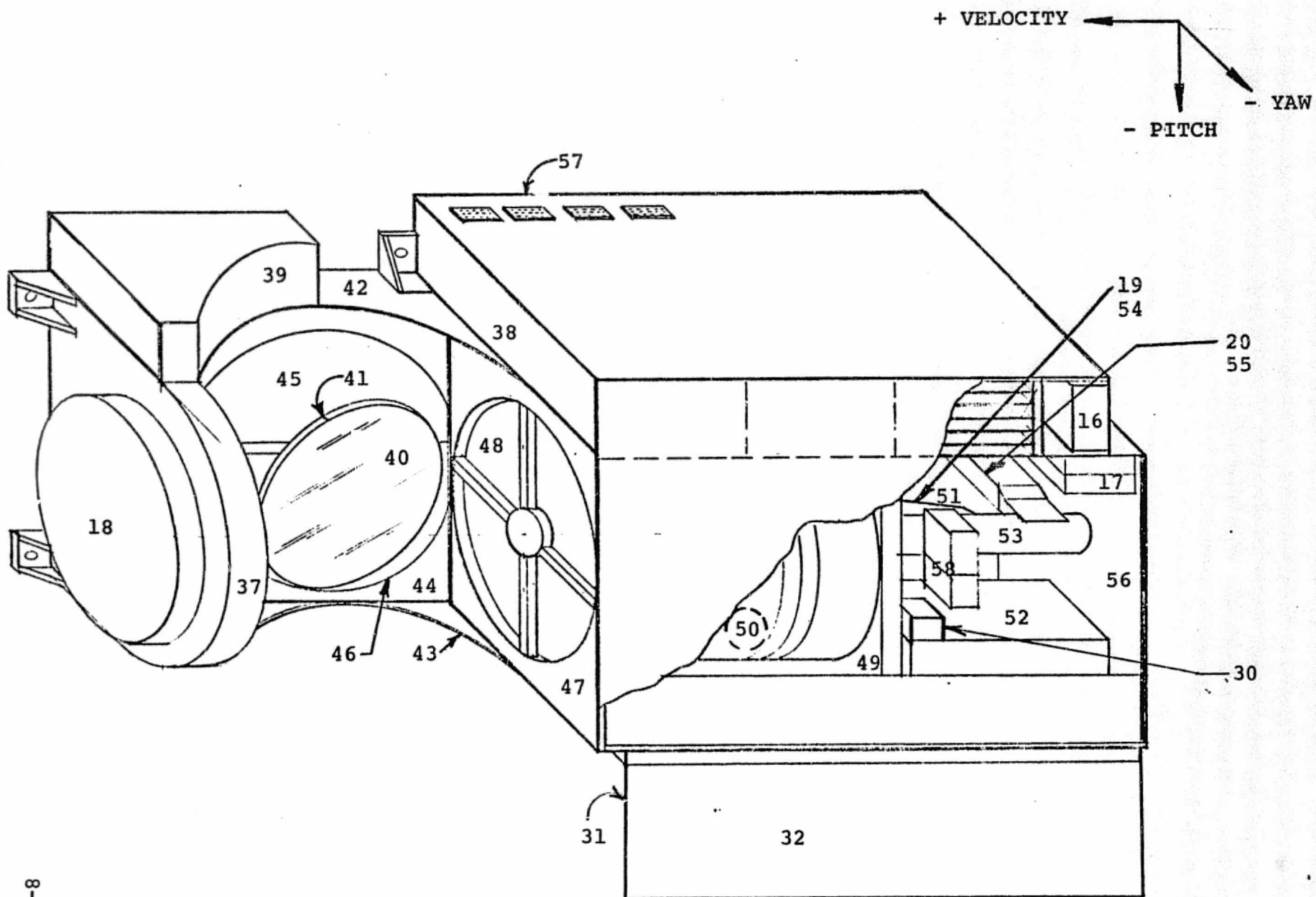


FIGURE B PICTORIAL NODE IDENTIFICATION - INSTRUMENT

<u>NODE NO.</u>	<u>NAME</u>	<u>MATERIAL</u>	<u>FINISH</u>
1	Power Converter	Nickel	None
2	+ -15V Regulator	P.C. Board	Solithane
3	Relay Bd 1 & 2 & 3	P.C. Board	Solithane
4	Patch Temp & TM	P.C. Board	Solithane
5	Telemetry #2	P.C. Board	Solithane
6	Aux Scan Logic	P.C. Board	Solithane
7	Scan Counter	P.C. Board	Solithane
8	Motor Logic	P.C. Board	Solithane
9	Black Body MUX	P.C. Board	Solithane
10	IR Post Amp	P.C. Board	Solithane
11	Daylight Post Amp	P.C. Board	Solithane
12	Ramp Calibration	P.C. Board	Solithane
13	Interface Logic #1	P.C. Board	Solithane
14	Interface Logic #2	P.C. Board	Solithane
15	Multiplexer	"	"
16	A/D Converter	P.C. Aluminum	Black Paint
17	Pre-Amplifier (vis)	Steel	Nickel
18	Scan Motor	Beryllium	Black Paint
19	Channel 1 Detector	Aluminum	Alodine
20	Channel 2 Detector	Aluminum	Alodine
21	Electronic Box, Anti-Sun	Magnesium	Dow 9
22	Electronic Box, Sun	Magnesium	Dow 9
23	Connector	Epoxy	Dow 9
24	Harness	Teflon	--
25	Electronic Box - Vel	Magnesium	Dow 9
26	Partition 1	Magnesium	Dow 9
27	Partition 2	Magnesium	Dow 9
28	Partition 3	Magnesium	Dow 9
29	Radiator 1	Magnesium	Dow 9
30	Pre-amplifier (IR)	Magnesium	Dow 9
31	Earth Shield, Specular	Aluminum	Specular
32	Earth Shield, Insul.	Mylar	Silver Teflon
33	Not Used		
34	Not Used		
35	Not Used		

<u>NODE NO.</u>	<u>NAME</u>	<u>MATERIAL</u>	<u>FINISH</u>
36	Not Used		
37	Scan Motor Hsg	Aluminum	Alodine, Black Paint
38	Radiator, Electronics	Magnesium	Silver Teflon
39	Scan PS	Magnesium	Black Paint
40	Scan Mirror Front	Beryllium	Aluminum
41	Scan Mirror Rear	Beryllium	Gold
42	Cavity, Sun	Magnesium	Black Paint
43	Cavity, A-Sun	Aluminum	Black Paint
44	Base Cavity	Aluminum	Black Paint
45	Cal Target L	Aluminum	Black Paint
46	Cal Target S	Aluminum	Black Paint
47	Bulkhead, Tele	Aluminum	Black Paint
48	Telescope	Invar	Black Paint
49	Bulkhead, Center	Aluminum	Alodine
50	Base, Telescope	Aluminum	Alodine, Black Paint
51	Base, Optic	Aluminum	Alodine, Black Paint
52	Cooler Housing	Aluminum	Gold
53	Telescope Optics	Aluminum	Alodine
54	Channel 1 Relay	Aluminum	Alodine
55	Channel 2 Relay	Aluminum	Alodine
56	End, Optics	Magnesium	Dow 9
57	Cover, Electronics	Magnesium	Dow 9, Black Paint
58	L.W. Relay	Aluminum	Alodine
59	Insulation + Velocity	Mylar	None
60	Insulation Anti-Sun	Mylar	None
61	Insulation - Velocity	Mylar	None
62	Insulation, Sun	Mylar	None
63	Insulation, Nadir	Mylar	None
64	Spacecraft	--	--

TABLE 1 (Continued)

<u>T</u> <u>Surface</u>	Min $\frac{\alpha}{\text{Max}}$	Min $\frac{\epsilon}{\text{Max}}$
Silver Teflon (.005)	.06 - .12	.74 - .78
3 M Black Velvet	.94 - .98	.89 - .93
Black Honeycomb Target	.98	.99
Gold Plate	.32 - .36	.04 - .08
Aluminum Scan Mirror	.08 - .16	.04 - .05
Kapton-Aluminized (.003)	.43 - .47	.77 - .83

Table II A Values of Surface Finishes Used On
External Surfaces

<u>Surface</u>	<u>E</u>
3 M Black Velvet	.91
Black Amodize	.85
Alodine	.85
Nickel Plating	.06
Deposited Aluminum	.05
Stainless Steel	.17
Teflon	.90
Solithane 113	.82

Table II B Value of Surface Finishes Used On
Internal Surfaces

<u>Material</u>	<u>Thermal Conductivity B/hr-in-F⁰</u>
Aluminum	10.65
Stainless Steel	.572
Invar	.517
Synthane G-10	.015
Fused Silica	.067
Beryllium	7.04
Copper	18.92
Magnesium	7.48
Heat Conductive Epoxy	.074

Table III Thermal Conductivity Values For
Materials Used in the AVHRR Instrument

TABLE IV NODAL TEMPERATURES FOR AVHRR/1 INSTRUMENT ON,
15°C CONTROL POINT, NOMINAL SURFACE FINISHES

	<u>28°</u>	<u>68°</u>	<u>0°</u>
1	28.47	28.52	28.24
2	36.95	36.69	36.40
3	24.90	24.59	24.29
4	22.60	22.19	21.97
5	24.36	24.12	23.85
6	26.63	26.45	26.17
7	25.56	25.40	25.11
8	26.85	26.68	26.40
9	23.03	22.80	22.55
10	27.84	27.44	27.23
11	31.27	31.04	30.79
12	28.68	28.50	28.22
13	25.90	25.73	25.44
14	26.16	25.98	25.70
15	27.02	26.80	26.55
16	28.58	28.28	28.00
17	22.73	22.06	21.96
18	20.66	15.08	23.31
19	22.71	20.65	18.62
20	22.65	20.60	18.58
21	18.68	17.81	17.73
22	20.55	20.17	19.99
23	22.52	23.16	22.60
24	16.94	18.96	17.93
25	22.60	22.35	22.08
26	21.27	20.75	20.58
27	21.09	20.58	20.41
28	20.70	20.15	20.00
29	18.32	17.29	17.18
30	18.58	17.54	17.43
31	18.01	16.95	16.78
32	18.02	16.95	16.79
33	18.32	17.29	17.18
34	18.32	17.29	17.18
35	18.33	17.30	17.18
36	19.33	17.30	17.18
37	20.13	14.65	22.24
38	18.22	17.91	17.41
39	18.99	14.01	17.96
40	25.86	14.98	57.30
41	25.86	14.98	57.27
42	18.24	14.02	17.69
43	17.53	13.25	17.11
44	17.72	13.33	17.17
45	17.65	13.06	16.88
46	18.05	13.14	17.38
47	16.88	14.35	15.87
48	28.75	21.04	10.79
49	17.42	16.45	16.36
50	16.43	15.30	15.74
51	16.20	15.73	15.62
52	17.55	16.40	16.16
53	20.76	18.57	16.35
54	21.04	18.93	16.84
55	21.04	18.93	16.83
56	17.73	16.91	16.71
57	7.61	12.44	10.47
58	20.26	18.32	16.53
59	-13.38	-9.19	-66.86
60	-99.11	-93.95	-102.57
61	-54.06	-49.20	-60.05
62	39.46	-21.43	34.44
63	-58.92	-51.19	-88.07
64	-269.44	-269.44	-269.44

ε .44 .26 .32

LOWER RADIATING AREA 1.26 ft.²

TABLE V NODAL TEMPERATURES FOR AVHRR/1 INSTRUMENT ON 15°C CONTROL POINT,
WORST CASE HOT AND COLD AND INSTRUMENT OFF WITH HEATERS

HOT ORBIT 28°	
N	CENT.
1	28.6
2	36.7
3	24.6
4	22.3
5	24.0
6	26.3
7	25.2
8	26.5
9	22.7
10	27.6
11	31.0
12	28.3
13	25.5
14	25.8
15	26.7
16	28.1
17	22.6
18	22.2
19	22.8
20	22.8
21	18.5
22	20.3
23	22.0
24	16.1
25	22.1
26	21.0
27	20.8
28	20.5
29	17.9
30	16.8
31	17.7
32	17.7
33	17.9
34	17.9
35	17.9
36	17.9
37	21.6
38	18.0
39	20.1
40	29.8
41	29.8
42	19.1
43	18.4
44	18.6
45	18.5
46	18.9
47	17.2
48	30.3
49	17.3
50	16.5
51	16.1
52	17.4
53	20.9
54	21.2
55	21.2
56	17.6
57	6.1
58	20.3
59	3.2
60	-97.8
61	-50.2
62	48.1
63	-52.5
64	-269.4

COLD ORBIT 68°	
N	CENT.
1	27.9
2	36.1
3	23.9
4	21.6
5	23.6
6	25.9
7	24.9
8	26.2
9	22.2
10	26.9
11	30.5
12	28.0
13	25.2
14	25.4
15	26.2
16	27.5
17	21.5
18	13.8
19	19.7
20	19.6
21	17.1
22	19.4
23	23.1
24	19.7
25	21.6
26	20.1
27	19.9
28	19.4
29	16.1
30	15.1
31	15.9
32	15.9
33	16.1
34	16.1
35	16.1
36	16.1
37	13.4
38	17.2
39	12.9
40	12.5
41	12.5
42	13.0
43	12.1
44	12.3
45	12.0
46	12.1
47	13.5
48	19.2
49	15.7
50	14.7
51	15.3
52	15.6
53	17.6
54	17.9
55	17.9
56	16.1
57	14.7
58	17.3
59	3.4
60	-91.5
61	-46.4
62	-11.2
63	-52.7
64	-269.4

COLD ORBIT OFF WITH HEATERS 68°	
N	CENT.
1	10.5
2	10.2
3	10.2
4	11.1
5	10.7
6	10.6
7	10.6
8	10.5
9	10.4
10	11.1
11	10.8
12	10.6
13	10.6
14	10.5
15	10.5
16	10.8
17	12.4
18	12.5
19	13.0
20	13.0
21	12.0
22	10.2
23	9.7
24	8.4
25	10.6
26	10.9
27	10.9
28	11.0
29	11.7
30	10.9
31	12.3
32	12.3
33	11.7
34	11.7
35	11.7
36	11.7
37	12.1
38	9.0
39	11.0
40	11.3
41	11.3
42	11.2
43	10.8
44	11.1
45	10.8
46	10.9
47	11.9
48	16.4
49	12.9
50	14.6
51	12.7
52	13.1
53	13.1
54	13.1
55	13.1
56	11.9
57	6.0
58	12.9
59	2.2
60	-91.6
61	-47.3
62	-12.3
63	-53.0
64	-269.4



**AEROSPACE/OPTICAL
DIVISION**

3700 E. Pontiac Street
Fort Wayne, Ind. 46803
(219) 423-9636 - TWX 810-332-1413

To: R. H. Foote

From: J. D. Crawford *JC*

Date: May 6, 1976

Revised: May 10, 1976

Subject: Revised Answers to MDR Question 15

Attached are Tables 1 and 2 which list the solar and earth inputs for the external nodes. Table 3 lists the radiant outputs for the external nodes. These values have been updated to the thermal runs dated 4/7/76.

/am

Attachment

Node Number	Description	NOMINAL 0° ORBIT BTU/HR			NOMINAL 28° ORBIT BTU/HR			NOMINAL 68° ORBIT BTU/HR		
		ER	ERTH	ALB	ER	ERTH	ALB	ER	ERTH	ALB
37	Scan Motor Housing	.0	2.6	.2	3.6	2.6	.8	.1	2.6	1.3
38	Radiator Electronics	.0	2.9	.2	11.3	2.9	1.1	14.8	2.9	1.6
39	Scan Power Supply	.0	2.6	.3	3.5	2.6	1.1	.3	2.6	2.2
40	Scan Mirror Front	61.4	7.2	.5	10.7	7.2	1.9	.1	7.2	3.1
41	Scan Mirror Rear	61.4	7.2	.6	10.7	7.2	1.9	.1	7.2	3.1
42	Cavity, Sun	.0	.4	.1	.0	.4	.1	.0	.4	.2
43	Cavity Anti-Sun	.6	.0	.0	1.5	.0	.0	.2	.0	.0
44	Base Cavity	.0	.0	.0	.0	0.0	.0	.0	.0	.0
45	Cal Target, Large	.0	5.3	.4	3.6	5.3	1.5	.1	5.3	2.6
46	Cal Target, Small	.6	4.0	.3	8.9	4.0	.8	.0	4.0	1.2
47	Bulkhead, Telescope	.0	2.2	.2	3.1	2.2	.6	.0	2.2	1.1
48	Telescope	.0	5.9	.4	21.2	5.9	1.5	11.2	5.9	2.7
59	Insulation + Velocity	.0	8.8	.7	39.8	8.8	1.4	41.4	8.8	4.5
60	Insulation Anti-Sun	.0	7.9	.0	0.0	7.9	1.9	.1	7.9	5.1
61	Insulation - Velocity	.0	12.9	1.0	1.0	12.9	3.4	.9	12.9	6.5
62	Insulation, Sun	143.6	17.6	4.1	153.2	17.6	6.8	34.3	17.6	10.0
63	Insulation, Nadir		28.9	7.3	36.5	29.0	26.1	31.1	29.0	50.3

TABLE 1

SOLAR AND EARTH INPUTS FOR THE AVHRR/1 EXTERNAL NODES, NOMINAL SURFACES FINISHES

Node Number	Description	WORST CASE COLD 68° ORBIT BTU/HR			WORST CASE HOT 28° ORBIT BTU/HR		
		ER	ERTH	ALB	ER	ERTH	ALB
37	Scan Motor Housing	.1	2.5	.9	3.8	2.7	1.0
38	Radiator Electronics	14.4	2.8	1.5	11.9	3.0	1.1
39	Scan Power Supply	.3	2.5	2.0	3.7	2.6	1.2
40	Scan Mirror Front	.1	7.0	2.5	11.3	7.4	2.2
41	Scan Mirror Rear	.1	7.0	2.5	11.3	7.4	2.2
42	Cavity, Sun	.0	.3	.1	.0	.4	.2
43	Cavity Anti-Sun	.2	.0	.0	1.6	.0	.0
44	Base Cavity	.0	.0	.0	.0	.0	.0
45	Cal Target, Large	.1	5.1	2.3	3.7	5.4	1.6
46	Cal Target, Small	.0	3.9	1.1	9.4	4.1	.8
47	Bulkhead, Telescope	.0	2.1	1.0	3.3	2.2	.6
48	Telescope	10.7	5.8	2.4	22.2	6.1	1.7
59	Insulation + Velocity	56.0	8.6	4.2	41.8	9.1	1.5
60	Insulation Anti-Sun	.1	7.7	4.8	.0	8.2	2.1
61	Insulation - Velocity	.9	12.5	6.1	1.1	13.3	3.6
62	Insulation, Sun	51.7	17.1	9.4	160.7	18.1	7.2
63	Insulation, Nadir	29.7	28.1	47.0	38.3	29.8	27.8

TABLE 2

SOLAR AND EARTH INPUTS FOR THE AVHRR/1 EXTERNAL NODES, HOT AND COLD CASES

Node Number	Description	NOMINAL SURFACE FINISHES			WORST CASE		OFF 22.8 WATT HEATERS WATTS
		QROUT 0° ORBIT WATTS	QROUT 28° ORBIT WATTS	QROUT 68° ORBIT WATTS	QROUT HOT WATTS	QROUT COLD WATTS	
37	Scan Motor Housing	4.3	4.1	3.8	4.1	3.8	3.7
38	Radiator Electronics	3.4	3.4	3.4	3.4	3.5	3.1
39	Scan Power Supply	1.8	1.9	1.7	1.8	1.7	1.7
40	Scan Mirror Front	.5	.3	.3	.3	.3	.3
41	Scan Mirror Rear	.9	.6	.5	.4	.6	.6
42	Cavity, Sun	.5	.5	.5	.5	.5	.5
43	Cavity Anti-Sun	.7	.7	.7	.7	.7	.7
44	Base Cavity	1.4	1.4	1.3	1.4	1.3	1.3
45	Cal Target, Large	4.2	4.2	3.9	4.3	3.9	3.8
46	Cal Target, Small	2.2	2.2	2.1	2.2	2.0	2.0
47	Bulkhead, Telescope	3.3	3.3	3.2	3.2	3.2	3.1
48	Telescope	3.7	4.7	4.2	4.6	4.2	4.0
44 50 51	LOUVERS	14.3	19.8	11.7	20.0	7.4	6.5
ϵ	EFFECTIVE ϵ OF LOUVERS	.32	.44	.26	.45	.16	.15

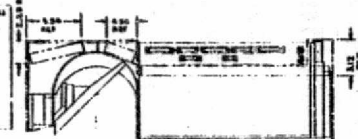
TABLE 3

RADIANT OUTPUTS FOR THE AVHRR/1 EXTERNAL NODES, NOMINAL AND WORST CASES

PHASE TELEMETRY
A/D & ELECTRONICS
MOTOR
SYSTEM LOGIC
CHANNEL 1
CHANNEL 2
CHANNEL 3
CHANNEL 4
CHANNEL 5
CHANNEL 6
CHANNEL 7
CHANNEL 8
CHANNEL 9
CHANNEL 10
CHANNEL 11
CHANNEL 12
CHANNEL 13
CHANNEL 14
CHANNEL 15
CHANNEL 16
CHANNEL 17
CHANNEL 18
CHANNEL 19
CHANNEL 20
CHANNEL 21
CHANNEL 22
CHANNEL 23
CHANNEL 24
CHANNEL 25
CHANNEL 26
CHANNEL 27
CHANNEL 28
CHANNEL 29
CHANNEL 30
CHANNEL 31
CHANNEL 32
CHANNEL 33
CHANNEL 34
CHANNEL 35
CHANNEL 36
CHANNEL 37
CHANNEL 38
CHANNEL 39
CHANNEL 40
CHANNEL 41
CHANNEL 42
CHANNEL 43
CHANNEL 44
CHANNEL 45
CHANNEL 46
CHANNEL 47
CHANNEL 48
CHANNEL 49
CHANNEL 50
CHANNEL 51
CHANNEL 52
CHANNEL 53
CHANNEL 54
CHANNEL 55
CHANNEL 56
CHANNEL 57
CHANNEL 58
CHANNEL 59
CHANNEL 60
CHANNEL 61
CHANNEL 62
CHANNEL 63
CHANNEL 64
CHANNEL 65
CHANNEL 66
CHANNEL 67
CHANNEL 68
CHANNEL 69
CHANNEL 70
CHANNEL 71
CHANNEL 72
CHANNEL 73
CHANNEL 74
CHANNEL 75
CHANNEL 76
CHANNEL 77
CHANNEL 78
CHANNEL 79
CHANNEL 80
CHANNEL 81
CHANNEL 82
CHANNEL 83
CHANNEL 84
CHANNEL 85
CHANNEL 86
CHANNEL 87
CHANNEL 88
CHANNEL 89
CHANNEL 90
CHANNEL 91
CHANNEL 92
CHANNEL 93
CHANNEL 94
CHANNEL 95
CHANNEL 96
CHANNEL 97
CHANNEL 98
CHANNEL 99
CHANNEL 100

SCHEMATIC PROFILE

LAUNCH	ACQUISITION	MANUAL	DECONTAMINATION
PHASE	PHASE	PHASE	PHASE
1	2	3	4
5	6	7	8
9	10	11	12
13	14	15	16
17	18	19	20
21	22	23	24
25	26	27	28
29	30	31	32
33	34	35	36
37	38	39	40
41	42	43	44
45	46	47	48
49	50	51	52
53	54	55	56
57	58	59	60
61	62	63	64
65	66	67	68
69	70	71	72
73	74	75	76
77	78	79	80
81	82	83	84
85	86	87	88
89	90	91	92
93	94	95	96
97	98	99	100



NOTES:
1. THE BLANKET OUTLINE IS SHOWN BY DIMENSION LINES.
2. THE BLANKET IS CAPTIONED.

* EST. 6 WATTS WITH
DOLBY CLEVER

SILVER TEFLON	AL	AL
BLACK	.76	.03
CAL. TARGET	.39	.38
BLACK HONEYCOMB	.39	.38
GO. D (BLACK HONEYCOMB)	.06	.34
AL SPECULAR	.08	.13
AL TAPE	.06	.13
KAPTON	.80	.46
SWIN (1-5 MM)	.09	.13
EQUVALENT BLANKET CONDUCTANCE	.018 TO .006 BTU/FT ² /HR	

CONVEX AREA	SO FT
1	.55
2	.40
3	.40

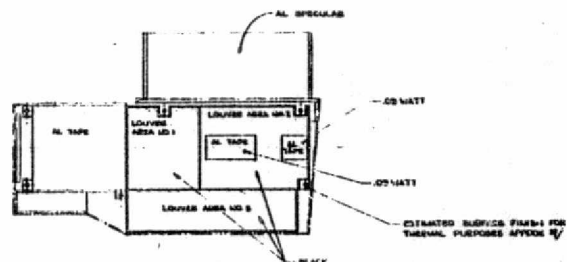
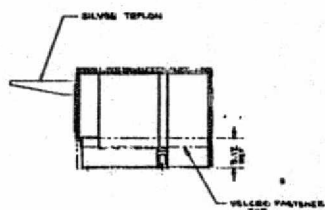
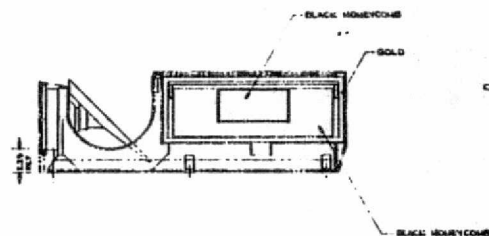
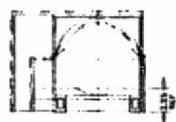
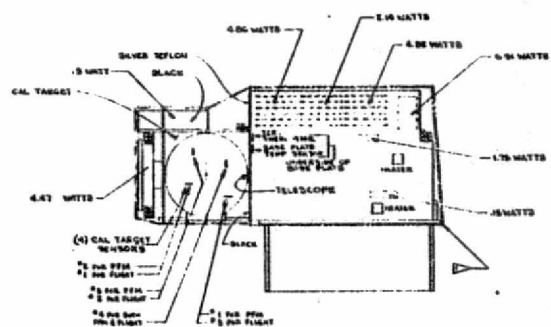


Figure 8.1

<p>AVHRR THERMAL INTERFACE DWG</p> <p>31558 8009976</p>	
<p>DATE: 11-1-77</p> <p>BY: [Signature]</p> <p>APP: [Signature]</p>	<p>DATE: 11-1-77</p> <p>BY: [Signature]</p> <p>APP: [Signature]</p>

REPRODUCIBILITY OF THE
ORIGINAL PAGE IS POOR

9.0 TEST AND CALIBRATION DATA

Resumes of test results for Engineering Model and Protoflight Model and DIR #40, Final Report of the Life Test Model are given in the following pages.

For detailed test results and calibration data, refer to

Alignment & Calibration Data Book,

AVHRR/1, ETM

Alignment and Calibration Data Book,

AVHRR/1, PFM

Test Report, AVHRR/1 PFM

AVHRR

RESUME OF ETM TEST RESULTS

SUMMARY OF MISCELLANEOUS ITEMS

<u>ITEM</u>	<u>SPEC LEVELS</u>	<u>MEASURED</u>
SIZE	MAX. 31" x 11" x 15"	EXCLUDING THERMAL BLANKET 30-1/4" x 9 3/4" x 14"
WEIGHT	60 LB. MAX.	58 LB. - 150Z (LESS THERMAL BLANKET)
ACCELERATION	18G LONGITUDINAL & 3G LATERAL FOR 1 MIN. + Z AND + X + Z AND + Y	NO PROBLEMS
VIBRATION	COVERED PREVIOUSLY	
ACOUSTICS	LEVELS REVIEWED AND COMPARED TO PAST PROGRAMS	NO PROBLEM NO TEST RUN
JITTER	$\pm 17 \mu\text{SEC}/98\%$	22.5V $\pm 8 \mu\text{SEC}/100\%$

CENTER OF GRAVITY	DOOR OPEN		DOOR CLOSE ACT
	EST	ACT	
X	3.42"	4.86"	4.72"
Y	11.8"	13.12"	13.12"
Z	2.73"	1.20"	1.27"

ETM AVHRR TEST RESULTS

PARAMETER	SPECIFICATION	MEASURED
CHAN 1 & 2 SIGNAL STABILITY	± 100 MV OVER TEMP. RANGE 10°C TO 30°C	NOT CHECKED DUE TO STABILITY OF VIS CAL. CHECK TGT.
CHAN 1 & 2 SPECTRAL RESPONSE	SEE PARA. 3.4.2 OF SPEC	CHAN 1 CUTOFF SLOPE .047 . ALL OTHER PARAMETERS OKAY. CHAN 2 ALL OKAY.
THERMAL CHAN. NE Δ T	$\leq 0.12\text{K}$ @ 300K	CHAN 3 0.06K CHAN 4 0.07K
CHAN 3 & 4 SIGNAL STABILITY	± 100 MV OVER TEMP RANGE 10°C TO 30°C	CHAN 3 CH 4 160 MV 41 MV
CHAN 3 & 4 SPECTRAL RESPONSE	SEE PARA 3.4.2 OF SPEC.	CHAN 3 CUTOFF SLOPE OUT. CHAN 4 ALL OKAY
SCAN JITTER	98% WITHIN \pm $16\mu\text{SEC}$	SCENE - 100% LINE - 100%
SCAN LINEARITY	LINE TO LINE: $\frac{1}{4}$ IFOV (98%) 20 MINUTES: 1 IFOV < 1 IFOV (98%)	< $\frac{1}{4}$ IFOV

ETM AVHRR TEST RESULTS

PARAMETER	SPECIFICATION	MEASURED	
		Scan	Cross Scan
IFOV Size to 50% POINTS	1.3 ± 0.2 MILLIRADIANS	CH 1 1.20 CH 2 1.30 CH 3 1.34 CH 4 1.30	CH 1 1.24 CH 2 1.26 CH 3 1.38 CH 4 1.28
CHANNEL REGISTRATION	ALL CENTERS WITHIN 0.10 MRAD	INITIALLY ≤ 0.07 MRAD AFTER VIB ≤ 1.0 MRAD	
SYSTEM MTF	>30% AT LIMITING FREQ	CH 1: 46% CH 2: 44%	CH 3: 39% CH 4: 37%
POLARIZATION SENSITIVITY	<10%, CHAN 1 + CHAN 2	CHAN 1 1.6% CHAN 2 12.9%	
S/N RATIO SOLAR CHANNELS	≤ 9.4 MVOLTS NOISE	CHAN 1: 2.0 MVOLTS CHAN 2: 1.3 MVOLTS	
SUN SCAN	SURVIVE AND RETURN TO CALIBRATION	SURVIVED: CHAN 1, 6MV CHAN 2: 25MV CHAN 3: 37 MV CHAN 4: 1 MV	
STRAY RADIANCE SUPPRESSION	<2% WITH PK SIGNAL NEAR AXIS	CH2 = 1.2% CH1 = 1.2%	
SCATTERED LIGHT SIGNAL	--	CHAN 1 & 2 -- NONE CHAN 4 - <3 NER IN HIGH SUN ORBITS	

ETM AVHRR TEST - RESULTS

PARAMETER	SPECIFICATION	MEASURED
SIGNAL AMPLITUDE CHAN 1 & 2	100% ALBEDO = $6.1 \pm .1V$ SPACE LOOK = $.25 \pm .05$	6.188V CH. 1 6.249V CH. 2 .250 VOLTS BOTH CHANNELS
SIGNAL AMPLITUDE CHAN 3 & 4	320K SCENE = $0.3 \pm .1V$ SPACE LOOK = $6.2 \pm .05$	CH 3 CH 4 .760 .931 6.187 6.256

ITEM	SPEC	MEASURED
COMMAND OPERATION		OPERATION AND DIGITAL TM LEVEL VERIFIED.
ANALOG TM		INSTRUMENT STATUS MEASURED.
TURN ON TRANSIENT	150% OF STEADY STATE	ELECTRONICS ON .6 AMP MOTOR ON .6 AMP COOLER HEAT ON 2.4 AMP
CONDUCTED RIPPLE	2% OF STEADY STATE	MOTOR ONLY LOW -6 MA MOTOR ONLY HIGH -6 MA ELECTRONICS & ALL CHANNELS -26 MA FULL INSTRUMENT -26 MA
SUSCEPTIBILITY	.25 VPP TO 1.5 KH .50 VP TO P TO 10 MHZ	MAX. SUSCEPTIBILITY AT 500 HZ, 0.9V P TO P

ITEM	SPEC	MEASURED
OVER-VOLTAGE	28V TO 39V	±15 V REGULATED VOLTAGES VARY 2 MV MAX FROM 26V TO 39V
AMPLIFIER ZEROING	CH 1 .250 ± 0.050 CH 2 .250 ± 0.050 CH 3 6.2 ± 0.050 CH 4 6.2 ± 0.050	251.119 MV 256.169 MV 6183.23 MV 6268.61 MV *INITIAL ZERO LEVEL SET PRIOR TO REDUC- TION OF NOISE
AMPLIFIER LINEARITY	± 6.25 MV	CH 1-2.27 MV MEASURE WITH CH 2 0 RAMP CAL AND CH 3-3.43 MV DATA CONVERTER CH 4 0
RAMP CAL RANGE	-0.1 TO +6.4	CH 1 6452 SWING CH 2 6585 SWING CH 3 6496 SWING CH 4 6498 SWING

ITEM	SPEC	MEASURED																		
AMPLIFIER DROOP	39% OF FULL SCALE (25 mv)	CH 1 .369 mv CH 2 .007 mv CH 3 5.47 mv CH 4 .50 mv																		
VERIFICATION OF TM IN DATA STREAM	--	<table> <tr> <td></td><td><u>TM</u></td><td><u>DATA</u></td></tr> <tr> <td>BB1</td><td>2320</td><td>2318.75</td></tr> <tr> <td>BB2</td><td>2389</td><td>2387.18</td></tr> <tr> <td>BB3</td><td>2379</td><td>2376.25</td></tr> <tr> <td>BB4</td><td>2439</td><td>2439.68</td></tr> <tr> <td>PATCH TEMP</td><td>3032</td><td>3033.11</td></tr> </table>		<u>TM</u>	<u>DATA</u>	BB1	2320	2318.75	BB2	2389	2387.18	BB3	2379	2376.25	BB4	2439	2439.68	PATCH TEMP	3032	3033.11
	<u>TM</u>	<u>DATA</u>																		
BB1	2320	2318.75																		
BB2	2389	2387.18																		
BB3	2379	2376.25																		
BB4	2439	2439.68																		
PATCH TEMP	3032	3033.11																		
BB SAMPLE TM	--	<table> <tr> <td></td><td><u>TM</u></td><td><u>DATA</u></td></tr> <tr> <td>CH 3</td><td>2173</td><td>2174.23</td></tr> <tr> <td>CH 4</td><td>4183</td><td>4179.26</td></tr> </table>		<u>TM</u>	<u>DATA</u>	CH 3	2173	2174.23	CH 4	4183	4179.26									
	<u>TM</u>	<u>DATA</u>																		
CH 3	2173	2174.23																		
CH 4	4183	4179.26																		
VOLTAGE CAL VERIFICATION	3 EARTH SCENE LEVELS 1 B.B. LEVEL DETECTOR DISABLED	VERIFIED																		

ITEM	SPEC	MEASURED
AUXILARY SCAN		SYNC PULSE TO COLLIMATOR TARGET NORMAL 45150 μ SEC . WITH AUX SCAN 45832 TO 45860 μ SEC JITTER $\pm 8 \mu$ SEC 97.027% $\pm 16 \mu$ SEC 99.499%

CALIBRATION EQUATIONS

RADIATOR TEMP	$^{\circ}\text{K}$	=	35.12V	+	141.7
PATCH POWER	.MW	=	$2V^2$		
PATCH TEMP LOW RANGE	$^{\circ}\text{K}$	=	5.16V	+	89.7
PATCH TEMP EX RANGE	$^{\circ}\text{K}$	=	45.12V	+	90.4
BB#1 TM	$^{\circ}\text{C}$	=	8.31V	+	3.424
BB#2 TM	$^{\circ}\text{C}$	=	8.31V	+	3.424
BB#3 TM	$^{\circ}\text{C}$	=	8.31V	+	3.424
BB#4 TM	$^{\circ}\text{C}$	=	8.31V	+	3.424
MOTOR CURRENT	MA	=	60V		
ELECTRONICS CURRENT	MA	=	196.5V		
EARTH SHIELD POSITION		=	($<2V$) c1	(2-4)MID	$>\Delta$ OPEN
ELECTRONICS TEMP	$^{\circ}\text{C}$	=	-5.82V	+	39.9
BASE PLATE TEMP	$^{\circ}\text{C}$	=	-7.75V	+	34.8
A TO D TEMP	$^{\circ}\text{C}$	=	-8.33V	+	86.15
MOTOR HOUSING TEMP	$^{\circ}\text{C}$	=	-7.75V	+	34.8
COOLER HOUSING TEMP	$^{\circ}\text{C}$	=	-7.75V	+	34.8
DETECTOR BIAS VOLTS		=	4.33V	-	21.33
BB IR CH3	$^{\circ}\text{C}$	=	$-1.1V^2$	-13.2V	+ 330.2
BB IR CH4	$^{\circ}\text{C}$	=	$-3V^2$	+11.3V	+ 302.3
OFFSET VOLTAGE	TM	=	1.33V		

ETM RADIANT COOLER PERFORMANCE

TEMPERATURE OF	ORIGINAL DESIGN	MEASURED	15°C BP WARMEST ORBIT
COOLER HOUSING	22°C	26.3°C	14.7°C (c)
OPTICS	25°C	23.4°C	19.6°C (c)
RADIATOR	170.9K	168.4K	166.0K
PATCH (a)	105.0K	105.6K	105.0K
CHAMBER MARGIN (b)	7.3K 25.6 MW	7.6K 27.2 MW	8.7K ± 0.6K 30.1 MW ± 1.8 MW
ORBITAL MARGIN (b)	10.0K 34.4 MW	10.2K 35.5 MW	11.3K ± 0.7K 38.0 MW ± 1.8 MW

(a) CONTROL POINT

(b) CALCULATED VALUES WITH RESPECT TO
CONTROL POINT

(c) FROM THERMAL ANALYSIS

AVHRR

RESUME OF PFM TEST RESULTS

PFM AVHRR TEST RESULTS

<u>ITEM</u>	<u>SPEC LEVELS</u>	<u>MEASURED</u>
SIZE	MAX. 31" x 11" x 15"	EXCLUDING THERMAL BLANKET 30.18" x 9-5/8" x 14.15"
WEIGHT	60 LB. MAX	59 - 15 oz (WITH THERMAL BLANKET)
ACCELERATION	NO TEST ON PFM	NA
POWER	27 WATTS	24.92 WATTS
VIBRATION	SEE SPEC. PARA. 4.4.4.3	PASSED 3RD VIBRATION PROBLEMS COVERED BY MFR'S
ACOUSTICS	NO TEST ON PFM	NA
JITTER	± 17 SEC/98%	MET SPEC AT B.P. 15° AND HIGHER SEE MFR 02526

CENTER OF GRAVITY	DOOR OPEN	DOOR CLOSE
X	4.77	4.68
Y	12.98	12.98
Z	1.14	1.24

PFM AVHRR TEST RESULTS

PARAMETER	SPECIFICATION	MEASURED
CHAN 1 & 2 SIGNAL STABILITY	± 100 MV OVER TEMP. RANGE 10°C TO 30°C	CHAN #1 = 25 MV CHAN #2 = 82 MV
CHAN 1 & 2 SPECTRAL RESPONSE	SEE PARA. 3.4.2 OF SPEC	CHAN #1 ALL OKAY CHAN #2 ALL OKAY
THERMAL CHAN. NEAT	≤ 0.12 K @ 300K	CHAN 3 .04°K CHAN 4 .06°K
CHAN 3 & 4 SIGNAL STABILITY	± 100 mv OVER TEMP RANGE 10°C TO 30°C	CHAN 3 CH 4 331.25 mv 61.56 *SEE MFR #02504
CHAN 3 & 4 SPECTRAL RESPONSE	SEE PARA 3.4.2 OF SPEC.	CHAN 3 ALL OKAY CHAN 4 ALL OKAY
SCAN JITTER	98% WITHIN \pm 17 SEC (1/2 IFOV)	SCENE - 99% LINE - 98% *SEE MFR #02526
SCAN LINEARITY	LINE TO LINE: $\pm 1/2$ IFOV (98%) 20 MINUTES: ± 1 IFOV (98%)	< 1/2 IFOV < 1 IFOV

PFM AVHRR TEST RESULTS

<u>PARAMETER</u>	<u>SPECIFICATION</u>	<u>MEASURED</u>
IFOV Size to 50% POINTS	1.5 ± 0.2 MILLIRADIANS	SCAN CROSS SCAN
		CH 1 1.38 CH 1 1.39
		CH 2 1.38 CH 2 1.41
		CH 3 1.54 CH 3 1.51
		*SEE MFR 02527
		CH 4 1.41 CH 4 1.41
CHANNEL REGISTRATION	ALL CENTERS WITHIN 0.10 MRAD	INITIALLY ≤ 0.08 MRAD
		AFTER VIB ≤ 0.08 MRAD
SYSTEM MTF	>30% AT LIMITING FREQ	CH 1: 49% CH 3: 39%
		CH 2: 48% CH 4: 45%
POLARIZATION	CHAN 1 ≥ 5%	CHAN 1 3.7 NADIR
SENSITIVITY	CHAN 2 ≥ 5.3%	CHAN 2 5.3 NADIR
S/N RATIO SOLAR CHANNELS	10.0 MVOLTS NOISE 3/1 @ .5% ALBEDO	CHAN 1: 1.83 MVOLTS
		CHAN 2: 1.89 MVOLTS
SUN SCAN	No TEST PFM	NA
STRAY RADIANCE SUPPRESSION	No TEST PFM	NA
SCATTERED LIGHT SIGNAL	No TEST PFM	NA

PFM AVHRR TEST RESULTS

PARAMETER	SPECIFICATION	MEASURED	
		CH 1	CH 2
SIGNAL AMPLITUDE	100% ALBEDO = $6.1 \pm .1V$	6051.52	6176.92
CHAN 1 & 2	SPACE LOOK = $.25 \pm .05$	256.25	251.24
		CH 3	CH 4
SIGNAL AMPLITUDE	320K $\pm 1^{\circ}K$ = $0.3 \pm .1V$	468.75	275.00
CHAN 3 & 4	SPACE LOOK = $6.2 \pm .05$	6212.50	6187.87

ITEM	SPEC	MEASURED
COMMAND OPERATION		OPERATION AND DIGITAL TM LEVEL VERIFIED.
ANALOG TM		INSTRUMENT STATUS MEASURED
TURN ON TRANSIENT (28V)		
ELECTRONICS	1.4A MAX. @ 20 MA/μSEC	680 MA - 3 MA/μSEC.
MOTOR	1.4A MAX. @ 20 MA/μSEC	680 MA - .56 MA/μSEC
COOLER HEAT	2.8A MAX. FOR 2 M.S.	2.8A FOR 500 μSEC
EARTH SHIELD	2.1A MAX. FOR 1 SEC	1.6A FOR .88 SEC
CONDUCTED RIPPLE (28V)		
MOTOR - LOW	18 MA P - P	5 MA P - P
MOTOR - HIGH	18 MA P - P	5 MA P - P
ELECT. & ALL CH'S	<20 Hz 3% (27 MA)	<20 Hz - 14 MA/>20 Hz - 2 MA
FULL INST.)	>20 Hz 1% (9 MA)	<20 Hz - 15 MA/>20 Hz - 5 MA
SUSCEPTIBILITY	.25 VPP TO 1.5 KHz .50 VP TO P TO 10 MHz	WORST CASE .8V @ 15 KHz.
CONDUCTED RIPPLE (+20V)	1 MA MAX.	NONE - DISCERNIBLE
CONDUCTED RIPPLE (+5V)	1 MA MAX.	NONE - DISCERNIBLE

ITEM	SPEC	MEASURED
OVER-VOLTAGE	28V TO 39V	±15 V REGULATED VOLTAGES VARY 0 MV - +5 V SUPPLY VARIES 32 MV.
AMPLIFIER ZEROING	CH 1 .250 ± 0.050 CH 2 .250 ± 0.050 CH 3 6.2 ± 0.50 CH 4 6.2 ± 0.50	250.00 MV 350.00 MV 6211.00 MV 6173.00 MV
AMPLIFIER LINEARITY	± 6.25 MV (±DATA CONV.)	CH 1 - 10.1 MV MEASURE WITH CH 2 10.4 MV RAMP CAL AND CH 3 6.25 MV DATA CONVERTER CH 4 8.3 MV
RAMP CAL RANGE	0.025 TO +6.475	CH 1 6506 SWING CH 2 6508 SWING CH 3 6499 SWING CH 4 6476 SWING

ITEM	SPEC	MEASURED				
AMPLIFIER DROOP	.39% OF FULL SCALE (25 mv)	CH 1	0	mv		
		CH 2	0	mv		
		CH 3	.1	mv		
		CH 4	6.11	mv		
VERIFICATION OF TM IN DATA STREAM	---		<u>TM</u>		<u>DATA</u>	
		BB1	1.247		1.243	
		BB2	1.276		1.268	
		BB3	1.321		1.309	
		BB4	1.319		1.309	
		PATCH TEMP	3.022		3.018	
BB SAMPLE TM	---		<u>TM</u>		<u>DATA</u>	
		CH 3	2.594		2.594	
		CH 4	4.653		4.659	
VOLTAGE CAL VERIFICATION	3 EARTH SCENE LEVELS 1 B.B. LEVEL DETECTOR DISABLED		1	2	3	4
		CH 1	1862	3493	5113	5922
		CH 2	1864	3494	5118	5925
		CH 3	1356	2975	4606	549
		CH 4	1362	2975	4587	567
		VERIFIED DET. DIS.				

ITEM	SPEC	MEASURED
AUXILIARY SCAN	NONE	SYNC PULSE TO COLLIMATOR TARGET NORMAL 42857.3 - 42800.0 WITH AUX 42812.8 - 42760.7 SCAN

CALIBRATION EQUATIONS

RADIATOR TEMP	$^{\circ}\text{K}$	=	35.12V	+	141.7
PATCH POWER	.MW	=	$2V^2$		
PATCH TEMP LOW RANGE	$^{\circ}\text{K}$	=	5.16V	+	89.7
PATCH TEMP EX RANGE	$^{\circ}\text{K}$	=	45.12V	+	90.4
BB#1 TM	$^{\circ}\text{C}$	=	8.31V	+	3.424
BB#2 TM	$^{\circ}\text{C}$	=	8.31V	+	3.424
BB#3 TM	$^{\circ}\text{C}$	=	8.31V	+	3.424
BB#4 TM	$^{\circ}\text{C}$	=	8.31V	+	3.424
MOTOR CURRENT	MA	=	60V		
ELECTRONICS CURRENT	MA	=	196.5V		
EARTH SHIELD POSITION		=	($<2V$) c1	(2-4)MID	$> \Delta$ OPEN
ELECTRONICS TEMP	$^{\circ}\text{C}$	=	-5.82V	+	39.9
BASE PLATE TEMP	$^{\circ}\text{C}$	=	-7.75V	+	34.8
A TO D TEMP	$^{\circ}\text{C}$	=	-8.33V	+	86.16
MOTOR HOUSING TEMP	$^{\circ}\text{C}$	=	-7.75V	+	34.8
COOLER HOUSING TEMP	$^{\circ}\text{C}$	=	-7.75V	+	34.8
DETECTOR BIAS VOLTS		=	4.33V	-	21.33
BB IR CH3	$^{\circ}\text{C}$	=	$-1.1V^2$	-13.2V	+ 330.2
BB IR CH4	$^{\circ}\text{C}$	=	$-3V^2$	+11.3V	+ 302.3
OFFSET VOLTAGE	TM	=	1.33V		

AVHRR S.N.

PFM

DATE

10-4-76

Q.C.

ENGINEER

L. OWENS

	CHANNEL 1		CHANNEL 2	
	SPEC.	MEASURED	SPEC	MEASURED
Short Wave 80% Wv'ln.	within 0.10 μ m of 50% Wv'ln.	.628	Within 0.02 μ m of 50% Wv'ln.	.720
Short Wave 50% Wv'ln.	0.55 \pm 0.05 μ m	.552	0.725 \pm .025 μ m	.710
Short Wave 5% Wv'ln.	within 0.14 μ m of 50% Wv'ln. AND $>$.46 μ m	.497	within 0.04 μ m of 50% Wv'ln*	.695
Long Wave 80% Wv'ln.	within 0.02 μ m of 50% Wv'ln.	.896	N.R.	
Long Wave 50% Wv'ln.	0.90 \pm 0.05 μ m	.904	N.R.	
Long Wave 5% Wv'ln.	within 0.04 μ m of 50% Wv'ln.	.938	N.R.	
Response between S.W. 80% Wv'ln. and L.W. 80% Wv'ln.	80% Min.	$>$ 80%	80% Min.	$>$ 80%
Out-of-Band Response	NASA Spec GSFC S-731-P-118 Rev. D Para. 3.4.2.1.5	OK	NASA Spec. GSFC S-731-P-118 Rev. D, Para. 3.4.2.2.6	OK
N.R. = No requirement * S.W. 5% Wv'ln. of Ch. 2 must always exceed 0.685 μ m ** or 0.65 μ m, whichever is greater				

TABLE 6
CHANNEL 1 & 2 SPECTRAL CHARACTERISTICS

14

8120269

AVHRR S.N.

PFM

DATE

10-7-78

Q.C.

ENGINEER

L. OWENS

	CHANNEL 3		CHANNEL 4	
	SPEC.	MEASURED	SPEC	MEASURED
Short Wave 50% Wv'ln.	10.5 ± 0.1 μm	10.52	3.55 ± 0.06 μm	3.59
S.W. 80% of 1st Peak Wv'ln.	See S.W. Slope	10.60	See S.W. Slope	3.63
S.W. 5% Wv'ln.	See S.W. Slope	10.40	See S.W. Slope	3.54
S. W. Slope*	< 3.0%	1.9%	< 3.0%	2.5%
Long Wave 50% Wv'ln.	11.5 ± 0.1 μm	11.45	3.93 ± 0.06 μm	3.98
L.W. 80% of 1st Peak Wv'ln.	See L.W. Slope	11.13	See L.W. Slope	3.95
L.W. 5% Wv'ln.	See L.W. Slope	11.67	See L.W. Slope	4.04
L.W. Slope*	< 5.0%	4.7%	< 3.0%	1.5%
Response between S.W. 80% Wv'ln. & L.W. 80% Wv'ln.	80% Min.	> 80%	80% Min.	> 80%
Response at Wv'ln. < 10.0 μm and > 12.0 μm	≤ 1%	< 1%	N/A	N.A.
Response at Wv'ln. < 3.40 and > 4.12 μm	N.A.	N.A.	≤ 1%	< 1%
Out-of-Band Response	NASA Spec. Para 3.4.2.3	5 OK	NASA Spec. Para. 3.4.2.4.5	OK

* Slope = $[(80\% \text{ of first peak Wv'ln.} - 5\% \text{ Wv'ln.}) \div 5\% \text{ Wv'ln.}] \times 100\%$

TABLE 7 - CHANNEL 3 & 4 SPECTRAL CHARACTERISTICS

15

8120269

9-24

100 %

10-7-76

90

80

70

60

50

40

30

20

10

CHANNEL 1 PTM
AVHRR/1 SPECTRAL
RESPONSE

— PREDICTED

- - - MEASURED

$\Delta\lambda = .0053 \mu$

.50

.60

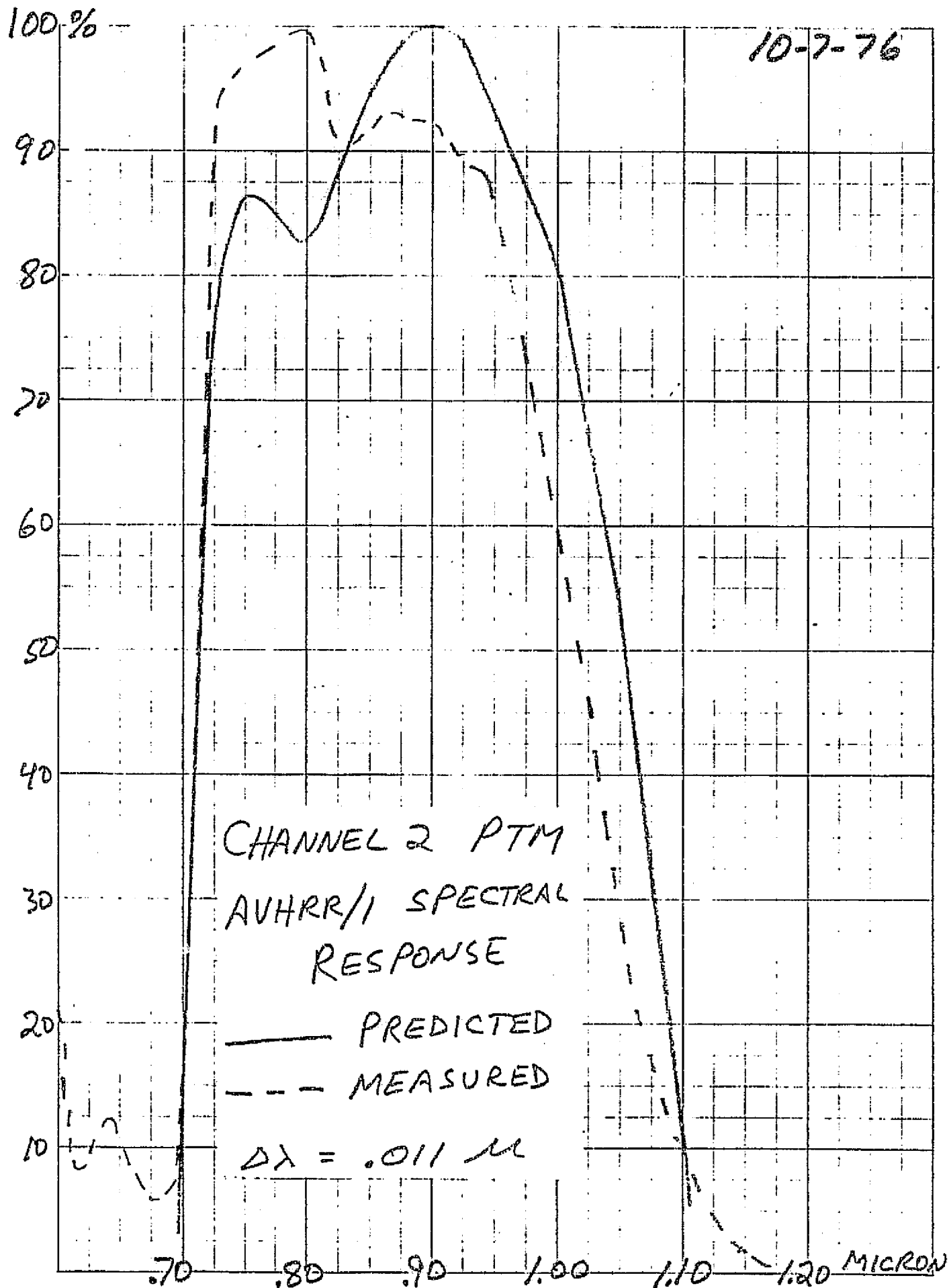
.70

.80

.90

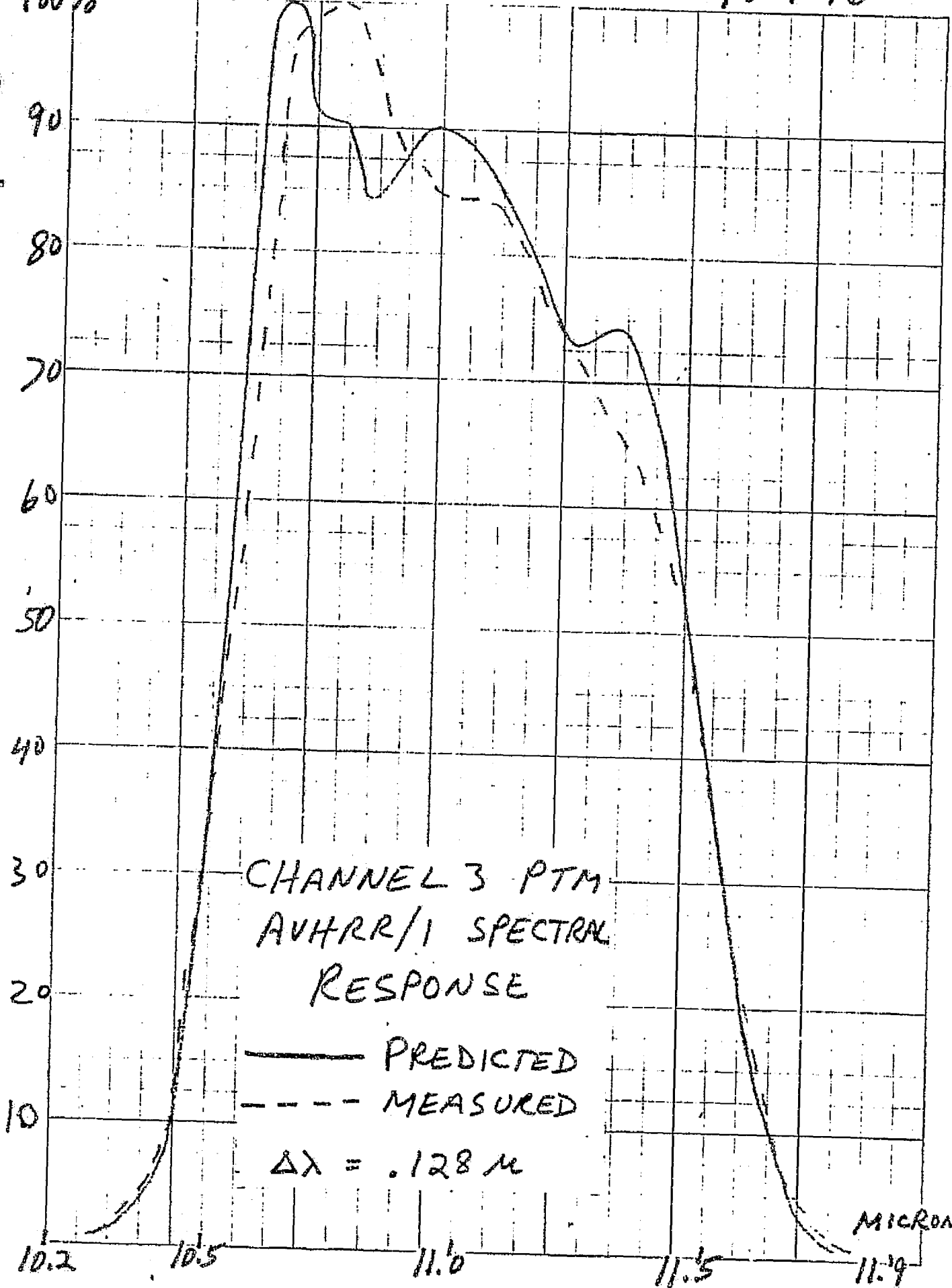
1.00

MICRON



10-7-76

100%



4 X 4 TO THE INCH 46 0253
100% 100% 100% 100% 100%
100% 100% 100% 100% 100%

10-7-76

100%

90

80

70

60

50

40

30

20

10

CHANNEL 4 PTM
AVHRR/1 SPECTRAL
RESPONSE

— PREDICTED

- - - MEASURED

$\Delta\lambda = .021 \mu$

3.5

3.6

3.7

3.8

3.9

4.0

MICRON

100%

10/15/76

4 X 4 TO THE INCH 46 0253
 10/15/76
 GEORGE S. FISHER CO.

90
80
70
60
50
40
30
20
10

.70 .80 .90 1.00 1.10 MICRONS

PTM
 — PREDICTED BASED
 ON ITT MEASURED
 MIRROR VALUES
 --- PREDICTED BASED
 ON VENDOR
 MIRROR VALUES



**AEROSPACE/OPTICAL
DIVISION**

3700 E. Pontiac Street
Fort Wayne, Ind. 46803
(219) 423-9636 - TWX 810-332-1413

To: R. Foote

From: C. L. Soest *CLS*

Date: December 22, 1976

Subject: DIR #40
AVHRR/L LTM Final Report

CC:
D. Melton
J. Stark

Ref: ITT 8120888 - Test Procedure for AVHRR Life Test
Model (LTM)

ITT 8009480 - Procedure for AVHRR LTM Scanner
Dismantling (with attached notes)

NASA/GSFC Memo by A. J. Babecki, "Examination of
Ball Bearings from the AVHRR Life Test"

Instruction

The AVHRR LTM Scanner was dismantled on March 17, 1976 for the purpose of investigation and analysis (primarily of the ball bearings). The scanner had operated in a vacuum in excess of 8500 hours and temperature cycled between 15°C and 35°C. The complete test plan is outlined in ITT 8120888 and the test data is recorded in the LTM Logbook.

The scanner was dismantled according to procedure 8009480 by ITT engineering personnel (J. Stark) and witnessed by GSFC personnel (E. Stengard). Appropriate notes were taken during the dismantling and are attached to the procedure.

Discussion

The motor was carefully disassembled and parts were checked for signs of wear and lubricant migration. No signs of lubricant migration was evident, and this was confirmed when the bearings were weighed. There were slight wear rings on the bearing journals of the rotor shaft, and small debris patterns on the front bearing cover, bearing spacer, and bearing nut.

The bearings were carefully weighed to check on weight loss of the lubricant, and then disassembled. The front bearing lost 1.5mg and the rear bearing lost 2.8mg of lubricant.

December 22, 1976

After the bearings were disassembled, they were cleaned and the wash solutions passed through a filter to collect particulates that might have been present. The filters were submitted to GSFC for analysis and the examination disclosed very little debris, and not enough for analysis.

The bearing races, balls, and ball retainers were examined by ITT personnel at magnifications up to 30X and then forwarded to GSFC for evaluation. NASA's examination confirmed our findings of very little wear on the bearings. The bearing races exhibited uniform ball tracks that were off center which indicated the presence of preload on the bearings. The balls did not show any wear rings and showed no evidence of wear.

Upon completion of the examination by NASA, the bearings were sent to Split Ballbearing for examination and preload measurement. Their measurements indicated a preload of 5 oz. A copy of their findings is attached.

Summary

After operating for over 8500 hours in a vacuum the LTM scan motor bearings exhibited very little wear and lost approximately 1.5 - 2.8mg of lubricant from approximately 27-29mg of total lubricant originally present. Jitter measurements were 100%, coast down time 2'-15", and running torque 0.8 oz-in.



MPB

Split Ballbearing

DIVISION OF MPB CORPORATION
HIGHWAY FOUR, LEBANON, NEW HAMPSHIRE 03766
TELEPHONE: 603-448-3900
TWX: 710-366-1661

August 24, 1976

ITT Aerospace/Optical Division
3700 E. Pontiac Street
Fort Wayne, Indiana 46803

Attention: Clarence Soest

Subject: Life Test Bearings, 3TAR 17-24-145
S/N 007

Dear Mr. Soest:

As you requested, we have reassembled the subject bearings and checked the preload. We find the preload to be approximately 5 oz. as compared to a spec of 1 1/2 to 3 1/2 lbs. This reduction in preload may be due to the diamond polishing which was performed at Goddard Space Flight Center. Historically, their polishing has reduced the preload on this type of bearing by approximately that amount.

The races appeared to be in excellent condition, showing only a very light frosted contact path which in no way had destroyed the geometry of the race.

We hope this answers your questions and are sorry for the initial mixup concerning these parts. Should you have any further questions please do not hesitate to contact this office or our Field Sales Engineer, William Cotton. The bearings are enclosed.

Regards,

Neal C. McBain

Neal C. McBain
Product Engineer

NCM/nl
cc: WC, Chic.
Enclosures

UNITED STATES GOVERNMENT

Memorandum

TO : Mr. M. J. Donohoe, Code 726

DATE: May 12, 1976

FROM : Mr. A. J. Babecki, Code 755
Materials Engineering Branch

SUBJECT: EXAMINATION OF BALL BEARINGS FROM THE AVHRR LIFE TEST

Background

The two 3TAR ball bearings, which were in the AVHRR scan motor life test for one year in vacuum, were submitted to this Code for examination after ITT-Ft. Wayne had disassembled and cleaned them. During the cleaning operation, ITT had passed the wash solutions through a filter pad to collect particulates, and that pad also was submitted.

Examination of the filter pad at magnifications up to about 30X disclosed very little debris, and certainly not enough for analysis.

During the life test, the spin axis had been kept vertical. Therefore, the two S/N 007 bearings are identified as top and bottom. Because of the simulated mirror mass that the bearings supported during the test, the bottom bearing should have experienced a heavier load than the top one. During the life test, the bearings rotated continuously at 360 rpm and were subjected to some thermal cycling.

Although this Code had polished the ball groove surfaces to remove the original coarse surface condition, the bearings were lubricated by ITT, reportedly with the recommended Krytox 143 AB oil. This lubrication included vacuum impregnation of the phenolic laminate ball cages and the addition of a small amount of free oil to the balls and grooves.

Examination

The bearings were visually examined at low magnification. It was noted that the inner races had one face stamped with Split Ball Bearing Co's identification and that the ball track on each was off-center in the ball groove away from the stamped face. Later it was learned that the stamped faces faced each other in the mechanism and, therefore, the



tracks indicated that the inner races were preloaded against each other (DB).

There had been some concern that the polishing operation would have removed enough metal from the races to remove the preload. However, the presence of ball tracks that were off center indicated that there was a preload of some value. Figure 1 pictures the ball tracks on the inner and outer races of the top bearing, and Figure 2 pictures them on the bottom bearing. The ball tracks were uniformly spaced and uniform in width around each race, which suggests that there was no looseness in the bearings as there might be with no axial preload. However, the track on the bottom bearing appeared to be slightly larger than on the top bearing, which would be expected considering the greater load that it carried.

Low power examination of the balls indicated that they were uniform in appearance, that they did not sport any wear rings, and that they did not show evidence of any significant wear. Figure 3 pictures the surface at high magnification of a randomly-selected ball from the bottom bearing. It is noted that the surface condition looks good. The figure also illustrates the as-polished surface condition of the ball groove and the slight change in it effected within the ball track of the bottom bearing. Figure 4 depicts the ball and track surfaces in the top bearing. Again, the changes effected by the life test operation were minimal.

A chemical analysis was made by IR spectrophotometry of a sample of the oil from the bearings at the conclusion of the life test. Mr. Fred Gross of this Code reported that the lubricant was not degraded and that it was, indeed, Krytox with a small amount of aliphatic hydrocarbons and esters that did not appear unusual.

Discussion

The examination of the bearings and oil, and the lack of wear debris on the filter pads show that there was an extremely small amount of wear of the bearings in the one year vacuum operation. Other information from ITT indicated that only 1.5-2.8 mgms. of oil was lost from the approximately 25 mgms. original quantity in each bearing. In addition, ITT reported seeing no oil film outside of the bearings, which indicates that there was no oil creep problem.

There is no doubt that the balls of the bearings floated on a film of oil with little or no metal-to-metal contact between them and the races. This desirable condition was due in part to the properties of the oil, but also to the fine surface finish given to the races by this Code. It is understood, however, that the flight bearings will not have races polished by this Code, although their surface finishes reportedly are better than the life test ones originally were.

If the flight bearings have surface finishes which are significantly rougher than the life test bearings after polishing, it is probable that the wear that is developed will be greater. How much greater is not known, but it may be significant if the axial preload is high and if the oil quantity for some reason is less than in the life test bearings.

Because the flight units may be in storage for a year or more before integration into the spacecraft, consideration will have to be given to the storage conditions to minimize contamination and to preserve the integrity of the lubricant. Such steps as sealing in a nitrogen atmosphere and periodic operation to spread the oil are minimum considerations. Perhaps vacuum sealing and witness mirrors and temperature limits also should be considered.

Recommendations

In order to gain confidence that the flight unit will perform as well as the life test model, it is recommended that

- 1) This Code be given a sample bearing of the new lot to inspect and return,
- 2) The axial preload applied be as low as practicable,
- 3) A greater quantity of oil be added if the bearing surface finishes are coarser than the life test bearings had, and
- 4) Adequate storage and periodic operation be incorporated in the plans.

Alfred J. Babicki

Alfred J. Babicki
Engineering Metallurgy Section

cc: 755 Distribution
Tiros-N Project List
J. Stern/325
D. Smith/921

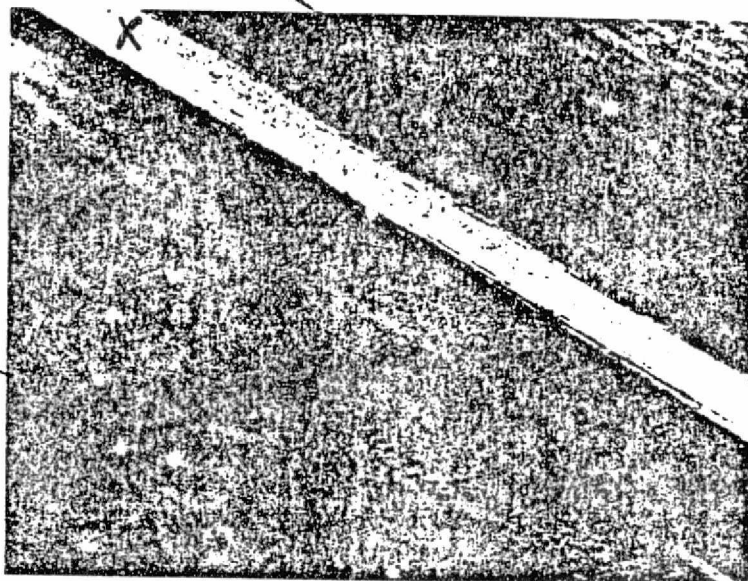
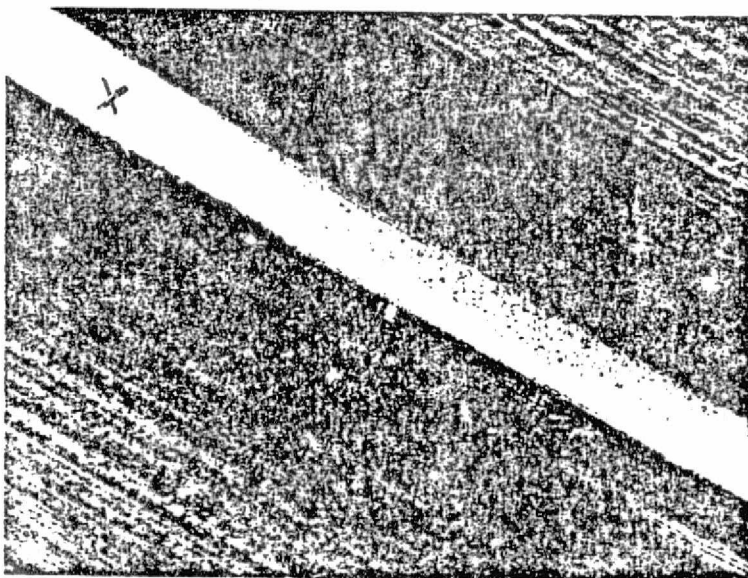


Figure 1

Ball groove (arrows)
and ball track (X)
on the inner race
of the top bearing.

22.5X



As above, but on
the outer race.

22.5X

REPRODUCTION OF THE
ORIGINAL FOR THE
FBI

REPRODUCIBILITY OF THE
ORIGINAL PAGE IS POOR

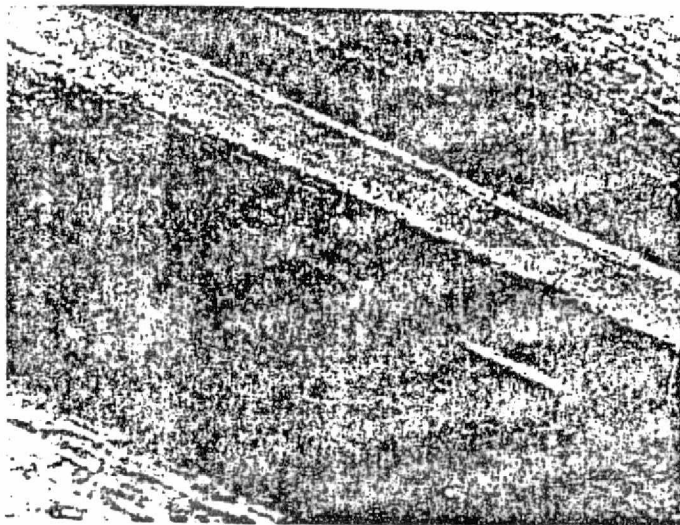
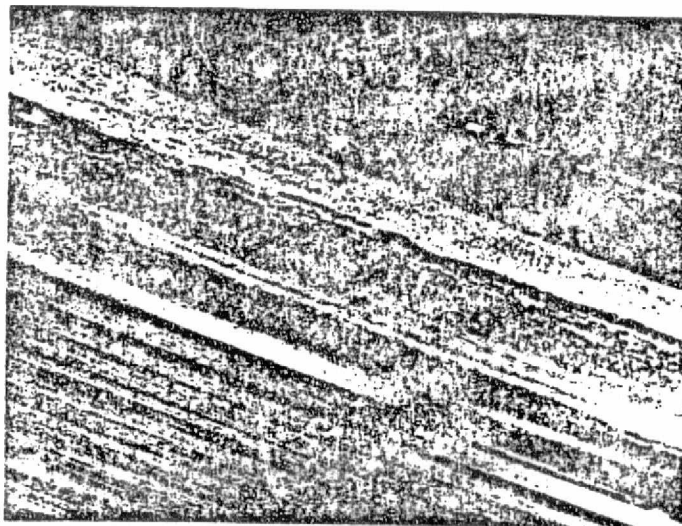


Figure 2

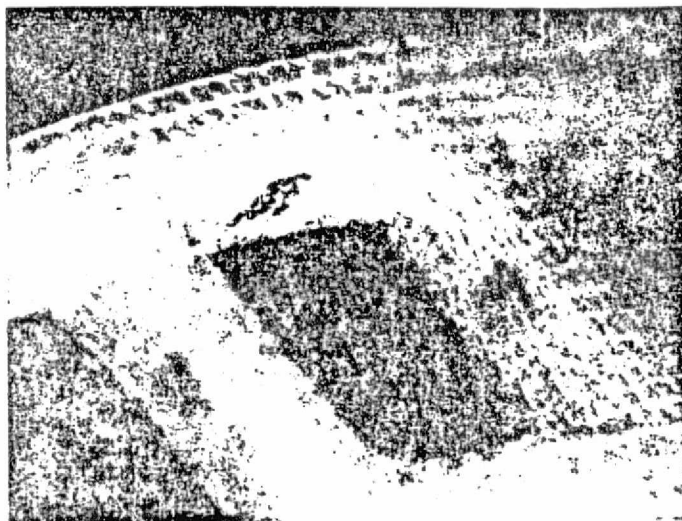
Ball groove and ball
track on the inner
race of the bottom
bearing.

22.5X



As above, but on the
outer race.

22.5X



Ball pocket of the
phenolic laminate
ball cage with rub
spots.

15X

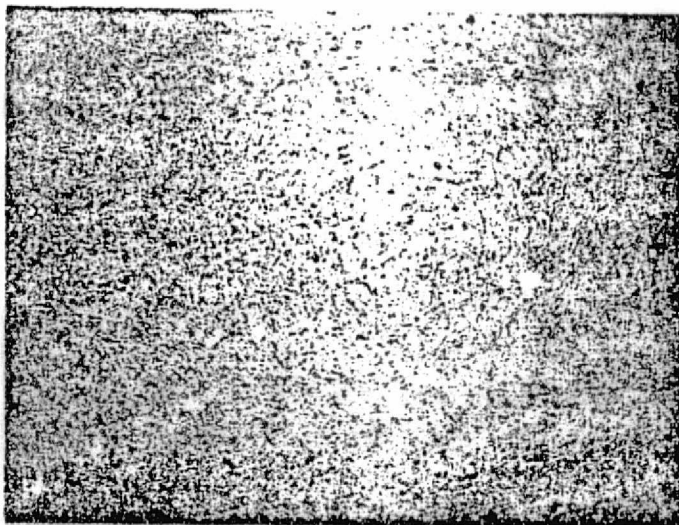


Figure 3
Surface of a ball
from the bottom
bearing appears flow-
less at 200X.



Polished surface of
the inner race ball
groove outside of
the ball track at
200X.



Surface of the ball
track on the inner
race of the bottom
bearing at 200X.

REPRODUCIBILITY OF THE
ORIGINAL PAGE IS POOR

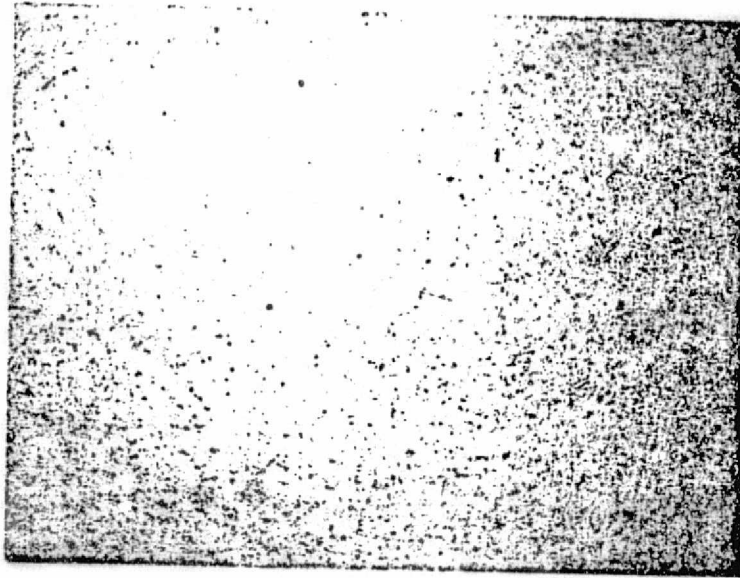


Figure 4


Surface of a ball
from the top bearing
at 200X.



Surface of the ball
track on the inner
race of the top bearing
at 200X.

REPRODUCIBILITY OF THE
ORIGINAL PAGE IS POOR

PROCEDURE
FOR
AVHRR LTM SCANNER DISMANTLING

REVISIONS DATE CHG BY ECH NO.		
PREP. BY <i>C. J. Smith 3-1-76</i>	 AEROSPACE/OPTICAL DIVISION <small>INTERNATIONAL TECHNOLOGY AND SYSTEMS CORPORATION</small> FORT WAYNE, INDIANA	ASSY. NO.
APPD. BY		DRAWING NO. 8009480 REV.
APPD. BY		SHEET 1 OF

ITT FW E-196

1.0 SCOPE

This procedure describes the order of disassembly and inspection of the LTM Scanner. The purpose of the procedure is to ensure that no data will be lost in disassembly of the motor prior to the investigation and analysis of all pertinent data.

2.0 INSTRUCTIONS

All LTM parts should be carefully handled with clear polyethylene gloves. Any pertinent data should be recorded below. Photograph parts as required.

LTM WAS AT PARTIAL VAC PRIOR TO CHECK

3.0 PROCEDURE

- 3.1 Measure LTM motor current in air at 22.5V 167 *mA*.
- 3.2 Measure coast down in air 1'-16.1". *TEMP 13°C*
- 3.3 Operate LTM motor for a minimum of 24 hours in vacuum (approx. 1 micron) and measure current at 22.5V 153.
- 3.4 Measure coast down in vacuum 2'-15.7".
- 3.5 Measure current at 22.5V in air 162.7.
- 3.6 Measure coast down in air 1'-55.5".
- 3.7 Remove motor from life test set-up and take to clean room environment. Carefully inspect assembly and note observations. Photograph if necessary. ✓
- 3.8 Check axial and radial play of shaft. Axial .
Radial .
- 3.9 Measure following torque at 22.5V. slip 4.9507-1M.
stall 5.0007-1M.
- 3.10 Make torque/current measurements on breadboard motor, and utilizing the breadboard motor as a drive source, measure running torque of the LTM running in the operational direction (CW looking at the motor from the mirror end). Measurements will be made with the motor in the horizontal position and 22.5V.

Breadboard Motor		
Torque	Current	RPM
No Load	170	360
0.5oz-in.	170	"
1.0	180.9	"
1.5	185.8	"
2.0	191.2	"
2.5	197.3	"
3.0	205.0	"
3.5	210.0	"
4.0	216.0	"
4.5	221.0	"
5.0	227.0	"
5.5	233.0	"
6.0	240.0	"

Current measurement of BB
motor while driving

LTM 179 ma

Resultant running torque
of LTM .807-in.

Torque	I	RPM
6.5	259	348
7.0	270	335
7.5	282	320
8.0	299	290
8.5	308	0
4.75	307	0

3.11 If possible, rotate entire assembly (BB motor driving
LTM motor) to the vertical direction and note any
change in current reading 174 ma.

3.12 Start disassembly of LTM with careful observations
along the way for any signs of debris, corrosion,
lubricant outside of bearings, evidence of binding,
cocking, walking of bearings on the shaft or housing,
walking of spacers, etc. Photograph if necessary.

* 3.13 Record front and rear bearing.

front (mirror end) SEE ATTACHED

rear (rotor end) NOTHING NOTED

3.14 Measure torque required to remove bearing retainer
nut 50 lb-in.

3.15 Remove bearings and spacers and visually examine at
magnification (~ 10x - 30x) for evidence of oil or
debris on the outside of bearings and separators.
Photograph as required.

3.16 Weigh bearing assembly to nearest 0.1 mgm

FROM = 17.76339 gms.
TO = 17.76494 gms.

MEASURE AIR GAP. UNIFORM & FREE
WITH .003 & .005 SPACERS

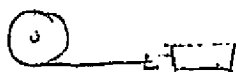
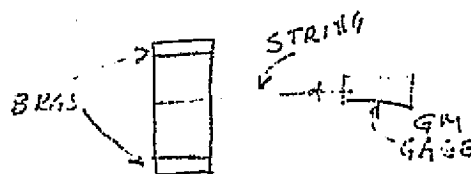
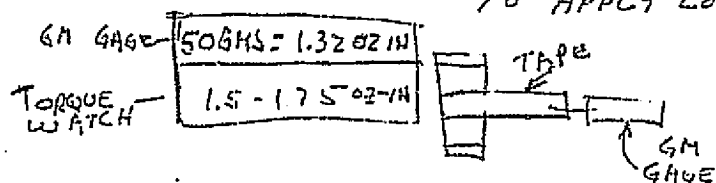
WEIGHED
APPROX 24:30
AND AFTER
AT 12:11
12:11

- 3.17 Examine interior of bearing at magnification for oil, debris, meniscus, non-wetting, etc. Photograph as required. *500 1/10 1/10 1/10 1/10*
- 3.18 Check bearing set for preload 710 ATC/02H.
- 3.19 Measure running torque with gram gage and torque watch 35 GMS @ .75" gm gage. = .92 OZ-IN
1.15 OZ-IN torque watch.
- 3.20 Disassemble bearing set and examine at magnification for debris and wear. Photograph as necessary.
- 3.21 Weigh retainer 50.074
49.106.
- 3.22 Clean metal parts in filtered freon, and filter wash after cleaning.
- 3.23 Examine filter at magnification. Photograph if necessary. Save wash and filter and send to GSFC for analysis.
- 3.24 Weigh dry metal parts 17.2594 GMS. 17.2671 GMS
- 3.25 Examine cleaned metal parts at magnification to 200x for evidence of wear, cracks on races, wear rings on balls, etc. Photograph as necessary.
- 3.26 Examine retainer pockets for wear at magnification. Photograph as necessary.
- 3.27 If bearing set has preload, send to SBB for measurement.

NOTE:

3.19 MEASUREMENT MADE ON 3-24-76 WITH TAPE ON O.D OF SPACER ONLY.

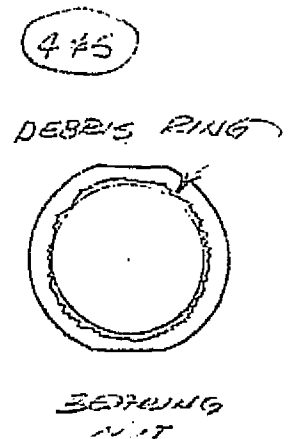
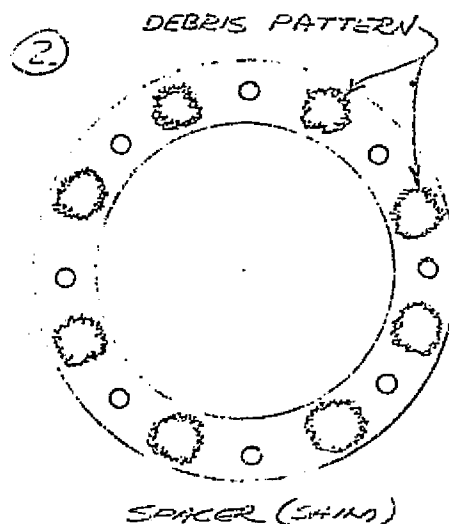
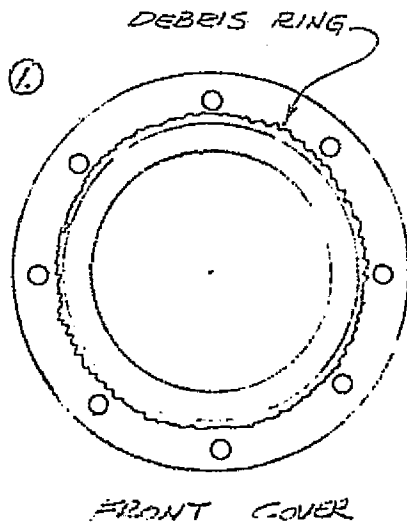
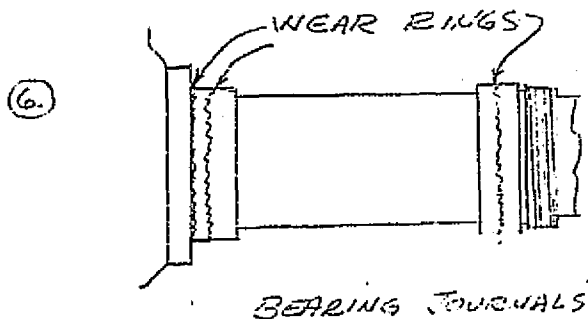
MEASUREMENT WAS REDONE ON 3-27-76 USING STRING TO APPLY LOAD TO GRAM GAGE.



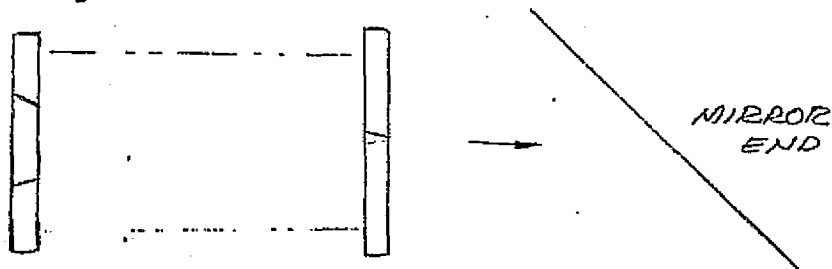
NOTES FOR 8009480

FRONT SIDE

1. Debris ring on front cover where contact with bearing is made.
2. Debris pattern of holes on spacer adjacent to
Obsolete lub. reservoir holes.
3. Nothing observed in bearing or races on examination while
still installed and nut tight.
4. Debris ring on each side of nut.
5. Debris ring on outside of spacer
- 3.15 6. Wear ring on ends of bearing journals and shoulder of step
on rotor end



7. Bearing I.D.'s show a couple of wear spots.
8. Bearing toward mirror has chevron toward mirror



9. Slight blade ring around bearing bore
and bores feel dry - no oil film detected.
- *10. (Front bearing)
 1. Balls have wear tracks (before disassembly) pattern
 2. Meniscus in bearing (Front bearing)
 3. No evidence of non wetting
 4. No debris buildup
 5. No large particles on balls or elsewhere.
 6. No rainbow effect
- *11. (Rear bearing)
 1. Is a meniscus
 2. No evidence of non wetting
 3. No debris or large particles
 4. No wear traces
 5. Rainbow effect on balls - lub.
 6. Surface of balls smoother than other bearing
 7. Seems to have more lub - observation and feel.

11	Wgt	17.76339 grams	<u>Front Bearing</u>	^
	"	17.76494 grams	<u>Rear Bearing</u>	/ \
Orig.	^	17.76492	/ \ 17.75777	(Test Plan)
	^	<u>17.76339</u>	/ \ <u>17.76494</u>	
	^	.00153 grams	.00283 grams	

- 3.20 > (1) Apparent wear track on inner race
(2) Congealed oil in groove - both races
(3) Balls clean, shiny, no evidence of wear
(4) No evidence of wear on retainer

Free oil on surface of cage

Wear spot on leading edge of ball contact point.

3.21 ⁵
/ \ .50299 (.50292)
^ .49106 (.49079)

10.0 LIST OF DESIGN INFORMATION REPORTS

Design Information Reports written on this program are listed below.

<u>DIR #</u>	<u>Subject</u>
1.	AVHRR Sensitivity - Harber/Koczor
2.	AVHRR Collimator - Diffraction Effects - R. Koczor
3.	Effects of Optical Surface Errors on Diffraction Limited MTF - R. Annable
4.	Approach to the Optical Alignment and Channel Registration of the AVHRR - R. Annable
5.	The Effect of Detectors on the Instrument Spectral Response, Part 1, Channels 3 & 4 - R. Koczor
6.	Theoretical Design to Meet the Polarization Requirements in Channels 1 and 2 - R. Annable
7.	Polarization Design and Analysis Based on OCLI Measured Data - R. Annable
8.	Using "Standard" Silicon Detectors for Channels 1 and 2 - R. Koczor
9.	Effect of Scan Mirror Power on Diffraction Limited MTF - R. Annable
10.	Visible In-Flight Calibration - R. Koczor
11.	Orientation of the Visible Calibration D.R.T. - R. Koczor
12.	Solar Channel Spectral Characteristics, Part 1 - R. Koczor
13.	Solar Channel Sensitivity - R. Koczor
14.	The Absence of Coma in an Afocal Pair of Confocal, Coaxial Parabolic Mirrors - R. Annable
15.	Heating of the Radiator Window for Contamination Protection - R. Annable
16.	AVHRR Test Collimator Design - R. Koczor
17.	The Effect of Collimator Aberrations on the Diffraction Limited MTF - R. Annable
18.	Worst Case Honeycomb Temperature Gradient in the In-Flight Thermal Calibration Target - R. Annable
19.	Cool Down and Decontamination Times for the Radiant Cooler - R. Annable
20.	Scanner Jitter, Linearity, and Alignment Tests - R. Koczor
21.	Optimization of IFOV Size and Shape, Pre-Sampling Filter, and Sample Rate - R. Foote
22.	Thermal Math Model Analysis - Crawford/Wright
23.	Thermal Math Model Analysis, OFF Instrument - Crawford/Wright
24.	Measurement of Low Emissivity - R. Koczor

DIR #Subject

25.	AVHRR Scan Motor Lubricant Evaluation and Selection - J. Stark
26.	AVHRR TM Calibration - N. Franklin
27.	MSM Vibration Test - J. Stark
28.	BBM Acceptance Test Results - Owens/Koczor
29.	Completion of Thermal Math Model - J. Crawford
30.	MSM Vibration #2 - J. Stark
31.	Effect of Loss of Radiant Cooler Temperature Regulation - R. Harber
32.	Worst Case Analysis - L. Roffelsen
33.	AVHRR MSM Vibration #3 - J. Stark
34.	Spectral Response Measurements on AVHRR ETM - R. Harber
35.	Pinning of Critical Parts - C. Soest
36.	Cooler Door Momentum - C. Soest
37.	Scattered Light Test Results of AVHRR BBM - R. Koczor
38.	Final Thermal Model Analysis - J. Crawford
40.	LTM Final Report - C. Soest
42.	AVHRR Data Amplifier Signal Droop - H. Kalina
43.	Channel 4 Coherent Noise in AVHRR PFM - R. Foote